CLASTIC DIAGENESIS AND POREFLUID EVOLUTION : AN ISOTOPIC STUDY, MAGNUS OILFIELD, NORTH SEA

A thesis submitted for the degree of
Doctor of Philosophy

by Calum Ian Macaulay B. Sc. (Aberdeen)

Department of Applied Geology,
University of Strathclyde.

August 1990

PAGINATED BLANK PAGES ARE SCANNED AS FOUND IN ORIGINAL THESIS

NO INFORMATION IS MISSING

CONTENTS

ABSTRACT

The Upper Jurassic Magnus Sandstone is a medium-grained feldspathic submarine fan sandstone, which was derived from the northwest and deposited in the East Shetland Basin as four stacked lobes. These formed a reservoir up to 200m thick within the Kimmeridge Clay oil source rocks. The oilfield was formed by uplift and subaerial erosion of a fault block from early to mid Cretaceous, followed by burial beneath Late Cretaceous mudstones and marls which form the seal.

Major diagenetic events within the reservoir sands comprise dissolution of feldspar and garnet and resultant precipitation of quartz overgrowths and kaolinite, followed by growth of magnesian siderite, ankerite and illite. The cement sequence is very similar in each of three wells studied along a 4km traverse from the crest to the flank of the field. The present day reservoir is buried to 3200m and 120°C, with a formation fluid salinity half that of seawater and a $\delta^{18}O$ +2‰.

Calcite cement is virtually absent, probably due to a lack of detrital shell carbonate. Siderite is distributed throughout the sandstone but localised around degrading detrital biotite grains and mud clasts. Rhombic crystals show distinct compositional evolution through three growth zones, and have more magnesian compositions downdip. This suggests different porefluid compositions across the field. Ankerite is only found close to mudstones, from where Fe and Mg were released during burial. These carbonates have $\delta^{13}C$ values which suggest a supply from decarboxylation of organic material.

Within each well, diagenetic mineral $\delta^{18}O$ values consisent with increasing temperature follow the mineral diagenetic sequence. Geothermal gradients of 45°Ckm^{-1} are inferred during rapid burial. The $\delta^{18}O$ values for each mineral are persistently 3-4‰ more negative for samples from the crest of the field than from the flank. This is interpreted to indicate persistently stratified porewaters during burial. The influence of isotopically negative meteoric-derived water in the crest contrasts with more marine-derived porewaters downdip. This surprising deduction suggests that diagenesis was dominated by local flow or diffusion and not by regional fluid movement. This oilfield perhaps represents an end member of the diagenetic spectrum.

ACKNOWLEDGEMENTS

I'd like to begin by thanking the two people who contributed so much to this work that it would not have been possible without them. Stuart Haszeldine, my official supervisor, and Tony Fallick are these two people. Stuart and Tony have been constant sources of encouragement and guidance, full of perception and innovation, and I owe them both a great deal. I also owe Tony a great many pints from the numerous Friday evenings during writing up when I arrived at "Duke's" penniless. Joe Hamilton helped conceive the project and was co-supervisor during my first year.

Rodger Connell of Marathon Oil in Aberdeen first encouraged my interests in diagenesis and pointed me towards Stuart at the Dept. of Applied Geology at Strathclyde University. I am indebted to him for his advice, and for keeping me in employment until I started at Strathclyde.

The Dept. of Applied Geology was both a revelation and inspiration to me. Mike Russell, Roger Anderton, Alan Hall, Iain Allison, George Bowes, Brian Bell and Jeff Harris have all contributed to some aspect of my work at various times. George is thanked especially for increasing my computing abilities from the search for the on/off switch to the point where I can now work a Mac - no mean feat- and for teaching me to play squash and running me ragged on court since. Murdo Mcleod and Dugie Turner provided first rate technical support and John Gilleece and Peter the Pigg, dab hands both, supplied excellent sections. Peter's Rolls Royce engineering expertise contributed to keeping my motorbike on the road.

I spent a great deal of time during this study at the Isotope Geology Unit of the Scottish Universities Research and Reactor Centre in East Kilbride. There, "Santa" Fallick and his staff taught me everything from sample preparation to flying the mass specs and data interpretation : many thanks to Terry Donelly the lab manager, Alison McDonald, Julie Gerc, Ward Scott, Adrian (Sulphur man) Boyce, Gawen (International Isotope Rescue) Jenkin, Pete Ainsworth, Jim Grey, Simon Kelly, Ray Burgess, Julian "Jos" Jocelyn, Fred "the Glassblower" Cornwallis, Andrew Tait, Gary and anyone else who I may have omitted.

Steve Rainey, my contact at BP, kept me on the straight and narrow and input usefull ideas. Cathy Brown, also at BP, took many of the SEM photomicrographs presented here.

Ed Stevens and Donald Herd at St. Andrews, and Peter Hill at Edinburgh, are thanked for their generous help with microprobe analyses.

Douglas McLean performed miracles in the dark room, often at notice so short that it was non-existent

I've had lots of fun and exchange of ideas over the past few years with members of the Diaboredom Gang and other friends, especially John Brint, Morgan Sullivan, Clark Fenton, Big Tam, his eminence the Big G, Pete Chung, Joe Crummy, Orla, Wobbly and Arshad.

I acknowledge receipt of a three year NERC grant, and provision of core material and data, through a CASE studentship, by BP.

I hope that I'll be able to repay my folks, Helen and Ian, and my brother Graham and sister Ann for their continuous support, financial, moral and edible. I couldn't have done it without them.

Extra special thanks and a big hug, for keeping me sane, to the gorgeous Hazel - my very best friend.

CHAPTER 1

1.1 INTRODUCTION

1.1.1 Original aims of the project

The isotopic compositions commonly observed in sandstone oil reservoir diagenetic minerals are usually interpreted to indicate diagenetic porefluids derived from meteoric water. This project was initiated to test the hypothesis that similar diagenetic mineral isotopic compositions could be produced by marine fluids interacting with clay minerals and organic debris. The reservoir to BP's Magnus oilfield northeast of Shetland was chosen as the testbed. As a deep-marine deposit buried beneath marine sediments, the only possible connection to a meteoric water supply was during the early Cretaceous. Wholesale flushing of the Magnus sandstones by meteoric fluids at this time had been invoked to explain the growth of diagenetic kaolinite (Rainey, 1987). The study was to sample several oilwells down and along structure, using core material supplied by BP, to gain isotopic, elemental and fluid inclusion data. The question was whether pre-kaolinite minerals would show isotopically marine porefluids derived from depositional waters in contrast to kaolinite and later minerals which might show meteoric-derived waters.

1.1.2 Rationale behind oilfield reservoir diagenesis studies

In the search for hydrocarbons the ability to predict oil and gas distribution and reservoir quality is vitally important to the industry. North Sea oil production peaked in about 1988. The attentions of oil and gas producers are necessarily, therefore, turning to increasing hydrocarbon recovery from existing reservoirs and to finding new reservoirs in deeper, more distant and more complex geological settings. Diagenesis is one of the fundamental pieces in the jigsaw that is reservoir characterisation.

Diagenesis encompasses the physical and chemical changes that occur in a sediment from deposition, through burial and reservoir filling, to metamorphism. Detrital minerals react with the porefluids as temperature and pressure increase with burial. Unstable minerals such as feldspars dissolve and new more stable diagenetic minerals precipitate. These dissolution and precipitation reactions can enhance and detract from reservoir porosity and permeability. Secondary porosity generated by

feldspar dissolution is commonly offset by precipitaion of new phases such as quartz overgrowths in both primary and secondary porosity. Permeability can be severely reduced by precipitation of clay minerals such as kaolinite and illite. The main application of the results of diagenetic studies is, therefore, to the descrption and prediction of reservoir quality in the subsurface. In the Upper Jurassic Magnus sandstones, detrital components have reacted with the porefluids and organic acids generated in the enclosing Kimmeridge Clay Formation, which was the hydrocarbon source rock. Quantitatively, the most important diagenetic minerals to have grown are quartz overgrowths, kaolinite, magnesian siderite, ankerite and illite. The most important minerals to dissolve were feldspars, micas and garnet.

An understanding of the origin and movement of the medium in which diagenetic reactions occur, namely the porefluid, is as important as understanding the reactions themselves. Porefluids carry dissolved ionic and organic species and can travel great distances through permeable rocks. Their origins can be inferred from their isotopic compositions. Analysis of diagenetic mineral isotopic composition allows, within certain constraints, interpretation of the isotopic composition of the porefluid from which that mineral precipitated if the temperature of precipitation is known. This is possible because, for a mineral formed at a given temperature in isotopic equilibrium with the porefluid, the isotopic composition of the mineral, the isotopic composition of the porefluid and the temperature of mineral growth are related by a fractionation factor. Numerous workers have calculated fractionation factors for different minerals through experiment and isotopic analyses of minerals formed in well constrained natural settings.

1.2 THE THESIS

This thesis comprises three papers which relate various aspects of the diagenetic history of the marine Magnus Sandstone :

The first (Chapter 2) is a short paper which reports a clear distinction between the isotopic compositions of very similar suites of diagenetic minerals from the crest of the oilfield where diagenetic mineral isotopic compositions are more negative and from the deeper flank where they are less negative. This is interpreted to reflect the retention through burial

diagenesis of a larger component of isotopically more negative meteoric-derived porewater in the crest of the field. Porewaters in the Magnus Sandstone were therefore stratified throughout diagenesis until the reservoir filled with hydrocarbons, some 35 million years after tectonic uplift allowed ingress of meteoric water. This scenario, which was a surprise to us, has not previously been reported from a hydrocarbon reservoir and implies that in this case diagenetic mineral constituents were locally derived. In many other oilfields ionic species which formed diagenetic minerals are interpreted to have been transported long distances by porefluid migration.

In Chapter 3 the chemical and isotopic compositions of diagenetic magnesian siderite and ankerite cements are examined in detail. Siderite grew in the raised pH environment around degrading detrital biotite grains from locally derived Fe and Mg. Carbon isotope values suggest that CO_2 was derived dominantly from the thermal decarboxylation of organic material in the Kimmeridge Clay mudstones. Later ankerite developed adjacent to mudstones, and is probably derived from dissolved ions expelled by mudstone compaction and CO_2 derived from slightly more advanced decarboxylation reactions. Both carbonate phases have oxygen isotope values which are more negative in samples from the crest of the field. Both phases are also more ferroan in the crest of the field and more magnesian at depth. This is interpreted to result from a larger component of meteoric-derived porewater in the crest of the field and a larger component of porewater derived from seawater at depth in the sandstone.

Chapter 4 discusses the diagenetic and isotopic evolution of the Magnus Sandstone through burial diagenesis. A variety of techniques were used to study the sandstone petrography, and oxygen ($\delta^{18}O$), hydrogen (δD), carbon ($\delta^{13}C$), sulphur ($\delta^{34}S$) and K/Ar dating isotope systems used to study the isotopic evolution of the porefluid. The paragenetic sequence of diagenetic minerals charts the chemical evolution of the porewaters with time and increasing burial temperatures. Original depositional marine bottom waters in the Magnus basin were reducing and promoted early diagenetic framboidal pyrite, glauconite and illite development. Tectonic uplift and subaerial erosion in the early Cretaceous exposed the sandstones to a shallow influx of meteoric water, which oxidised early framboidal pyrite in the crest of the field. Subsidence and burial beneath thick mid-Cretaceous

and younger sediments lead to increasing temperatures in the Magnus Sandstone which promoted mineral/fluid reactions. As temperatures increased toward 80°C organic acids were expelled from the enclosing Kimmeridgian mudstones and promoted detrital feldspar and garnet dissolution The results of $\delta^{18}O$ analyses suggest that quartz overgrowths developed at temperatures as low as 40°C, and continued until at least 100°C. Kaolinite developed mostly at about 80°C. Late diagenetic pyrite $\delta^{34}S$ results indicate that the sulphur isotopic system was closing, and magnesian siderite (85°C) and ankerite (90°C) developed as organic reactions continued, as described in Chapter 3. Finally, fibrous illite developed at about 100°C. Hydrocarbons filled the reservoir by 55 Ma, but illite continued to grow beneath the oil pool. In each of the three wells studied, a similar paragenetic sequence was observed and all the diagenetic minerals analysed show the same trend of more negative oxygen isotope values in crestal samples than downdip. Kaolinite and illite δD values mirror this trend. In each well the diagenetic mineral $\delta^{18}O$ values record the isotopic evolution of the porefluids towards more positive values through porefluid/sediment interaction, yet the influence of an isotopically negative meteoric-derived porewater in the crest of the field is recorded throughout diagenesis.

1.3 REFERENCE

Rainey S.C.R.,1987, Sedimentology, diagenesis and geochemistry of the Magnus Sandstone Member, Northern North Sea. (Ph.D. thesis) : University of Edinburgh.

CHAPTER 2

SEDIMENTARY BASIN POREWATERS REMAIN STRATIFIED DURING 35 MYR RAPID SUBSIDENCE: MAGNUS OILFIELD, NORTH SEA

C.I.Macaulay*, R.S.Haszeldine*, & A.E.Fallick^.

* Department of Geology and Applied Geology,
University of Glasgow, Glasgow G12 8QQ, Scotland.
^ Scottish Universities Research and Reactor Centre,
East Kilbride, Glasgow G75 0QU, Scotland.

2.1 ABSTRACT

The palaeo-hydrology of sedimentary basins is of great interest to oil and minerals geologists, geochemists and basin modelling engineers. Some type of fluid flow movement within a basin is generally expected to have transported the solutes and solvents required to form an ore deposit - or to have transported the ions which form diagenetic mineral cements to an oilfield sandstone. Fluid flow may be the result of gravity, thermal convection, compaction- induced basin dewatering or seismic valving. We have attempted to study the effects of fluid movement in a giant oilfield in the North Sea by using conventional isotopic and petrographic techniques to characterise diagenetic minerals. In contrast to our expectations, we find that porewaters of distinctly different compositions existed within four kilometers of each other, and within the same uniform sandstone. This is shown by separated clusters of diagenetic mineral isotopic data from the crest and from the flank of the field. These same differences persisted from earliest burial, through 2km of subsidence to oil migration - a timespan of 35 Myr. Therefore during this period the oilfield fluids were stratified and static, and no homogenisation of the fluids occurred across the field. Mass transport of material to cement the sandstone was presumably dominated by diffusion, not fluid flow. Oil has been trapped for a further 55 Myr, implying that this oilfield has been a discrete hydrologic compartment for 90 Myr.

2.2 INTRODUCTION

The Upper Jurassic Kimmeridgian (152-154 Ma) Magnus Sandstone Member forms the major reservoir to the "giant" Magnus oilfield in the East Shetland Basin (Figure 1a). These sediments were deposited as midfan lobes in a sand-rich submarine fan system derived from the west (Rainey, 1987 ; De'Ath and Schuyleman, 1981). Fine-medium grained arkosic sandstones form a 200m thick porous sandstone unit sandwiched within the Kimmeridge Clay Formation (KCF) mudstones, and regionally decrease in grain size and thickness eastwards. Four depositional lobes have been identified (Rainey, 1987). Several of these lobes are separated by mudstone beds which act as pressure barriers within the reservoir. Following deposition, Lower and Mid-Cretaceous structural movements caused uplift, tilting and subaerial erosion of the Jurassic sequence, at which time meteoric water is inferred to have entered the Magnus Sandstone, dissolved detrital feldspars, and displaced the depositional marine water at the top (crest) of the fault block (De'Ath and Schuyleman, 1981).

During subsequent burial beneath marine sediments, temperature and pressure-related changes in the Magnus Sandstone and surrounding Kimmeridge Clay Formation resulted in the dissolution of detrital mineral phases such as feldspars, garnets and micas and the formation of new diagenetic mineral phases. Detrital mineral dissolution and diagenetic mineral precipitation events in the Magnus Sandstone are very similar to those seen petrographically in many other oilfield sandstones (Milliken et al.,1981 ; Bjorlykke et al., 1988).

2.3 APPROACH

The same petrographic sequence of diagenetic minerals is observed in each of the three wells studied, which lie only 3 km. apart (Figure 1b). Therefore we assume in this paper that the same minerals grew at approximately the same times and temperatures in each well until diagenesis was halted by reservoir filling with hydrocarbons. Volumetrically, the most important of the diagenetic minerals, in

their petrographically determined paragenetic sequence, are quartz overgrowths (which continued to grow throughout diagenesis), kaolinite, magnesian siderite, ankerite and illite.

When these silicate and carbonate minerals grew, the stable oxygen isotopes of the surrounding pore water were partitioned into each mineral to a degree described by an isotope fractionation factor. At equilibrium the isotopic fractionation factor for each mineral depends on temperature. So, a given mineral formed at the same temperature in equilibrium with pore fluids of different isotopic compositions will record different $\delta^{18}O$ values, and these $\delta^{18}O$ values can be related back to the oxygen isotopic composition of the different pore fluids (Friedman and O'Neil, 1977) . In the Magnus Sandstone, separated clusters of isotopic data measured for the same mineral in different wells imply isotopic differences between the crestal porewater and downdip porewater. For each mineral formed during the diagenetic sequence, the separation of isotopic values in different wells is retained. We deduce that the porewaters remained static and were not homogenised by fluid flow during diagenesis. The differences in measured isotope ratios are not dependent upon the exact fractionation ratio used, the exact temperature of growth, or the exact isotopic ratios of the ancient waters. We argue below that throughout diagenesis an isotopically light pore fluid was retained in the crest of the structure whereas an isotopically heavier pore fluid was retained downdip. Likely original end-member pore fluid isotopic compositions were isotopically light (more negative $\delta^{18}O$) Lower Cretaceous meteoric fluid with a probable $\delta^{18}O$ of -7‰ (extrapolated from Taylor and Forester,1971, and Fallick et al.,1985), isotopically heavier (more positive $\delta^{18}O$) marine pore water with $\delta^{18}O$ of -1.2‰ (Shackleton and Kennett, 1975 ; Brint et al., 1990b) and isotopically evolved (i.e. $\delta^{18}O$ rich) pore fluid.

We have studied three wells which fall on a W/E cross-section through the Magnus field from the structural crest to the oil/water contact (Figure 1b) . Because depositional sandstone lobes are separated by thin mudstones, samples for analysis were collected from those lobes which are present in all three wells.

2.4 METHODS

The major diagenetic minerals have been separated in our laboratory from sandstone core samples. Oxygen isotope analyses ($\delta^{18}O$) of all the appropriate mineral phases were performed. From these mineral analyses, we can (via fractionation equations (Friedman and O'Neil, 1977) characterise the oxygen isotope geochemistry of the pore fluid which precipitated each of the minerals within the sandstone in these different wells. The relevant mineral separation and analytical isotope techniques are conventional (Brint, 1990a,b). Sample depths range from 2945.7m. in well 211/12-1 on the structural crest to 3355.3m. in well 211/12a-9 downdip. The results of isotopic analyses are reported relative to Standard Mean Ocean Water, SMOW (Craig, 1961).

2.5 RESULTS

2.5.1 Quartz

Quartz overgrowth $\delta^{18}O$ analyses were performed using the mass-balance technique of Milliken et al.(1981), which requires that the ratio of diagenetic quartz overgrowth to detrital quartz grain in each sample be known accurately. To this end we have established quartz overgrowth percentages on polished thin sections (Figure 3) using a cathodoluminescence detector on an electron microscope. In each case the grain mount used for point count analysis was prepared from the same quartz separate that was used for isotopic analysis. Quartz abundance analyses by different methods (grid overlay and image processing of backscatter photographs) on the same sample typically give agreement within 0.5%, suggesting that the greatly improved imaging from cathodoluminescence enhances the accuracy of Milliken`s method. No extensive pressure solution is observed between detrital quartz grains within these sandstones, precluding this as a source of quartz cement, and suggesting instead that silica cement was supplied by diffusion from adjacent mudrocks (Bjorlykke et al., 1988) and from detrital mineral dissolution within the sandstone. Our analyses suggest that quartz cement is more abundant

(10-20 %) within rare thin (less than 1m) sandstones surrounded by mudstones, than in thicker (tens m) sandstone units (5-10 %) which form the typical oilfield reservoir. Unpublished quartz overgrowth fluid inclusion data (B.P.) show that homogenisation temperatures near the oilfield crest are similar to those on the flank. In addition salinity data, limited by small inclusion sizes, shows a range from 0.2-4.6 wt% equivalent NaCl (9 measurements) in a well in the south of the field, one value of 2.6% from the northern crestal region and one value of 0.5% from a well in the far north of the field. None of these wells were sampled in our isotopic study. Our isotopic results for quartz overgrowths are $\delta^{18}O$ = +23.9 to 25.9‰ (x= 24.7‰) for crestal well 211/12-1 samples and +28.2 to 30.1‰ (x=29.0‰) for downdip well 211/ 12a-9 samples (Fig.4a). Assuming that the quartz overgrowth development in the crestal well was synchronous with that downdip, and that overgrowths in the crestal well grew at no higher a temperature than those downdip, the $\delta^{18}O$ data suggest that the crestal pore fluid had a $\delta^{18}O$ 2-3‰ more negative than that downdip. Therefore the crestal pore fluid during quartz formation had retained a significant meteoric-derived component, whereas the downdip pore fluid had retained some isotopically heavier marine or evolved fluid dominated component.

2.5.2 Kaolinite

Hurst and Irwin (1982), related kaolinite morphology to crystal growth rates and suggested that acidic ion-undersaturated meteoric pore fluids promoted rapid detrital mineral dissolution and subsequent development of coarse-grained, skeletal, vermiform kaolinite. In marine sandstones, however, diagenetic kaolinite is commonly fine-grained, euhedral and blocky. Kaolinite from the crestal wells 211/12-1 and 211/12a-M1 is dominantly coarse-grained (10-30μm) and commonly vermiform, whereas downdip in 211/12a-9 kaolinite is generally less than 10μm and blocky, suggesting that ion supply for kaolinite development was faster in the crestal region. $\delta^{18}O$ values for kaolinite in the crestal well 211/12-1 ranges from +13.5 to +14.9‰ (x= 13.6‰) whereas downdip in 211/12a-9 values are more positive and range from +15.5 to +17.5‰ (x=16.4‰)(Fig.4b). This

suggests that the crestal vermiform kaolinites grew more rapidly, and from a pore fluid with a significantly larger component of isotopically light meteoric-derived pore fluid, than the blocky kaolinites downdip. Kaolinite hydrogen isotope (δD) analyses agree with the $\delta^{18}O$ data in that crestal well 211/12-1 kaolinite δD values are significantly more negative than the values from kaolinite downdip in well 211/12a-9 (Figure 4f). However, the possibility exists of interpretational complexities such as hydrogen isotope exchange (Longstaffe, 1989 : Bird and Chivas, 1988) and the influence of organic compounds in the pore water within which the kaolinite grew. Therefore we shall not attempt here to use δD values as direct indicators of porewater hydrogen isotope composition at the time of kaolinite growth.

2.5.3 Magnesian siderite and ankerite

Magnesian siderite and ankerite cements post-date kaolinite formation, and again both show the same isotopic separation with isotopically lower values in the crestal sandstones and higher values downdip (Figure 4c,d). Siderite values in 211/12-1 range from +13.6‰ to +18.2‰ (x=16.0‰). The bulk of the siderite data from 211/12a-9 lie between +16.5‰ and +18.6‰ (x=17.6‰) but when a single result at +14.1‰ is included the mean is +16.9‰. Ankerite ranges are from +17.1‰ to +19.1‰ (x=17.7‰) in 211/12-1 and from +20.9‰ to +21.6‰ (x=21.4‰) in 211/12a-9.

Whereas siderite development is commonly intimately associated with detrital biotite degradation, ankerite cement in the sandstone is developed only within about 10m of the Upper and Lower Kimmeridge Clay and thick mudstone interbeds.This observation suggests that ions have migrated from mudstones into the sandstones in concentrations high enough to promote ankerite cementation.

2.5.4 Illite

Illite was the last diagenetic mineral to form (McHardy et al., 1982) prior to oil migration into the reservoir. $\delta^{18}O$ results of illite from updip well 211/12-1 range from +9.1 to +13.0‰ (x=11.5‰) whereas

higher values ranging from +12.9 to +15.5‰ (x=14.6‰) were recorded from 211/12a-9 downdip (Fig.4e). Again assuming that the illites in the oil zone are all coeval, the data suggest that even at this latest stage of diagenesis isotopically lighter waters still persisted in the structural crest. Interestingly, illite δD data show the same trend as kaolinite (Figure 4f), with more negative results from crestal samples. The assumption of age equivalence can be tested in future via K/Ar dating. Our available K/Ar age dates in 211/12a-9 are 55 Ma ±2.4 from illite at the base of the oil pool and 41 Ma ±1.3 from the water zone. These dates firstly constrain the period of diagenesis to a 35 Myr timespan (starting with subsidence in the Upper Cretaceous at 90 Ma); secondly date the time that diagenesis ceased due to oil migration into the reservoir; and thirdly suggest that illite growth may have continued beneath the oil/water contact.

2.6 DISCUSSION

The isotopic data (Figure 4) can be satisfied by several models :

1. The same diagenetic minerals grew in nearby sectors of the oilfield from a fluids of uniform, or different, isotopic compositions, and at different times and different temperatures, to give the same petrographic sequence with consistently different isotopic signatures. We consider this unlikely.

2. The same diagenetic minerals grew in nearby sectors of the oilfield in a dynamic flow system such as thermally-driven porewater overturn. Systematic differences in isotopic composition were maintained by a buffering exchange with a reservoir of fluid having a pronounced meteoric signature in the crest of the field, and by exchange downdip with silicates (carbonates are only present in trace quantities throughout the field). However, silicate dissolution is ubiquitous and uniform across the field, and mudstone barriers separate sandstone lobes, limiting large scale porefluid overturn (Bjorlykke et al 1988).

3. The diagenetic minerals grew at similar temperatures and at around the same time from stratified fluids which were isotopically different in nearby sectors of the oilfield. This fits most easily with the known geology, subaerial exposure and subsidence of the oilfield, and is our strongly preferred interpretation.

2.7 CONCLUSIONS

During shallow burial from the late Jurassic to the mid Cretaceous (Figure 2) the hydrologic system of the Jurassic sediment package was open, but with the onset of mid Cretaceous marine sedimentation and subsidence it was closed and preserved its isotopic stratification (Fig.1b). We have not proven this here but diagenetic mineral growth was accompanied by isotopic evolution of the surrounding pore water towards heavier values (many North Sea oilfields have present-day formation water compositions of $\delta^{18}O$ around +2‰ (Brint, 1990b ; Glassmann et al., 1989 ; Egeberg and Aagaard, 1989). The isotopic evidence shows this process has occurred in both the crest and base of the Magnus structure, but in pore waters of different origin, during the 35 million years and 2km of rapid subsidence (Figure 2) during which diagenesis took place.

Concepts of fluid flow in sedimentary basins have been dominated by models of continuous fluid throughput, whether by meteoric influx driven by hydrostatic head (Bjorlykke, 1979 ; Bethke, 1986), upward compactional fluid drive from the basin centre (Galloway, 1984), sediment subsidence through a stationary fluid column (Bjorlykke et al., 1988), fluid convection within the sediment (Wood and Hewett, 1984), or by seismic valving (Sibson et al., 1975; Burley, 1986). In this Magnus study, which may be a special case, we have shown that an isotopic difference in sandstone pore waters between the structural crest and 3km downdip was preserved during diagenesis. We cannot envisage any large scale movement of pore fluid in the Magnus sandstone during burial, either by flow of compactional waters or by convection. Diagenetic mineral cements probably grew by diffusional ion supply, yet the Magnus Sandstones have a mineralogy and diagenetic sequence very similar to other oilfields (Milliken et al., 1981; Bjorlykke et al., 1988).

Diagenesis was halted by oil migration which displaced the original pore fluids and filled the present oilfield structure by 55 Ma. Since then oil has been trapped in the field and only limited diagenesis has continued below the oil/water contact. Even at the present day, therefore, the low-density oil at the top of the structure remains a fluid-flow backwater receiving oil from the basin but not transmitting it onwards. The sandstones at the top of the Magnus oilfield have remained hydraulically restricted from those downdip for 90 Myr.

2.8 ACKNOWLEDGEMENTS

This research was carried out at the Department of Applied Geology, University of Strathclyde, and at the Scottish Universities Research and Reactor Centre Isotope Geology Unit whilst in receipt of a NERC grant. Core was provided through a CASE studentship with B.P. Exploration, who do not necessarily agree with our views. We thank P.J. Hamilton, Anton Kearsley at Oxford Polytechnic, and Oxford Instruments for discussion and use of CL equipment. Typescript was improved after comments by F.J. Longstaffe and two anonymous "Geology" referees. The SURRC is supported by NERC and the Scottish Universities.

2.9 REFERENCES

Bethke C.M.,1986, Hydrologic constraints on the genesis of the Upper Mississippi Valley mineral district from Illinois Basin brines : Economic Geology v.81, p. 233-249.

Bird M.I. and Chivas A.R., 1988, Stable isotope evidence for low temperature kaolinite weathering and post-formational hydrogen-isotope exchange in Permian kaolinites ; Chemical Geology (IGS) v. 72, p. 249-265.

Bjorlykke K., Mo A., and Palm E., 1988, Modelling of thermal convection in sedimentary basins and its relevance to diagenetic reactions : Marine and Petroleum Geology, v. 5, p. 338-350 .

Bjorlykke K.,1979, Diagenesis in Mesozoic sandstones from Spitzbergen and the North Sea - A comparison : Geologische Rundschau v. 68 no.3, p. 1152-1171.

Brint J. F., Haszeldine R.S., Fallick A.E., Hamilton P.J., Brown S., 1990a, The formation and origin of carbonate cemented zones in Brent sandstones of the Dunlin field, Northern North Sea, Journal of Sedimentary Petrology (in press).

Brint J.F.,Haszeldine R.S.,Hamilton P.J.,Fallick A.E.,Brown S. 1990b Isotope diagenesis and palaeofluid movement in the Brent sandstones, Northern North Sea, Bulletin of the American Association of Petroleum Geology (submitted).

Burley S.D., 1986, The development and destruction of porosity within Upper Jurassic reservoir sandstones of the Piper and Tartan fields, Outer Moray Firth, North Sea ; Clay Minerals v. 21, no. 4, p. 649-694.

Craig H.,1961, Standard for reporting concentrations of deuterium and oxygen-18 in natural waters : Science v.133, p.1833-1934 .

De-Ath N.G. and Schuyleman S.F., 1981, The geology of the Magnus oilfield, in Brooks J. and Glennie K.W., eds., Petroleum Geology of the Continental Shelf of North-west Europe , Heyden & Son, London, p. 342-351.

Egeberg P.K. and Aagaard P., 1989, Origin and Evolution of Formation Waters from Oilfields on the Norwegian Shelf : Applied Geochemistry v. 4, p. 131-142 .

Fallick A.E., Jocelyn J., Donnelly T., Guy M., and Behan C.,1985, Origin of agates in volcanic rocks from Scotland : Nature v. 313, p. 672-674 .

Friedman I. and O"Neil J.R.,1977, Compilation of Stable Isotope Fractionation Factors of Geochemical Interest in Fleischer M., ed., Data of Geochemistry , U.S. Geol. Survey 6th ed., Chapter KK, Paper 440KK.

Galloway W.E.,1984, Hydrogeologic regimes of sandstone diagenesis, in McDonald D. A. and Surdam R.C.,eds., Clastic Diagenesis : American Association of Petroleum Geologists Memoir no. 37, p. 3-13.

Glassman J.R., Lundegard P.D.,Clark R.A.,Penny B.K., & Collins I.D., 1989, Geochemical evidence for the history of diagenesis and fluid migration Brent sandstone, Heather field, North Sea : Clay Minerals v. 24, p. 255-284 .

Hurst A. and Irwin H., 1982, Geological Modelling of Clay Diagenesis in Sandstones : Clay Minerals v.17, p. 5-22.

Longstaffe F.J. and Ayalon A.,1989, Hydrogen isotope variations of diagenetic clay minerals from Cretaceous clastic rocks, Western Canada Sedimentary Basin ; Abstract : 9th International Clay Conference, Strasbourg, France.

McHardy W.J., Wilson M.J. and Tait J.M., 1982, Electron microscope and X-ray diffraction studies of filamentous illitic clay from sandstones of the Magnus field : Clay Minerals v.17, p. 23-29.

Milliken K.L.,Land L.S.and Loucks R.G. ,1981, History of burial diagenesis from isotopic geochemistry, Frio formation, Brazoria County, Texas : Bulletin of the American Association of Petroleum Geology, v. 65, p. 1397-1413.

Rainey S.C.R.,1987, Sedimentology, diagenesis and geochemistry of the Magnus Sandstone Member, Northern North Sea. (Ph.D. thesis) : University of Edinburgh.

Shackleton N.J. and Kennett J.P.,1975, Palaeotemperature history of the Cenozoic and the initiation of Antarctic glaciation : oxygen and carbon isotope analyses in DSDP sites 277, 279 and 281 in Kennett J.P., Houtz R.E. et al., eds., " Initial Reports of the Deep Sea Drilling Project ", XXIX, Washington, p. 743-755 .

Sibson R.H., Moore McM. and Rankin A.H., 1975, Seismic pumping - a hydrothermal fluid transport mechanism : Journal of the Geological Society of London v. 131, p. 653-659.

Taylor H.P.Jr., and Forester R.W.,1971, Low $\delta^{18}O$ igneous rocks from the intrusive complexes of Skye, Mull and Ardnamurchan, Western Scotland : Journal of Petrology v.12, p. 465-497 .

Wood J.R. and Hewett T.A.,1984, Reservoir diagenesis and convective fluid flow in McDonald D. A. and Surdam R.C.,eds., Clastic Diagenesis : American Association of Petroleum Geologists Memoir no. 37, p. 99-111.

2.10 FIGURE CAPTIONS AND FIGURES

Figure 1a. Location of the Upper Jurassic Magnus oilfield, which lies in a basin distinct from the cluster of Middle Jurassic oilfields to the south and east.

b. Cross-section through the Magnus field showing location of the three wells studied , stratigraphic position of the Magnus Sandstone Member between the Upper Kimmeridge Clay Formation (UKCF) and Lower Kimmeridge Clay Formation (LKCF), and stratified nature of the pore fluid.

Figure 2 Burial history curve for the Magnus Sandstone Member. Isotopic temperature estimates and K/Ar age dating of illite constrain timing of cementation.

Figure 3 Cathodoluminescence photomicrograph shows obvious distinction between light grey luminescing detrital quartz grain (dq) and dark overgrowth (og) in a sample from the main reservoir sandstone at 3218.0m, 211/12a-9. Photo by Anton Kearsley, using an Oxford Instruments Cathode Luminescence SEM detector.

Figure 4 (a-e): Mean and standard deviation (vertical bar) results of oxygen isotope analyses of the major diagenetic mineral phases plotted against mineral formation temperature and pore water isotopic composition . Siderite curves are calculated from modal values. Each diagenetic mineral records the same isotopic trend : a higher proportion of isotopically "lighter" (less positive) meteoric-derived pore water updip in the crest near the early Cretaceous erosion surface and a higher proportion of "heavier" (more positive) marine-derived pore water downdip. Errors on replicate isotope analyses are typically ±0.2‰ in these samples. The error for quartz is compounded by potential point count errors giving ±0.5‰ overall.(f.) Hydrogen isotope (δD) results for both kaolinite and illite also record more negative results from crestal samples. (Note : Stable isotope ratios (R) are conventionally reported in the δ‰ notation relative to a standard, here SMOW, where $\delta‰ = (R_{sample}/R_{SMOW}-1)10^3$.

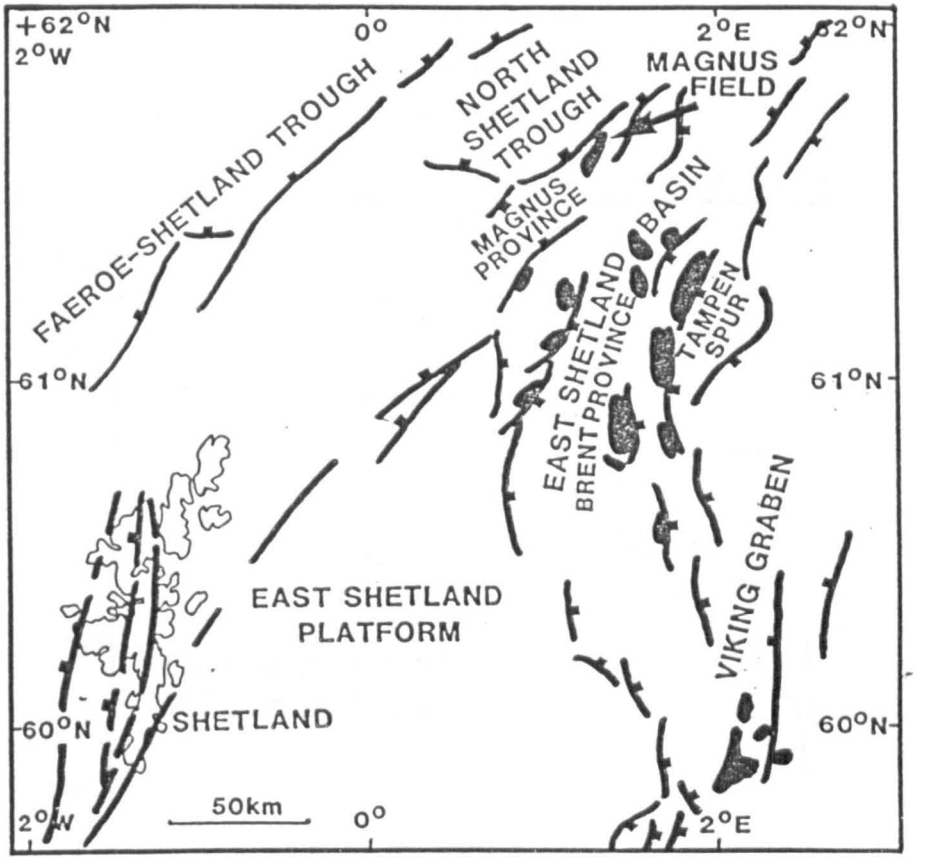

Figure 1a

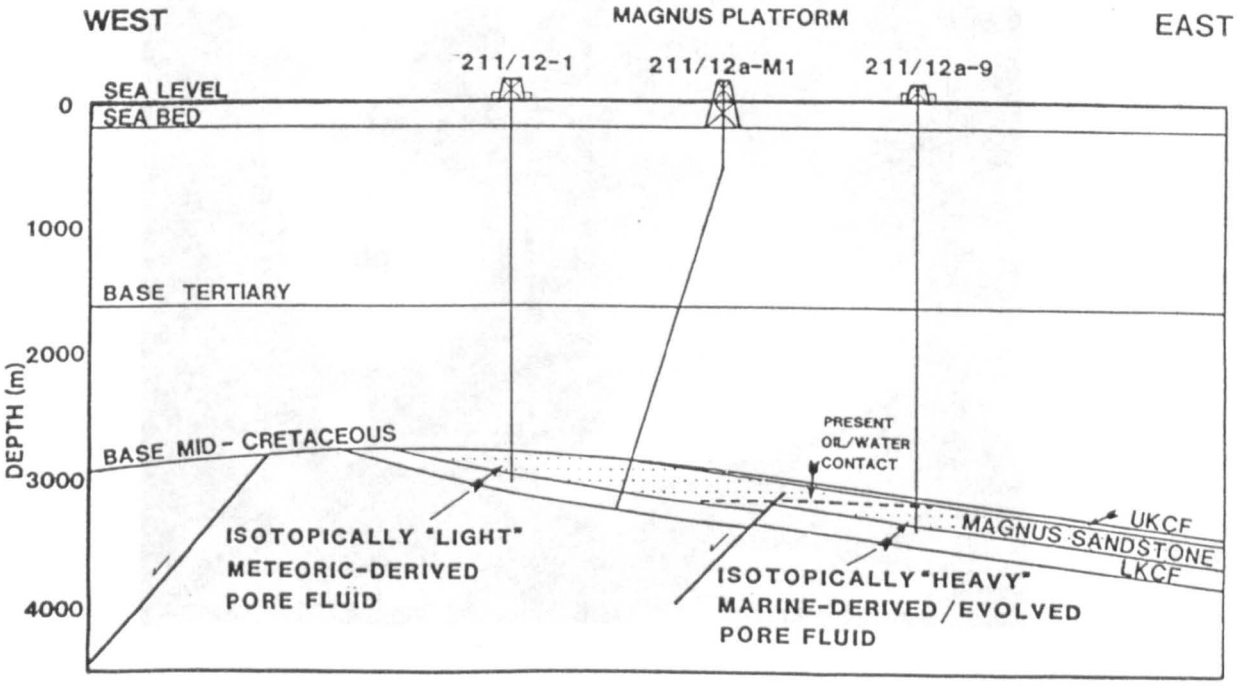

Figure 1b

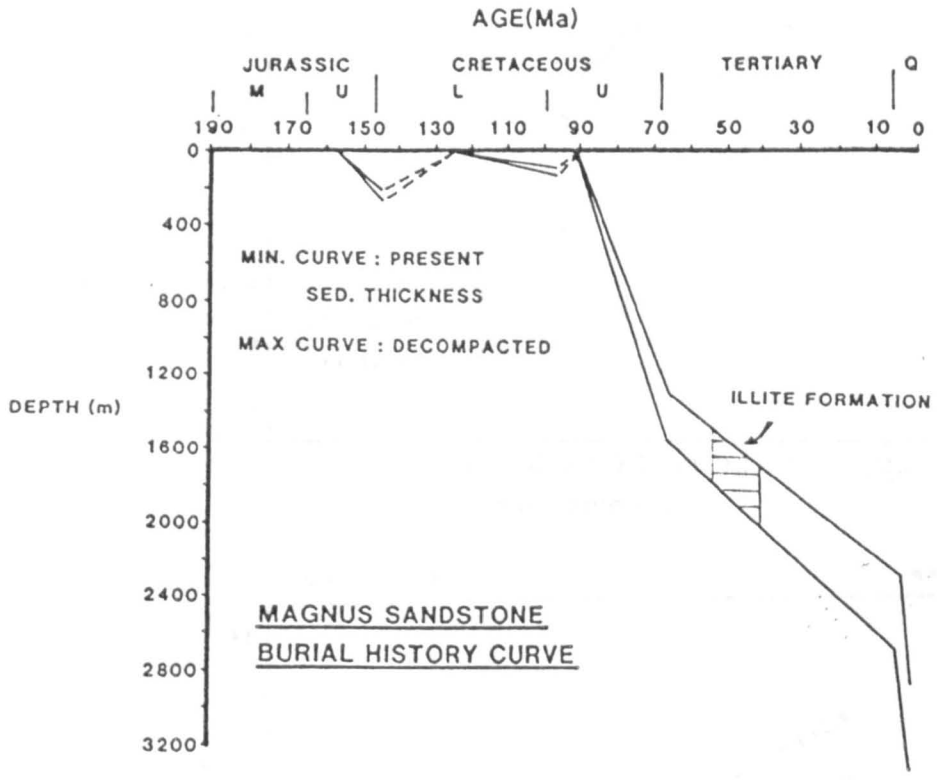

Figure 2

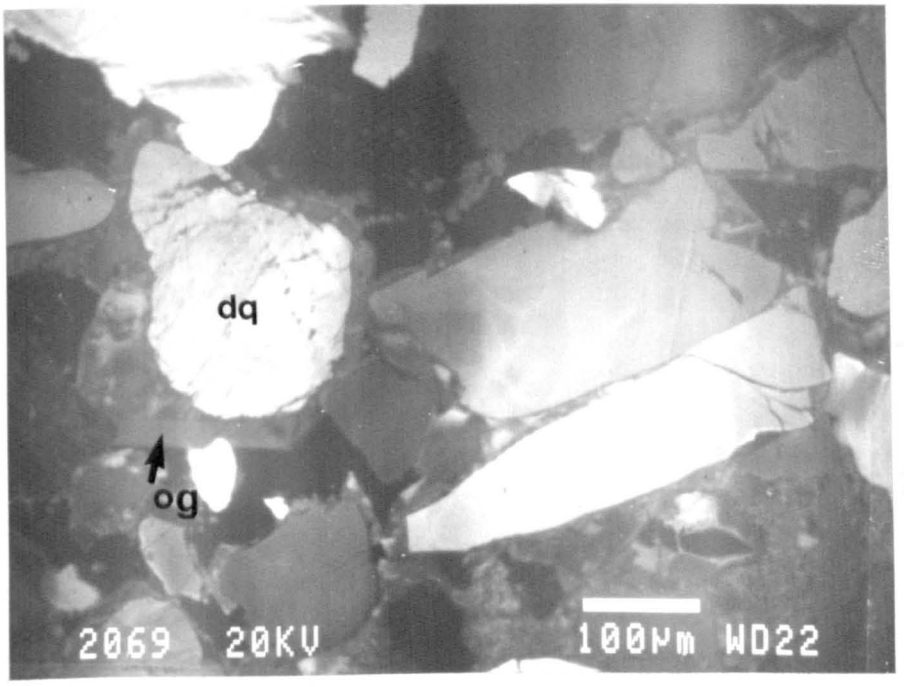

Figure 3

a.

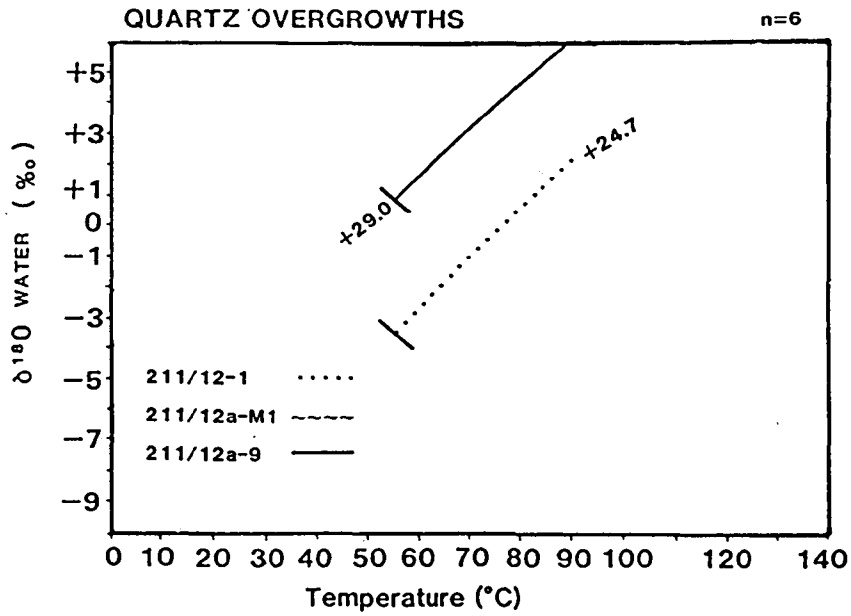
QUARTZ OVERGROWTHS
n=6
δ18O WATER (‰)
+5
+3
+1
0
−1
−3
−5
−7
−9
+29.0
+24.7
211/12-1
211/12a-M1
211/12a-9
0 10 20 30 40 50 60 70 80 90 100 120 140
Temperature (°C)

b.

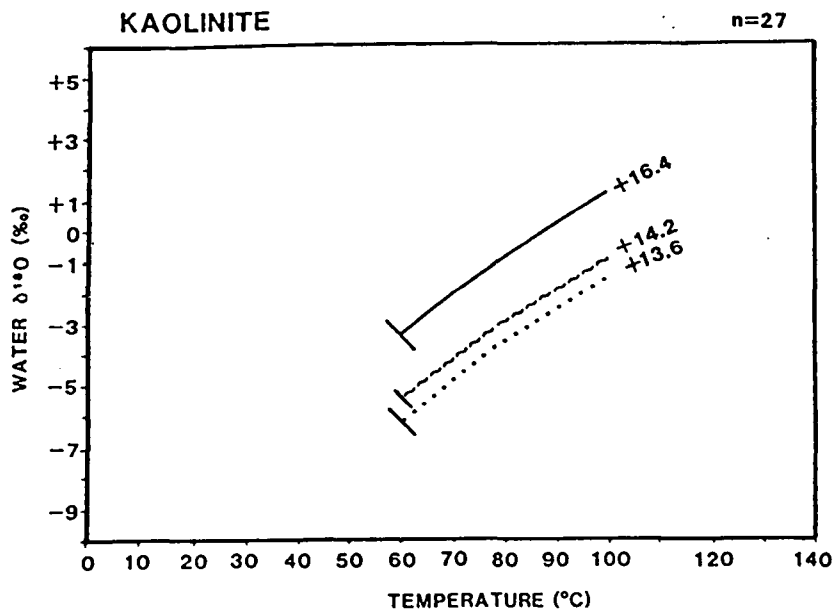
KAOLINITE
n=27
WATER δ18O (‰)
+5
+3
+1
0
−1
−3
−5
−7
−9
+16.4
+14.2
+13.6
0 10 20 30 40 50 60 70 80 90 100 120 140
TEMPERATURE (°C)

c.

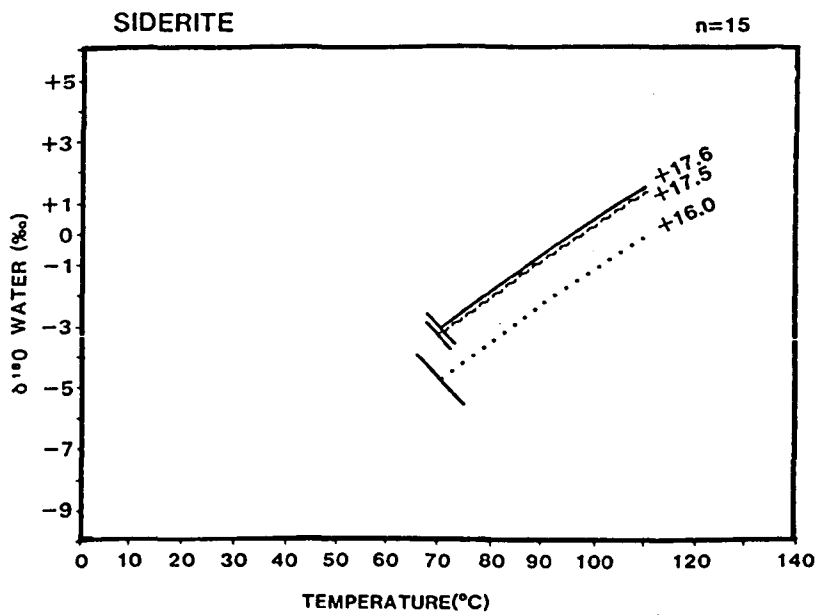
SIDERITE
n=15
δ18O WATER (‰)
+5
+3
+1
0
−1
−3
−5
−7
−9
+17.6
+17.5
+16.0
0 10 20 30 40 50 60 70 80 90 100 120 140
TEMPERATURE(°C)

Figure 4

d.

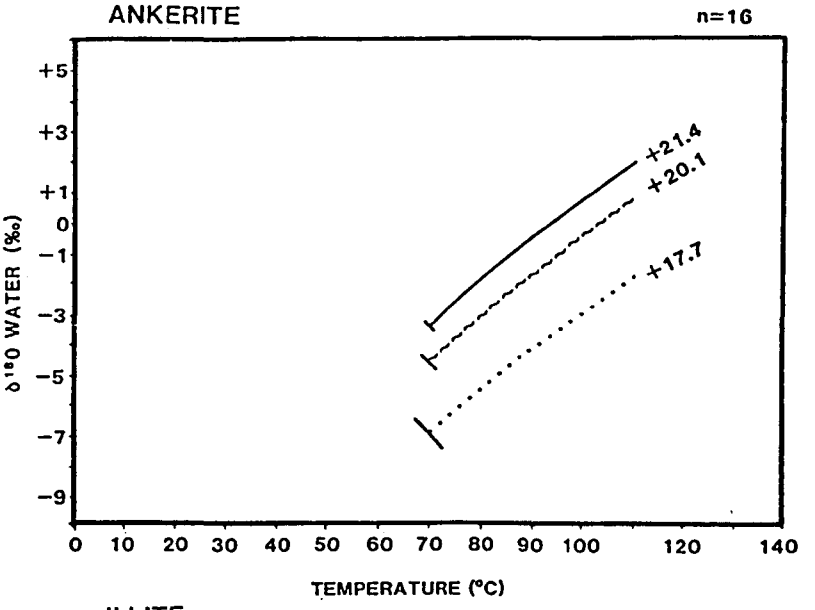

e.

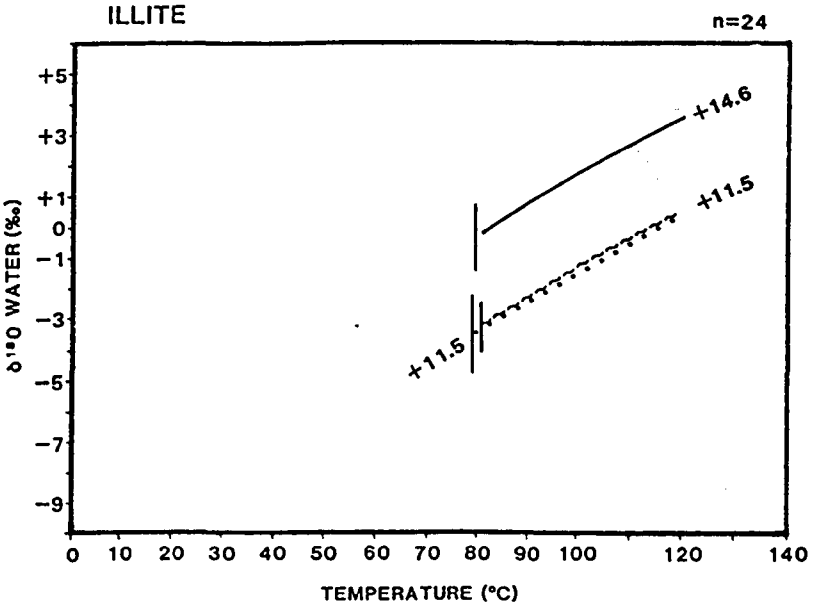

Figure 4 continued

f.

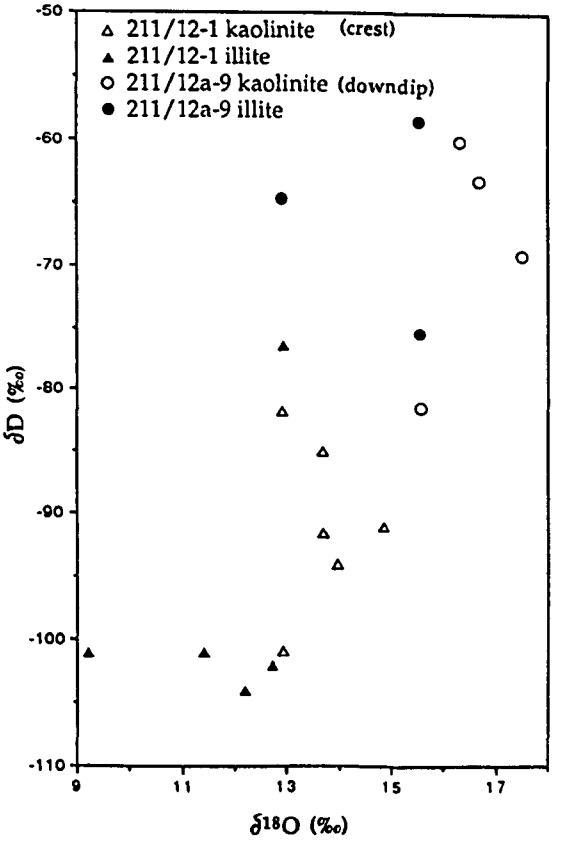

CHAPTER 3

DISTRIBUTION, CHEMISTRY, ISOTOPIC COMPOSITION AND ORIGIN OF DIAGENETIC CARBONATES : MAGNUS SANDSTONE, NORTH SEA.

C.I.Macaulay*, R.S.Haszeldine*, & A.E.Fallick^.

* Department of Geology and Applied Geology,
University of Glasgow, Glasgow G12 8QQ, Scotland.
^ Scottish Universities Research and Reactor Centre,
East Kilbride, Glasgow G75 0QU, Scotland.

3.1 ABSTRACT

The distribution of diagenetic carbonates in the Upper Jurassic marine turbidite Magnus Sandstone is controlled by original depositional facies and by detrital mineralogy. Diagenetic early calcite occurs as very rare discrete rhombic grains. Diagenetically late (post quartz overgrowth and kaolinite) magnesian siderites have developed throughout the reservoir sandstone and are commonly intimately associated with decomposed detrital biotite grains. Poikilotopic ankerite cement postdates calcite and siderite and occurs only adjacent to mudstone beds and in thin sandstones within mudstone beds.

The common association of siderites with decomposed detrital biotites indicates that Fe and Mg for siderite growth were transported only short distances and that siderite grew in a localised, more alkaline chemical field caused by biotite breakdown . Compositional zonations are commonly observed in backscatter electron images of magnesian siderites and reflect fluctuations during the chemical evolution of the pore water. All magnesian siderites show the same trend of evolution from relatively magnesian compositions to more ferroan then back to more magnesian. However, differences in the absolute Mg and Fe abundances in magnesian siderites in different wells reflect differences in pore water chemistry between wells. The deepest siderites are most magnesian, and developed in pore fluid with a larger component of marine-derived/evolved water, whereas the siderites from the crest of the field, beneath the Mid-Cretaceous unconformity, are most ferroan, and developed in pore fluid with a higher proportion of meteoric-derived water. This implies distinct, stratified, fluids during diagenesis. Ankerite developed due to release of Mg, Fe, Ca and HCO_3^- ions from mudstones into adjacent sandstones following dissolution of detrital minerals, probably by organic acids.

Both siderite and ankerite record more negative $\delta^{18}O$ values at the crest of the oilfield than downdip, reflecting the retention during burial diagenesis of a higher component of meteoric water in the crest of the field below the Lower to Mid-Cretaceous unconformity than downdip. Diagenetic porefluid contained a higher component of marine-derived porewater downdip.

3.2 INTRODUCTION

The Magnus oilfield lies 160km northeast of the Shetland Islands in the Magnus Province of the East Shetland Basin, UK northern North Sea (Figure 1a). Part of an Upper Jurassic submarine fan system, the reservoir consists of mid-fan feldspathic turbidite sandstones, named the Magnus Sandstone Member (De'Ath and Schuyleman, 1981), within the Kimmeridge Clay Formation (KCF). The KCF mudstones act as source rocks for the reservoir and are divided into Upper and Lower formations wherever the Magnus Sandstone Member is present . Located on the south-eastward dipping flank of an early Cretaceous fault block, the eastward downdip limit of the oilfield is defined by the oil/water contact and the western margin by depositional pinch-out to the north and south but by sub-Cretaceous erosional unconformity in the central crestal region (Figure 1b,c).

Grainsize decreases downdip to the east, as also does the sandstone/shale ratio (Rainey, 1987), indicating a westerly sediment source. Average reservoir sandstone porosity is 22%, with a range of permeabilities from 50-1000mD (Rainey, 1987). Major controls on porosity and permeability are structural depth and resultant compaction, distance from source and grain size, diagenetic secondary porosity development and cementation.

Burial beneath a thick "layer-cake" mudstone and marl stratigraphy from the mid-Cretaceous resulted in compaction, detrital mineral dissolution and diagenetic mineral precipitation as the Magnus sediments sought chemical equilibrium in response to increased burial stress, temperature and organic maturation. The generalised paragenetic sequence for the Magnus Sandstone, shown in Figure 2, is dominated by the alteration and dissolution of detrital micas and feldspar and the development of quartz overgrowths, kaolinite, magnesian siderite, ankerite and illite. Growth of these diagenetic minerals has reduced reservoir quality.

The turbiditic sub-arkosic Magnus sandstones are interbedded with, and enclosed by, organic-rich Kimmeridge Clay Formation mudstones. These were subaerially exposed and eroded during two periods of structural uplift and tilting at base- and mid-Cretaceous times, during which meteoric water was inferred to have penetrated the Magnus Sandstone (De'Ath and Schuyleman, 1981). Oxygen isotopic studies of the major diagenetic silicate

and carbonate minerals have confirmed meteoric water penetration (Macaulay et al., Chapter 2). These indicate that, during burial from the mid-Cretaceous until reservoir filling, porewaters across the field remained isotopically stratified - with a higher component of meteoric-derived porewater at the crest of the field than downdip.

3.3 ANALYTICAL METHODS

3.3.1 Carbonate petrography and composition

Thirty three samples of the Magnus Sandstone from wells 211/12-1, 211/12a-M1 and 211/12a-9, and two samples each from 211/12-3A and 211/12-6, were studied (Figure 1b,c). An impregnated part-polished thin section of each sample was petrographically examined and point counted (500 counts) for grain size and composition. The number of carbonate phases present was verified by X-ray diffraction. Thin sections were examined using Technosyn Mark 1 cold cathode luminescence microscopy. Textures were examined by scanning electron microscopy, energy-dispersive X-ray detection (SEM-EDX) and back-scatter electron imaging. Carbonate compositional data were obtained by electron microprobe analyses of fully polished thin sections, and results were normalised to 100mol% Fe+Mn, Mg and Ca.

3.3.2 Isotopic analyses

Samples for isotopic analysis were disaggregated and sieved and the 160-250μm size fraction selected for heavy liquid (1,1,2,2 tetrabromoethane) separation of carbonate grains from silicates. Purified carbonate samples were passed through a magnetic separator to isolate ferroan dolomite/ankerite from siderite, and sample purities were checked by XRD. Pure mineral separates were plasma ashed in oxygen to destroy any organic matter. CO_2 gas was produced from calcite for isotopic analysis by overnight reaction with 100% phosphoric acid at 25°C (McCrea, 1950) and corrected using standard procedures (Craig, 1957). Ferroan dolomite/ankerite underwent reaction for 5 days at 25°C (Land, 1980). Aliquots of ankerite samples were also reacted at 100°C and relevant fractionation factors applied (Rosenbaum and Sheppard, 1986) but no significant differences in carbon or

oxygen isotope composition of the carbonates were observed. Siderite was reacted with phosphoric acid at 100°C for 1 hour (Rosenbaum and Sheppard, 1986). Oxygen isotope fractionation factors

$$\alpha = \frac{(^{18}O/^{16}O)_{CO_2}}{(^{18}O/^{16}O)_{carb.}}$$

used were : calcite a= 1.01025 (Longstaffe and Ayalon, 1987), siderite α = 1.00881 (Rosenbaum and Sheppard 1986) and ankerite α = 1.01169 (Land, 1980). Oxygen and carbon isotope data are presented in the standard δ‰-notation relative to the PDB standard for carbon (Craig 1957) and both the PDB and SMOW standard for oxygen (Craig, 1961).

3.4 CARBONATE PETROLOGY

3.4.1 Calcite

Only a few grains of calcite were observed in sandstone from the wells studied ; three in 211/12a-M1 and one in 211/12a-9. Calcite occurs as discrete individual grains 50-200μm across. The only constraint observed on the timing of calcite development in the diagenetic sequence is that it predates ankerite (Figure 3).

3.4.2 Magnesian siderite

Magnesian siderite comprises discrete individual rhombs and clusters of rhombs 100-200μm in length infilling pore space. Also, aggregates of small siderite rhombs 10-30 μm in length replace detrital biotite grains and mud clasts (Figure 4a,b,c). Biotite-replacing magnesian siderite commonly occurs with associated cubic and/or octahedral pyrite. This has been reported in many Jurassic Brent Group North Sea oilfield sandstones (Bjorlykke and Brensdal, 1986 ; Brint , 1989). Magnesian siderite has developed in both primary intergranular porosity (Figure 4a) and secondary feldspar dissolution porosity (Figure 5a), and often replaces pore-filling kaolinite which was the product of feldspar dissolution (Figure 5b). Note also in Figure 5b that kaolinite post-dates the growth of diagenetic quartz overgrowths. Thus, siderite growth is constrained petrographically by earlier

feldspar dissolution, quartz overgrowth and kaolinite development and by later ankerite development (Figure 5c).
Magnesian siderite exhibited no cathodoluminescence due to quenching resulting from its high Fe+Mn content (Sommer, 1972, Pierson, 1981), but useful textural and compositional information was gathered using backscattered electron imaging (see section on microprobe analyses).

3.4.3 Ankerite

These iron rich magnesian carbonates have dolomite-type composition $Ca(MgFe^{2+}Mn)(CO_3)_2$, the term ankerite being applicable when 20% or more of the Mg sites are filled by Fe^{2+} or Mn (Deer et al., 1966). Most of the carbonates of this type in the Magnus Sandstone were found to contain sufficient Fe^{2+} to be termed ankeritic in composition (Appendix 1). They occur as individual pore-filling crystals up to several hundred microns across and as poikilotopic cements (Figure 5c).These may completely fill the porosity of thin sandstones which are surrounded by mudstones (Figure 6).

3.5 CARBONATE DISTRIBUTION

3.5.1 Calcite

Calcite is not a common diagenetic mineral in the Magnus Sandstone. Only four grains were identified during this study, one from downdip well 211/12a-9 and three from intermediate well 211/12a-M1, although non-ferroan calcite concretions have been found in a recent core from a crestal well, 211/12a-M10 (D. Emery, BP, pers. comm. 1989). One reason for the scarcity of calcite may be restricted Ca supply : detrital shell material is very scarce in the Magnus sediments, leaving only original marine porewater and limited plagioclase as a source of Ca.

3.5.2 Magnesian siderite

Siderite abundance commonly varies between 0.5 to 3.0% as determined by point counting of thin sections (500 points per section), but may reach 8%. All thin sections studied contained some diagenetic siderite except for a sample at 3248.0m in 211.12a-9, which is a thin sandstone (40cm) within a thick mudstone (20m) (Figures 6 and 7). Siderite is frequently associated

with degraded detrital biotite and detrital mud clasts. It has also developed in proximity to partially dissolved detrital almandine (Fe rich) garnets, which are more abundant in crestal well 211/12-1 and can locally form up to 8% of the sandstone. Raised pH in proximity to degrading detrital micas is well documented as an important factor in allowing precipitation of diagenetic carbonate minerals (Boles and Johnson, 1983).

Thus siderite distribution is controlled primarily by redistribution, internal to the sandstone, of ions released by the breakdown of detrital ferromagnesian silicates, in common with many other North Sea oilfield sandstones (Bjorlykke and Brensdal, 1986, Brint , 1989).

3.5.3 Ankerite

Ankerite closely postdates siderite in the diagenetic sequence, but shows a distribution which indicates a different ion source. It is much more abundant close to mudstones (Figure 7), to the extent that thin sandstones within mudstones are completely cemented with ankerite to the exclusion of porosity (ankerite constituting 22% rock volume at 3248.0m in 211/12a-9). Within the main reservoir sandstone, ankerite has precipitated only within ~ 10m of thick mudstone units. No ankerite has been detected in sandstones more distant than this from mudstones. Immediately adjacent to mudstone margins ankerite may constitute from 2-3% to 8-9% of the sandstone.

This intimate association between ankerite cement and mudstones reflects Ca, Mg, Fe, Mn and HCO_3^- transfer from mudstones into sandstones (Evans, 1989) The 10m maximum distance from mudstones at which ankerite has developed probably reflects the distance beyond which relevant ion concentrations fell below that required for ankerite precipitation. Ion transfer may have occurred by both ion diffusion and advection during compactional fluid loss from mudstones.

Unlike siderite, ankerite does not show any obvious nucleation relationship with detrital minerals, except occasionally with almandine garnet. In the Magnus Sandstone, almandine garnet commonly displays preferential etching textures along rhombic crystal faces. Ankerite development post-dates this rhombic etching (Figure 8). Hansley (1987) noted the same effect in Upper Jurassic marine sandstones from the Morrison Formation, New

Mexico, and attributed this particular style of etching to the action of organic acids. This explanation is also applicable to the organic-rich Magnus sediments. Examples have been observed in backscatter images where ankerite forms euhedral overgrowths on these etched rhombic garnet faces. Garnet dissolution may have contributed to Fe supply for ankerite development.

3.6 CARBONATE MICROPROBE ANALYSES

3.6.1 Calcite

Calcite is rare , but slightly more (still <<1%) was observed in intermediate well 211/12a-M1 than in downdip well 211/12a-9, but none was detected in crestal well 211/12-1. In 211/12a-M1 calcite compositions range from 99.9 mol % Ca, with only 0.1 mol % Mg and no detectable Fe+Mn, to 99.2 mol % Ca, 0.8 mol % Mg and no Fe+Mn, to 99.94 mol % Ca, 0.02 mol % Mg and 0.04 mol % Fe + Mn. Calcite (one grain) downdip in 211/12a-9 had a composition of Ca 99.93 mol % and 0.07 mol % Fe + Mn (Table 1)

WELL	Fe+Mn	Mg	Ca
211/12a-M1	0-0.04	0.1-0.8	99.2-99.9
211/12a-9	0.07	0	99.93

Table 1 : Calcite compositional data (mol %)

3.6.2 Magnesian siderite

Magnesian siderites are late diagenetic carbonates in the Magnus Sandstone. They postdate development of secondary dissolution porosity in feldspar and the resultant pore-filling kaolinite (Figure 5a). Siderites predate ankerite cement precipitation (Figure 5c). Siderites from the Magnus Sandstone fall in the compositional fields of sideroplesite (5-30 mol% $MgCO_3$), pistomesite (30-50 mol% $MgCO_3$) and breunnerite (5-50 mol% $FeCO_3$) (Deer at al, 1966). Commonly, compositional zonations are observed in individual magnesian siderite grains in back-scattered electron images (Figure 4a). Two and three-zoned rhombs are observed. Comparison of backscatter and scanning electron images precludes topographic variations in siderite surfaces in

polished sections being the cause of zonations : grain topography and zone boundaries are not coincident.

In crestal well 211/12-1 rhomb compositions fall in the more ferroan sideroplesite/pistomesite fields whereas downdip in 211/12a-9 compositions fall within the fields of pistomesite and breunnerite (Figure 9). The analyses from 211/12a-M1 lie in the same fields as the 211/12a-9 rhombs.

Updip in well 211/12-1 the composition of the central zone in three-zoned magnesian siderites ranges from Fe + Mn 64-70 mol %, Mg 30-36 mol % and Ca 1-5 mol %. Downdip in 211/12a-9 central zone compositions range from Fe + Mn 38-64 mol %, Mg 37-62 mol % and Ca 1-20 mol % (Table 2).
The compositional field of the middle zones of three-zoned rhombs coincides with the inner zone of two-zoned rhombs. Often the inner zones of three-zoned rhombs have ragged edges, suggesting that dissolution of the original inner zone occurred before precipitation of the middle zone. This dissolution may have continued to near completion in two-zoned rhombs, or alternatively, nucleation of two-zoned rhombs may have occurred independent of remnant inner zones.

The compositional range of the middle zones of three-zoned rhombs/inner zones of two-zoned rhombs is Fe + Mn 75-87 mol % in 211/12-1 and Fe + Mn 65-82 mol % in 211/12a-9. Mg ranges from 37-41 mol % in 211/12-1 and 18-25 mol % in 211/12a-9. Ca ranges from 1-8 mol % in 211/12-1 and from 0.5-20 mol % in 211/12a-9.

Outer zone compositional ranges in 211/12-1 for both 2 and 3 zoned rhombs are Fe + Mn 59-63 mol %, Mg 37-41 mol % and Ca 2-6 mol %. The compositions of outer zones in 211/12a-9 are split into two distinct groups with no apparent relationship between compositional variation and the number of zones. Both compositional groups have similar Ca ranges of between 2-9 mol %. One group has relatively high Fe + Mn of 52-58 mol % and Mg of 42-48 Mol % , a composition similar to the inner zone of three zoned rhombs. The other group is considerably more magnesian with Fe + Mn ranges of 28-34 mol % and Mg of 66-72 mol %.

	Well	Fe+Mn	Mg	Ca
Centre zone :	211/12-1	64-70	30-36	1-5
3-zoned siderites	211/12a-9	38-64	37-62	1-20
Inner zone of 2-zoned/	211/12-1	75-87	37-41	1-8
middle zone of 3-zoned	211/12a-9	65-82	18-25	0.5-20
Outer zone (both types)	211/12-1	59-63	37-41	2-6
	211/12a-9	52-58	42-48	2-6
	211/12a-9	28-34	66-72	2-9

Table 2 : Siderite zone compositional data (mol %) from updip well 211/12-1 and downdip well 211/12a-9 (Appendix 1).

Figure 10a, b and c shows how magnesian siderite compositions evolved through time as the zones formed. This siderite compositional evolution reflects pore water chemistry evolution, on both a very localised scale and a fieldwide scale. In all three wells the earliest formed siderite, represented by the inner zone of 3 zoned siderites, was relatively Mg rich. Pore waters then became more Fe rich as recorded by the middle zone of 3 zoned siderites and the inner zone of 2 zoned siderites, before becoming more magnesian again during outer zone precipitation. Ca concentrations remained roughly constant during siderite precipitation. In general, magnesian siderite is more ferroan in the crestal of the field and more magnesian downdip, so that although siderites show the same sense of compositional evolution fieldwide, abundances of Mg and Fe change from the crest downdip. This probably reflects the higher proportion of Mg-rich marine-derived porewater downdip and the higher proportion of relatively Fe-rich and Mg-poor meteoric-derived water in the crest (Rainey, 1987).

3.6.3 Ankerite.

Figure 11 shows a plot of ankerite compositional data for the three wells studied. Obvious differences between wells are apparent.

WELL	Fe+Mn	Mg	Ca
211/12-1	10-25	17-27	56-67
211/12a-M1	4 -12	30-38	55-62
211/12a-9	7 -17	33-43	42-52

Table 3 : Ankerite compositional data (mol %)

Ankerites in crestal well 211/12-1 are more Fe rich whereas those downdip in 211/12a-9 are less ferroan and more magnesian, with intermediate well 211/12a-M1 recording intermediate compositions (Table 3). When the data of Rainey (1987) are included on Figure 11 the compositional fields of ankerite from 211/12a-M1 and 211/12a-9 overlap. These compositional variations record porewater chemical variations at the time of ankerite precipitation. Again, more Fe in crestal porewaters and more Mg downdip might feasibly be explained by a higher proportion of meteoric-derived water near the crestal erosion surface (Rainey 1987, Macaulay et al, Chapter 2) and a higher proportion of marine-derived porewater downdip, distant from the erosion surface.

Excess Ca is also notable in ankerites, especially in wells 211/12-1 and 211/12a-M1. Although not observed in the few calcite grains studied, this may represent replacement of calcite by ankerite (Deer et al., 1962, Boles, 1978, Kantorowicz, 1985) or structural effects such as periodic structural modulation (Reeder, 1983).

Backscatter electron images of ankerite show subtle sector, concentric and banded zonations in all wells. These reflect very minor compositional differences (Figure 8).

3.7 Discussion and conclusions from compositional data

Calcite composition data are too few to allow significant cross-field comparison. Siderite and ankerite both show similar compositional trends, but no uniformity of composition, across the oilfield. This contrasts with the compositional uniformity of diagenetic carbonates across the Brent Group sandstones (Brint , 1989) which were precipitated by large-scale flow of pore-fluid. Hence, the compositional data suggest that diagenetic carbonates

developed in a static pore-fluid regime in the Magnus Sandstone. Higher proportions of marine-derived porewater downdip and meteoric-derived porewater at the crest of the field resulted in siderite and ankerite compositions being more magnesian downdip and more ferroan updip.

3.8 CARBONATE ISOTOPE ANALYSES

3.8.1 Calcite

In the wells studied, calcite is not present in sufficient quantities for separation and isotopic analysis. However, advanced technologies such as laser isotopic analysis and ion microprobe analysis should enable isotopic analysis of individual carbonate grains in the future.

3.8.2 Magnesian siderite

As descibed previously, magnesian siderite rhombs commonly exhibit 2 or 3 growth zones in back scatter electron microscopy. These different zones reflect compositional changes resulting from fluctuating porewater chemistry during siderite precipitation. It is possible, therefore, that fluctuations in the isotopic composition of the pore fluid also occurred during siderite precipitation. In this study quoted isotopic ratios for magnesian siderites are bulk values because the analytical procedure for carbonates involves complete reaction of whole grains with acid.

3.8.2.1 Strontium ($^{87}Sr/^{86}Sr$) isotope results and interpretation

Magnesian siderite $^{87}Sr/^{86}Sr$ ratios were measured for two pure samples from 211/12a-9 and gave initial results of 0.7126 and 0.7127 (3206.0m, 3355.3m). These highly radiogenic results reflect supply of radiogenic strontium from the decomposition of detrital biotite grains with which siderite is commonly associated (Faure, 1986, Brint et al, 1989)

3.8.2.2 Carbon ($\delta^{13}C$) and sulphur ($\delta^{34}S$) isotope results and interpretation

The overall spread in $\delta^{13}C$ results from wells 211/12-1, 211/12a-M1 and 211/12a-9 is from -8.0 to -14.6‰PDB (Figure 12a) (Table 4). Within individual wells ranges are : 211/12-1 -8.0 to -14.1‰ ($x = -10.7 \pm 2.4$ (1σ)), 211/12a-M1 -8.9 to -11.1‰ ($x = -9.7 \pm 0.8$) and 211/12a-9 -8.8 to -14.6‰ ($x = -11.6 \pm 2.1$). No statistically meaningful separation in $\delta^{13}C$ ratios between wells is evident, suggesting that the CO_2 source for siderite development was not dissimilar in all three wells.

Several sources have been recognised of dissolved bicarbonate in porewaters for carbonate precipitation during burial diagenesis (Irwin et al, 1977, Curtis and Coleman, 1986). Marine reservoir bicarbonate, with $\delta^{13}C \sim 0$‰, can be determined by isotopic analysis of shell material which grew contemporaneously with sedimentation. In this study only one such sample of shell debris was found, at 3119.9m. in 211/12a-9, and its $\delta^{13}C$ was measured as + 1.4‰ ($\delta^{18}O$ 0.5‰PDB, +31.4‰SMOW). This suggests fully marine depositional water in terms of isotopes, and therefore implies marine salinity and cation content. The shell has *not* recrystallised. Brint et al (1989) showed that locally dissolved shell fragments can be an important source of bicarbonate for precipitation of new carbonate minerals. However, the scarcity of detrital shell material, or evidence for its previous existence, in the Magnus Sandstone for the wells studied suggests that dissolution and reprecipitation of shell material was not an important source of bicarbonate. Of course, the original marine depositional water would have contained significant dissolved bicarbonate. Other sources of CO_2 for bicarbonate production are related to the modification of organic material incorporated in the sediment. These are, with increasing burial depth : aerobic oxidation ($\delta^{13}C$ -25‰), bacterial sulphate reduction ($\delta^{13}C$ -25‰), bacterial

WELL	DEPTH (m)	$\delta^{13}C$	$\delta^{18}Opdb$	$\delta^{18}Osmow$
211/12-1	2963.4	-9.2	-15.0	15.2
211/12-1	2975.4	-11.8	-13.8	16.4
211/12-1	2976.6	-10.2	-13.5	16.7
211/12-1	2978.6	-14.1	-16.6	13.6
211/12-1	2983.7	-8.0	-12.0	18.2
211/12a-M1	3030.2	-9.4	-12.0	18.3
211/12a-M1	3030.4	-9.0	-14.0	16.2
211/12a-M1	3042.8	-11.1	-12.8	17.4
211/12a-M1	3059.8	-9.7	-12.5	17.7
211/12a-M1	3064.0	-9.4	-11.8	18.4
211/12a-9	3184.5	-14.6	-16.0	14.1
211/12a-9	3240.0	-11.9	-11.6	18.6
211/12a-9	3262.7	-11.7	-13.5	16.7
211/12a-9	3355.3	-8.8	-12.8	17.4

Table 4 : Mangesian siderite carbon and oxygen isotopic data (‰).

fermentation ($\delta^{13}C$ +15‰) and thermally-induced abiotic decarboxylation ($\delta^{13}C$ -10 to -15‰) (Figure 12b).

The timing of magnesian siderite growth can be estimated texturally, isotopically and by indirect age dates. Spatially, magnesian siderite often occurs not with early framboidal pyrite but beside cubic and octahedral pyrite (Figures 4b,c). Petrographic relationships suggest that they grew at similar times. The pyrite $\delta^{34}S$ analyses (Table 5 and Figure 13) show this late cubic pyrite to have relatively high $\delta^{34}S$ (approaching that of Jurassic seawater sulphate). Presumably it formed in a system closed to sulphur replenishment, and not in a shallow sulphate reduction zone. In the presence of pyrite, siderite growth through bicarbonate supply from organic matter degradation by sulphate reduction is indicated ($\delta^{13}C$ -25‰), whereas

without pyrite, bicarbonate supply by iron reduction of organic matter is more likely ($\delta^{13}C$ -25‰) (Curtis and Coleman, 1986).

WELL	DEPTH (m)	$\delta^{34}S$	MORPHOLOGY
211/12a-9	3184.5	4.4	mixture
211/12a-9	3206.0	-13.0	framboidal
211/12a-9	3240.0	7.8	cubic>framboidal
211/12a-9	3248.0	15.7	cubic
211/12a-9	3262.7	-0.3	mixture
211/12a-9	3313.3	-8.7	framboidal
211/12a-9	3355.3	-1.2	mixture

Table 5 : Pyrite $\delta^{34}S$ (‰) data - 211/12a-9

Dating of illite , the last diagenetic mineral to form, in well 211/12a-9 by the K/Ar method shows diagenesis ceased at 55-41 Ma (Macaulay et al., Chapter 2) (Figure 14). This gives a maximum depth of burial at the time of illite growth of approximately 1.6-2 km. Siderite postdates quartz overgrowth and kaolinite development, but predates illite and has $\delta^{18}O$ values indicative of growth in warm (~ 90°C) water. Therefore siderite probably grew at around 1.5km burial depth.

The source of CO_2 for siderite growth could simplistically represent a mixture of CO_2 from primary marine bicarbonate ($\delta^{13}C$ 0‰), bacterial fermentation of organic matter ($\delta^{13}C$ +15‰) and abiotic thermal decarboxylation of organic matter ($\delta^{13}C$ -10 to -25‰). However, gradual thermal degradation of organic matter results in carbon isotope fractionation as CO_2 is liberated. Isotopically light carbon is preferentially incorporated into CO_2 as heavy carbon is retained in the organic parent. This process begins at about 80°C, which is close to the temperature at which siderite is interpreted to have formed. Observed siderite $\delta^{13}C$ values between -8 to -14 ‰PDB may not therefore be simply a mixture of end-member CO_2 sources, but the heterogenous result of an ongoing thermally induced organic degradation and related C-isotope fractionation process. In their study of oilfield formation waters, Carothers and Kharaka (1979) found highly variable $\delta^{13}C$ values for HCO_3^- at temperatures between 80 and 100°C. This is also around the same temperature at which organic acids are generated in volume (Surdam et al., 1984, Crossey et al.,1986). In summary, siderite was a late burial cement, forming at about 1.5 km in a semi-closed

isotope system. Intergrowth with cubic pyrite indicates bicarbonate supply from organic matter degradation perhaps accompanying sulphate reduction. Sulphate-reducing bacteria cannot survive temperatures as high as the 90°C inferred for diagenetic siderite, which is intergrown with late cubic pyrite. Krouse et al (1988), however, leave open the possibility that sulphate reduction can occur in the presence of hydrocarbons at temperatures as low as, perhaps, 90°C. The measured $\delta^{13}C$ values for Magnus Sandstone magnesian siderites record a significant contribution from CO_2 derived from maturation of organic matter.

3.8.2.3 Oxygen ($\delta^{18}O$) isotope results and interpretation

Separate groups of siderite $\delta^{18}O$ values are distinguishable among the three wells studied (Figure 15a, b). Crestal well 211/12-1 siderites record the most negative range of values, whereas downdip well 211/12a-9 records the least negative (Table 4). In 211/12-1 $\delta^{18}O$ ranges from -16.6 to -12.0‰PDB (+13.6 to 18.2‰SMOW, x= +16.0‰ ± 1.7(1σ) or +16.6 if the one very negative value of -16.6‰ is excluded), in 211/12a-M1 from -14.0 to -11.8‰PDB (+16.2 to 18.4‰SMOW, x= +17.5‰ ± 0.9) and in 211/12a-9 from -16.0 to -11.6‰PDB (+14.1 to 18.6‰SMOW, x= +16.9‰±1.7 if the one very negative value of 14.1‰ is included or +17.6‰ ±0.8 if it is excluded).

Petrographic observations indicate that across the field siderite grew at the same stage of the paragenetic sequence. If siderite had formed from detrital biotite breakdown in a pore fluid which was isotopically homogenous throughout the Magnus Sandstone, then measured siderite $\delta^{18}O$ values would imply that the crestal (more negative $\delta^{18}O$) siderites formed at higher temperature than those downdip. There is no geologic evidence in favour of this scenario. It is most plausible that siderite development was controlled by biotite degradation. Therefore crestal siderites must have grown in a pore fluid with $\delta^{18}O$ 2-3‰ more negative than that downdip (for wider discussion see Macaulay et al., Chapter 2).

Using the range in mean siderite $\delta^{18}O$ values between wells (Figure 15b), a siderite formation temperature of 84 -98°C is implied were the pore fluid wholly unevolved marine-derived water with $\delta^{18}O$ of -1.2‰, or 44-55°C were the pore fluid wholly unevolved meteoric-derived water with $\delta^{18}O$ of -7‰. Also, compactional mudstone dewatering would input evolved

marine depositional water to the sandstone ($\delta^{18}O$ -1‰ or more positive). In reality the pore fluid was probably an isotopically and chemically evolved mixture of marine and meteoric-derived waters, with a greater component of meteoric-derived water towards the crestal Mid-Cretaceous unconformity (Figure 1c) and a greater component of depositional marine-derived pore fluid downdip. Considering the burial and diagenetic history of the Magnus Sandstone (illite K/Ar date =55Ma from the oil reservoir (Figure 14) - see Chapter 2) and the progressive evolution of pore fluid $\delta^{18}O$ toward heavier ratios through water/rock interaction, siderite most likely grew in the higher temperature bracket discussed above (i.e. 84 - 98°C).

The apparent overlap of values from 211/12a-9 with the other wells is the result of one very negative result of 14.1‰SMOW. The modal $\delta^{18}O$ value for downdip 211/12a-9 siderites is less negative than 211/12a-M1 values. Kantorowicz (1982) recorded a diagenetically-late siderite $\delta^{18}O$ data set from the Ninian oilfield comparable to that from 211/12a-9, with one similarly low value at +14‰SMOW, which may represent local higher temperature siderite development on the flank.

3.8.3 Ankerite

In backscatter electron images ankerite displays various types of zonation which implies that, like siderite, ankerite isotope results reflect a mineral separate bulk value for each particular sample depth.

3.8.3.1 Strontium ($^{87}Sr/^{86}Sr$) isotope results and interpretation

Ankerite $^{87}Sr/^{86}Sr$ was measured from one pure sample in 211/12a-9 (3206.0m) and gave an initial strontium result of 0.7103, a lower ratio than that measured for siderite. This again reflects incorporation of radiogenic strontium released from detrital mineral dissolution (Faure, 1986, Brint et al, 1989), but radiogenic strontium ratios in the Magnus Sandstone were probably diluted by mixing of water released from mudstones with sandstone porewater in the 10m zone, around mudstones, in which ankerite developed.

3.8.3.2 Carbon ($\delta^{13}C$) isotope results and interpretation

Ankerite $\delta^{13}C$ across the oilfield ranges from -7.7 to -13.6‰PDB (Table 6), a range similar to, but slightly more negative than that exhibited by siderite. Ranges within individual wells are as follows : 211/12-1 -10.6 to -13.6‰ (x = -12.1 ± 1.5 (1σ)), 211/12a-M1 -9.5 to -12.8‰ (x = -10.7 ±1.1) and 211/12a-9 -7.7 to -13.4‰ (x= -10.9 ±2.4) (Figure 16). As with siderite there is no significant difference in ankerite $\delta^{13}C$ values among the three wells. Two ankerite samples from 211/12-6 in the north of the Magnus field (Figure 1b) gave results of -6.7‰ and -6.1‰, and two samples from 211/12-3A in the south gave -10.1‰ and -9.9‰. Petrographic relationships show that ankerite cement post-dates magnesian siderite growth. This is in keeping with bicarbonate for siderite and ankerite development being sourced from similar progressive organic breakdown reactions or mixtures of marine, fermentation and decarboxylation CO_2, and also with ankerite having an overall more negative $\delta^{13}C$. Note that this negative carbon supply for siderite and ankerite texturally post-dates dissolution textures in feldspars and garnets, which are independently inferred to result from organic acids. It is also worthy of note that ankerite with the lowest measured $\delta^{13}C$ in this study of -13.4‰ is from ankerite cement in a thin sandstone (40cm) within a thick shale unit (20m) at 3248,0m in 211/12a-9 (Figure 7). Ankerite in this sandstone incorporated a higher proportion of organic decarboxylation-sourced CO_2 (-15‰) from the enclosing shales than the thicker sandstones.

3.8.3.3 Oxygen ($\delta^{18}O$) isotope results and interpretation

Ankerite $\delta^{18}O$ values from wells 211/12-1, 211/12a-M1 and 211/12a-9 form distinct separate groups (Figure 17 and Table 6). Results from 211/12-1 range from -11.8 to -13.8‰PDB (17.1 to 19.1‰SMOW,x=17.7 ± 1.2 (1σ)), from -9.7

WELL	DEPTH (m)	$\delta^{13}C$	$\delta^{18}Opdb$	$\delta^{18}Osmow$
211/12-1	2954.5	-10.6	-11.8	19.1
211/12-1	2971.4	-12.1	-13.5	17.1
211/12-1	2978.6	-13.6	-13.8	17.1
211/12a-M1	2936.6	-10.7	-11.2	19.4
211/12a-M1	2951.9	-12.8	-10.7	20.3
211/12a-M1	2952.1	-11.5	-9.7	20.4
211/12a-M1	2976.4	-10.4	-10.1	20.5
211/12a-M1	2976.6	-9.7	-10.3	20.3
211/12a-M1	2996.1	-10.8	-10.2	20.4
211/12a-M1	2996.2	-9.5	-10.2	20.5
211/12a-M1	3042.8	-9.3	-11.2	19.3
211/12a-M1	3064.0	-11.4	-11.3	19.2
211/12a-9	3206.0	-10.6	-9.0	21.3
211/12a-9	3248.0	-13.4	-8.7	21.6
211/12a-9	3249.2	-11.9	-8.9	21.4
211/12a-9	3355.3	-7.7	-9.3	20.9
211/12-3A	3069.9	-9.9	-7.6	23.1
211/12-3A	3074.6	-10.1	-7.8	22.8
211/12-6	3019.9	-6.7	-8.4	22.2
211/12-6	3081.1	-6.1	-8.2	22.4

Table 6 : Ankerite carbon and oxygen isotopic data (‰).

to -11.3‰PDB (19.2 to 20.5‰SMOW, x=20.1 ± 0.5) in 211/12a-M1 and from -8.7 to -9.3‰PDB (20.9 to 21.6‰SMOW, x=21.4 ± 0.3) in 211/12a-9. The samples from 211/12-6 gave values of -8.4 and -8.2‰PDB (22.2 and 22.4‰SMOW) and those from 211/12-3A -7.8 and -7.6‰PDB (22.8 and 23.1‰SMOW).

Following the same argument presented for the distinct groups of $\delta^{18}O$ values obtained for siderite, with lower values near the crestal erosion surface and higher values downdip, it is evident that ankerite also precipitated in porewaters which had $\delta^{18}O$ 2-3‰ more negative at the crest of the oilfield compared to downdip. Ankerites have been demonstrated to occur immediately adjacent to mudstones. Temperature-related clay transformation and, more importantly, detrital mineral breakdown reactions in the thick mudstones presumably released water, Fe, Mg, Mn, Ca and HCO_3^- which diffused or were advected up to 10 metres into the sandstones to precipitate ankerite cements. The shales in all three wells were deposited in nearly identical marine conditions (Rainey, 1987). Due to the small depth, and hence temperature, difference between crestal and downdip wells the isotopic composition of compactional water released from mudstones in different wells was probably similar. The trend of more negative $\delta^{18}O$ at the structural crest of the oilfield must therefore relate to the isotopic composition of the sandstone porewater.
As a late diagenetic cement, ankerite formed at a temperature of 82-98°C if unevolved marine porewater with $\delta^{18}O$ of -1.2‰ is assumed for well 211/12a-9. Porewater isotopic composition evolution towards higher $\delta^{18}O$ values since burial, through water/rock interaction, means that these are minimum temperatures. The present day formation water isotopic composition has $\delta^{18}O$ of approximately +2‰ (BP analysis ; S. Rainey pers. comm.). A maximum ankerite formation temperature of 105-110°C is obtained using this water $\delta^{18}O$. Present day reservoir temperature is approximately 120°C.

3.9 Summary and discussion of isotope data

The high initial $^{87}Sr/^{86}Sr$ ratios in siderite reflect Sr supply from breakdown of detrital biotite. $\delta^{13}C$ values indicate that decarboxylation of organic matter was important in supplying CO_2 for siderite growth. Oxygen isotope analyses indicate that siderite grew at about 84-98°C, assuming an evolved meteoric-derived or marine-derived porewater with $\delta^{18}O$ -1‰. At a maximum burial depth of 1.6km for siderite growth this implies a high geothermal gradient of 52-60°C km^{-1}, considerably higher than the present-day 30°C km^{-1}. An alternative model for siderite growth could be that it grew in porewater with a more negative $\delta^{18}O$ at lower temperatures. However, decarboxylation influenced $\delta^{13}C$ and the texturally late position of siderite in the diagenetic

sequence argue against this. More negative $\delta^{18}O$ for siderite in the crest than downdip indicate retention in the crest of a meteoric-derived water lens.

Ankerites also formed under a high geothermal gradient in isotopically evolved porewaters which retained a meteoric ($\delta^{18}O$) influence in the crest of the field. Mg was supplied from original porewaters (hence more Mg-rich downdip - Figure 11) and also from mudrock reactions, so ankerite is located only close to muds. High initial $^{87}Sr/^{86}Sr$ ratios suggest supply from silicates within the muds. More negative $\delta^{13}C$ for ankerite than for siderite imply that, later in the paragenetic sequence, carbon supply was more strongly influenced by organic sources.

A schematic representation of the development of diagenetic carbonate minerals in the Magnus sandstones is shown in Figure 18.

3.10 CONCLUSIONS

1. Calcite is the earliest formed diagenetic carbonate preserved in the Magnus Sandstone, but is very scarce. Dissolution of rare shell material, plagioclase dissolution and original marine Ca were the most likely sources of Ca. The significance of original marine Ca, given meteoric-water dilution of the original marine porewater is speculative.

2. Magnesian siderite formed in both primary and secondary feldspar porosity throughout the Magnus Sandstone. The intimate association between degraded detrital biotite and diagenetic siderite points to biotite as the most important source of Fe, Mg and Sr and suggests that a local geochemical environment with raised pH was important for siderite growth. This is confirmed by the very high initial $^{87}Sr/^{86}Sr$ ratios in siderites derived from detrital biotite breakdown. Formation of late cubic and octahedral pyrite exhausted local sulphate supply and allowed siderite development.

3. Three compositional growth zonations in siderite grains are present in all three wells from the crest of the field to the flank. In all three wells a similar trend of compositional evolution through time is observed, in both two and three zoned rhombs. First-formed siderite was relatively magnesian, then compositions became more ferroan, before compositions returned to being at least as magnesian as the first stage. These individual grain variations overprint a fieldwide variation where siderite is more ferroan in the crestal samples and more magnesian downdip. This reflects the greater influence of Fe-rich meteoric-derived water in the crest and the greater influence of marine-derived Mg-rich porewater downdip.

4. Siderite $\delta^{13}C$ of -8.0 to -14.6‰PBD reflect the importance of organic matter in sourcing CO_2. These results could reflect either CO_2 generated at a particular stage in organic maturation (at about 80°C) at which a particular fractionation of C-isotopes is prevalent and/or a mixture of marine bicarbonate (0‰), bacterial fermentation (+15‰) and abiotic thermally-induced decarboxylation (-10 to -25‰). Siderite $\delta^{18}O$ values are more

negative for samples from crestal well 211/12-1 than in downdip well 211/12a-9. This reflects the retention of a meteoric-derived water lens, derived from mid-Cretaceous subaerial erosion, in the structural crest of the field. $\delta^{18}O$ values of x= +16.0‰SMOW in the crest and x= +17.6‰ downdip constrain siderite formation to temperatures of 84 to 96°C, assuming an evolved or marine-derived porewater with $\delta^{18}O$ -1‰.

5. Ankerite post-dates siderite formation and has only formed in the Magnus Sandstone within 10m of mudstones and in thin sandstones within mudstones. Pre-ankerite etching of detrital garnets along rhombic faces suggests that organic acids had been generated and were present in significant quantities at this time. These acids dissolved unstable detrital grains resulting in Ca, Mg, and Fe+Mn for ankerite development being transported from mudstones into adjacent sandstones, probably by advection or diffusion.

6. The range of ankerite $\delta^{13}C$ is more negative than that for siderite (-7.7 to -13.6‰) supporting ankerite formation, shortly after siderite, from CO_2 produced by slightly more advanced decarboxylation of organic matter in surrounding mudstones. The results of $\delta^{18}O$ analyses show a cross-field stratification with more negative ratios in the crest. Again this reflects retention of a crestal meteoric-derived water lens. These oxygen isotope ratios indicate that ankerite grew at 80 to 110°C.

7. Oxygen isotope analyses of both siderite and ankerite suggest an elevated geothermal gradient of around 60°C km^{-1} in the oilfield during rapid subsidence in the late Cretaceous.

8. The isotopic evolution of $\delta^{13}C$, closed system $\delta^{34}S$ values and stratified $\delta^{18}O$ from crest to flank of the field make it very difficult to envisage any large scale porewater movements. This is strongly supported by the parallel, but distinct, geochemical fingerprints of zoned siderite cements from the crest to the flank of the field, and different ankerite compositions from the crest to the flank.

3.11 ACKNOWLEDGEMENTS

The authors thank the staff of the Isotope Geology Unit, SURRC, East Kilbride, for their help with mineral separations and analyses. Dr. Ed Stephens and Donald Herd of the Geology Department, Saint Andrews University, and Dr Peter Hill of the Geology Deparment, Edinburgh University, were instrumental in the microprobe analyses. SEM assistance was provided by Cathy Brown at BP, Aberdeen, and Pete Ainsworth at the Dept. of Geology and Applied Geology, Glasgow University. C.I.M. acknowledges receipt of NERC grant no. GT4/86/GS/102, and provision of core material from BP through a CASE studentship.

3.12 REFERENCES

Baldwin B. and Butler C.O., 1985, Compaction curves : Bulletin of the American Association of Petroleum Geologists v. 69, p. 622-626.

Bjorlykke K. and Brensdal A., 1986, Diagenesis of the Brent Sandstone in the Statfjord field, North Sea : in Gautier D.L., ed., Roles of Organic Matter in Sediment Diagenesis, Society of Economic Palaeontologists and Mineralogists Special Publication 38, p. 157-167.

Boles J.R., 1978, Active ankerite cementation in the subsurface Eocene of Southeast Texas : Contributions to Mineralogy and Petrology v. 68, p. 13-22.

---------- and Johnson, 1983, Influence of mica surfaces on pore-water pH : Chemical Geology v. 43, p. 303-317.

Brint J. F., (1989) Isotope diagenesis and palaeofluid movement: Middle Jurassic Brent Sandstones, North Sea: Unpublished Ph.D. thesis, University of Strathclyde, UK.

Carothers W.W. and Kharaka Y.K., 1980, Stable carbon isotopes of HCO_3^- in oil-field waters - implications for the origin of CO_2 : Geochimica et Cosmochemica Acta v. 44, p 323-332.

Claypool G.E., Holsen W.T., Kaplan I.R., Sakai H. and Zak I., 1980, The age curves of sulfur and oxygen isotopes in marine sulfate and their mutual interpretation : Chemical Geology v. 28, p. 199-260.

Craig H., 1957, Isotopic standards and isotopic correction factors for mass spectrometric analysis of carbon dioxide : Geochimica et Cosmochimica Acta v. 12, p. 133-149.

---------- 1961, Standards for reporting concentrations of deuterium and oxygen-18 in natural waters : Science v. 133, p. 1833-1834.

Crossey L.J., Surdam R.C. and Lahann R., 1986, Application of organic/inorganic diagenesis to porosity prediction. : In Gautier D.L., ed., Roles of Organic Matter in Sediment Diagenesis : S.E.P.M. Special Publication No. 38, p. 147-156.

Curtis C.D. and Coleman M.L., 1986, Controls on the precipitation of early diagenetic calcite, dolomite and siderite concretions in complex depositional sequences. : In Gautier D.L., ed., Roles of Organic Matter in Sediment Diagenesis : S.E.P.M. Special Publication No. 38, p. 23-34.

De-Ath N.G. and Schuyleman S.F., 1981, The geology of the Magnus oilfield. : In Brooks J. and Glennie K.W., eds., Petroleum Geology of the Continental Shelf of North-west Europe , Heyden & Son, London, p. 342-351.

Deer W.A., Howie R.A. and Zussman J., 1962, Rock-forming Minerals v. 5, p.371 - non-silicates, John Wiley and Sons, New York.

---------- 1966, An Introduction to the Rock Forming Minerals p.494 : John Wiley and Sons, New York.

Evans I.J., 1989, Geochemical fluxes during shale diagenesis, an example from the Ordovician of Morocco. : In Miles, ed., Water-Rock Interaction WRI-6, p. 219-222 : Balkema, Rotterdam.

Faure G., 1986, Principles of Isotope Geology (2nd. ed.) : John Wiley and Sons, Canada 589p.

Hansley P.L., 1987, Petrologic and experimental evidence for the etching of garnets by organic acids in the Upper Jurassic Morrison Formation, NW New Mexico : Journal of Sedimentary Petrology v. 57 no. 4, p. 666-681.

Irwin H., Curtis C.D. and Coleman M., 1977, Isotopic evidence for source of diagenetic carbonates formed during burial of organic-rich sediments : Nature v. 269, p. 209-213.

Kantorowicz J.D., 1982, Diagenetic modelling in Middle Jurassic clastic sediments from the Ravenscar Group, Yorkshire, and the Brent Group, Northern North Sea : Unpublished Ph.D. Thesis, University of Hull.

_____1985, The origin of authigenic ankerite from the Ninian field, UK North Sea : Nature v. 315, p. 214-216.

Krouse H.R., Viau C.A., Eliuk L.S., Veda A. and Halas S., 1988, Chemical and isotopic evidence of thermochemical sulphate reduction by light hydrocarbon gases in deep carbonate reservoirs : Nature v. 333, p. 415-419.

Land L.S., 1980, The isotopic and trace element geochemistry of dolomite : the state of the art. : In Zenger D.H., Dunham J.B. and Ethington R.L., eds., Concepts and Models of Dolomitization : S.E.P.M. Special Publication No. 28, p. 87-110.

Longstaffe F.J. and Ayalon A., 1987, Oxygen-isotope studies of clastic diagenesis in the Lower Cretaceous Viking Formation, Alberta : implications for the role of meteoric water. : In Marshall J.D., ed., Diagenesis of Sedimentary Sequences : Geological Society Special Publication No. 36, p. 277-296.

Macaulay C.I., Haszeldine R.S. and Fallick A.E., 1990, Sedimentary basin porewaters remain static during 35Myr rapid subsidence : Magnus oilfield, North Sea : Chapter 2, this volume.

McCrea J.M., 1950, On the isotope chemistry of carbonates and a palaeotemperature scale : Journal of Chemical Physics v. 18, p. 849-857.

Pierson B.J., 1981, The control of cathodoluminescence in dolomite by iron and manganese : Sedimentology v. 28, p. 601-610.

Rainey S.C.R.,1987, Sedimentology, Diagenesis and Geochemistry of the Magnus Sandstone Member, Northern North Sea. (Ph.D. thesis) : University of Edinburgh.

Reeder R.J., 1983, Crystal chemistry of the rhombohedral carbonates, in Reeder R.J., ed., Carbonates : Mineralogy and Chemistry, Reviews in Mineralogy v. 11, Mineralogical Society of America, p. 32.

Rosenbaum J. and Sheppard S.M.F., 1986, An isotopic study of siderites, dolomites and ankerites at high temperatures : Geochimica et Cosmochimica Acta v. 50, p. 1147-1150.

Sommer S.E., 1972, Cathodoluminescence of carbonates. 1. Characterization of cathodoluminescence from carbonate solid solutions. 2. Geological applications : Chemical Geology v. 20, p. 121-149.

Surdam R. C., Boese S.W. and Crossey L.J., 1984, The chemistry of secondary porosity. : In McDonald D.A. and Surdam R.C., eds., Clastic Diagenesis : A.A.P.G. Memoir 37, p. 127-150.

3.13 FIGURE CAPTIONS

Figure 1a. Magnus oilfield location map.

b. The Magnus oilfield is defined to the east by the oil/water contact, and to the west by subcrop of the Magnus Sandstone beneath Cretaceous marine sediments and by depositional pinchout to the north and south.

c. Cross section through the Magnus oilfield showing the location of the three wells studied, and the Magnus Sandstone between the Upper and Lower Kimmeridge Clay Formations (UKCF, LKCF) below the mid-Cretaceous unconformity. Well -1 to well -9 is 3km

Figure 2. Generalised paragenetic sequence for the Magnus Sandstone. Hollow bars are dissolution events.

Figure 3. Backscatter electron image showing ankerite (A) enclosing and postdating rare calcite (C).

Figure 4a. Backscatter electron image showing zoned magnesian siderite (S) developed in primary porosity.

Figure 4b. Backscatter electron image showing in situ replacement of detrital biotite (B) by magnesian siderite (S).

c. Backscatter electron image showing intimate growth of magnesian siderite (S) This suggest growth through ion supply from detrital biotite (B) and mud clasts (MC). Bright specks are pyrite.

Figure 5a. Backscatter electron image showing magnesian siderite (S) developed in secondary porosity produced by detrital feldspar (F) dissolution.

Figure 5b. Magnesian siderite (S) 200 μm across replacing pore-filling kaolinite (K)

Figure 5c. Backscatter electron image showing zoned magnesian siderite (S) predating ankerite (A) development.

Figure 6. A 40cm thin sandstone from 3248m in 211/12a-9 which is enclosed in 20m of mudstone is completely cemented by silica (Si) and later ankerite. Ankerite (A) constitutes 22% of the sandstone in this sample. Field of view 200mm.

Figure 7. Magnesian siderite and ankerite distribution in 211/12a-9 as determined by point counting (500 counts per section). White areas represent reservoir sandstone, and black areas mudstone.

Figure 8. Backscatter image showing preferential etching of detrital almandine garnet (G), producing rhombic crystal faces. This was probably caused by organic acids, and predates ankerite (A) precipitation.

Figure 9. Variations in siderite compositions from well to well : crestal (211/12-1) siderite is more ferroan and that downdip (211/12a9) more magnesian.

Figure 10a. Magnesian siderite compositional trends from inner to outer zones as determined by electron microprobe analyses : 211/12-1 (oilfield crest).

b. Magnesian siderite compositional trends from inner to outer zones as determined by electron microprobe analyses : 211/12a-M1 (near crest).

c. Magnesian siderite compositional trends from inner to outer zones as determined by electron microprobe analyses : 211/12a-9 (downdip flank).

Figure 11. Variations in ankerite compositions between wells : crestal (211/12-1) ankerites are more ferroan and those downdip (211/12a-9) more magnesian.

Figure 12a. Graph of carbon vs. oxygen isotopic composition of magnesian siderite samples (in‰ relative to PDB standard). No overall correlation is apparent.

b. Variations in carbon isotope composition of CO_2 sourced by organic matter with increasing depth of burial (after Irwin et al., 1977).

Figure 13. The depth distribution of pyrite $\delta^{34}S$ values in 211/12a-9. Most negative values represent early framboidal pyrite formation in an open sulphate system and least negative values late cubic and octahedral pyrite formed in a more closed sulphate system. Jurassic seawater sulphate had $\delta^{34}S \sim 16 \pm 1.5‰$ (Claypool et al, 1980).

Figure 14. Burial history curve for the Magnus Sandstone derived for well 211/12a-9 using decompaction ratios described by Baldwin and Butler (1985). K/Ar date constrains illite (the last diagenetic phase) formation to 55Ma in the oil zone and 41Ma in the water zone below.

Figure 15a. Plot of modal $\delta^{18}O$ (and one standard deviation) values for magnesian siderite from 211/12-1, 211/12a-M1 and 211/12a-9 (relative to SMOW, after Macaulay et al., 1990). Note the separation of more negative crestal ratios and less negative downdip ratios.

b. Plot of ranges of $\delta^{18}O$ for magnesian siderite from 211/12-1, 211/12a-M1 and 211/12a-9.

Figure 16. Graph of carbon vs. oxygen isotopic composition of ankerite samples (relative to PDB standard).

Figure 17a. Plot of mean $\delta^{18}O$ values (and one standard deviation) for ankerite from 211/12-1, 211/12a-M1 and 211/12a-9 (relative to SMOW, after Macaulay et al., 1990).

Figure 17b. Plot of ranges of $\delta^{18}O$ for ankerite from 211/12-1, 211/12a-M1 and 211/12a-9.

Figure 18. A schematic representation of the development of diagenetic carbonate minerals in the Magnus sandstone.

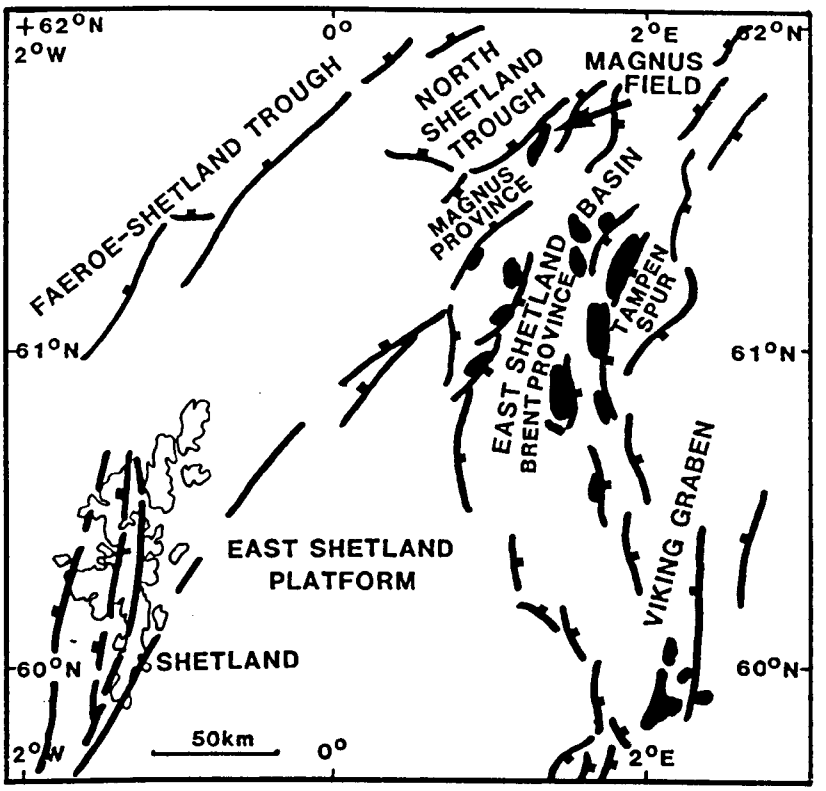

Figure 1a.

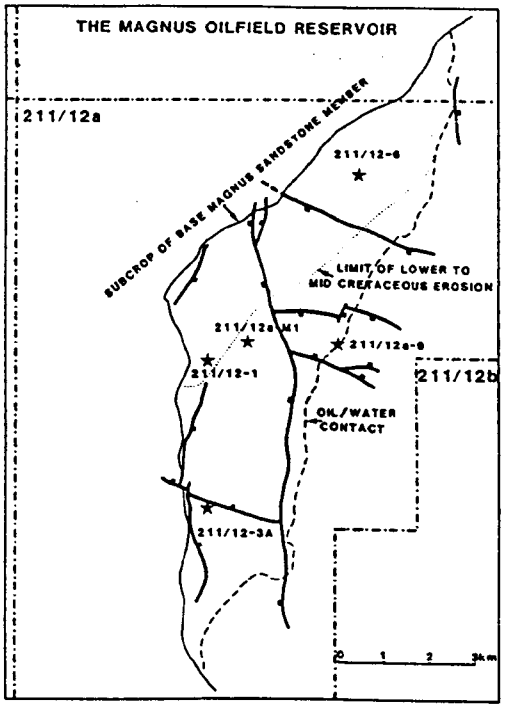

Figure 1b.

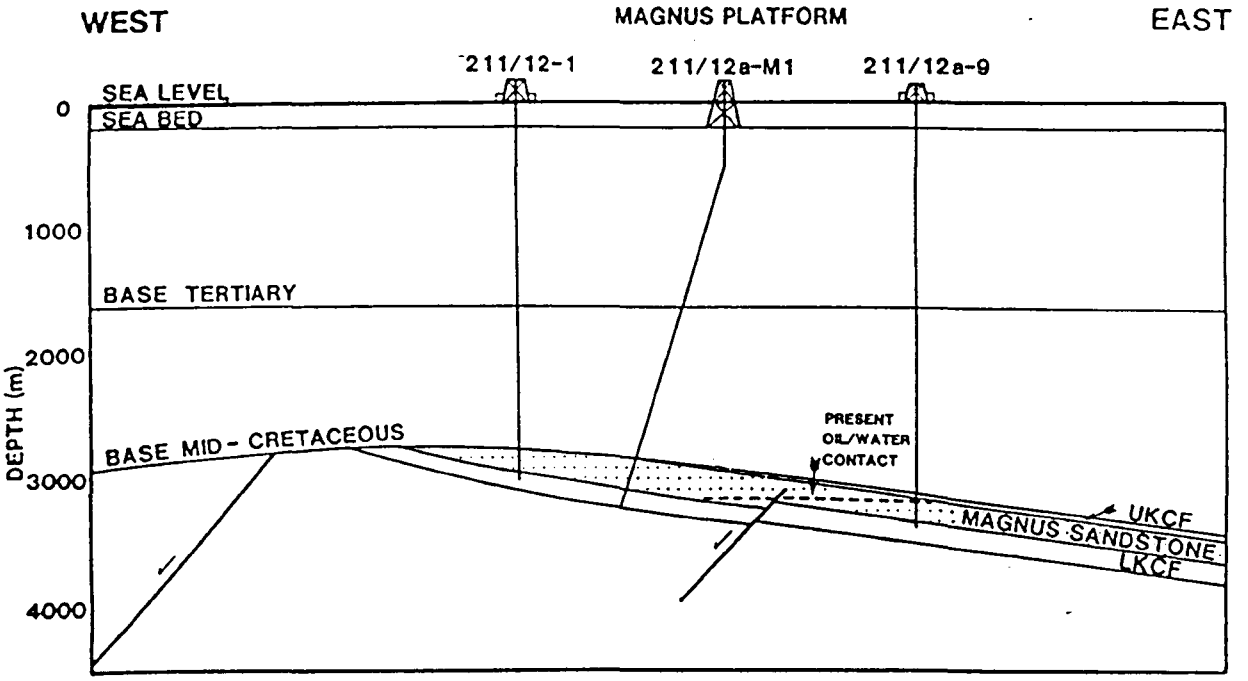

Figure 1c.

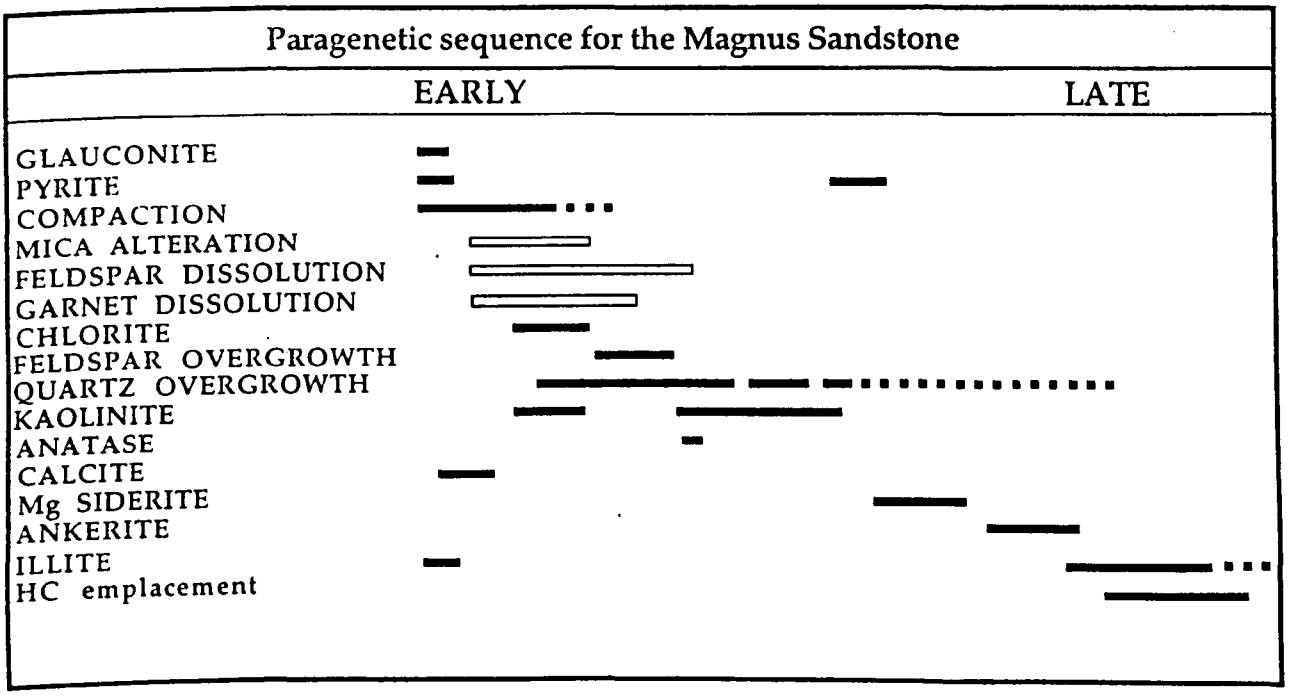

Figure 2.

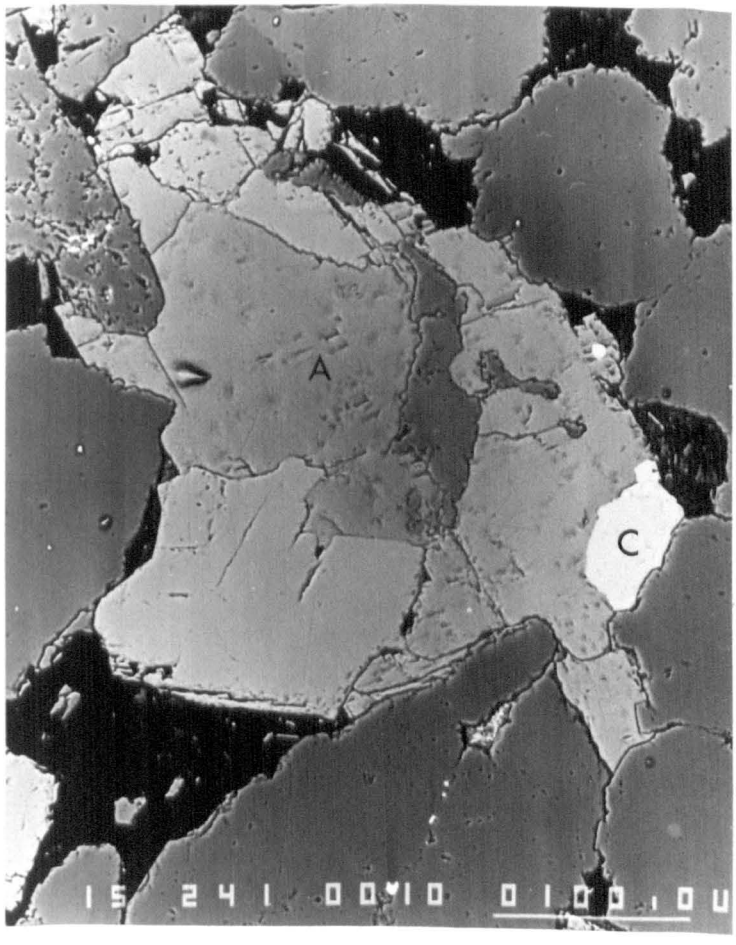

Figure 3.

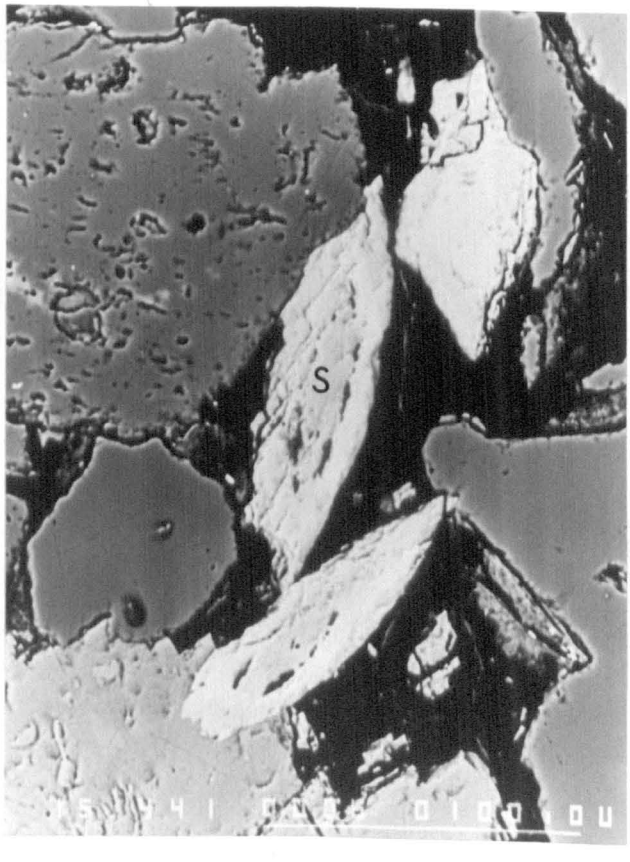

Figure 4a.

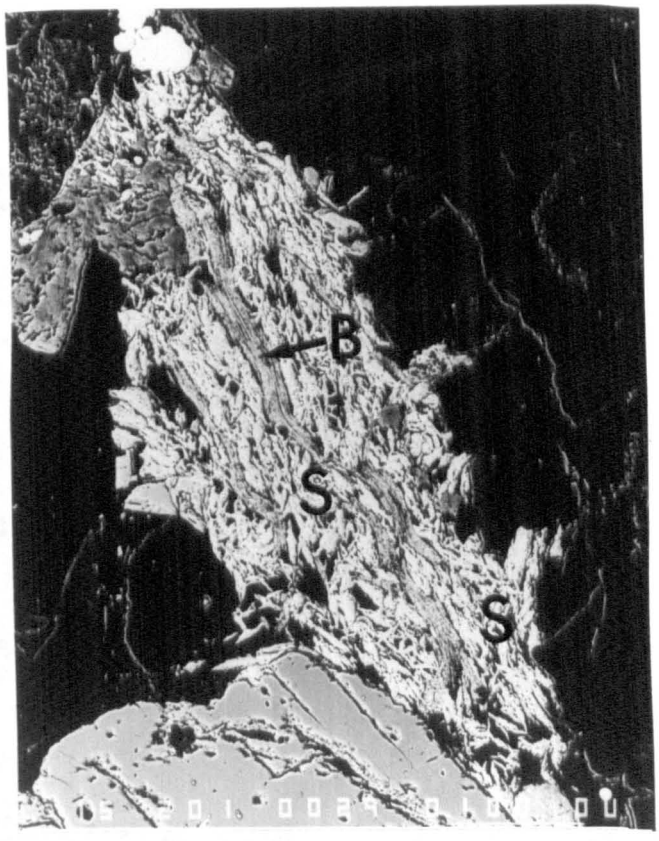

Figure 4b.

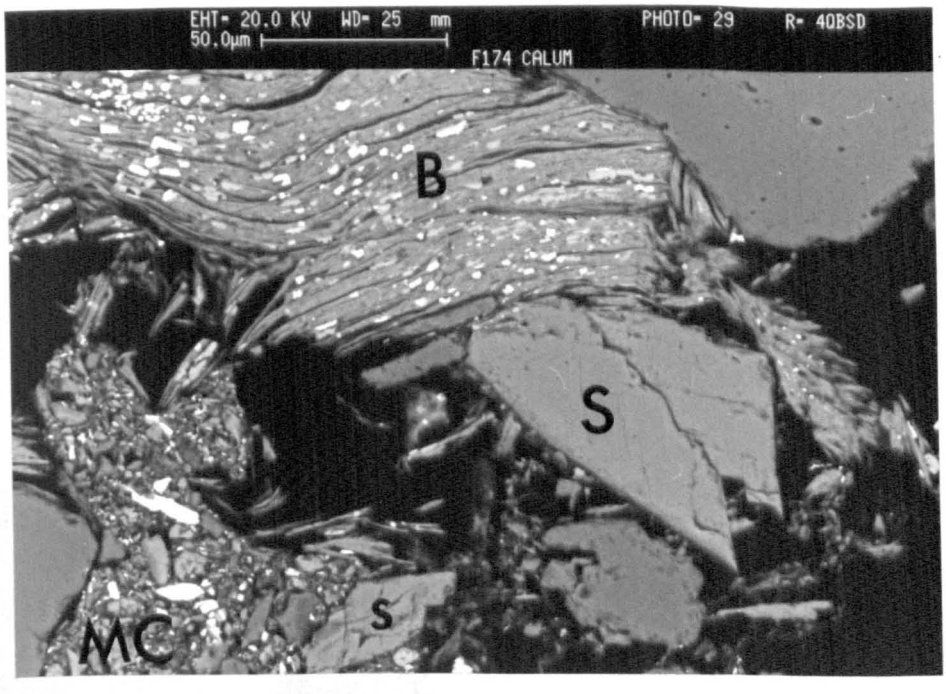

Figure 4c.

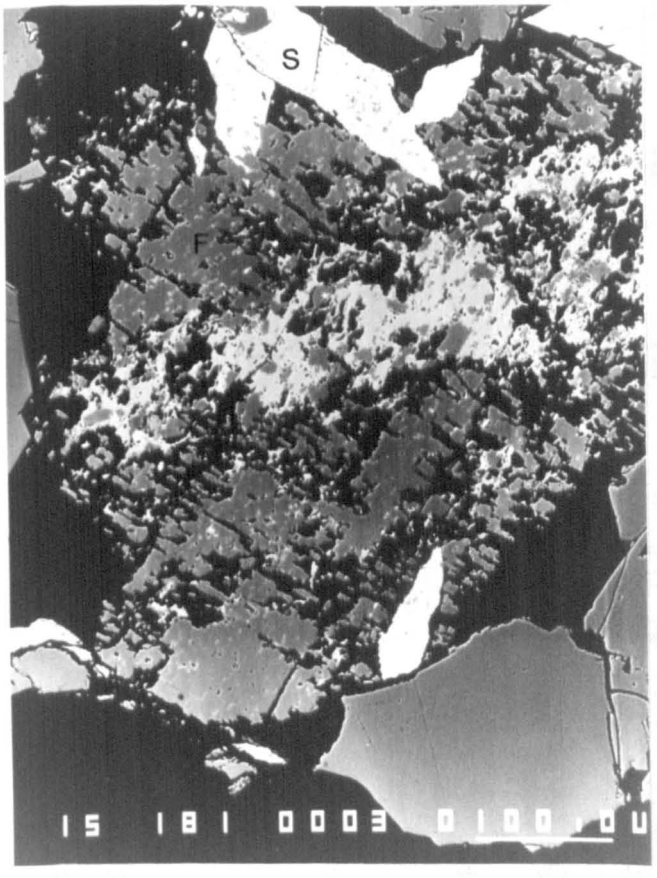

Figure 5a.

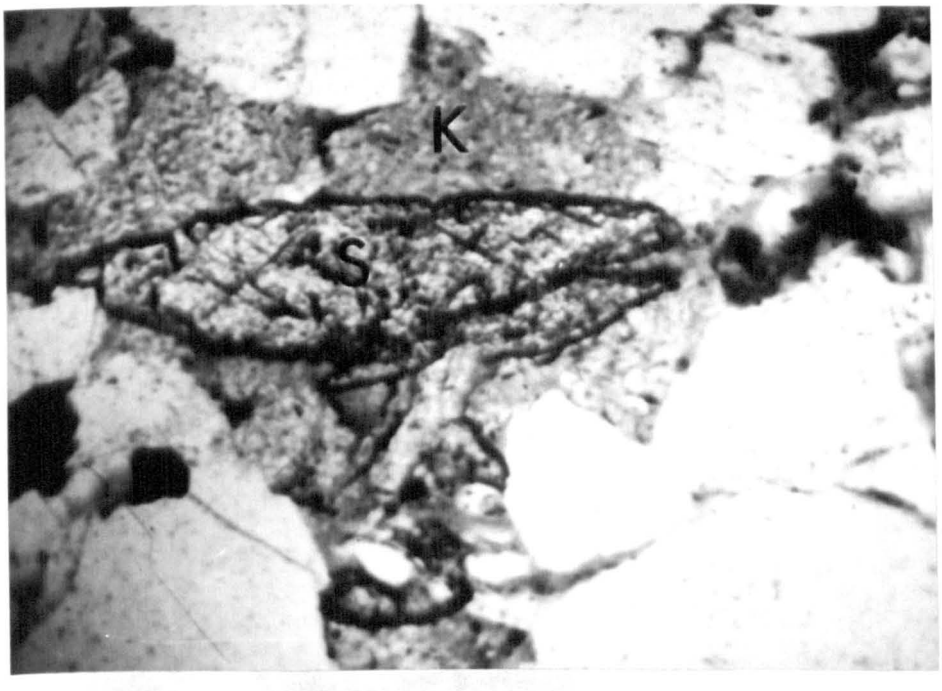

Figure 5b

Figure 5c.

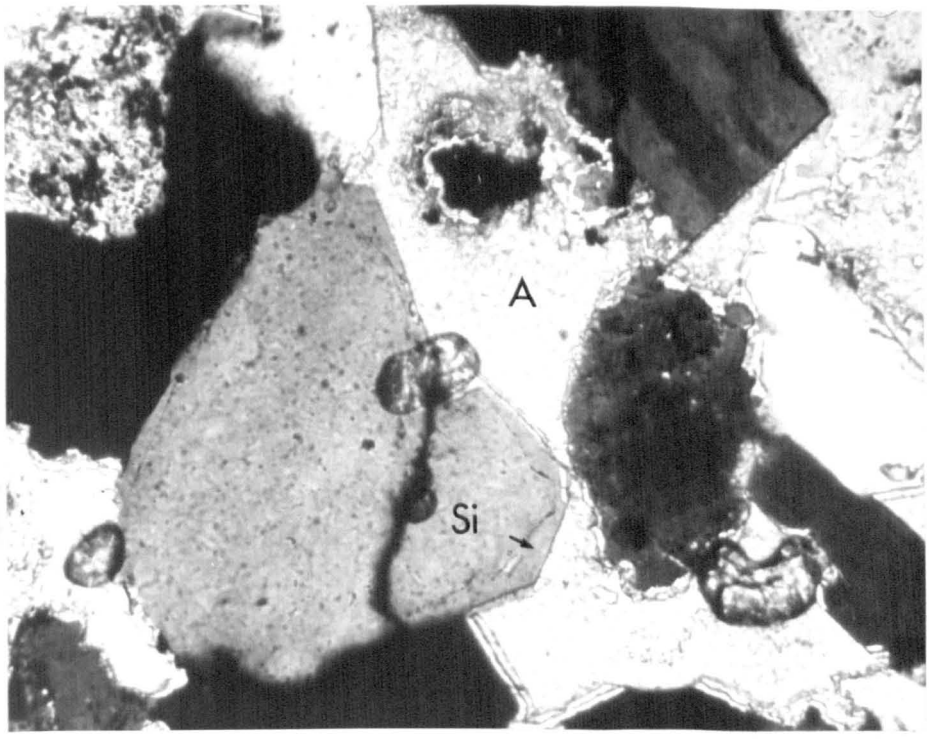

Figure 6.

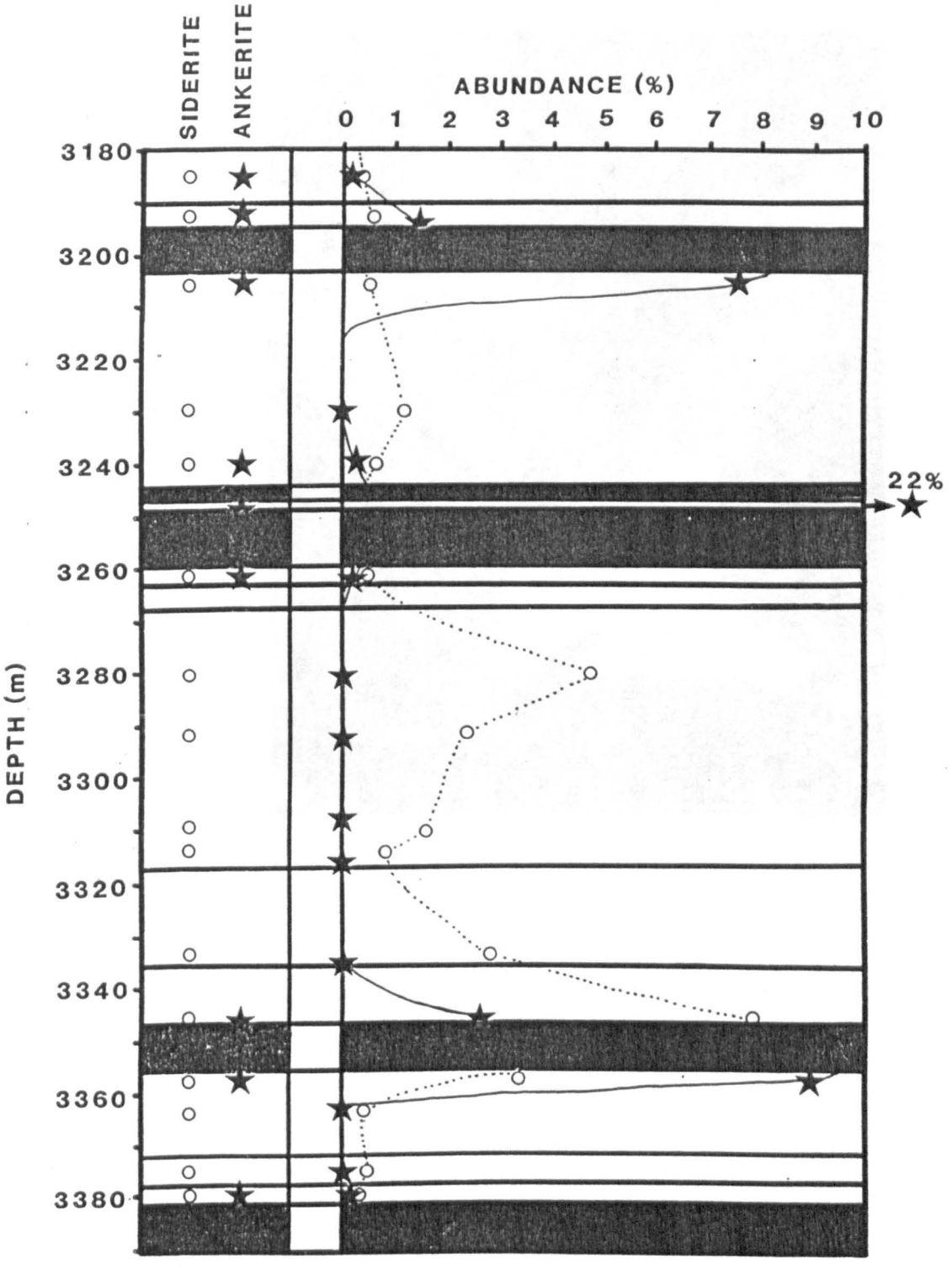
SIDERITE
ANKERITE
ABUNDANCE (%)
0 1 2 3 4 5 6 7 8 9 10
DEPTH (m)
3180
3200
3220
3240
3260
3280
3300
3320
3340
3360
3380
22%

Figure 7.

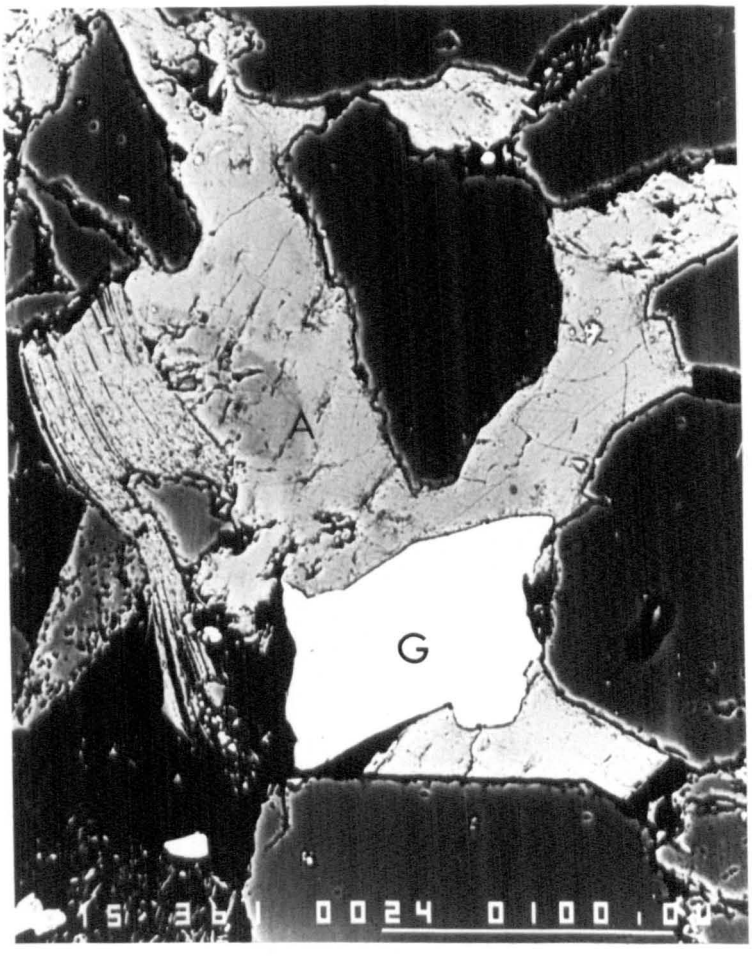

Figure 8.

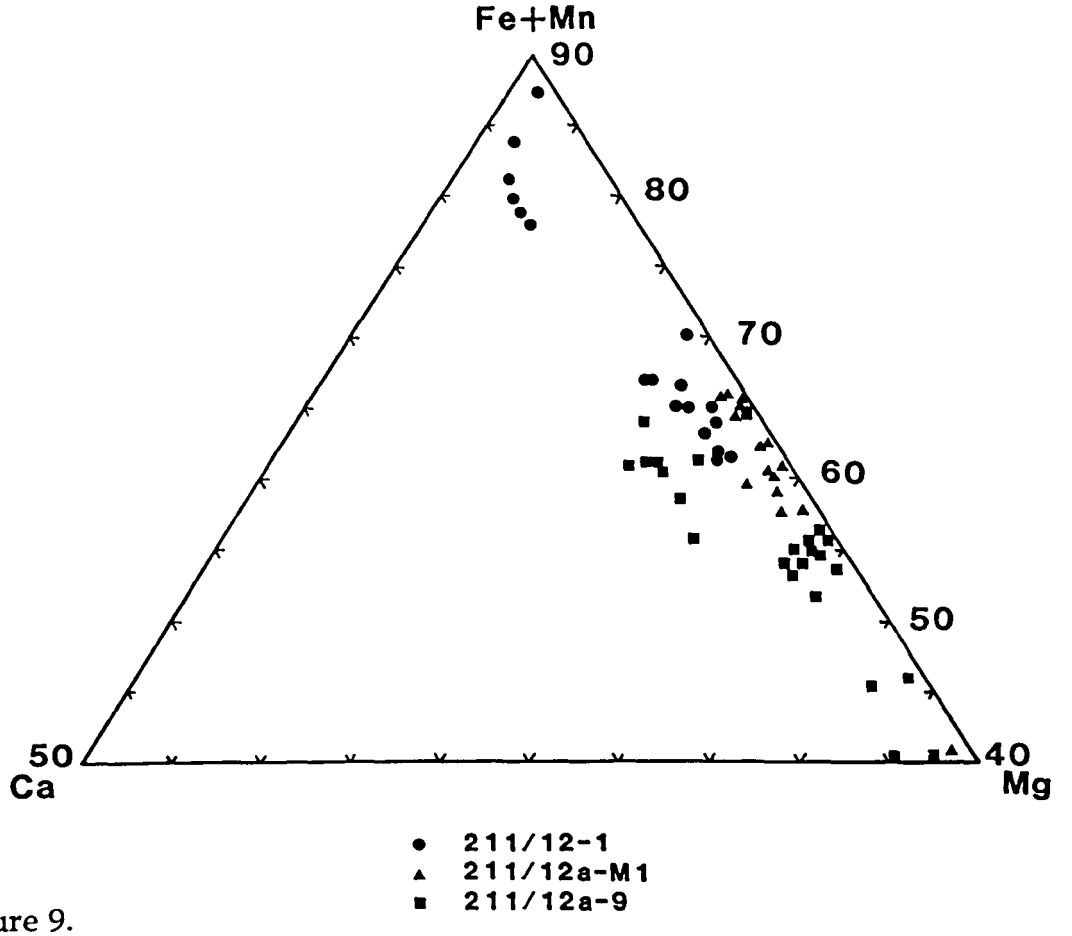

Figure 9.

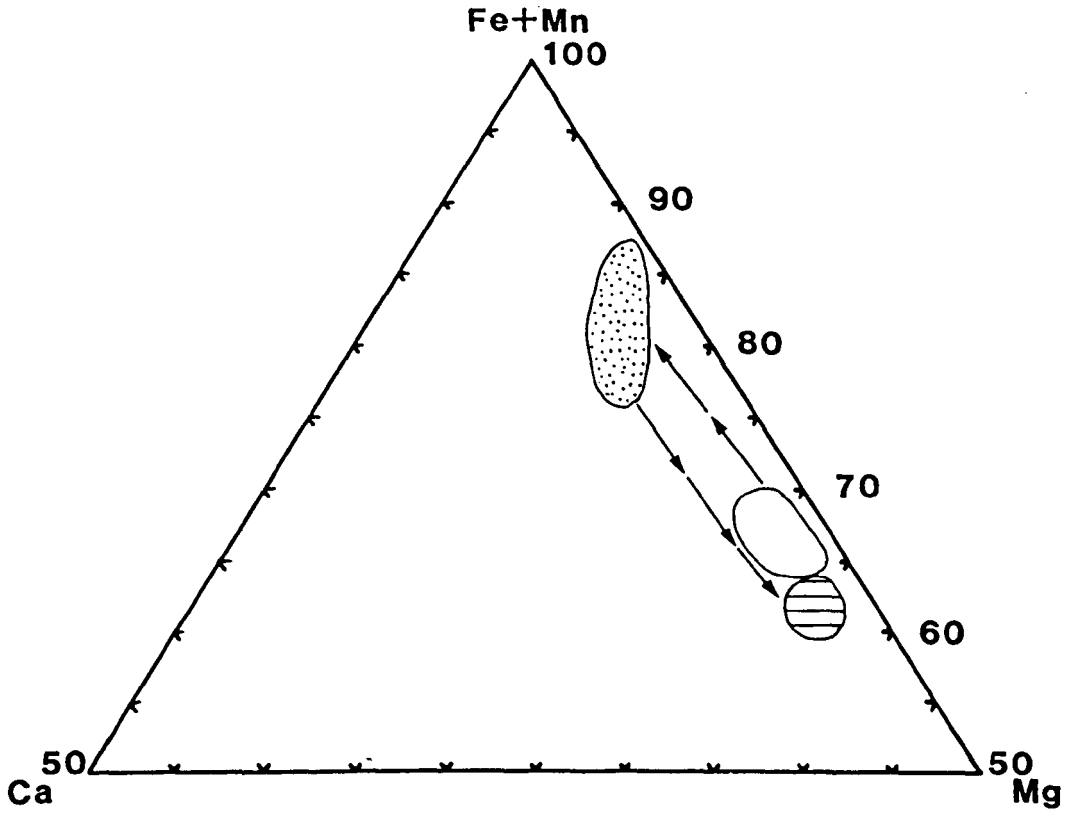

Figure 10a.

Inner zone of 3-zoned magnesian siderites.
Middle zone of 3-zoned/inner zone of 2-zoned magnesian siderites.
Outer zone of both 2 and 3-zoned magnesian siderites.

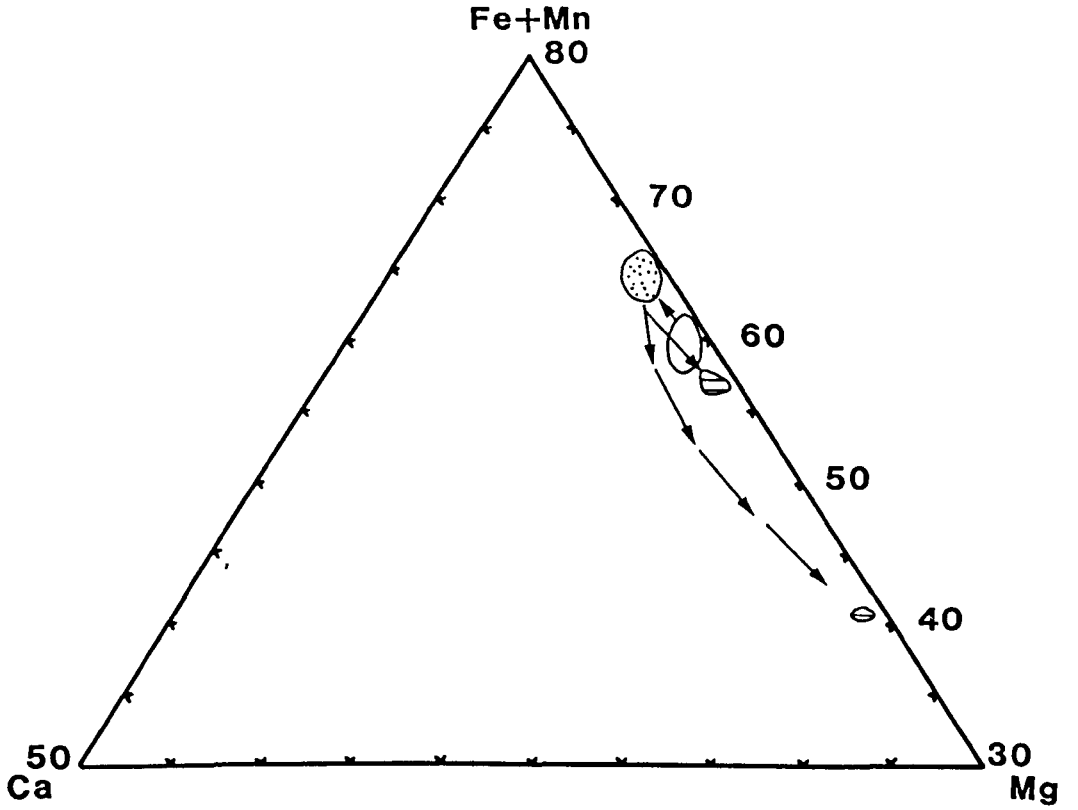

Figure 10b.

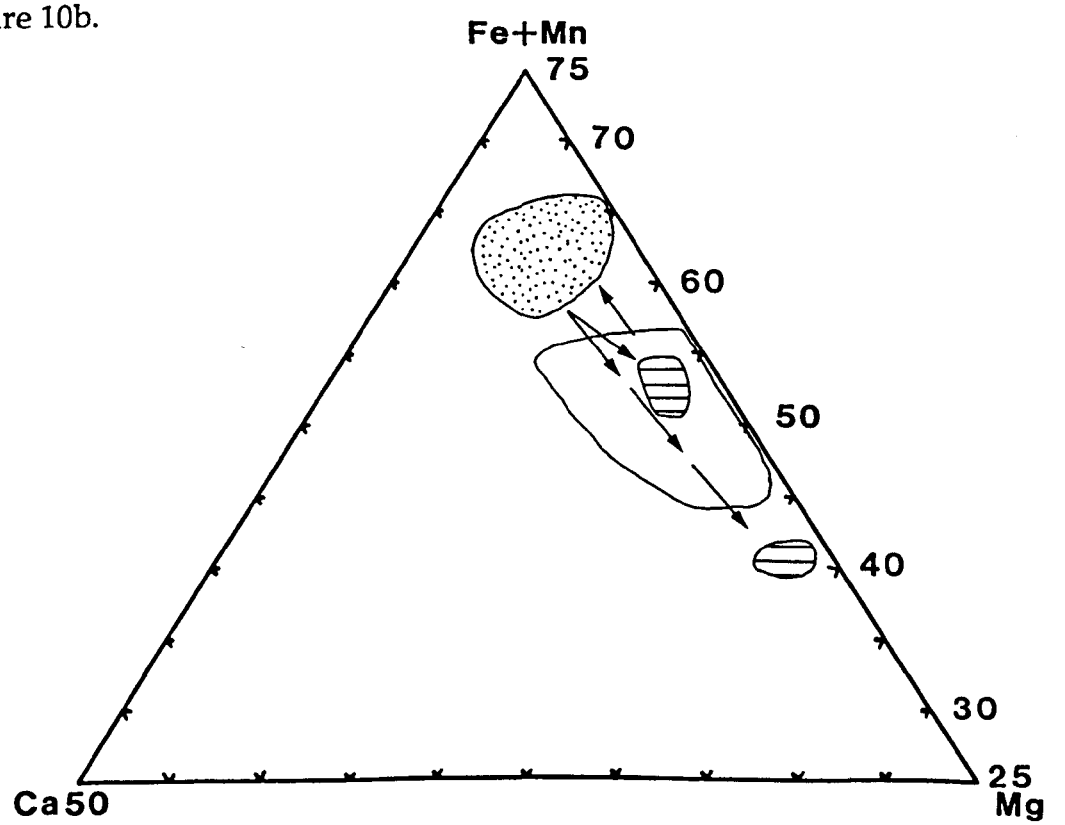

Figure 10c.

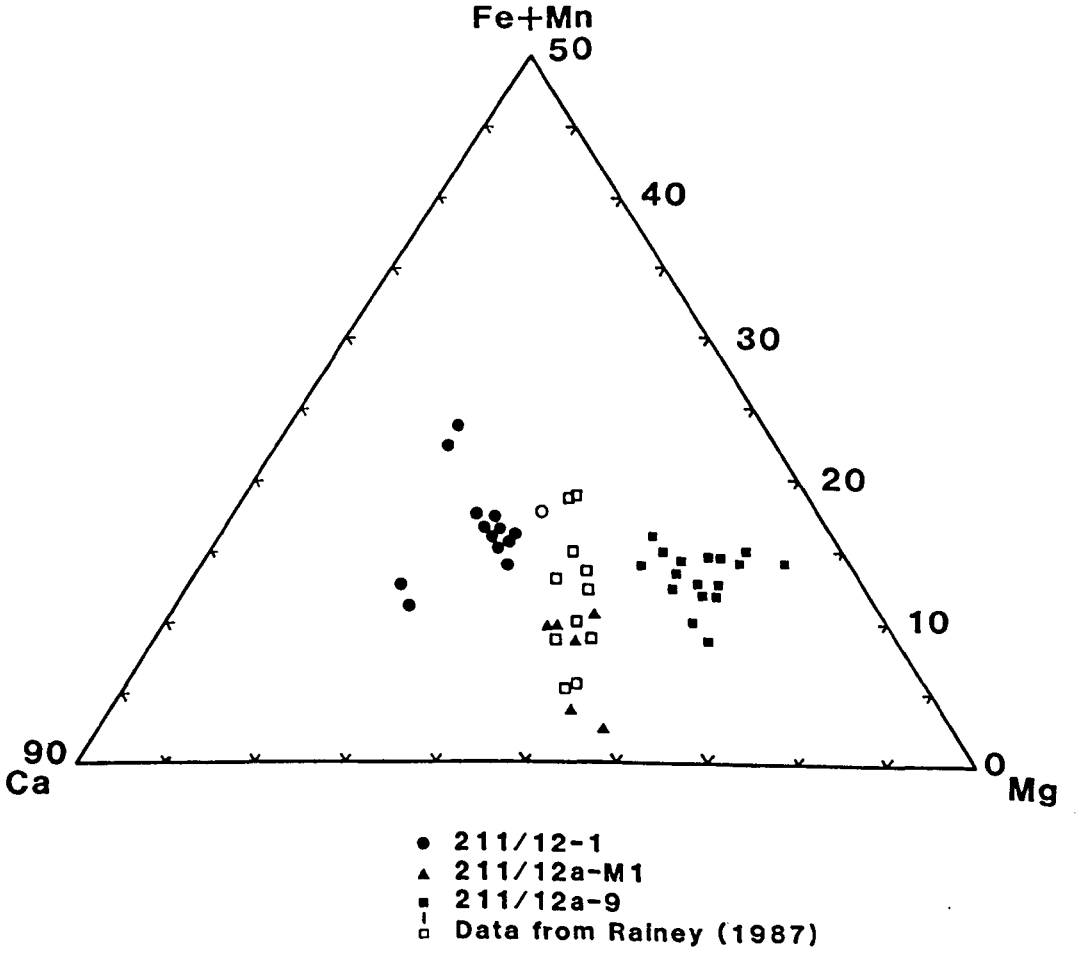
Fe+Mn
50
40
30
20
10
0
Mg
90
Ca
211/12-1
211/12a-M1
211/12a-9
Data from Rainey (1987)

Figure 11.

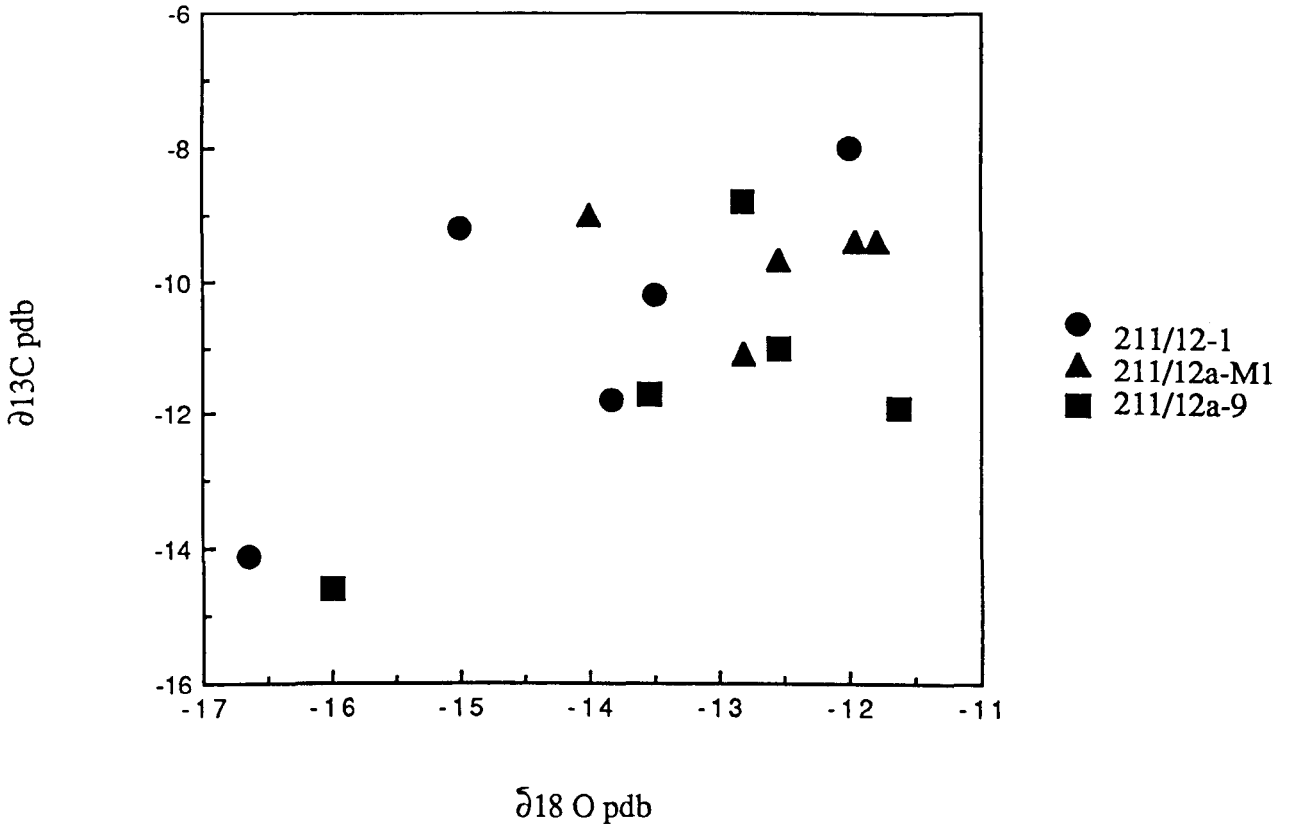

Figure 12a.

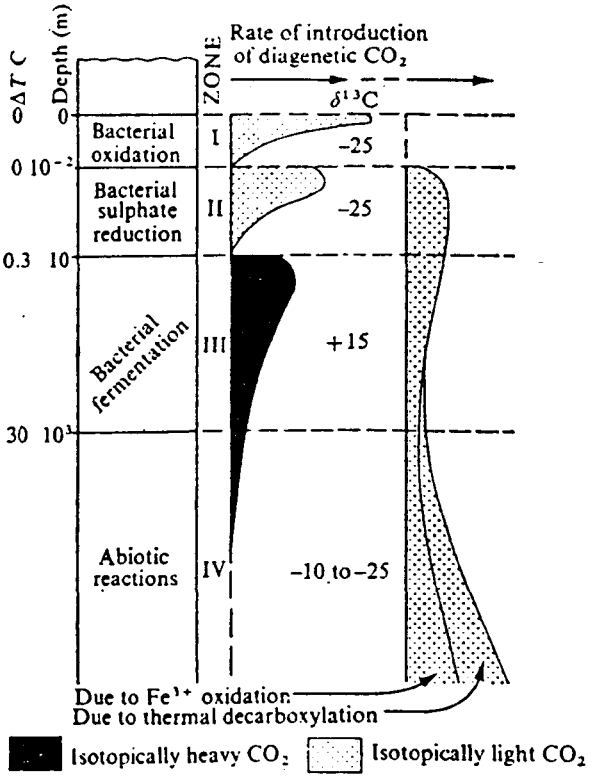

Figure 12b.

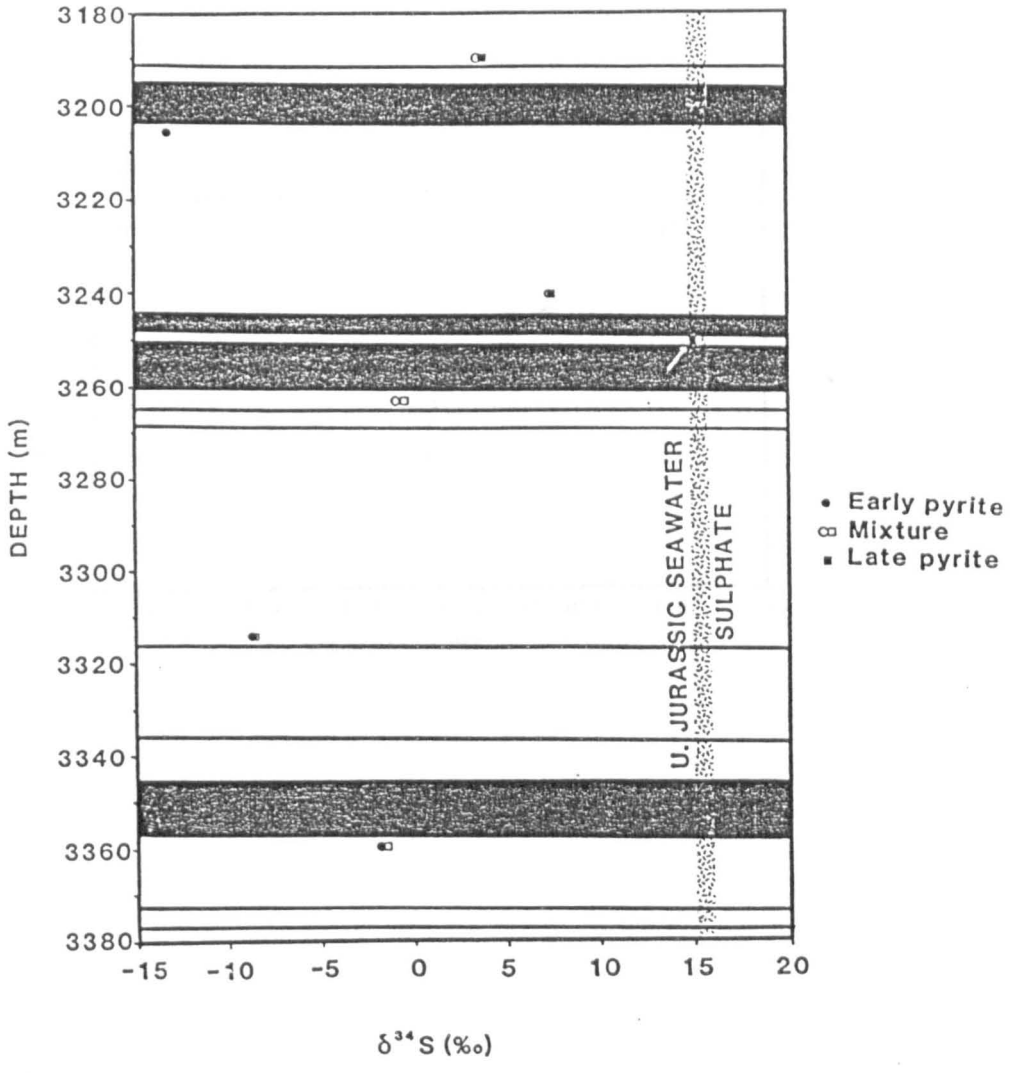

Figure 13.

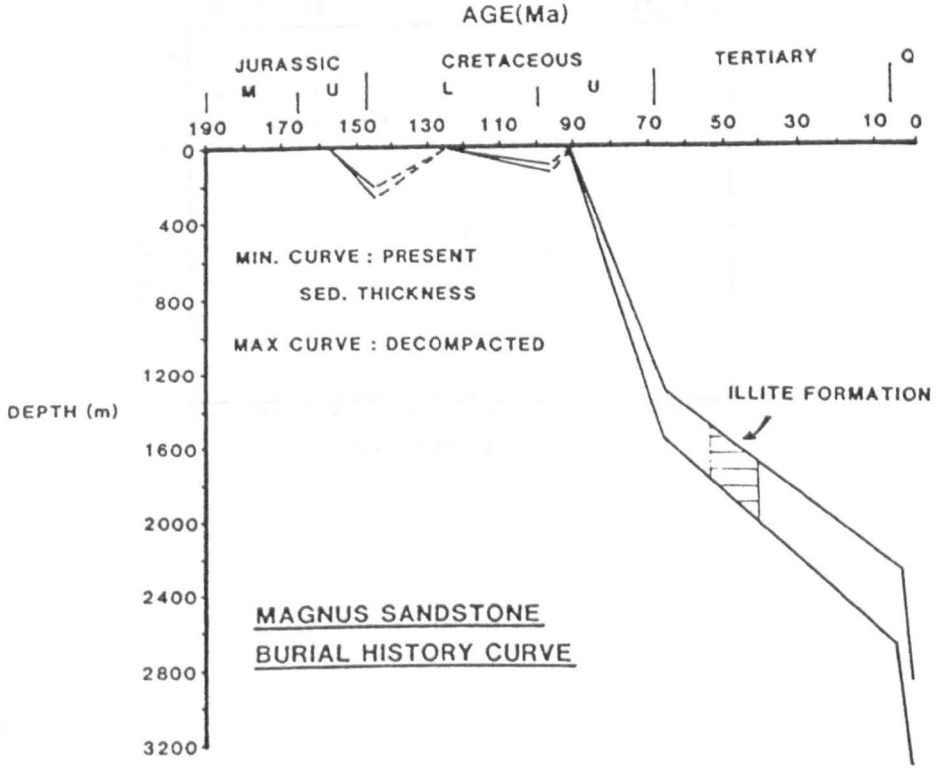

Figure 14.

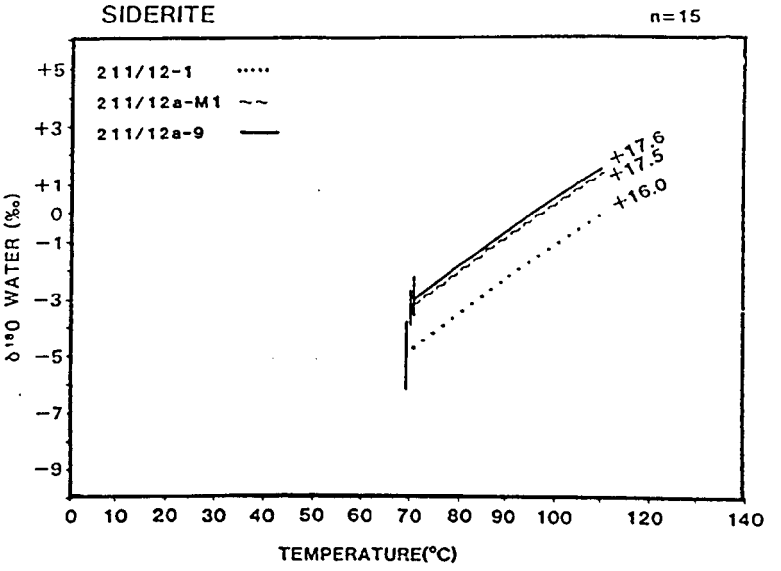

Figure 15a.

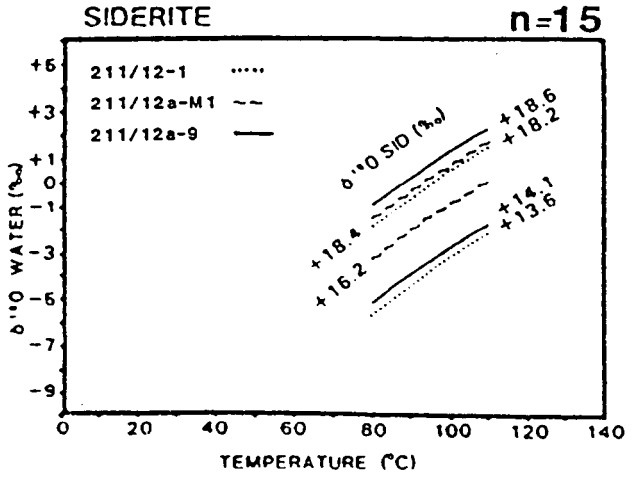

Figure 15b.

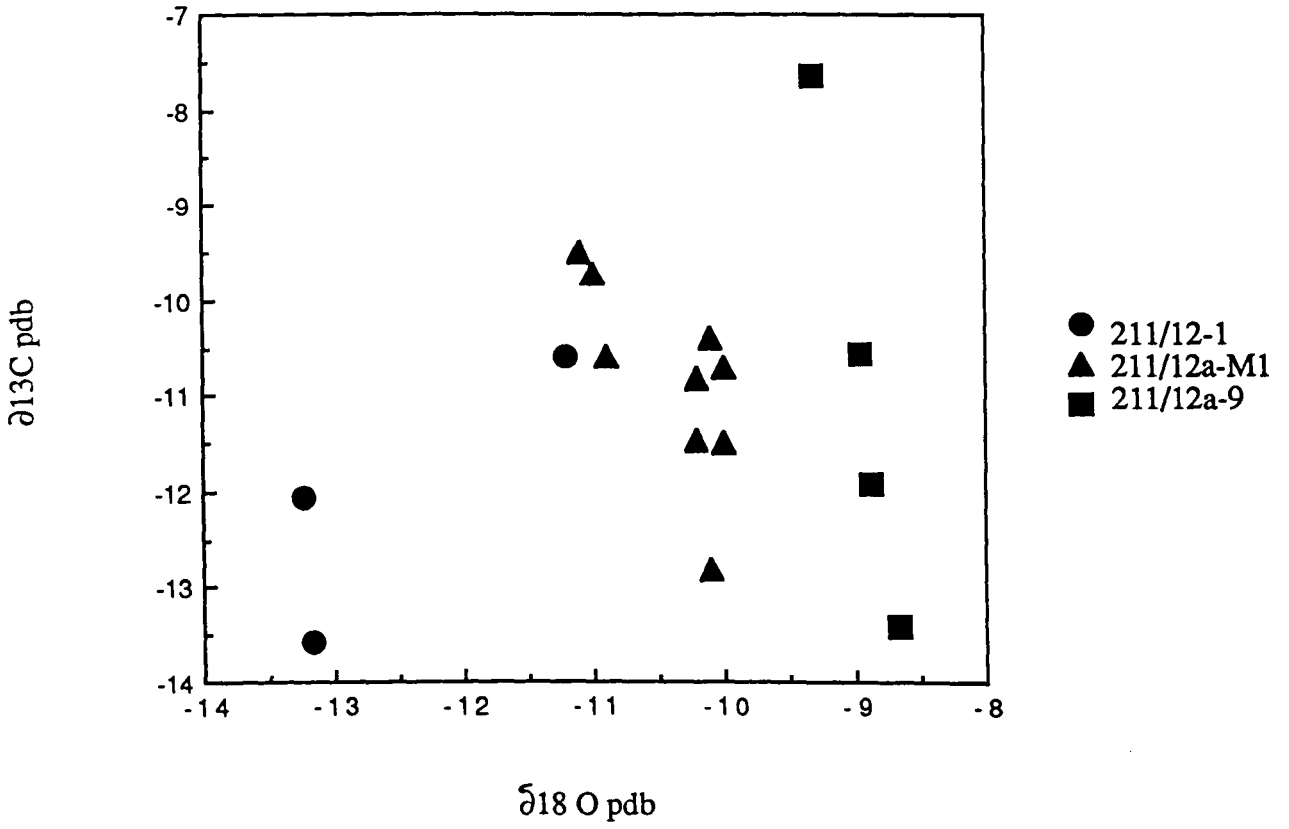
-7
-8
-9
-10
-11
-12
-13
-14
-14
-13
-12
-11
-10
-9
-8
∂13C pdb
∂18 O pdb
211/12-1
211/12a-M1
211/12a-9

Figure 16.

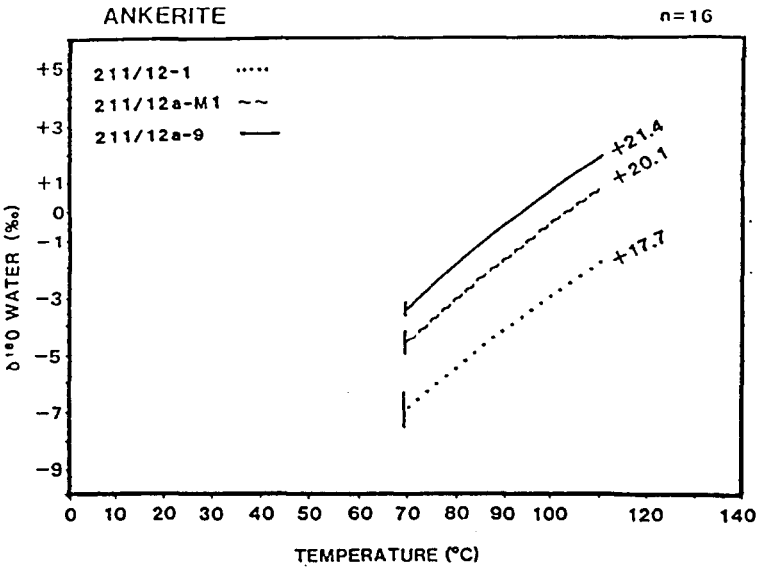

Figure 17a.

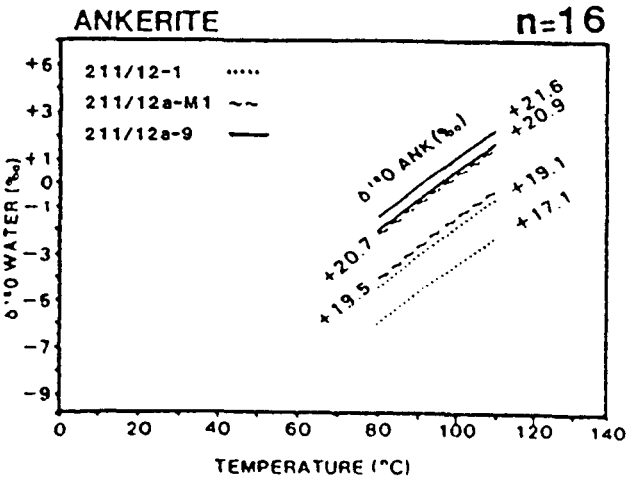

Figure 17b.

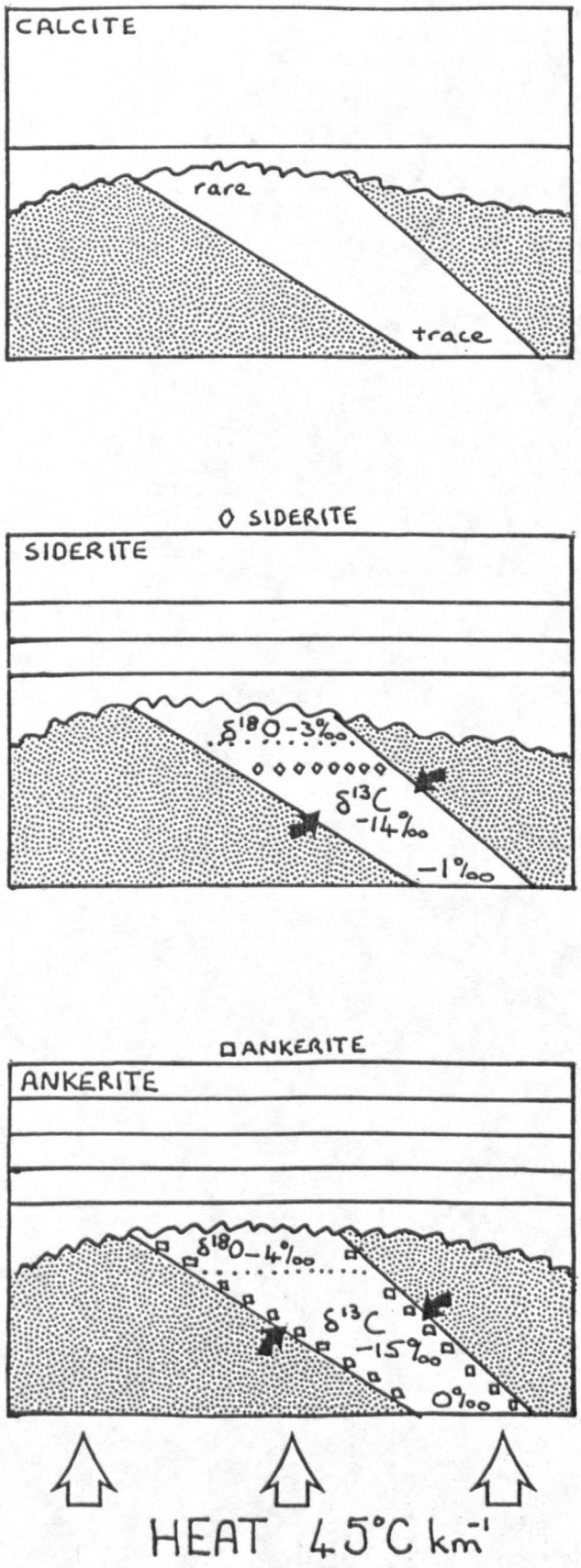
CALCITE
rare
trace
◊ SIDERITE
SIDERITE
δ18O-3‰
δ13C
-14‰
-1‰
□ANKERITE
ANKERITE
δ18O-4‰
δ13C
-15‰
0‰
HEAT 45°C km-1

Figure 18

CHAPTER 4

AN ISOTOPIC STUDY OF DIAGENESIS AND PORE FLUID EVOLUTION IN THE MAGNUS SANDSTONE, NORTH SEA.

C.I.Macaulay*, R.S.Haszeldine*, & A.E.Fallick^.

* Department of Geology and Applied Geology,
University of Glasgow, Glasgow G12 8QQ, Scotland.
^ Scottish Universities Research and Reactor Centre,
East Kilbride, Glasgow G75 0QU, Scotland.

4.1 ABSTRACT

The isotopic compositions of diagenetic minerals from the Upper Jurassic Magnus Sandstone, northern North Sea, were studied to reconstuct the history of porewater composition during diagenesis. Core samples were examined from three wells which lie on a cross-section of the field from the crest to the oil/water contact. A very similar diagenetic sequence was observed in each well, comprising early long-lived quartz overgrowth formation, kaolinite growth, dissolution of feldspar and garnet, followed by growth of magnesian siderite, ankerite and finally illite.

Each diagenetic mineral shows the same pattern in oxygen isotopic composition - consistently more negative values from crestal samples than from deep samples. This is interpreted to reflect retention, in the crest of the field, of a larger component of meteoric-derived pore fluid, which entered the Magnus Sandstone during periods of subaerial erosion from the Upper Jurassic to Mid Cretaceous. During burial diagenesis, the oxygen isotopic composition of the pore fluid evolved to more positive values through time in each well. However fluids from the crest and the flank of the field remained distinct.

The spatial and quantitative distribution of diagenetic minerals suggests not only that local detrital mineral dissolution supplied many of the ions required for diagenetic mineral growth, but also that Si, Ca, Mg, Fe, CO_2 and organic acids were imported from the surrounding Kimmeridge Clay mudstones.

4.2 INTRODUCTION

4.2.1 Geological setting of the Magnus oilfield

In 1974 BP drilled wildcat well 211/12-1 on a structural high northeast of the Shetland Islands. This well found oil-bearing sands in deep water facies of Kimmeridgian age, which became the Magnus field. The Magnus oilfield is located in blocks 211/12 and 211/7, 160km north-east of the Shetland Islands (Figure 1) within the Magnus province, adjacent to the Brent Province, of the East Shetland Basin (De'Ath and Schuyleman, 1981). Upper Jurassic sub-arkosic sandstones form the reservoir, and dip eastwards at 11°. These sandstones are interpreted by De'Ath and Schuyleman (1981) to have been deposited rapidly by a submarine fan which prograded rapidly eastwards into a syndepositional basin during the Kimmeridgian. Depositional thicknesses vary laterally from 202m in 211/12a-9 to 2m in 211/12-4 7km away. Reworked early Oxfordian palynomorphs occur throughout the early Kimmeridgian Magnus sandstone ; De'Ath and Schuyleman (1981) cite this as supporting evidence of a turbiditic depositional mechanism. These same authors introduced "Magnus Sandstone Member" as the formal name for the sandstone sequence occurring within the Kimmeridge Clay Formation : the Kimmeridge Clay is the oil source rock for the reservoir. Well 211/12-5 was used by De'Ath and Schuyleman (1981) as a reference for the Magnus stratigraphy (Figure 2). Since then, the thin Upper Jurassic turbidite sandstones of the Penguin field reservoir have been discovered 12km to the east of Magnus, suggesting the lateral extent of Magnus reservoir sandstones to the east.

The reservoir is 16km long and 4 km wide with an area of 34km^2 (Figure 3). Its base and eastern margin is defined by the oil/water contact, at 3150m subsea, and the western margin by depositional pinchout to the north and south, but by Lower and Mid Cretaceous erosion in the central crestal region (Figure 3). The reservoir is estimated to contain over 1 billion barrels of oil, 565 million of which are estimated to be recoverable (Rainey, 1987). Production began in 1983 and has since levelled at 120000 BOPD.

4.2.2 Structure

To the south-east of the Magnus province lies the Brent province, the most productive hydrocarbon region of the North Sea. Hydrocarbon accumulations occur in Middle Jurassic sandstones on the westward dipping flanks of tilted Jurassic fault blocks. Some of these faults may have originated in the late Triassic during early development of the Viking Graben. However, most of the faults probably had a Devonian or Carboniferous origin (Haszeldine & Russell 1977) and had large syndepositional motions in the Triassic (Glennie 1984). Syndepositional rift faulting occurred in the Lower and Upper Jurassic, with minor thermal subsidence and normal faulting in the Middle Jurassic (Badley et al, 1990). Some fault movement continued throughout the Jurassic, before and after sandstone deposition. Poor quality Middle Jurassic sandstones lie below the Magnus field. Fault alignment in the Magnus area is north/south in the southern part but moves to northeast/southwest in the north (Figure 1). Hay (1978) relates this change to rotation of basement fault blocks along transcurrent faults, but De'Ath and Schuyleman (1981) interpret the change to reflect the influence of the post-Jurassic North Shetland Trough to the North. The southern flank of this basin hosts the Magnus oilfield in the south-eastward dipping flank of a fault block which formed in the early Cretaceous due to rapid subsidence of the trough.

Following rapid deposition of the Magnus Sandstone during the Kimmeridgian followed by Upper Jurassic marine mudstones, early Cretaceous tectonic movements along north-east/south-west structures caused uplift, tilting and erosion of the Jurassic sediments. The Magnus structure was formed at this time. Lower Cretaceous sediments then onlapped this structure before Mid-Cretaceous erosion removed Lower Cretaceous and Jurassic sediments, especially from the northern part of the field. Meteoric water is invoked to have invaded the Magnus Sandstone at this time and to have caused kaolinitisation of detrital feldspars (De'Ath and Schuyleman, 1981). The field was sealed by Upper Cretaceous muds and marls (in contrast to the Brent and Statfjord fields which were sealed by Upper Jurassic or Lower Cretaceous shales). Rapid subsidence and deposition persisted until the late Tertiary. A cross section from NW to SE

through the field , including the three wells studied, is shown in Figure 4a, and the burial history is depicted in Figure 4b. The reservoir is now at its maximum burial and dip, and shows 400m maximum difference in depth between crestal and downdip samples studied. If temperatures were governed solely by conduction, then the maximum temperature difference between crest and flank would be 14 C at present, and18°C for a rift-setting geothermal gradient of 45°Ckm^{-1}.

4.2.3 Petroleum source rocks

The mudstones of the Kimmeridge Clay are considered to be the dominant source rock in the East Shetland Basin and contain type 2 kerogen (Barnard and Cooper, 1981). This consists of a mixture of bacterially degraded algal debris of marine planktonic origin (amorphous liptinite) and degraded humic matter of terrigenous origin (amorphous vitrinite). This amorphous component is mixed with variable amounts of particulate vitrinite (woody debris) and inertinite - highly altered (oxidised or burnt) material of land plant origin. Land plant spores and marine algae are present in trace amounts. Total Organic Carbon ranges from 1-30% in the Kimmeridge Clay, although weighted averages in any section usually range from 5-10%, being higher towards depocentres (Bernard and Cooper, 1981). Magnus crude is a light oil of API 39°, supporting its link with the high sapropelic kerogen content Kimmeridge Clay source rocks (De'Ath and Schuyleman, 1981).

In the East Shetland Basin, the Kimmeridge Clay and its equivalents lie at depths of >3000m over most of the area (Day et al, 1981). From the present maturity gradient, Goff (1983) calculates that the oil-generating window extends from 2500-4500m with peak generation at around 3250m. Therefore the Upper Jurassic shales are mature over much of the basin area. Peak generation occurred during the Palaeocene in the Viking Graben and during the late Eocene in the deeper parts of the East Shetland Basin. Migration distances in Magnus are short, only a few kilometres (Barnard and Cooper, 1981), and the reservoir sandstones interfinger downdip with Kimmeridge Clay Formation source rocks.

4.2.4 Magnus Sandstone facies

The Magnus Sandstone Member comprises four stacked depositional lobes of submarine fan sandstones (Rainey, 1987) : the lowermost unit, lobe 1, is confined to the central area of the field and contains about 3% of the oil-in-place; lobe 2 is present over most of the field except the northern extremity and contains about 59% of the oil-in-place ; lobe 3 is present mainly in the north of the field and contains about 38% of the oil-in-place. Lobe 4, recognised in the cored interval of 211/12a-9, is of minor importance to the reservoir and thickens into the basin by offlap to the north east. Extensive sealing shale barriers caused non-uniform reservoir depletion as a result of production. The main barriers identified were between lobes 1 and 2 and between lobes 2 and 3. Secondary restrictions to fluid flow between wells are caused by faulting (Atkinson, 1985). Thick bedded sandstones (Facies A of Rainey, 1987) represent the most common lithofacies in Magnus cores, and bed thicknesses range from an average of 2.67m in crestal well 211/12-1 to 1.66m in downdip well 211/12a-9 (Rainey, 1987). Rainey (1987) identified four other facies in the Magnus Sandstone member : Facies B which consists of medium bedded very fine-fine grained sanstones with moderate sorting which were deposited by "classical" turbidity currents ; Facies C which comprises thinly interbedded sandstones, siltstones and mudstones ; Facies D which consists of sediments affected by post-depositional mass movements such as slumping and debris flows ; Facies E which consists of organic-rich mudstones with thin laminations of siltstone and very fine-grained sandstone. In 211/12-1 Facies A comprises 77.8% of the total facies thickness of 48.19m. The remainder is made up of Facies B 8.7%, Facies C 11.1% and Facies E 2.4%. Facies D is absent in 211/12-1. Downdip in well 211/12a-9 Facies A comprises 65.7% of the total facies thickness of 204.2m, Facies B 7.0%, Facies C 7.5%, Facies D 5.8% and Facies E 13.9%. Beds commonly fine upwards, with increasing mica towards the top. Grain size is mostly fine-medium but occasionally coarse, and sorting is generally poor. Grain sphericity is subangular to subrounded. Rainey (1987) found no evidence of bioturbation, suggesting that depositional conditions were anoxic.

4.2.5 Detrital mineralogy

Detrital mineralogy was determined by examination of 43 thin sections. The results of point-count data (500 counts per section) are presented in Tables 1-3 for wells 211/12-1, 211/12a-M1 and 211/12a-9. The detrital mineralogy will be expressed as a % of whole rock volume. Monocrystalline quartz forms up to 60% whereas polycrystalline quartz is relatively rare and always less than 5%. Feldspars, dominantly orthoclase, comprise 10-20% with minor albite and microcline. Mica, dominantly muscovite, constitutes 0.6-2.6%. Detrital clay clasts comprise 0.6 to 17.2% and are more abundant in finer grained thinner sandstone beds. Rock fragments of quartz and feldspar, and quartz and mica (Rainey, 1987), are minor constituents.
Heavy minerals, dominantly pink almandine garnets, can form up to 2%. Other minor-trace components are organic fragments, zircons, rutile and tourmaline.
Minus cement porosities range from 15 to 32% and are generally lowest in fine grained sandstones interbedded with mudstones and highest in thick bedded Facies A sandstones.

4.3 Analytical techniques

Petrography was studied by standard optical microscopic examination of thin sections impregnated with blue epoxy. Scanning Electron Microscopy (SEM) was performed using a Jeol 35CF and a Cambridge Instruments S360 with Link AN 10000 Eds system. Cathodoluminescence studies utilised a Technosyn cold cathode luminescence 8200 Mk 2 unit. SEM cathodoluminescence analyses were performed on a Cambridge Instruments S360 SEM with an Oxford Instruments CL detector.
Fluid inclusion microthermometry was attempted using a Linkam TH600 heating/freezing stage (Shepherd, 1981) mounted on a Leitz Dialux 20-EB binocular microscope with long working distance condenser lens giving magnification of x1250. Double polished fluid inclusion wafers 40-100μm thick were prepared by the method of Crosbie (1981).

Bulk sandstone and mineral separate mineralogy analyses were performed by X-ray diffraction (XRD). Oriented samples were sedimented in acetone onto glass slide mounts and air dried. Analyses were run on a Philips 3kw diffractometer using Fe filtered Co-Ka radiation with 0.5 divergence,

antiscatter slits and a 0.1° micron receiving slit for clays and a 1° divergence, antiscatter slits and 0.1° micron receiving slit for whole rock.

4.4 ISOTOPIC ANALYSES

4.4.1 Sample preparation methods

Quartz overgrowth oxygen isotope analyses were performed by the method described by Milliken et al (1981). This derives the $\delta^{18}O$ value of overgrowths by a mass balance method, involving analysis of detrital quartz grains with overgrowths attached and detrital quartz grains from which overgrowths have been removed using HF. Overgrowth abundance, originally underestimated by thin-section point-counting, was more accurately obtained (to ±1% whole rock) using SEM cathodoluminescence.

Clay separates were obtained by sieving off the <160μm fraction then using standard gravity settling and centrifuging techniques described by Jackson (1979). Sample purities were checked by XRD and SEM.

Carbonate minerals and pyrite were separated from the 160-250μm fraction by 1,1,2,2 Tetrabromoethane heavy liquid separation and experimentation with a Frantz Isodynamic magnetic separator. Sample purity was checked by XRD.

4.4.2 Oxygen isotope analysis of silicate minerals.

Oxygen was liberated from approximately 10mg samples of purified silicate minerals (quartz, kaolinite or illite) by oxidation reaction with ClF_3 (Borthwick and Harmon, 1982) in nickel reaction vessels at 650°C. The oxygen was cleaned and reduced to CO_2 using a vacuum extraction line similar to that described by Clayton and Mayeda (1963). The oxygen yield was determined by comparing the starting weight of mineral with the number of micromoles of gas produced. A VG-SIRA 10 mass spectrometer was used to analyse the CO_2

4.4.3 Hydrogen isotope analysis of kaolinite and illite.

Hydrogen was extracted from kaolinite and illite (30-50mg samples) by heating samples under vacuum to release bound hydrogen, mostly as water vapour. Water is converted to hydrogen by reaction with hot uranium. Samples were placed into platinum crucibles which had previously been heated to 1500°C for >3 hours, and the sample + crucible was evacuated and degassed at 120°C overnight prior to hydrogen extraction. Details of the technique are described by Jenkin (1988). The hydrogen yield was determined by comparing the starting weight of mineral with the number of micromoles of gas produced. The extracted hydrogen was analysed using a VG Micromass 602B mass spectrometer.

4.4.4 Sulphur isotope analysis of pyrite

Pyrite (~5mg samples) was reacted with excess Cu_2O as an intimate mixture at 1070°C to produce SO_2 (after Robinson and Kusakabe, 1975) The SO_2 was analysed for $\delta^{34}S$ on an Isospec 44 mass spectrometer modified for SO_2.

4.4.5 K/Ar dating of illite

Illite ages were calculated by combining the K percentage, obtained by flame photometry of around 10mg of illite, and an argon value obtained by standard mass spectrometry. Approximately 50mg of pure sample was used, after overnight degassing at 100°C, to remove any adsorbed water.

4.4.6 Standards

Throughout this study oxygen and hydrogen isotopic variations in silicate minerals are reported relative to Standard Mean Ocean Water (SMOW : $\delta^{18}O$, δD 0‰) as defined by Craig (1961). The NBS 28 standard gave values of 9.6‰±0.2SMOW during the course of these analyses, and a kaolinite laboratory standard, calibrated using NBS 30 which has δD -64‰, gave values of δD -55‰±2SMOW. Carbon and oxygen isotope variations in carbonate minerals are reported relative to the Peedee Belemnite (PDB : $\delta^{13}C$ 0‰) (Craig, 1957), and additionally for oxygen, to SMOW. NBS 20 standards gave $\delta^{18}O$ 26.5‰±0.2 SMOW and $\delta^{13}C$ -1.2‰±0.2PDB. Variations in sulphur isotope ratios are reported relative to the Canyon Diablo Troilite (CDT : $\delta^{34}S$

0‰) after Thode et al (1961). Reproducibility of results is to within ±0.2‰ for $\delta^{18}O$, $\delta^{13}C$ and $\delta^{34}S$ analyses, with the exception of quartz overgrowth analyses where point count errors lead to a reproducibility of ±0.5‰. Reproducibility for δD analyses is ±2‰.

4.4.7 Sampling strategy

Typical reservoir sandstones, sandstones from within mudstones and mudstones were sampled. All samples were studied in thin-section and by SEM prior to isotopic analysis. Samples were collected from lobes 1, 2 and 3 in all wells and, in addition, from lobe 4 in 211/12a-9.

4.5 DIAGENETIC MINERAL PETROGRAPHY

The generalised paragenetic sequence for the Magnus Sandstone is described below and shown in Figure 5. Optical microscopy, Scanning Electron Microscopy (SEM) and EDS analyses, cathodoluminescence and backscattered electron imaging were employed in the determination of the paragenetic sequence.

4.5.1 Glauconite

Glauconite is a mica mineral which is found almost exclusively in marine sediments, although in many respects it can validly be considered as a clay mineral similar to illite (Deer, Howie and Zussman,1966). It forms at the interface between oxidizing and reducing environments in sediments, where Fe^{3+} is transiently available in solution (Ireland et al, 1983). In the Magnus Sandstone it is present in very minor amounts (<<1%) as rounded grains or pellets 100-200μm in diameter. These pellets are generally dull green or green/brown when viewed in thin section in plane polarised light and lack internal features. Often glauconite pellets are observed to have been compactionally deformed and squeezed into the pore spaces between detrital silicate grains, indicating that they were originally soft and ductile. Glauconites contain both ferric and ferrous iron which indicates that they form under moderately reducing conditions of the type which occur commonly through the action of sulphate reducing bacteria on decaying organisms (Deer, Howie and Zussman,1966).

4.5.2 Illite 1

Early diagenetic illite occurs as "hand-like" plates and fronds which are developed perpendicular to detrital grain surface. Although not volumetrically significant, this early illite may have been an important substrate for the nucleation of later fibrous pore-filling illite. McHardy et al (1982) showed that critical-point drying of preserved samples is essential for analysis of reservoir illite morphology : critical-point dried samples contain a dense basketwork of fine interwoven late illite fibres whereas air-dried illite has collapsed onto pore margins Care must therefore be exercised in the distinction of early and collapsed late illite. Early illite shows blunt terminations to fronds, suggesting dissolution, and is overgrown by later diagenetic quartz (Figure 6).

4.5.3 Pyrite 1

Two distinctly different morphologies of the iron sulphide pyrite have developed during the diagenesis of the Magnus Sandstone. An early diagenetic form is framboidal, and each 10μm framboid is clearly observed to be composed of tightly packed individual octahedral crystallites (Figure 7). Both solitary and clustered framboids occur. Framboids form close to the sediment/water interface through the action of anaerobic sulphate-reducing bacteria. Fisher and Hudson (1987) have identified four prerequisites for pyrite formation :

1. Anoxic conditions in which the bacteria may function.
2. Sulphate supply - chiefly seawater sulphate.
3. Appropriate organic material as a substrate for the sulphate-reducing bacteria.
4. Iron for the conversion of H_2S to iron sulphide.

The marine turbidite sandstones of the Magnus Sandstone Member and the enclosing Kimmeridge Clay Formation satisfied all these conditions at deposition, and during shallow burial until the first of several phases of uplift began in the early Cretaceous (Figure 4b). As well as forming framboids, pyrite replaced organic matter. Small pyrite concretions (~

10mm) are developed in silty bands in the Kimmeridge Clay. The bedding in the mudstones has been compressed and deformed around these, demonstrating their pre-compaction growth. The sandstones in wells 211/12-1 and 211/12a-M1 in the crest of the field contains very little or no framboidal pyrite compared to distal well 211/12a-9, suggesting that Early Cretaceous meteoric water ingress may have oxidised the early diagenetic framboidal pyrite.

4.5.4 Kaolinite 1

Early diagenetic kaolinite is not a common mineral : estimates of its abundance suggest that it forms less than 5% total kaolinite. It is developed across the field in the form of clustered fine grained euhedral crystals (<5μm) and coarse grained (>30μm) sheets which are the direct result of muscovite degradation (Bjorlykke and Brensdal, 1986). Quartz overgrowths can almost completely enclose the early euhedral kaolinite (Figure 8). Dissolution of vulnerable detrital grains such as feldspars, partially dissolved or fractured in transport, may have contributed to early kaolinite growth.

The occurrence of diagenetic kaolinite in sandstone and its relationship to unstable framework grains has been established for many years (Fuchtbauer, 1974 ; Nagtegaal, 1978). Bucke and Mankin (1971) recognised that a combination of factors was important for kaolinite formation :

1. low pH
2. K feldspar as a source of Al and Si.
3. Low K^+ activity eg. illite as a K^+ acceptor.
4. Water filled pores as a medium for ion transport.

These conditions existed early during the burial of the Magnus Sandstone, with the qualification that meteoric water as well as organic matter were likely sources of acid for feldspar dissolution, and muscovite was an important additional source of Al and Si.

4.5.5 Calcite

Calcite is not a common diagenetic mineral in the Magnus Sandstone. Only four grains were identified during this study, one from downdip well 211/12a-9 and three from intermediate well 211/12a-M1, although non-ferroan calcite concretions have been found in a recent core from a crestal well, 211/12a-M10 (D. Emery BP, pers. comm. 1989). One reason for the scarcity of calcite may be restricted Ca supply : detrital shell material is very scarce in the Magnus sediments, leaving only limited plagioclase as a source of Ca.

4.5.6 Secondary porosity

Dissolution of K-feldspar has created significant secondary porosity in the Magnus sandstone (Figures 9 to 11a), as is discussed later in the section on cement distribution. Further minor secondary porosity has been contributed by garnet dissolution(Figure 11b). Mineral dissolution which releases cations in solution can occur in significant quantities only in the presence of an acid (Land et al, 1987). Feldspar dissolution is controlled by the rate of reaction at the crystal surface. Where a surface reaction is the rate-limiting step, reaction rates are much more sensitive to temperature than those where transport of products or reactants to or from the crystal face is the rate-limiting step. Thus with burial and increased temperature reaction rates increase (Giles and Marshall, 1986). Creation of secondary porosity is balanced by precipitation of diagenetic quartz overgrowths, kaolinite and very minor titanium oxides in pore space as a result of detrital mineral dissolution.

Sources of acid include inorganic and organic processes (Land et al, 1987 ; Giles,1987). Inorganic sources include reverse weathering reactions involving silicate minerals in shales and thermally driven oxidation reactions involving sulphur and/or iron (Bjorlykke, 1983 ; Edman and Surdam, 1986), meteoric water (Bjorlykke, 1983) and mixing corrosion (Plummer, 1975). Organic sources include acidic fluids generated from CO_2 produced by thermal maturation of organic matter (Schmidt and McDonald, 1979) and organic, dominantly acetic, acids generated during thermal maturation of organic matter (Surdam et al, 1984). Acid generated from organic sources would have to migrate into the Magnus Sandstone without

being neutralised by reactions internal to the enclosing Kimmeridge Clay mudstones (Giles and Marshall, 1986). However, Kimmeridge Clay mudstones from the Magnus field contain very little or no carbonate (Rainey, 1987), and acid migration distances to the Magnus Sandstone are short.

Isotopic and textural data discussed later suggest that widespread feldspar dissolution occurred during late diagenesis at elevated temperatures, and not during early exposure to meteoric water. Late diagenetic carbonate minerals have $\delta^{13}C$ values indicative of CO_2 generated by thermal decarboxylation of organic matter. Detrital garnet grains are etched along rhombic faces in a manner akin to that described by Hansley (1987) as being the distinctive result of organic acid leaching. The Magnus Sandstone is sealed within the unusually organic-rich Kimmeridge Clay. Organic acid producing processes are therefore suggested to be the dominant acid source which has resulted in mineral dissolution, although in other oilfield studies (Lundegard et al, 1984 ; Giles and Marshall, 1986 ; Land et al, 1987) material balance calculations indicate that organic acid sources are insufficient to account for observed secondary porosity. Land et al (1987) postulate that if organic acids and CO_2 are the proton sources involved in mineral dissolution, then they must be synthesised from reaction of kerogen with water or some other oxygen source.

4.5.7 Diagenetic feldspar

Feldspar overgrowths occur both as albite overgrowths on detrital plagioclase grains and orthoclase (K feldspar) overgrowths on detrital potassium feldspar grains. K feldspar overgrowths are by far the most abundant. Usually, feldspar overgrowths comprise <<1% of the whole rock, however locally they can form up to 2% (eg 211/12a-M1, 2952.1m) as determined by 500 count per thin section point counts. Overgrowths range in size from individual euhedral crystallites <10μm long (pure orthoclase composition), as developed on the extensively dissolved detrital potassium feldspar grain in Figure 9, to grain rimming cements up to 30μm thick eg Figures 10 (pure albite composition), 11a(pure orthoclase composition). Feldspar overgrowths usually display obvious optical discontinuity with their detrital hosts. K feldspar overgrowths are preserved on detrital hosts displaying many degrees of dissolution. In some examples K feldspar

overgrowths around the perimeter of an empty pore space may be the only evidence of a pre-existing detrital potassium feldspar grain. In others overgrowths are developed around partially sericitised detrital grains and in others still around completely fresh host grains. This suggests that feldspar dissolution occurred before and after feldspar overgrowth development. In backscatter electron images diagenetic K feldspar has also been observed to heal fractures and cracks in detrital potassium feldspar grains (Figure 10).

Textural relationships observed in thin sections and SEM indicate that K feldspar overgrowths developed prior to or contemporaneous with quartz overgrowth formation ie. relatively early in the diagenetic sequence. Dissolving detrital grains such as feldspar (Figure 11a) and garnet (Figure 11b) were ion sources at this time.

The scarcity of diagenetic albite has made difficult its firm timing in the diagenetic sequence. It has been observed only as euhedral overgrowths up to 30μm thick growing into free pore space. Overgrowths observed in well 211/12a-9 have a pure albite composition. Analysis of feldspar abundance in the Magnus Sandstone compared to feldspar dissolution from point counts (Tables 1-6), shows that potassium feldspar is now considerably more abundant than plagioclase, both in terms of original deposition mineralogy and diagenetic feldspar. Potassium feldspar has suffered considerably more dissolution than plagioclase. This, and the burial depth of only 3200m, combine to explains the relative scarcity of albitization in the Magnus Sandstone (the most obvious alternative sources of minor Na are from seawater or smectite->illite reactions : present day Magnus formation water has a salinity approximately half that of seawater (De'Ath and Schuyleman, 1981) and the detrital clays of the Kimmeridge mudstones contain only 20% smectite at most (Dypvik, 1983 ; Hansen and Lindgreen, 1989)). The albitization reaction of Boles (1982) and Boles and Coombs (1977) requires substantial amounts of Si and Na to proceed, and temperatures in excess of 120°C.

4.5.8 Quartz overgrowths

Quartz cementation in the form of syntaxial overgrowths on detrital quartz grains is ubiquitous throughout the Magnus Sandstone in the wells studied. Overgrowths range in size from individual tiny crystal euhedra 1-20μm

across (Figure 12a) to grain rimming cements 60 μm thick (Figure 12b). Grain rimming overgrowths develop either through coalescence of individual euhedra or development of dominant euhedra which envelop surrounding euhedra (Pittman, 1972). In addition, rare outgrowths or long prismatic overgrowths up to 100μm in length have been observed (Figure 13). Quartz overgrowth abundances from thin-section point-counts range from 0.6 to 8.2% whole rock, but the results of SEM CL analyses, discussed later, suggest that these are underestimates.

Quartz overgrowth development here is inferred to be by direct precipitation of silica from solution, producing well ordered alpha-quartz (McBride, 1989). Overgrowths develop with the same crystallographic orientation as, and in optical continuity with, the detrital host grain. In thin section quartz overgrowths were identified by their prismatic terminations, "clean" appearence compared to the inclusion-rich detrital grains and by poorly developed lines of small fluid inclusions along the detrital grain/overgrowth boundary (Figure 14). Boundary inclusions and "dust rims" are the most commonly used indicators of the detrital grain margin. However, in the Magnus examples no dust lines are present and boundary inclusions are usually poorly developed. Late quartz precipitation along capillary pores may have obscured dust rims (Pittman, 1972), or any detrital "dust" clays may have dissolved during meteoric flush. Poor overgrowth/detrital host distinction causes problems both for measuring quartz precipitation temperatures by fluid inclusion microthermometry, and for point count determination of the abundance of quartz overgrowths.

Cathodoluminescence studies of detrital quartz grains in polished thin sections showed both red/brown colours, indicitave of a metamorphic source, and blue colours indicitave of a plutonic source (Zinkernagel, 1978). Diagenetic quartz overgrowths from the Magnus Sandstone remained non-luminescent even under instrument operating conditions in which Brent Sandstone quartz overgrowth examples luminesced dull red/brown (Brint, 1989). However SEM cathodoluminescence (SEM CL) studies of Magnus Sandstones allowed delineation of at least three growth zones within some overgrowths (Figure 15), and chaotic turbid growth zones in others. These zones are perhaps related to factors such as lattice order and ionic substitution, especially by Al^{3+} in the quartz overgrowth (Matter and Ramseyer, 1985). Henry et al (1986) documented variable Al^{3+} concentrations as a source of complex zoning in overgrowths. Other North Sea oilfields from which complex zoning in quartz overgrowths have been reported

include Piper (Burley 1986) and Alwyn (Hogg, 1987). Textural observations from SEM images often show stepped overgrowths, which most likely developed by periodic precipitation of new layers (Figure 16).
Thin section petrography, SEM, and SEM cathodoluminescence observations indicate that quartz overgrowths had developed relatively early in diagenesis and prior to kaolinite 2 formation (Figure 12b). Quartz overgrowths continued to develop through diagenesis and are at least partly cogenetic with illite, the last diagenetic mineral to form, as evidenced by overgrowths enclosing the ends of illite fibres (McHardy et al, 1981 ; Rainey, 1987) (Figure 17).

4.5.9 Kaolinite 2

Most of the kaolinite in the Magnus Sandstone grew in this period, forming 2.2-12.4% whole rock. Kaolinite infills both primary and secondary porosity. Diagenetic kaolinite in the Magnus Sandstone displays morphological differences across the field. SEM, backscatter electron and thin section petrography show that kaolinite in the crestal area from wells 211/12-1 and 211/12a-M1 is predominantly vermiform (Figure 18), whereas downdip in 211/12a-9 it is mostly blocky in character (Figure 19). Hurst and Irwin (1982) studied the relationship between kaolinite morphology and porewater composition. According to their model, a meteoric-derived water flux results in rapid generation of "nutrient" ions (Al^{3+}, Si) in solution through dissolution of unstable detrital grains such as feldspar and mica. Consequent rapid kaolinite growth results in a vermiform texture. In the absence of meteoric porewater flux, such as in a shale-enclosed marine sandstone, kaolinite growth would be expected to proceed more slowly, leading to finer grained euhedral kaolinite with a crystallinity more akin to the ideal kaolinite a:b:c ratio of 0.5 : 1 : 0.8 (Deer, Howie and Zussman, 1966), where a is the thickness of the crystal, b the length and c the breadth.

De'Ath and Schuyleman (1981) first suggested that during Lower-mid Cretaceous erosion of the Magnus Sandstone the reservoir was probably exposed to meteoric water which may have caused kaolinitisation of the feldspars. Rainey (1987) suggested that the occurrence of kaolinite in close association with degraded feldspars suggests that Al^{3+} was conserved. Using bulk geochemical methods, he found that kaolinite distribution showed no systematic relationship with proximity to the overlying unconformity

surfaces and concluded that meteoric water penetrated all parts of the reservoir to the same degree. Point count data obtained from thin sections in this study suggest slightly greater abundance of kaolinite downdip in the sandstones of well 211/12a-9 (Figure 20), compared to 211/12-1 and 211/12a-M1. Emery et al (1988) studied core from 0-9m below the unconformity in an unreleased Magnus crestal well. Their petrographic study found that potassium feldspar concentration increased from 9% to 18% total rock, increasing away from the unconformity, whilst natural gamma log showed an increase in K concentration from 0.9 - 1.8% across the same 9m of sandstone. The presence of relict dissolved potassium feldspar in oversized pores, plus enhanced porosity and permeability, demonstrated this to be the result of enhanced feldspar dissolution near the unconformity.

In a study of kaolinite in the mid-Jurassic Gullfaks field of the Norwegian sector of the North Sea, Bjorkum et al (1990) concluded it to be unlikely that much kaolinite, formed during exposure, is preserved in the sandstone underlying the late Cimmerian unconformity, except immediately below the unconformity. This is because the sandstone erosion rate during tectonic rotational elevation of the fault block was probably faster than the feldspar dissolution front propagation rate. They, like Emery et al (1988), observed only a very local (<10m) zone of kaolinitisation adjacent to unconformities in marine sandstones which were low in detrital kaolinite and had not been exposed to immediate post-depositional meteoric flushing.

4.5.10 Pyrite 2

Late diagenetic pyrite is cubic or octahedral in morphology and is less common than framboidal pyrite in deep well 211/12a-9. Late diagenetic pyrite occurs in the Magnus sandstone in all the wells studied. Crystals range in size from 10-50μm across. Commonly this late pyrite is associated in space, and by implication in time, with degradation of detrital biotite grains and mud clasts (Figure 21), and the development of diagenetic magnesian siderite rhombs. Cubic pyrite has also nucleated and grown on earlier framboidal pyrite.

4.5.11 Magnesian siderite

Magnesian siderite comprises discrete individual rhombs and clusters of rhombs 100-200μm in length infilling primary and secondary pore space. Also, aggregates of small siderite rhombs 10-30 μm in length replace detrital biotite grains and mud clasts (Figure 22). Biotite-replacing magnesian siderite commonly occurs with associated cubic and/or octahedral pyrite. This has been reported in many Brent Group North Sea oilfield sandstones (Bjorlykke and Brensdal, 1986 ; Brint, 1989), and explained theoretically by Boles and Johnson (1983). Magnesian siderite has developed in both primary intergranular porosity and secondary feldspar dissolution porosity , and often replaces pore-filling kaolinite which was the product of feldspar dissolution (Figure 23a,b). Note also in Figure 23a that kaolinite post-dates the growth of diagenetic quartz overgrowths. Thus siderite growth is constrained petrographically by earlier feldspar dissolution, quartz overgrowth and kaolinite development, and by later ankerite development (Figure 24).

4.5.12 Chlorite

Only trace amounts of chlorite were observed. One sample from 211/12a-M1 exhibited "rosette" structure chlorite. Each rosette is composed of several plates ~ 5μm in diameter. Most of the observed chlorite was present in the "beehive" form, which is unusual (Welton, 1984), and in this case can be directly attributed to be the result of detrital biotite replacement. Chlorite plate size in the "beehive" structure is also ~ 5μm (Figure 25). Note that later quartz overgrowths have enveloped some of these diagenetic chlorite plates.

The studies of Hayes (1970), Boles and Franks (1979) and Curtis et al (1985) indicate that diagenetic chlorites in sediments form under conditions of moderate to deep burial at temperatures between 60 to 150°C. The delicate "rosette" morphology suggests growth from porewater solutes, whereas the "beehive" structure is obviously a replacement of precursor biotite. Boles and Franks (1979) thought the illitization reaction to be the source of Fe^{2+} and Mg^{2+}, whilst Iijima and Matsumoto (1982) argued for the reaction of siderite with kaolinite to produce berthierine. Both of these reactions produce acid which, if quantitatively significant, could affect the stability of other phases present. Reduction of oxidised iron causes an increase in

alkalinity (Curtis, 1985) and would favour coprecipitation of ferroan carbonates such as ankerite. Octahedral substitution of Al^{3+} for Fe^{3+} in glauconite through burial diagenesis (Ireland et al, 1983) is a possible source of oxidised iron in the Magnus sandstones.

4.5.13 Ankerite

Ankerite occurs both as individual pore-filling crystals up to several hundred microns across and as poikilotopic cements (Figure 14) which are most common adjacent to mudstones.These may completely fill the porosity of thin sandstones which are enclosed in mudstones, suggesting that reactions occurring during mudstone diagenesis may have released Ca, Mg, Fe and CO_2 for ankerite development. Ankerite clearly post-dates quartz overgrowths and magnesian siderite in the diagenetic sequence, but is intergrown with the tips of late diagenetic illite fibres (Figure 26).

4.5.14 Illite 2

Late diagenetic filamentous illite has important implications for reservoir quality. Delicate fibrous illite was observed in crestal wells 211/12-1 and 211/12a-M1, but is more abundant in downdip well 211/12a-9. McHardy et al (1982) described characteristic extensive pockets or mats of intertwined ribbons, often radiating out from stiffer, thicker laths. These thicker laths formed in early diagenesis. Illite also replaces kaolinite, with delicate illite fibres bridging between kaolinite plates (Figure 27). 211/12a-9 was cored mainly through the water leg, and K/Ar dates suggest that illite continued to grow beneath the oil/water contact after diagenesis had been arrested in the oil pool (see following isotope section). Reduction in sandstone permeability because of filamentous illite migration and blocking of pore throats was postulated by Gray and Rex (1966), and the detrimental effect of illite morphology itself was established by Seeman (1979). In a recent study of diagenetic illites from Brent Group sandstones in the Cormorant field, Kantorowicz (1990) described a similar sequence of illite development to that seen in Magnus. He contrasted the physical sizes of illite particles in the Magnus and Cormorant fields with thicker illite particles from Rotliegendes sandstones which have been buried to high temperatures (>100°C) for 50-60 Myr using a concept analogous to TTI heating for organics (Lopatin, 1976). Illite particles from Magnus are very thin (10Å), and are the thinnest illite

particles that can exist (Nadeau, 1985). Their growth was probably kinetically controlled requiring temperatures approaching 100°C (Bjorkum and Gjelsvik, 1988). The Magnus Sandstones have been buried to 100°C only during the last 10-25 Myr (Kantorowicz, 1990) and so their delicate morphology is the result of rapid growth over a short time span.

4.6 CEMENT DISTRIBUTION

Distribution of quartz, kaolinite, magnesian siderite and ankerite cements are plotted on generalised sedimentary logs for wells 211/12-1, 211/12a-M1 and 211/12a-9 in Figures 28-33. Plots were compiled from data obtained by point counting of thin sections (500 counts per section). It is important to note that the grainsize of the sandstone samples is very similar. This minimises the possibility of differences in original % feldspar in different samples due to grain size differences - as is a problem for diagenetic studies in other sandstones. Thus, all the sandstones samples can be equally compared.

Quartz overgrowth and kaolinite data are plotted against detrital feldspar content (Figures 28-30). The plots for all three wells show an antithetic (ie. high feldspar = low quartz and kaolinite) relationship between feldspar content and quartz and kaolinite cementation. This suggests that feldspar dissolution was an important source of ions for quartz and kaolinite cement. Assuming that original sandstone feldspar abundances were approximately equal throughout the Magnus sandstone and that Al^{3+} was conserved (Curtis, 1983), the probable reaction was:-

Reaction 1

$$2KAlSi_3O_8 + 2H^+ + H_2O \rightarrow Al_2Si_2O_5(OH)_4 + 4SiO_2 + 2K^+$$

Orthoclase Kaolinite

If the reaction products are not removed from the sandstone, leached feldspar will reprecipitate 60% kaolinite and 40% quartz by volume (Bjorlykke, 1983). Quantification of this reaction using point-count data of the abundances of quartz and kaolinite cements and the amount of feldspar dissolution are presented in Tables 4-6. Partially dissolved feldspars were

normalised as being 50 % dissolved on average and added to the percentage of completely dissolved feldspars to derive the figure for total percentage feldspar dissolution. Kaolinite point-count data as presented are not corrected for microporosity between crystals which could be as high as 50% for loosely packed blocky kaolinite, but probably less for more closely packed crystals in the crestal vermiform variety . SEM cathodoluminescence analyses of polished thin sections show that point-count determination of quartz overgrowth abundances are underestimates, sometimes by as much as half (Table 7). These underestimates result from the difficulty of distinguishing, by standard optical petrography, between detrital and diagenetic quartz when dust rims or boundary inclusions between detrital host grain and overgrowth are poorly developed or undeveloped. Even with these point counts systematically over-estimating %kaolinite and under -estimating %quartz overgrowth, feldspar dissolution can account for a significant proportion of diagenetic quartz precipitated in most, but not all, of the Magnus Sandstone samples observed. Silica must therefore have been imported to the sandstone. Alternative possible sources of silica are still needed : dissolution of biogenic silica such as sponge spicules and other unstable detrital minerals such as micas and garnets, clay transformation reactions such as smectite->illite (Foscoles and Powell, 1979), pressure solution between quartz grains and efflux of silica from mudstones. Evans (1989) and Astin and Evans (1990) calculate that 10-20% of the solid volume of shales may be lost during burial diagenesis (>1km depth), primarily through quartz dissolution.

Point-counted kaolinite volumes are typically less than calculated theoretical volumes for kaolinite produced through detrital feldspar dissolution in crestal wells 211/12-1 and 211/12a-M1, but are higher in deep well 211/12a-9. Kaolinite point-count data are rather subjective in that a pore filled with kaolinite contains considerable microporosity and therefore point counted kaolinite abundances are probably overestimates. Also, kaolinite formed through degradation of other detrital minerals such as muscovite, a common reaction in the Magnus Sandstone, is not accounted for in the calculations from Reaction 1, and can be significant contributers (Bjorlykke and Brensdal, 1986). Nevertheless, the data suggest that more kaolinite has formed from feldspar dissolution in deep water-wet well 211/12a-9 than in the crestal wells. Hayes and Boles (1990) reported similar observations from sandstones of the San Joaquin basin, where they suggested that higher concentrations of organic acids in deep sandstones,

more isolated from meteoric water recharge were important for Al^{3+} mobilisation. Curtis (1983) demonstrated the importance of organic acid complexing and pH for Al^{3+} mobility during feldspar dissolution and kaolinite precipitaion.

Magnesian siderite and ankerite distribution plots (Figures 31-33) show the same patterns in all three wells. In each well, magnesian siderite is distributed throughout the Magnus Sandstone. This probably reflects the distibution of detrital biotite grains and mud clasts, close to which magnesian siderite is commonly observed to have developed (Figure 23). Ankerite cementation has occurred adjacent to mudstones, and a thin sandstone within a mudstone bed is completely ankerite cemented (211/12a-9, 3248.0m). This strongly suggests that mudstones were an important source of ions (Ca^{2+}, Fe^{2+}, Mg^{2+}) and CO_2 for ankerite cementation. An association between mudstones and ankerite cementation has been noted previously from Magnus sediments by Rainey (1987) and from other submarine turbidite localities (Gawthorpe, 1987).

SEM studies indicate that late diagenetic illite is abundant in deep well 211/12a-9, principally below the oil/water contact. Critical point drying techniques were not employed in this study and the results of McHardy et al (1982) and Kantorowicz (1990) suggest that this technique is essential both for "in-situ" quantitative and qualitative illite observation (additionally, samples must be prepared from preserved core). However, the data of Kantorowicz (1990) for Magnus illite wettability also suggest that a higher abundance of filamentous late diagenetic illite has developed in the water zone. This is supported by the younger illite K/Ar age date from water zone illite of 41.8± 1.3 Myr from a 0.1-0.5μm sample compared to a sample of <0.1μm in the oil zone which was dated at 56.6± 2.3 Myr (Table 9). In any one sample the finest illite size fraction should represent the last illite to have formed and therefore record the youngest age. Illite most likely continued to grow in the water zone after oil migration had arrested diagenesis in the reservoir.

4.7 STABLE ISOTOPE ANALYSES

Isotopes of an element are atoms whose nuclei contain the same number of protons but a different number of neutrons. Stable isotopes are fractionated

by natural processes such as geochemical reactions, and because these processes are reasonably well understood it is often possible to infer aspects of geological processes from the isotopic composition of rocks or minerals (O'Neil, 1986).

This study deals with the use of the stable isotopes of oxygen ($^{18}O/^{16}O$), hydrogen (D/H), carbon ($^{13}C/^{12}C$) and sulphur ($^{34}S/^{32}S$) to trace the physicochemical variations and diagenetic evolution of the mineral/water/organic system of the Magnus Sandstone.

In his review of the use of stable isotopes as tracers in clastic diagenesis, Longstaffe (1989) outlined ten important questions which can be tackled using stable isotopes :

1. What is the temperature at which a specific diagenetic mineral crystallised?
2. What is the maximum temperature to which a sedimentary basin has been heated?
3.What is the origin of formation water in a sedimentary basin?
4. How has the composition of diagenetic porewaters evolved and why?
5. Have diagenetic minerals retained their original isotopic compositions, or have they undergone exchange with formation waters?
6. What was the water/rock ratio during diagenesis?
7. Has diagenesis proceeded in an open or closed system?
8. What are the sources (organic, inorganic) and reaction pathways involved in the fixation of oxygen, hydrogen, carbon and sulphur in diagenetic minerals?
9. What constraint can be placed on variations in redox conditions during diagenesis?
10. On what scale and by what mechanism has mass transport occurred within the sedimentary basin during diagenesis ?

This paper is an attempt to address these questions for diagenesis in the Magnus Sandstone.

4.7.1 Original pore fluid isotopic composition

The isotopic composition of Jurassic seawater has been calculated as $\delta^{18}O$

-1.2‰ by Shackleton and Kennett (1975). Extrapolation between a Devonian meteoric water value of $\delta^{18}O$ -5‰ (Fallick et al, 1985) and an Eocene value of -12‰ (Taylor and Forester, 1971) provides a value for Upper Jurassic to Mid-Cretaceous meteoric water of at least as negative as -7‰.

4.8 RESULTS OF ISOTOPIC ANALYSES

The results of isotopic analyses of individual diagenetic minerals are reported and discussed for individual wells 211/12-1 (crest), 211/12a-M1 (intermediate) and 211/12a-9 (downdip) (Figure 4a) as well as more generally. This is because each well shows internally consistent values for each individual mineral, but these are different and separate from well to well, as reported in Chapter 2.

4.8.1 Pyrite 1

Measured $\delta^{34}S$ ratios for early diagenetic framboidal pyrite and discussion of these results are included in the section on late diagenetic pyrite. The results show a large fractionation from Jurassic seawater sulphate indicating pyrite development through bacterial sulphate reduction in a system open to seawater sulphate.

4.8.2 Quartz overgrowths

Six results were obtained from oxygen isotope analyses of quartz overgrowths, using the mass-balance method described by Milliken et al (1981), Fisher and Land (1986) and Brint (1989). Initially the method of Lee and Savin (1985) was attempted but proved unsuccessful. This method involved weakening the detrital grain/quartz overgrowth boundary with acid and then shaking off the overgrowths in an ultrasonic bath for isotopic analysis ; it has been successfully applied to samples where the grain/overgrowth boundary is delineated by obvious dust lines or trails of boundary inclusions. However, as described in the petrography section, dust lines are absent in Magnus examples and boundary inclusions are scarce ; overgrowths are therefore firmly attached to their detrital hosts over a large part of the area beneath the overgrowth. As a result, in the ultrasonic bath detrital grains were found to be fracturing along structural weaknesses

rather than the desired effect of overgrowths detaching from detrital hosts. The resultant homogenous detrital quartz $\delta^{18}O$ ratios measured are shown in Table 9. The finest size fractions should have shown more positive values had they been pure overgrowth separates (Lee and Savin, 1985 ; Brint, 1989).

Three samples were successfully analysed from crestal well 211/12-1 and three from downdip well 211/12a-9 by the mass-balance method described by Milliken et al (1981), Fisher and Land (1986) and Brint (1989). Samples were chosen initially for their high diagenetic quartz content as determined by petrographic point counting. Accurate determination of quartz overgrowth abundance was achieved using SEM CL images of grain mounts prepared from the same sample as was used for isotopic analsysis. In all samples quartz overgrowths in leached aliquots had been completely removed by HF, In unleached aliquots of the same sample percentage overgrowth was compared by two methods : 1. overlaying photographic images of 50-60 grains with 1mm grid and counting relative % detrital and diagenetic quartz ; and 2. cutting the overgrowths and grains from traced images prepared from photographs and weighing. These methods gave excellent agreement, typically to ±0.5% quartz overgrowth. Thankfully, recent computer image analysis techniques make this process considerably less labour intensive. Quartz overgrowth oxygen isotope results are shown in Table 10a. Measured $\delta^{18}O$ values for quartz overgrowths from 211/12-1 range from 23.9 to 25.9‰ ($x=24.7$, $1\sigma=1.6$, $n=3$) and from 28.2 to 30.1‰ ($x=29.0$, $1\sigma=1.5$, $n=3$) in 211/12a-9 (Figure 34).

Assuming that quartz overgrowths grew in isotopic equilibrium with their contemperaneous pore fluids it is possible for any given temperature to infer the oxygen isotopic composition of the pore fluid at the time of overgrowth development. However, petrographic observations show that significant quantities of quartz overgrowth had developed early in diagenesis prior to kaolinite formation, and that overgrowths also enclose the ends of fibres of illite, the last diagenetic mineral to form. Furthermore, SEM cathodoluminescence studies show the presence of at least three growth zonations within quartz overgrowths (Figure16). Therefore the measured quartz overgrowth $\delta^{18}O$ ratios must be bulk values reflecting an average for the whole period of diagenetic quartz precipitation. Inferred pore fluid $\delta^{18}O$ compositions must also, therefore, be averaged values. However,

it is assumed here that quartz diagenesis events affected all samples to the same degree and that quartz overgrowths formed at around the same temperature and time across the field (as is indicated by the very similar diagenetic sequence fieldwide, and the statistically indistinguishable groups of fluid inclusion temperatures measured by BP from various wells ; Appendix 2). Consequently, at any given temperature the pore fluid in the crestal sandstones of well 211/12-1 must have been at least 3‰ more negative than those in downdip well 211/12a-9 and more likely ~5‰ (Figure 34). This most likely reflects a higher proportion of isotopically negative meteoric-derived water, introduced during Lower-Mid Cretaceous subaerial erosion, in the crestal sandstones. Alternative scenarios are discussed and rejected in Chapter 1. The small spread of ratios measured for quartz overgrowths from each individual well could indicate that the $\delta^{18}O$ signature of one of the quartz precipitation events may have swamped the others, if indeed the others were significantly different, but the small number of samples hinders more detailed interpretations.

Were the temperature of quartz overgrowth formation well constrained, then the oxygen isotope composition of the pore fluid involved could be calculated, assuming equilibrium fractionation. Twenty four fluid inclusion wafers from the three wells 211/12-1, 211/12a-M1 and 211/12a-9 were prepared for this purpose. Unfortunately, fluid inclusions were too scarce and too small for reliable homogenisation temperatures to be measured. Fluid inclusions tend to be biggest in quartz precipitated rapidly at high temperature (Roedder, 1984), intimating that Magnus quartz overgrowths may have developed slowly and/or at relatively low temperatures. However, some quartz overgrowth fluid inclusion data were collected from Magnus sandstones by BP, which show a range in temperatures from 75-116°C in the oil zone. Recently evidence has emerged (Osborne and Haszeldine, 1990) which suggests that in the North Sea Basin fluid inclusions have re-equilibrated to present day burial temperatures by leakage or distortion. This problem is well documented for diagenetic carbonate minerals (Goldstein, 1986 ; Prezbindowski and larese, 1987 ; Barker and Goldstein, 1990). An alternative model for hot fluid inclusion temperatures from a reservoir oil zone in the Haltenbanken area, offshore mid-Norway, is proposed by Walderhaug (1990). Walderhaug suggested continued quartz precipitation in the oil zone by silica diffusion from stylolites and grain/grain contacts through irreducible water as a

mechanism to explain oil zone quartz overgrowth temperatures equal to the present day burial temperatures.
Hence quartz overgrowth formation temperatures may not be accurately constrained by fluid inclusion temperatures, but the value of 75°C from the BP data will be taken as the nearest to the start of overgrowth development. It is not known if this is a boundary inclusion temperature and therefore representative of earliest overgrowth formation.

4.8.3 Kaolinite 2

Kaolinite samples from all three wells 211/12-1, 211/12a-M1 and 211/12a-9 were purified by settling and centrifuging and checked for purity by XRD and SEM examination prior to isotopic analysis. Oxygen and hydrogen isotope results for kaolinite are shown in Table 11.

Crestal well 211/12-1 kaolinite $\delta^{18}O$ results range from 12.5 to 14.9‰, with a mean of 13.6‰ (1σ=0.7, n=10), and δD results range from -61.1 to -101.4‰ with a mean of -85.8‰ (1σ=12.1, n=8).
Intermediate well 211/12a-M1 kaolinite $\delta^{18}O$ ratios are between 13.7 to 15.3‰ with a mean of 14.2‰ (1σ=0.5, n=8). No hydrogen isotope data for kaolinite was obtained from this well.
Downdip kaolinite from well 211/12a-9 gave $\delta^{18}O$ ratios of between 15.5 and 17.5‰ with a mean of 16.4‰ (1σ=0.7, n=6), and δD ratios between -60.2 and -81.0‰ with a mean of -68.2‰ (1σ=9.2, n=4).
No meaningful variation in oxygen or hydrogen isotope ratios with depth or sample grain size was observed.

In each individual well a spread of kaolinite $\delta^{18}O$ ratios of around 2‰ implies, for constant porefluid $\delta^{18}O$ during kaolinite growth, a temperature "window" of around 20°C through which kaolinite developed. Note that this arguement cannot be applied to explain $\delta^{18}O$ isotopic variations between kaolinites developed penecontemporaneously in crestal and downdip wells without invoking a higher temperature at the crest of the field than downdip. Since this is thought unlikely, we suggest that porefluid $\delta^{18}O$ regimes were different.

Detrital feldspar is commonly observed to suffer significant alteration and dissolution in oilfield situations, coincident with theoretically significant

production of organic acids and CO_2 from organic maturation in shales at about 80°C (Surdam, 1984 ; Crossey et al, 1986 ; Lundegard and Land, 1986 ; Shock, 1988), (Figure35). Preservation of extremely delicate skeletal feldspar petrography in the Magnus Sandstone shows feldspar dissolution to have been a relatively late (post-compaction) event, and it presumably resulted in kaolinite precipitation. Assuming the same temperature of 80°C for kaolinite growth, and penecontemoraneous kaolinite growth across the field, it is possible to reconstruct the pore fluid $\delta^{18}O$ across the field at the time of kaolinite development. Using the mean kaolinite $\delta^{18}O$ from each well it follows that pore fluid ranged in $\delta^{18}O$ from -3.4‰ in crestal well 211/12-1 to -1‰ in downdip well 211/12a-9 (Figure 36). (Absolute pore fluid oxygen isotope compositions derived in this way are, of course, dependent on the assumed kaolinite formation temperature). The pore fluid in the crest of the field must, then, have contained a significantly higher proportion of low $\delta^{18}O$ meteoric-derived porewater than the sandstones downdip. This is supported by the more negative δD ratios measured from crestal kaolinites (discussed later).

4.8.4 Pyrite

In the Magnus Sandstone pyrite has formed during both early and late diagenesis. Early pyrite has both replaced organic material and formed framboids. Framboids probably result from the inversion of greigite to pyrite (Sweeney and Kaplan, 1973). Preserved early pyrite is only observed in the deepest well studied, 211/12a-9. The Kimmeridge Clay Formation mudstones, which enclose the Magnus Sandstone, also contain abundant framboidal pyrite as well as occasional small (<10mm) pyrite nodules. Late diagenetic pyrite is octahedral or cubic and has formed throughout the Magnus Sandstone, especially where organic debris is rich. Often it is associated with degraded detrital biotite and diagenetic magnesian siderite. Pyrite $\delta^{34}S$ analyses of pyrite from the Magnus Sandstone display a range of results from -13 to +15.7‰CDT (Table 12). The overlying Cretaceous marls are heavily pyritised by framboids, which have a $\delta^{34}S$ of -47.7‰.

Ocean water is a major source of sulphate. In the Upper Jurassic, seawater sulphate had a $\delta^{34}S$ of about +16‰ (Claypool et al, 1980). During early diagenesis at low temperatures sulphate is reduced to sulphide by anaerobic bacteria such as Desulfovibrio desulfuricans. The resultant H_2S is rich in ^{32}S

but the exact fractionation is variable for natural systems. Claypool et al (1980) and Nakai and Jensen (1964) take a 40‰ fractionation to represent the aqueous sulphate-solid sulphide system, but experimental systems show lesser fractionation,.only up to 27‰ (Faure, 1986). Sulphur isotopic studies can indicate the "openness" of the sulphate system, in that in an open system the $\delta^{34}S$ values of H_2S produced through bacterial activity will be constant whereas if sulphate supply is restricted a Rayleigh-type fractionation leads to dissolved sulphate having increasing $\delta^{34}S$ values as its concentration falls. Thus, pyrite $\delta^{34}S$ becomes more positive in a closed system as sulphate reduction continues. Longstaffe (1989) cautions, however, that the behaviour of sulphur isotopes in sedimentary systems, and their relationship to "open" or "closed" systems is complex.

Raiswell (1982) and Gautier (1985) showed that early framboidal pyrite tends to have lower $\delta^{34}S$ ratios than late cubic or octahedral pyrite from the same sample. Pyrite samples were separated from sandstones and examined petrographically to distinguish relative quantities of early and late pyrite, and separates were hand-picked in an attempt to obtain pure samples of early and late pyrite. These efforts were complicated by aggregates of pyrite of ambiguous morphology and by framboidal grains with later cubic overgrowths. Hence the range of pyrite $\delta^{34}S$ values is a minimum range. The most successful separations yielded a $\delta^{34}S$ of -13‰ for framboidal pyrite and +15.7‰ for cubic/octahedral pyrite.

The early framboidal pyrite $\delta^{34}S$ of -13‰ represents a 29‰ fractionation from Upper Jurassic seawater sulphate and pyrite growth either in a system open to seawater sulphate and/or the first sulphate reduction, which is the same in an open or closed system. Euhedral pyrite with $\delta^{34}S$ of +15.7‰ was separated from a 40cm thin sandstone within a 20m thick mudstone from well 211/12a-9. Only a tiny fractionation can have occurred if this pyrite formed from sulphate with a $\delta^{34}S$ of +16‰, and may, therefore, represent a small scale example of a "closed" sulphate system. Measured pyrite $\delta^{34}S$ ratios between -13 and +15.7‰ represent mixtures of early and late pyrite, whether it be as separate grains or as early framboids overgrown by late cubic pyrite.

Late euhedral pyrite is petrographically constrained to have formed at about the same time as late diagenetic magnesian siderite (probably just earlier -

low dissolved sulphate is an important parameter controlling magnesian siderite formation (Curtis and Coleman, 1986)). Fe was supplied by degrading detrital biotite. By association, therefore, late pyrite formed at temperatures in excess of 80°C, which is the temperature threshold for the survival of sulphate-reducing bacteria. An alternative sulphate-reduction mechanism is provided by Krouse et al (1988). They encountered subsurface environments in which chemical and carbon isotope data argue for thermochemical sulphate reduction by light hydrocarbon gases at temperatures as low as 90°C. Obviously this mechanism has potential in hydrocarbon reservoirs such as the Magnus Sandstone.

The measured $\delta^{34}S$ of -47.7‰ from framboidal pyrite extracted from Cretaceous marls overlying the Magnus Sandstone is very low compared to the Magnus examples. Seawater sulphate $\delta^{34}S$ values may have dropped marginally to +15‰ during the early Cretaceous (Claypool et al, 1980), but not enough to explain this 62‰ fractionation. It has been suggested that for bacterial sulphate reduction at extremely slow rates of reduction fractionations may approach theoretical equilibrium values of -74‰ at 25°C (Fisher and Hudson, 1987 ; Trudinger and Chambers, 1973). Slow specific reduction rates, or the addition of isotopically light sulphate by the reoxidation of sulphide, may be responsible (Fisher and Hudson, 1987).

4.8.5 Magnesian siderite

Magnesian siderite occurs throughout the Magnus Sandstone as discrete or clustered rhombs, and is commonly spatially associated with degraded detrital biotite. Variations in magnesian siderite compositions can be simplified to : more ferroan in the crest of the field and more magnesian downdip. Details of chemical variations are described in Chapter 3. Petrographic and SEM observations indicate that magnesian siderite post-dates kaolinite in the diagenetic sequence. Like quartz overgrowths and kaolinite, magnesian siderite displays isotopic variations across the field. Magnesian siderite euhedra display obvious growth zonations in backscatter electron images and so isotopic results are bulk figures homogenising isotopic contributions from each growth zone. Isotope results are tabulated in Table 13.

Magnesian siderite separates from crestal well 211/12-1 gave a range of $\delta^{18}O$ ratios from 13.6 to 18.2‰ SMOW, mean 16.0‰ (1σ=1.7, n=5) (or -16.8 to -12.4‰ PDB) and $\delta^{13}C$ from -8.0 to -14.1‰PDB. Intermediate well 211/12a-M1 values are $\delta^{18}O$ 16.2 to 18.4‰ SMOW, mean 17.5‰ (1σ= 0.9, n=5), (-14.3 to - 12.1‰PDB) and $\delta^{13}C$ from -9.0 to -11.1‰PDB. Downdip well 211/12a-9 magnesian siderite ratios range from $\delta^{18}O$ 14.1 to 18.6‰SMOW, mean 16.9‰ (1σ= 1.7, n=5) (-16.0 to -11.6‰PDB) or 17.6‰ (1σ= 0.8, n=4) if the one vey low value of 14.1‰ is excluded, and $\delta^{13}C$ -8.8 to -14.6‰PDB.

The similarity in $\delta^{13}C$ ratios across the field (Figure 37a) suggest a common reservoir of CO_2, with a substantial component of CO_2 derived from degradation of organic material (Irwin et al, 1977).
Developing the argument presented for quartz overgrowths and kaolinite, if a slightly hotter temperature of formation of 85°C is assumed for magnesian siderite than kaolinite, then pore fluid $\delta^{18}O$ composition during magnesian siderite formation ranged from -2.9‰ in the crest of the field to -1‰ downdip (Figure 37b). A significantly higher proportion of meteoric-derived porewater was therefore still present in the crest of the field during magnesian siderite growth, than downdip.

4.8.6 Ankerite

Poikilotopic ankerite cement is developed generally only within 10m of mudstone units in the Magnus Sandstone in the wells studied, and is most abundant in downdip well 211/12a-9. It has cemented thin sandstones within mudstones to the complete exclusion of porosity. Ankerite cement commonly encloses, and therefore post-dates, magnesian siderite rhombs. Like magnesian siderite, ankerite shows a general chemical compositional variation across the field from more ferroan in the crestal region to more magnesian downdip. Zoned chemical variations within individual crystals, although much less pronounced than those observed in magnesian siderite rhombs, again mean that measured isotopic values for ankerite separates are bulk values.

In common with the previous diagenetic minerals, ankerite shows distinct differences in measured $\delta^{18}O$ values across the field from crest to oil/water contact. Isotope results are shown in Table 14.

Values from crestal well 211/12-1 samples range from $\delta^{18}O$ 16.6 to 18.8‰SMOW, mean 17.7‰ (1σ=1.2, n=3) (-13.8 to -11.8‰ PDB) and $\delta^{13}C$ -10.6 to -13.6‰PDB. Ankerites from intermediate well 211/12a-M1 gave a range from $\delta^{18}O$ 19.2 to 20.5‰SMOW, mean 20.1‰ (1σ=0.5, n=9) (-11.3 to -10.1‰ PDB) and $\delta^{13}C$ -9.3 to -12.8‰PDB. Downdip deep well 211/12a-9 ankerites range from $\delta^{18}O$ 20.9 to 21.6‰SMOW, mean 21.4‰ (1σ=0.3, n=4) (-9.3 to -8.7‰ PDB) and $\delta^{13}C$ -7.7 to -13.4‰PDB.
Two separates of ankerite from well 211/12-6 in the north of the field (Figure 2) yielded values of $\delta^{18}O$ 22.2 and 22.4‰SMOW (-8.4 and -8.2‰PDB respectively) and $\delta^{13}C$ -6.7 and -6.1‰PDB. Sandstone from well 211/12-3A to the south also has ankerite cements, two samples of which gave $\delta^{18}O$ of 22.8 and 23.1‰SMOW (-7.8 and -7.6‰PDB respectively) and $\delta^{13}C$ -10.1 and -9.9‰PDB. Overall, the ankerite $\delta^{13}C$ data are slightly more negative than for earlier magnesian siderite, reflecting increased influence of isotopically negative carbon produced by organic decarboxylation at the time of ankerite growth.

Ankerite $\delta^{18}O$ data indicate pore fluid $\delta^{18}O$ compositions of around -4‰ in the crest of the field and 0‰ downdip in 211/12a-9 for an assumed ankerite growth temperature of 90°C (Figure 38). Slightly more positive pore fluid $\delta^{18}O$ compositions must be invoked for ankerite development at 90°C in the sandstones in the north and south of the field (ie more positive due to higher input of isotopically positive shale-derived water or lesser input of isotopically negative meteoric-derived water). Ankerite oxygen isotope data uphold the hypothesis of a greater component of isotopically more negative meteoric-derived pore fluid in the crest of the field. Downdip, where the mudstone/sandstone ratio is higher, pore fluid is inferred to have been more positive.

4.8.7 Illite 2

Illite is the last diagenetic mineral to have formed in the Magnus Sandstone before the reservoir filled with oil. McHardy et al (1981) studied Magnus illite in detail and described its hairy morphology and detrimental effect on

sandstone porosity and especially permeability. SEM obsevations from this study and those of McHardy et al (1981) and Rainey (1987) show that illite development was contemperaneous with the last phases of quartz overgrowth and ankerite cementation. Table 15 contains the isotopic data for illite.

Illite separated from reservoir sandstone core from crestal well 211/12-1 has $\delta^{18}O$ values of between 9.1 and 12.9‰ with a mean of 11.5‰ (1σ=1.7, n=7), and δD between -76.4 and -125.3‰ with a mean of -98.8‰ (1σ=16.0, n=7). From intermediate well 211/12a-M1 illite $\delta^{18}O$ is between 9.5 and 12.9‰ with a mean of 11.5‰ (1σ=1.0, n=18), and δD ratios between -89.7 and -90.9‰ with a mean of -89.8‰ (1σ=0.2, n=3). $\delta^{18}O$ for illite from downdip well 211/12a-9 range from 12.9 to 15.5‰ with a mean of 14.6‰ (1σ=1.5, n=3), and δD between -58.5 and -75.3‰ with a mean of -66.1‰ (1σ=8.5, n=3).

For a minimum assumed illite formation temperature of 100°C, (after Kantorowicz, 1990 and discussed later in the isotope discussion) pore fluid $\delta^{18}O$ values of -1.2‰ in the crest of the field and +1.7‰ downdip are inferred (Figure 39). In common with the oilfields of the Brent province (Brint, 1989), and others in the northern North Sea (Glasmann, 1989), present day Magnus formation water has a $\delta^{18}O$ of ~ +2‰ (D. Emery BP, pers comm). As with kaolinite, illite δD data from crestal samples are more negative than those downdip, and are discussed in detail later.

4.9 INTERPRETATION AND SYNTHESIS OF ISOTOPE DATA

Figure 40 outlines the approach used in the interpretation of the isotopic evolution of the rock/water/organic system of the Magnus Sandstone Member. Initial parameters to the system include palaeosurface temperature, geothermal gradient, water/rock ratio, isotopic composition of original end-member pore fluids and the burial history. Final parameters include the present-day formation temperature, the present-day formation water oxygen isotope composition and salinity, K/Ar dates for the formation of diagenetic illite which grew last in the diagenetic sequence and perhaps slightly lower water/rock ratio.
Between the two lies the interpretation of the diagenetic mineral growth sequence and its compatibility with the isotopic composition of the diagenetic minerals. The interpretation must consider factors such as the

reasons for the isotopic evolution path, the nature of the isotopic system - open or closed, the possibilities of isotopic exchange, isotopic and chemical mass transport, variations in redox conditions and their relationship to burial depth, temperature and time.

According to Longstaffe (1983) and Brint (1989), during diagenesis, the oxygen and hydrogen isotopic composition of neoformed minerals are functions of :

1. The temperature of mineral formation.
2. The isotopic composition of the pore fluid.
3. The mass balance between oxygen and hydrogen isotopes of mineral and fluid.
4. The stable isotope fractionation factor between diagenetic mineral and fluid.
5. The extent to which isotopic equilibrium was maintained between diagenetic mineral and fluid.
6. The extent and nature of isotopic exchange between diagenetic mineral and fluids.

Important uncertainties to be borne in mind during interpretation of diagenetic mineral isotopic data , pointed out by Ayalon and Longstaffe (1988) and Brint (1989), are :

1. The potential reequilibration of diagenetic minerals.
2. The mineral curves generated from isotopic fractionation equations are subject to experimentally-derived understanding of the fractionation factor at low temperatures for mineral-water pairs. These are particularly poorly constrained for kaolinite (<400°C : Liu and Epstein, 1984 ; <200°C : Lambert and Epstein, 1980) and illite (29-120°C : Yeh, 1980).
3. Sample purity even after application of sample purification techniques and checks.

4.9.1 Definition of initial parameters

A subtropical, possibly seasonal, climate for NE Scotland is postulated from a study of shale detrital clay mineralogy by Hurst (1985). In this climate grew lush vegetation, much of which was swept into the North Sea basin in

various stages of degradation (Barnard and Cooper, 1981). This resulted in reducing water conditions in the restricted, initially landlocked basin. Static water conditions and high algal production rates led to deoxygenation of bottom waters in deeper parts of the basin and accumulation of organic-rich sediments.
Land surface temperatures in the Jurassic and Cretaceous (Hallam, 1982 ; Savin, 1977) were almost certainly higher than those of today at equivalent latitudes. Palaeogeographic reconstructions during the Mesozoic by Smith and Briden (1977) indicate that the East Shetland Basin was just north of 40°N.

On deposition, well sorted sandstones have a porosity of 35-40% (Pettijohn, 1975). High initial porosities in the Magnus Sandstone are shown by high minus-cement porosities of up to 32% without correction for compaction.

The estimated isotopic composition of Jurassic seawater was $\delta^{18}O$ -1.2‰ and Upper Jurassic to Mid Cretaceous meteoric water -7‰ or lower. Rainey (1987) notes that in the Magnus area the sedimentary basin was relatively closed and had a high riverine input, so depositional marine waters may have been slightly diluted by meteoric water. A buoyant meteoric water lens entering a relatively saline basin would be expected to affect surface waters considerably more than deep marine waters, in which the Magnus Sandstone turbidites were deposited. However, a turbidite flow will carry its own water with it, but settles out by mixing and dilution with the surrounding water.

4.9.2 Final parameters

Present-day bottom hole temperatures of 115-120°C corrected from logs give a geothermal gradient of 35°C/km^{-1} for present day surface temperatures around 5°C. Constraints on illite formation suggest that, in the past, geothermal gradients may have been significantly higher in the Magnus basin. A K/Ar age date from illite at the base of the oil pool of 55Myr implies a burial depth of 2km (Figure 4b). Taking the growth temperature for Magnus illite as 100°C (Kantorowicz, 1990), a geothermal gradient of 45°C is implied with a surface temperature of 10°C in the Paleocene/Eocene. Carstens and Finstad (1981) believe that high Jurassic geothermal gradients

>35°C/km^{-1} are related to flow of hot fluid from depth up faulted Jurassic blocks. On the western flank of the actively subsiding Rhine Graben geothermal gradients of 77°C/km^{-1} have been recorded (Doebl et al, 1974), again probably the result of thermal waters rising through the fault system. If quartz overgrowth fluid inclusion data (75-116°C) are taken as representative of quartz overgrowth formation temperatures, then even higher geothermal gradients than 45°C/km^{-1} would be required because the majority of quartz diagenesis predates illite growth. This problem confronted Brint (1989), studying the diagenesis of middle Jurassic Brent sandstones, who explored other possible heat sources such as crustal thinning and Tertiary igneous activity, but invoked a hypothesis of pulsed hot fluid migration from deeper in the basin.

Porosity in the Magnus Sandstone was reduced by compaction and burial diagenesis until present conditions were met. Core analysis porosities of 20-30% are recorded near the crest of the field and 10-25% further downdip. These high water/rock ratios, and limited flow of sandstone porewater, indicate that the "sealed" Magnus sediments formed a rock buffered isotopic system. Present day formation water analyses are $\delta^{18}O$ around +2‰ and salinity around half that of seawater (De'Ath and Schuyleman, 1981).

The Magnus Sandstone is overpressured by 2000psi (virgin pressure was 6638psi at a datum of 3050m depth ; Atkinson, 1985) and is interpreted as a closed pressure system (no leakage nor input from deeper in the basin) by Buhrig (1989). All the reservoir zones are overpressured, although in some wells the uppermost sands were at lower lower pressure than the lowermost sands, and in some wells pressure build up tests showed the proximity of reservoir barriers.

4.9.3 Interpretation of the isotopic evolution of the Magnus Sandstone from initial to final parameters.

A considerable volume of literature now exists documenting the isotopic evolution of pore fluids in reservoir sandstones through diagenesis. Longstaffe (1989) reviews the uses of stable isotopes in such studies, and some important North Sea aspects are reported by Hamilton et al (1987), Jourdan et al (1987), Glasmann et al (1989) and Brint (1989). In all these examples pore fluid compositions evolve towards heavier values through

water/rock interaction, and this is reflected in the isotopic composition of diagenetic minerals. Diagenetic silicate minerals are resistant to oxygen isotope exchange at sedimentary temperatures, but hydrogen isotopes are less reliable, especially in clays. A notable exception is post-growth clay mineral hydrogen isotope exchange due to an high volume influx of meteoric water deep into the Western Canada Sedimentary basin (Longstaffe and Ayalon, 1989)

The diagenetic history of the Magnus Sandstone can be divided into early and late burial diagenesis, early occurring in original depositional marine porewater before early Cretaceous exposure to meteoric water (Figures 4b and 5).

4.9.4 Early diagenesis

Following deposition of the Magnus Sandstone in the reducing, stagnant marine pore water of the Magnus basin, diagenetic minerals began to form at shallow burial depths (cms- few metres). Pellets of glauconite probably originated at the oxidising/reducing boundary in the sediments from faecal pellets derived from the fauna in the overlying oxygenated water strata. Platey illite probably also grew at around this time perpendicular to detrital grain surfaces, indicating that it is diagenetic and not a filtrate. Utilising the large amount of organic matter available, sulphate-reducing bacteria reduced seawater sulphate to form framboidal pyrite. Negative $\delta^{34}S$ of -15‰ for framboidal pyrite indicate that at this time the sulphur isotope system was open to seawater sulphate.
Scarce early calcite, which is common in Brent facies containing shell debris and forms a concretion in a crestal well not examined in this study, has a marine isotopic signature of $\delta^{13}C$ +1‰ and $\delta^{18}O$ +29‰ SMOW (pers comm, S. Rainey, BP), indicating growth at about 20°C. One reason for the scarcity of calcite may have been the virtual absence of detrital shell material, which is an important Ca source in Brent sandstones. From the Upper Jurassic to the mid-Cretaceous, the sandstone was uplifted and exposed to meteoric water. This destroyed early pyrite in the shallow wells, but did not penetrate deeply into the sandstone and extra dissolution porosity only occurs within a few metres of the unconformity. Perhaps during this time K^+ was released from detrital biotite breakdown, and chlorite replaced the biotite. Early kaolinite

grew as fine grained blocky plates and as a relacement of muscovite as the sandstones became buried and their temperature increased.

4.9.5 Late burial diagenesis

With increasing temperature, diagenetic reactions in the Magnus sandstone became increasingly influenced by organic reactions occurring in the surrounding Kimmeridge Clay. Detrital K feldspar was quantitatively the most reactive sandstone component. K feldspar overgrowths developed on dissolved or adjacent K feldspar grains in volumes locally approaching 2% whole rock. Feldspars dissolved due to elevated temperatures (>60°C) and the action of organic acids. In the crest of the field, which had been subject to subaerial erosion, acid meteoric-derived waters may have been an important solvent component, whilst downdip, where mudstone/sandstone ratios increase, organic acids released from mudstone maturation may have dominated. Detrital garnets downdip in 211/12a-9 show strongly etched rhombic faces, a phenomenon ascribed by Hansley (1987) to the action of organic acids. Etching is similar but less well developed on garnets from the crestal wells. Organic acid etching of garnet occurred prior to pore filling kaolinite 2 growth (Figure 12b).
A very similar diagenetic evolution is inferred to have occurred in the three wells studied because in each well the petrographically observed diagenetic sequence is the same, sandstone depositional composition is homogenous across the field and the three wells are less than 4km apart. Only 400m depth difference separates the top of the crestal well (211/12-1) from the base of the deepest (211/12a-9). For a high geothermal gradient of 45°C/km^{-1} a maximum temperature difference between crest and downdip of 18°C can be inferred. Thermally controlled mineral reactions could be visualised as occurring as the Magnus Sandstone sank with burial through various temperature thresholds (Bjorlykke, 1983). Feldspar dissolution probably began in earnest with the thermal destruction of bacteria at 60-80°C which allowed a rise in the concentration of organic acids produced in the initial stages of organic maturation (Figure 35).
The products of feldspar dissolution were quartz overgrowths and pore filling kaolinite. Observed feldspar dissolution is not sufficient to account for the abundance of diagenetic quartz, but is sufficient to account for diagenetic kaolinite. More kaolinite is present in deep well 211/12a-9 where Al^{3+} has been complexed and better conserved by higher concentrations of

organic acids. Silica must have been imported in solution to the Magnus Sandstone, most probably from the surrounding Kimmeridge Clay mudstones. Silica solubility may have been enhanced by organic compound complexing (Bennet and Siegel. 1987 ; Bennet et al. 1988) and ferrous-ferric iron reactions in clays (Morris and Fletcher, 1987).

4.9.5.1 Quartz overgrowths

Quartz overgrowth $\delta^{18}O$ values are different between the crest and base of the field. Crestal (211/12-1) $\delta^{18}O$ values range from 23.9 to 25.9‰ and downdip from 28.2 to 30.1‰ (Figure 34). Were the quartz overgrowth formation temperature confidently known, then the isotopic composition of the coexistent porefluid could be calculated. Fluid inclusion temperatures of 75-116°C may have been affected by post-formation reequilibration toward present day reservoir temperatures of 115-120°C. Even application of the minimum 75°C fluid inclusion temperature yields values which are clearly too positive bearing in mind the original pore fluid isotopic compositions (meteoric -7‰ ; marine -1.2‰). Crestal pore fluid $\delta^{18}O$ calculated from the quartz values is -0.9 to +0.9‰, and downdip from +3.5 to 5‰. Note that the crestal pore fluid is around 4‰ more negative than the downdip porefluid, suggesting a considerably larger component of meteoric-derived (-7‰) pore fluid in the crest than downdip. It is not possible to produce this effect by decending isotopically negative porewaters being heated.
Even at a lower temperature of 60°C, calculated porewater $\delta^{18}O$ values are, from the crest -2 to -4‰ , and from downdip +0.6 to 2.0‰. The quartz overgrowth $\delta^{18}O$ data would therefore indicate that the bulk of the overgrowths precipitated at below 60°C, and probably nearer 40-50°C. Silica could be supplied at such low temperatures by dissolution of microfossil amorphous silica such as sponge spicules and the onset of pressure solution. Quartz overgrowth SEM CL studies showed that overgrowths contain at least three growth zones, so a zone of overgrowth precipitated from isotopically positive shale-derived silica-rich waters might offer part explanation. Quartz overgrowth development continued at least until the early stages of illite 2 growth.

4.9.5.2 Kaolinite 2

Widespread kaolinite 2 precipitation followed the main phase of quartz overgrowth development. Early kaolinite 1 is quantitatively insignificant in terms of separation for analysis. Again a distinction of $\delta^{18}O$ values between crest and downdip was recorded. Crestal kaolinite $\delta^{18}O$ is 12.5 to 14.9‰ and downdip 15.5 to 17.5‰ (Figure 36). For a temperature of 80°C (maximum organic acid generation) these translate to a porewater $\delta^{18}O$ from -5 to -2.8‰ in the crest to -2.0 to -0.2‰ downdip. As feldspar and other detrital minerals (positive $\delta^{18}O$) dissolved, quartz overgrowths and kaolinite precipitated and the porewater $\delta^{18}O$ composition evolved to more positive values in both crest and downdip. Reduction in water/rock ratio with compaction may have increased the influence of rock buffering on the isotopic system.

4.9.5.3 Pyrite 2

Late diagenetic pyrite with $\delta^{34}S$ +15.7‰, close to Jurassic seawater sulphate values (+16‰) grew at temperatures around 80°C through Fe supply from detrital biotite dissolution and possibly thermochemical sulphate reduction in a relatively closed sulphur isotopic system.

4.9.5.4 Magnesian siderite

Rising maturation levels in the Kimmeridge Clay released CO_2 from organic matter which was incorporated into diagenetic carbonate minerals. Magnesian siderite developed from Fe and Mg released from biotite dissolution in porewaters locally alkaline and depleted in sulphate due to late pyrite growth. $\delta^{13}C$ values from crest downdip are consistent with a common CO_2 source, -8,0 to -14.1‰ indicating a significant CO_2 contribution from abiotic thermal decarboxylation of organic matter (Irwin et al, 1977). The virtual absence of shell debris to dissolve and the dilution of depositional marine water by meteoric water suggest that organic sources of CO2 were predominent. Once more an oxygen isotope separation from crest to downdip is indicated by the range in magnesian siderite $\delta^{18}O$ from 13.6 to 18.2‰ in the crest (mean 16.0‰) and 14.1 to 18.6‰ downdip (mean 17.6‰) (Figure 37). Growth at slightly higher temperature than kaolinite of 85°C would indicate a range in porewater $\delta^{18}O$ from -5 to -0.8‰ (mean -2.8‰) in the crest and -4.5 to -0.2‰ (mean -1.1‰) downdip. The large overlap of data

caused by one particularly negative result in each of the wells 211/12-1 and 211/12a-9 might reflect long periods of growth in isotopically changing porewaters, or different mixes of growth zones with different $\delta^{18}O$ in the bulk data.

4.9.5.5 Ankerite

Following magnesian siderite growth ankerite precipitated close to mudstones. It too has indistinguishable $\delta^{13}C$ values from crest to downdip, again suggesting a common CO_2 source (range -7.7 to -13.6‰). Ankerite mean $\delta^{13}C$ (-11.0‰, 1σ=1.6, n=16) is slightly more negative than that for siderite (-10.7‰, 1σ=1.9, n=15), reflecting slightly higher organic-derived CO_2 contribution. Crestal/downdip separation is from $\delta^{18}O$ 17.1 to 19.7‰ in the crest to 20.9 to 21.6‰ downdip. For a growth temperature of 100°C porefluid $\delta^{18}O$ in the crest of the field was -3.2 to -2.0‰ and downdip from 0.2 to 0.7‰ (Figure 38).

4.9.5.6 Illite

Illite probably grew at about 100°C, the result of continued feldspar dissolution and kaolinite degradation. Crestal illite $\delta^{18}O$ ranges from 9.1 to 12.9‰, equivalent to a water value of -3.6 to -0.2‰, and downdip from 12.9 to 15.5‰, equivalent to water of +0.2 to 2.6‰.

4.10 DISCUSSION

The mineral oxygen isotope data indicate that throughout diagenesis a higher proportion of isotopically negative (probably originally about -7‰) meteoric-derived porewater was retained in the crest of the field. The values measured for the different minerals, together with their paragenetic sequence suggest that the oxygen isotopic composition of the pore fluid evolved from originally negative values to more positive values (Figures 34-39). The pathway of this evolution can be only approximately constrained with the present data. Consider a first alternative, that the present-day porefluid $\delta^{18}O$ value of +2‰ was homogenous across the field (water sample location not known). By this hypothesis, the pore fluid in the crest of the field, which at the time of quartz precipitation was some 3-4‰ more negative (Figure 34), must have evolved considerably more than that

downdip. As a second, more likely, alternative, the pore fluids at the crest (Figure 41a), centre (Figure 41b) and flank (Figure 41c) of the field could have evolved along parallel curves throughout diagenesis, until oil filling of the reservoir. The illite $\delta^{18}O$ data suggest that only illite from 211/12a-9 was in equilibrium with water of $\delta^{18}O$ +2‰ at 100°C. Illites from the other wells were growing in equilibrium with waters up to 4‰ more negative (Figure 39).

The interpretation of the present-day water +2‰ value is ambiguous, because reservoir filling may also have pushed the water column down and preserved the original water stratification, so that porefluid originally from the crest of the field was displaced to just below the oil/water column. By contrast, oil migration and reservoir filling may have homogenised the porefluids. Whichever the case, K/Ar dates for illite from beneath the oil/water contact, and increased illite abundance, indicate that illite continued to grow in the water zone after diagenesis was arrested in the oil reservoir, and it is this illite which could have been in equilibrium with water of $\delta^{18}O$ +2‰ at 100°C, and is still in equilibrium with today's reservoir conditions. It is possible that porewater in 211/12a-9 became slightly more negative as the reservoir was filled and crestal porewaters were displaced downwards, and these have since evolved back to $\delta^{18}O$ +2‰.

Two end-member possibilities to explain the observed isotopic separation between crest and downdip are :-

1. The whole Magnus sandstone was flushed with meteoric water then mudstone decompactional water from the surrounding Kimmeridge Clay invaded the sandstone, having a most pronounced effect downdip where the mudsone/sandstone ratio is higher. However early diagenetic framboidal pyrite is preserved downdip in 211/12a-9, suggesting that there was no meteoric flush there, and the narrow zone of intense feldspar weathering below the unconformity suggest that meteoric water was not an effective immediate solvent to great depth.
2. Meteoric water penetration into the Magnus sandstone was only shallow (<400m depth) and a significant proportion of original depositional marine-derived water remained downdip, to be added to during burial by marine water released from mudstones through compaction and water expelled by clay mineral reactions. Compositional data for both siderite and ankerite

show more iron updip and more magnesium downdip, supporting Mg-rich marine-derived water downdip.

A third (theoretical) dynamic fluid model might involve the mixing of isotopically negative fluid from a landward upland area, driven up faults to the crest of the field where it mixed with isotopically more positive basinal-derived fluids. However, the retention of isotopically stratified porefluids through diagenesis would require a prolonged fluid-mixing status quo during burial, and argues against mass transport of dissolved components through homogenising processes such as convection. Samples were collected from the most permeable horizons in all three wells to characterise most likely fluid pathways. If fluid transport occurred along discrete aquifers (eg Whitney and Northrop, 1987), then any differences in porefluid isotopic composition within individual wells were not recorded. Nor were incursions of basinal hot fluids recorded, which have been invoked to explain hot fluid inclusion temperatures in other oilfields (Burley, 1986 ; Brint, 1989). Also, the early development of overpressures inhibits fluid movement.

Some ions for growth of diagenetic minerals must have been derived locally from within the sandstone and surrounding mudstones. This is supported by the relationship between dissolved feldspar and diagenetic kaolinite and degraded biotite and diagenetic magnesian siderite. Siderite growth was sustained by Fe and Mg released from the breakdown of detrital biotite and by carbon dioxide from surrounding mudstones ; ankerite developed from ions released from these mudstones. However, silica was supplied via feldspar dissolution, and was exported from mudstones giving rise to the excess of quartz overgrowth compared to feldspar-derived quartz, and quartz overgrowth precipitation continued throughout diagenesis. At elevated temperatures of around 100°C kaolinite destabilised and illite developed. An illite K/Ar age date of 55 million years from the base of the oil pool suggests that the reservoir was filled, and diagenesis in the reservoir arrested, by the Upper Paleocene/Lower Eocene.

4.10.1 Kaolinite and Illite Hydrogen Isotope Ratios

Values of δD for both crestal kaolinite and illite are considerably more negative than those downdip, as has already been demonstrated for $\delta^{18}O$ (Figures 42a, b and 43). Crestal kaolinite mean δD is -85.8‰, 1σ=12.1, n=8 and illite -98.9‰, 1σ=16 and n=7, whereas downdip kaolinite mean δD is -68.2‰, 1σ=9.2, n=4 and illite -66.1‰, 1σ=8.5 and n=3. Calculation of water δD values from these measured values (from Liu and Epstien, 1980 for kaolinite and Yeh, 1980 for illite) gives crestal porewater δD of -66‰ and downdip -48‰ during kaolinite growth at an assumed temperature of 80°C and -62‰ in the crest and -32‰ downdip during illite growth at an assumed temperature of 100°C. For a Lower Cretaceous meteoric water with $\delta^{18}O$ -7‰ the expected equivalent δD, from $\delta D = 8\delta^{18}O + 10$, should be -46‰. Seawater $\delta^{18}O$ and δD is assumed to be 0‰ (Figure 43 is a plot of the clay mineral hydrogen and oxygen isotope data) although melting of polar icecaps could result in more negative values, perhaps up to -1‰ and -10‰ respectively (Shakleton, 1967 ; Dansgaard and Tauber, 1969 ; Taylor, 1979 ; Savin and Yeh, 1981). In most sedimentary basins that have been studied, the hydrogen isotopic composition of the pore fluid evolves towards more positive values in the same way that oxygen does (for review see Longstaffe, 1989), but to a lesser extent because the amount of hydrogen in minerals compared to water is very small.

The calculated δD values for the porewaters in which kaolinite and illite grew are therefore more negative than the value of - 46 ‰ calculated for meteoric water with $\delta^{18}O$ -7‰. If Lower-Mid Cretaceous meteoric -derived water had $\delta^{18}O$ values much more negative than -7‰, then these quickly become incompatible with diagenetic mineral growth temperatures, especially for quartz overgrowths. Various possibile explanations of the unusually negative δD data are examined below :

1. Sheppard and Charef (1986) suggest that if hydrogen in organic matter dominates the total hydrogen in fluids through dehydration, oxidation or exchange reactions, this H2O bearing fluid (called organic water by Sheppard and Charef, 1986) is likely to be strongly depleted in deuterium. The term organic water only implies that there is a recognisable organic water contribution and Sheppard and Charef (1986) proposed H-isotope

compositions for organic water in the range -90 > dD > -250‰. The O-isotope compositions of organic waters are probably controlled by the $\delta^{18}O$ values of the reservoir rocks and the temperature of exchange, and will therefore be similar to formation water values (Sheppard, 1986). Sheppard and Charef (1986) chose -90‰ as a practical cut off because δD values of organic waters could be higher than -90‰ but then they become indistinguishable from formation and metamorphic waters. It is therefore extremely difficult to assess the H-isotope contribution of organic water in an ancient sedimentary diagenetic system.

2. Isotopically negative Tertiary meteoric water with δD -85‰ (Fallick et al, 1985) somehow infiltrated the Magnus sediment package. This is unlikely because of the 1000m of Cretaceous mudstones and marls overlying the Upper Jurassic Magnus sediments.

3. Isotopic exchange occurred between clay minerals and isotopically depleted hydrocarbons in the oil reservoir, either directly or using a minor aqueous phase as an intermediary. Kaolinite hydrogen isotopic exchange has been reported in the literature through interlayer water (Bird and Chivas, 1988 ; Longstaffe and Ayalon, 1989), and could be conceived for surface exchange in high surface area illites. However it would be considerable coincidence that kaolinite and illite had both exchanged to the same hydrogen isotopic end compositions in the crest and separately downdip. Also in no other North Sea oilfield has post-formation isotopic exchange of clays been reported (Table 16)

4. Local climatic effects might have influenced the isotopic composition of meteoric water in the Magnus basin in the early Cretaceous. Tropical oceanic islands with high relative humidity show a low deuterium excess, with a meteoric water line slope of near six (Sheppard and Charef, 1986). Barnard and Cooper (1981) suggested that the abundant organic matter deposited nearshore in the Kimmeridgian resulted from rich tropical vegetation growing on the surrounding landmasses. Application of the MWL back through time must therefore be made with caution, although no solid evidence exists to indicate that ancient meteoric water isotopic systematics were significantly different from present meteoric water relationships (Sheppard, 1986)

Figure 44 summarises the diagenetic evolution of the Magnus Sandstone from deposition to the present day.

4.11 CONCLUSIONS

1. Prior to early Cretaceous uplift and erosion, framboidal pyrite, glauconite and platey illite developed in the marine porewaters of the Magnus Sandstone.

2. Subaerial erosion allowed *shallow* ingress of meteoric water into the Magnus Sandstone in the Lower to Mid-Cretaceous.

3. Rapid burial beneath thick Cretaceous and Tertiary sediments sealed the Magnus Sandstone and promoted overpressuring.

4. With increasing temperature, maturation of organic matter in the surrounding Kimmeridge Clay mudstones resulted in organic acid production and dissolution of detrital micas, feldspars and garnets.

5. Quartz overgrowths (<60-≥100°C) and kaolinite (~80°C) grew as a result of feldspar dissolution. Fluid inclusion temperatures range from 75°C to 116°C, which is too hot to explain the estimated porewater oxygen isotope compositions and the measured $\delta^{18}O$ of quartz overgrowth. These temperatures are thought to have been reset during burial. Kaolinite morphology is predominantly vermiform in the crestal region and blockier downdip.

6. Magnesian siderite (~85°C) developed close to degrading biotite flakes and ankerite (~90°C) adjacent to mudstones. Both have negative $\delta^{13}C$ values indicative of an important component of CO_2 derived from thermal decarboxylation, ankerite more so than siderite.

7. Increasing temperature and porefluid alkalinity encouraged fibrous illite formation as kaolinite began to destabilise at around 100°C.

8. Each diagenetic mineral records the influence of a fluid of meteoric derivation in the crest of the field. Quartz overgrowths, kaolinite, siderite, ankerite and illite from crestal samples consistently have more negative $\delta^{18}O$ values.

9. When the reservoir filled with oil diagenesis was arrested, but fibrous illite continued to grow in the water zone. Only illite from water zone deep well 211/12a-9 is in isotopic equilibrium with the present day porewater which has $\delta^{18}O$ +2‰.

10. Diagenetic kaolinite and illite both show more negative δD values from crestal samples, although these values are more negative than would be expected even if the clays all grew from Lower Cretaceous meteoric-derived pore water. Even so, these values imply that during burial diagenesis a larger component of isotopically negative meteoric-derived porewater remained in the crest of the field. Porewaters downdip were isotopically more positive, reflecting a larger component of marine-derived porewater and water derived from mudstone dewatering.

4.12 ACKNOWLEDGEMENTS

The authors thank the staff of the Isotope Geology Unit, SURRC, without whom this work would not have been possible. Cathy Brown of BP and Pete Ainsworth of the Dept. of Geology and Applied Geology, Glasgow University, are thanked for their assistance with SEM work, and in addition P.A. for his patience in SEM CL studies. Steve Rainey of BP provided informative discussion and supervision. CIM acknowledges receipt of NERC grant no. GT4/86/GS/102. Core material was supplied through a CASE studentship with BP.

4.13 REFERENCES

Astin T.R. and Evans I.J., 1990, Volume loss through silicate dissolution during shale diagenesis : Implications for modelling the compaction and maturation histories of clastic sequences : Abstracts IAS 1990, Nottingham.

Atkinson, J.P. 1985, The use of reservoir engineering in the development of the Magnus oil reservoir : Soc Petrol Engineers 13979/12 Offshore Europe 85 Conference

Ayalon A. and Longstaffe F.J. 1988 Oxygen isotope studies of diagenesis and pore water evolution in the western Canada sedimentary basins: evidence from the Upper Cretaceous Basal Belly River Sandstone, Alberta: Journal of Sedimentary Petrology v. 58 p.489-505.

Badley M., Roberts A. and Yielding G., 1990, Subsidence in the Viking Graben and the tectonic setting of the Brent Group : Abstracts, Structure, sedimentology, diagenesis, hydrocarbons, and production geology : Brent Sandstones, North Sea, Joint meeting of the British Sedimentological Research Group and the Petroleum Group, London, March 1990, ISBN 0 85261 290 7.

Barker C.E and Goldstein R.H., 1990, A fluid inclusion technique for determining maximum temperature in calcite and its comparison to the vitrinite reflectance geothermometer : In press, Geology v. 18.

Barnard P.C. and Cooper B.S., 1981, Oils and source rocks of the North Sea area. In : Illing L.V. and Hobson G.D. eds., Petroleum Geology of the Continental Shelf of North West Europe, Heyden and Son, London, p. 169-175.

Bennet P. and Siegel D.I., 1987, Increased solubility of quartz in water due to complexing in organic compounds : Nature v. 326, p. 684-686.

Bennet P.C., Melcer M.E., Siegel D.I. and Hasset J.P., 1988, The dissolution of quartz in dilute aqueous solutions of organic acids at 25°C : Geochimica et Cosmochimica Acta v. 52, p. 1521-1530.

Bird M.I. and Chivas A.R., 1988, Stable isotope evidence for low temperature kaolinite weathering and post-formational hydrogen-isotope exchange in Permian kaolinites : Chemical Geology (IGS) v. 72, p. 249-265.

Bjorkum P.A. and Gjelsvik N., 1988, An isochemical model for formation of authigenic kaolinite, K feldspar and illite in sediments : Journal of Sedimentary Petrology V. 58 no. 3, p. 506-511.

Bjorkum P.A., Rune M., Walderhaug O. and Hurst A., 1990, The role of the late Cimmerian unconformity for the distribution of kaolinite in the Gullfaks field, northern North Sea : Sedimentology v. 37, p. 395-406.

Bjorlykke K., 1983, Diagenetic reactions in sandstones. In : Parker A. and Sellwood B.W. eds., NATO ASI Series C Mathematical and Physical Sciences v. 115, p. 169-214.

_____ and Brensdal A., 1986, Diagenesis of the Brent Sandstone in the Statfjord field, North Sea. In : Gautier D.L., ed., Roles of Organic Matter in Sediment Diagenesis, Society of Economic Palaeontologists and Mineralogists Special Publication 38, p. 157-167.

_____, 1988, Sandstone diagenesis in relation to destruction and preservation of porosity. In : Diagenesis 1, Chingarian G.V. and Wolf K.H. eds., Elsevier Science Publishers B.V., Amsterdam.

Boles J.R. and Coombs D.S., 1977, Zeolite facies alteration of sandstones in the Southland Syncline, New Zealand : Journal of Science v. 277, p. 982-1012.

_____ and Franks S.G, 1979, Clay diagenesis in Wilcox sandstones of southwest Texas : implications of smectite diagenesis on sandstone cementation : Journal of Sedimentary Petrology v. 49 no. 1, p. 55-70.

_____,1982, Active albitization of plagioclase, Gulf Coast Tertiary : American Journal of Science v. 282, p. 165-180.

_____ and Johnson K.S., 1983, Influence of mica surfaces on pore-water pH : Chemical Geology v. 43, p. 303-317.

Borthwick J. and Harmon R.S., 1982, A note regarding ClF_3 as an alternative to BrF_5 for oxygen isotope analysis : Geochimica et Cosmochimica Acta v. 46, p. 1665-1668.

Brint J.F., 1989, Isotope diagenesis and palaeofluid movement : Middle Jurassic Brent Sandstones, North Sea : Unpublished Ph.D. thesis, University of Strathclyde,UK.

Bucke D.P.J. Jr. and Mankin C.J., 1971, Clay mineral diagenesis within interlaminated shales and sandstones : Journal of Sedimentary Petrology v. 41 no. 4, p. 971-981.

Buhrig C., 1989, Geopressured Jurassic reservoirs in the Viking Graben : modelling and geologic significance : Marine and Petroleum Geology v. 6, p. 31-48.

Burley S.D.,1986, The development and destruction of porosity within Upper Jurassic reservoir sandstones of the Piper and Tartan fields, Outer Moray Firth, North Sea : Clay Minerals v. 21 no. 4, p. 649-694.

Carothers W.W. and Kharaka Y.K., 1980, Stable carbon isotopes of HCO_3^- on oilfield waters-implications for the origin of CO_2 : Geochimica et Cosmochimica Acta v. 44, p. 323-332.

Carstens H. and Finstad K.G., 1981, Geothermal Gradients of the Northern North Sea Basin, 59-62°N. In : Illing L.V. and Hobson G.D., eds., Petroleum Geology of the Continental Shelf of North West Europe, Heydon and Son, London, p. 152-161.

Claypool G.E., Holsen W.T., Kaplan I.R., Sakai H., and Zak I. , 1980, The age curves of sulphur and oxygen isotopes in marine sulphate and their mutual interpretation : Chemical Geology v. 28, p. 199-260.

Clayton R.N. and Mayeda T.K., 1963, The use of bromine pentafluoride in the extraction of oxygen from oxides and silicates for isotopic analysis : Geochimica et Cosmochimica Acta v. 27, p. 43-52.

Coplen T.B. and Hanshaw B.B., 1973, Ultrafiltration by a compacted clay membrane, I. Oxygen and hydrogen isotopic fractionation : Geochimica et Cosmochimica Acta v. 37, 2295-2310.

Craig H., 1957, Isotopic standards for carbon and oxygen and correction factors for mass spectrometric analysis of carbon dioxide : Geochimica et Cosmochimica Acta v. 12, p. 133-149.

Craig H., 1961, Isotopic variations in meteoric waters : Science v. 133, p. 1702-1703.

Crosbie T., 1981, Polished wafer preparation for fluid inclusion and other studies : Transactions of the Institute of Mining and Mietallurgy v. 90, B82-83.

Crossey L.J., Surdam R.C. and Lahann R., 1986, Applications of organic/inorganic diagenesis to porosity prediction. In : Gautier D.L., ed., Roles of organic matter in sediment diagenesis : S.E.P.M. Special Publication No. 38, p. 147-155.

Curtis C.D., 1983, Link between Aluminium Mobility and Destruction of Secondary Porosity : Bulletin of the American Association of Petroleum Geologists v. 67 no. 3, p. 380-384.

_____, Hughes C.R., Whiteman J.A. and Whittle C.K., 1985, Compositional variation within some sedimentary chlorites and some comments on their origin : Mineralogical Magazine, v. 49, p. 375-386.

_____ and Coleman M.L., 1986, Controls on the precipitation of early diagenetic calcite, dolomite and siderite concretions in complex depositional sequences. In : Gautier D.L., ed., Roles of organic matter in sediment diagenesis : S.E.P.M. Special Publication No. 38, p. 23-34.

Dansgaard W. and Tauber H., 1969, Glacier oxygen-18 content and Pleistocene ocean temperatures : Science v. 166, p. 499-502.

Day G.A., Cooper B.A., Anderson C., Burgers W.F.J., Ronnevik H.C. and Schoneich H., 1981, Regional Seismic Structure Maps of the North Sea. In : Illing L.V. and Hobson G.D. eds., Petroleum Geology of the Continental Shelf of North West Europe, Heyden and Son, London, p. 76-84.

De'Ath N.G. and Schuyleman S.F., 1981, The Geology of the Magnus Oilfield. In : Illing L.V. and Hobson G.D. eds., Petroleum Geology of the Continental Shelf of North West Europe, Heyden and Son, London, p. 342-351.

Deer W.A., Howie R.A. and Zussman J., 1966, An Introduction to the Rock Forming Minerals p.494 : John Wiley and Sons, New York.

Doebl F., Heling D., Homann W., Karweil J., Teichmuller M. and Welte D., 1974, Diagenesis of Tertiary clayey sediments and included dispersed organic matter in ralation to geothermics in the Upper Rhine Graben. In : Illies J.H. and Fuchs K. eds., Approaches to Taphrogenesis, Schweizerbartsche Verlagsbuchshandlung, Stuttgart, p. 192-207.

Dypvik H., 1983, Clay mineral transformation in Tertiary and Mesozoic sediments from the North Sea : Bulletin of the American Association of Petroleum Geologists v. 67 no. 1, p. 160-165.

Edman J.D., and Surdam R.C. 1986 Organic-inorganic reactions as a mechanism for porosity enhancement in the Upper Cretaceous Ericson Sandstone, Green River Basin, Wyoming. : In: Gautier D.L. (ed) Roles of organic matter in sediment diagenesis. Soc. Econ. Paleontol. Mineral. Spec. Publ. 38, Tulsa, Ok. p.85-110.

Emery D., Myers K. and Young R., 1988, Geophysica and diagenesis reveal subaerial exposure of the Magnus Sandstone : Abstracts of the 27th Annual Meeting of the British Sedimentological Research Group, Cambridge.

Evans I.J.,1989, Geochemical fluxes during diagenesis : an example from the Ordovician of Morocco. In Miles D.L. ed., Water-rock Interaction VI, Balkema, Rotterdam, p. 219-222.

Evans I.J., 1990, Quartz dissolution during shale diagenesis - implications for quartz cementation in sandstones : Abstracts of IAS, Nottingham.

Fallick A.E., Jocelyn J., Donnelly T., Guy M., and Behan C.,1985, Origin of agates in volcanic rocks from Scotland : Nature v. 313, p. 672-674 .

Faure G.,1986, Principles of Isotope Geology, 2nd Edition, Wiley and Sons, New York, 589p..

Fisher I.St.J. and Hudson J.D., 1987, Pyrite formation in Jurassic shales of contrasting biofacies. In Brooks J. and Fleet A.J. eds., Marine Petroleum Source Rocks, Geological Society Special Publication No. 26, p. 69-78.

Fisher I.St.J. and Land L.S., 1986, Diagenetic History of Eocene Wilcox Sandstones, South Central Texas : Geochimica et Cosmochimica Acta v. 50, p. 551-561.

Foscoles A.E. and Powell T.G., 1979, Catagenesis in shales and occurrence of authigenic clay in sandstone, North Sabine well H-49, Canadian Arctic Island : Canadian Journal of Earth Science v. 16, p. 1309-1314.

Fuchtbauer H., 1974, Sediments and Sedimentary Rocks 1 : E. Schweizerbart'sche Verlagsbuchshandlung, Stuttgart, 464pp..

Gautier D.L., 1985, Interpretation of early diagenesis in ancient marine sediments. In : Gautier D.L. ed., Relationship of Organic Matter and Mineral Diagenesis, SEPM Short Course no. 17, p. 6-78.

Gawthorpe R.L., 1987, Burial dolomitization and porosity development in a mixed carbonate-clastic sequence : an example from the Bowland Basin, northern England : Sedimentology v. 34, p. 533-558.

Giles M.R., and Marshall J.D., 1986, Constraints on the development of secondary porosity in the subsurface: re-evaluation of processes : Marine and Petroleum Geology v. 3, p.243-255.

Giles M.R., 1987, Mass transfer and problems of secondary porosity creation in deeply buried hydrocarbon resevoirs : Marine and Petroleum Geology v. 4, 188-204.

Glasmann J.R., Lundegard P.D., Clark R.A., Penny B.K. and Collins I.D., 1989, Geochemical evidence for the history of diagenesis and fluid migration, Brent Sandstone, Heather field, North Sea : Clay Minerals v. 24, p. 255-284.

Glennie K.W., 1984, The structural framework and the pre-Permian history of the North Sea area. In : Glennie K.W. ed., Introduction to the Petroleum Geology of the North Sea, Blackwell Scientific Publications, London, p. 25-62.

Goff J.C., 1983, Hydrocarbon generation and migration from Jurassic source rocks in the East Shetland Basin and Viking Graben of the northern North Sea : Journal of the Geological Society of London v. 140, p. 445-474.

Goldstein R.H., 1986, Reequilibration of fluid inclusions in low temperature calcium-carbonate cement : Geology v. 14, p. 792-795.

Graf D.L., Friedman I. and Meents W.F., 1965, Origin of saline formation waters II. Isotopic fractionation by shale microppore systems : Illinois Geological Survey Circular 393, 32pp..

Gray D.H. and Rex R.W., 1966, Formation damage in sandstones caused by clay dispersion and migration : Clays and Clay Minerals V. 14, p. 355-366.

Hallam A., 1982, The Jurassic climate, in Studies in Geophysics : Climate in Earth History, National Academy Press, Washington D.C., p. 159-163.

Hamilton P.J., Fallick A.E., MacIntyre R.M., and Elliot S., 1987, Isotopic tracing of the provinence and diagenesis of Lower Brent Group Sandtones, North Sea. In Brooks J. and Glennie K.W. eds., Petroleum Geology of North West Europe, Graham and Trotman, London, p. 939-949.

Hansen P.L. and Lindgren H., 1989, Mixed layer illite/smectite diagenesis in Upper Jurassic claystones of the North sea and onshore Denmark : Clay Minerals v. 24 no. 2, p. 197-214.

Hansley P.L., 1987, Petrologic and experimental evidence for the etching of garnets by organic acids in the Upper Jurassic Morrison Formation, NW New Mexico : Journal of Sedimentary Petrology v. 57 no. 4, p. 666-681.

Haszeldine R.S. and Russell M.J., 1987, The Late Carboniferous northern North Atlantic Ocean : implications for hydrocarbon exploration from Britain to the Arctic. In : Brooks J. and Glennie K.W. eds., Petroleum Geology of North West Europe, Graham and Trotman, London, p. 1163-1175.

Hay J.T.C., 1978, Structural development in the northern North Sea : Journal of Petroleum Geology v. 1 no. 1, p. 65-77.

Hayes J.B., 1979, Polytypism of chlorite in sedimentary rocks : Clays and Clay Minerals v. 18, p. 285-306.

Hayes M.J. and Boles J.R., 1990, Volumetric relations between dissolved plagioclase and kaolinite in San Joaquin basin sandstones : Implications for aluminium mobility : Abstracts of the Annual Convention of the American Association of Petroleum Geologists, San Fransisco .1990

Henry D.J., Toney J.B., Suchecki R.K. and Bloch S., 1986, Development of quartz overgrowths and pressure solution in quartz sandstones : evidence from cathodoluminescence backscattered electron imaging and trace element analysis on the electron microprobe : Abstract from the Geological Society of America Abstract Program v. 18, p. 635.

Hogg A.J.C., Jourdan A., Sellier E. and Pearson M., 1987, Cathodoluminescence of Quartz cements in Brent Group sandstones, South Alwyn, northern North Sea : Abstracts of the 26th Annual Meeting of the British Sedimentological Research Group, University of Aberdeen, Absract no. 60.

Hurst A. and Irwin H., 1982, Geological modelling of clay diagenesis in sandstones : Clay Minerals v. 17, p. 5-22.

Hurst A., 1985, The implications of clay mineralogy to palaeoclimate and provenance during the Jurassic in NE Scotland : Scottish Journal of Geology v. 21 no. 2, p. 143-160.

Hutcheon B. and Friedman I., 1969, Geochemistry and origin of formation waters in the Western Canada Sedimentary Basin I, Stable Isotopes of hydrogen and oxygen : Geochimica et Cosmochimica Acta v. 33, p. 1321-1349.

Iijima A. and Matsuomoto R, 1982, Berthierine and chamosite in coal measures of Japan : Clays and Clay Minerals v. 30, p. 264-274.

Ireland B.J., Curtis C.D. and Whiteman J.A., 1983, Compositional variation within some glauconites and illites and implications for their stability and origins : Sedimentology v. 30, p. 769-786.

Irwin H., Coleman M.L. and Curtis C.D., 1977, Isotopic evidence for several sources of carbonate and distinctive diagenetic processes in organic rich Kimmeridgian sediments : Nature v. 269, p. 209-213.

Jackson M.L., 1979, Soil chemical analyses - advanced course 2nd edition : Published by the author, Madison, Wisconsin 53705, 895p.

James A.T and Baker D.R., 1976, Oxygen isotope exchange between illite and water at 22°C : Geochimica et Cosmochimica Acta v. 40, p. 235-239.

Jenkin G.R.T., 1988, Stable isotope studies in the Caledonides of SW Connemara, Ireland : Unpublished Ph.D. thesis, University of Glasgow.

Jourdan A., Thomas M., Brevant O., Robson P., Somme F. and Sullivan M., 1987, Diagenesis as a control of the Brent Sandstone reservoie properties in the Greater Alwyn area (East Shetland Basin). In : Brooks J. and Glennie K.W. eds., Petroleum Geology of North West Europe, Graham and Trotman, London, p. 951-961.

Kantorowicz J.D., 1990, The influence of variations in illite morphology on the permeability of Middle Jurassic Brent Group sandstones, Cormorant Field, UK North Sea : Marine and Petroleum Geology v. 7, p. 66-74.

Kharaka Y.K., Berry A.F. and Friedman I., 1973, Isotopic composition of oilfield brines from Kettleman North Dome, California, and their geologic implications : Geochimica et Cosmochimica Acta v. 37, p. 1899-1908.

Krouse H.R., Viau C.A., Eliuk L.S.,Veda A. and Halas S., 1988, Chemical and isotopic evidence of thermochemical sulphate reduction by light hydrocarbon gases in deep carbonate reservoirs : Nature v. 333, p. 415-419.

Lambert S.J. and Epstein S., 1980, Stable isotope investigations of an active geothermal system in Valles Caldera, Jemez Mountains, New Mexico : Journal of Volcanological and Geothermal Research v. 8, 111-129.

Land L.S., Milliken K.L. and McBride E.F. 1987 Diagenetic evolution of Cenozoic sandstones, Gulf of Mexico sedimentary basin: Sedimentary Geology v.50 p.195-225.

Lawrence J.R., 1970, $^{18}O/^{16}O$ and D/H ratios of soils, weathering zones and clay deposits : Ph.D thesis, California Institute of Technology, Pasadena, California 263pp..

Ledoux R.L. and White J.L., 1964, Infrared studies of OH^- groups in expanded kaolinite : Science v. 143, p, 244-246.

Lee M. and Savin S.M., 1985, Isolation of diagenetic overgrowths on sand grains for oxygen isotope analysis : Geochimica et Cosmochimica Acta v. 49, p. 497-501.

Lewis C.R. and Rose S.C., 1970, A theory relating high temperatures and overpressures : Journal of Petroleum Technology v. 22, p. 11-16.

Liu K-K and Epstein S., 1984, The hydrogen isotope fractionation between kaolinite and water : Isotope Geoscience v. 2, p. 335-350.

Longstaffe F.J., 1989, Stable Isotopes as Tracers in Clastic Diagenesis, in I.E. Hutcheon ed., Burial Diagenesis, Mineralogical Association of Canada Short Course Series v. 15, p.201-277.

---------- and Ayalon A.,1989, Hydrogen isotope variations of diagenetic clay minerals from Cretaceous clastic rocks, Western Canada Sedimentary Basin ; Abstract : 9th International Clay Conference, Strasbourg, France.

Lopatin N.V., 1976, K opredeleniyu vliyaniya temperatury i geologicheskogo vremeni na katageneticheskiye protsessy uglefikatsii i neftegazoobrazovaniya (the influence of temperature and geologic time on the catagenetic processes of coalification and petroleum and gas formation). In : Issledovaniya organicheskogo veshchestva sovremennykh i iskopayemykh osakdov, Moscow, Nauka Press, p. 361-366.

Lundegard P.D., Land L.S. and Galloway W.E. 1984 Problem of secondary porosity: Frio Formation (Oligocene) Texas Gulf Coast : Geology v. 12, p.399-402

_____ and Land L.S., 1986, Carbon dioxide and organic acids : their role in porosity enhancement and cementation, Paleogene of the Texas Gulf Coast. In Gautier D.L., ed., Roles of organic matter in sediment diagenesis : S.E.P.M. Special Publication No. 38, p. 129-146.

Matter A. and Ramseyer K., 1985, Cathodoluminescence microscopy as a tool for provenance studies of sandstone. In Zuffa G.G. ed., Provenancs of Arenites, NATO ASI, Reidel, p. 191-211.

McBride E,F., 1989, Quartz cement in Sandstones : A Review : Earth Science Reviews V. 26, p. 69-112.

McHardy W J., Wilson M.J. and Tait J.M., 1982, Electron microscope and X-ray diffraction studies of filamentous illitic clay from sandstones of the Magnus field : Clay Minerals v. 17, p. 23-29.

Milliken K.L., Land L.S. and Loucks R.G., 1981, History of burial diagenesis determined from isotopic geochemistry, Frio Formation, Brazoria County, Texas : Bulletin of the American Association of Petroleum Geologists v. 65, p. 1397-1413.

Morris R.C. and Fletcher A.B., 1987, Increased solubility of quartz following ferrous-ferric iron reactions : Nature v. 330, p. 558-561.

Nadeau P.H., 1985, The physical dimensions of fundamental clay particles : Clay Minerals v. 20, p. 499-514.

Nagtegaal P.J.C., 1978, Sandstone - framework instability as a function of burial diagenesis : Journal of the Geological Society of London v. 135, p. 101-105.

Nakai N. and Jensen M.L., 1964, The kinetic isotope effect in the bacterial reduction and oxidation of sulfur : Geochimica et Cosmochimica Acta v. 28, p. 1893-1912.

O'Neil J.R. and Kharaka Y.F., 1976, Hydrogen and oxygen isotope exchange reactions between clay minerals and water : Geochimica et Cosmochimica Acta v. 40, p. 241-246.

_____ 1986, Theoretical and experimental aspects of isotopic fractionation. In : Valley J.W., Taylor H.P. Jr. and O'Neil J.R. eds., Stable isotopes in high temperature geological processes, Mineralogical Society of America Reviews in Mineralogy v. 16, p. 1-40.

Osborne M. and Haszeldine R.S., 1990, Fluid inclusions in diagenetic quartz record oilfield burial temperatures, not precipitation temperatures : submitted to Geology.

Pettijohn F.J., 1975, Sedimentary rocks, Third Edition, Harper and Row, New York, p. 77, 628pp..

Pittman E.D., 1972, Diagenesis of quartz in sandstones as revealed by scanning electron microscopy : Journal of Sedimentary Petrology v. 42, p. 507-519.

Plummer L.N. 1975 Mixing of seawater with calcium carbonate ground water: Geological Soc. of America Memoir 142 p.219-236.

Prezbindowski D.R. and Larese R.E., 1987, Experimental stretching of fluid inclusions in calcite - implications for diagenetic studies : Geology v. 15, p. 333-336.

Rainey S.C.R., 1987, Sedimentology, diagenesis and geochemistry of the Magnus Sandstone Member, northern North Sea : Unpublished Ph.D. thesis, University of Edinburgh.

Raiswell R., 1982, Pyrite texture, isotopic composition and the availability of iron : American Journal of Science v. 282, p. 1244-1263.

Robinson B.W.and Kusakabe M., 1975, Quantitative preparation of SO_2 for $^{34}S/^{32}S$ analyses from sulphides by combustion with cuprous oxide : Analytical Chemistry v. 47, p. 1179-1181.

Roedder E., 1984, Fluid Inclusions : Mineralogical Society of America Review in Mineralogy v. 12, p. 12.

Savin S., 1977, The history of the earth surface temperature during the past 100 million years : Annual Reviews in Earth and Planetary Science v. 5, p. 319-355.

------- and Yeh H-W., 1981, Stable isotopes in ocean sediments, in Emiliari C. ed., The Sea Volume 7, The Oceanic Lithosphere, John Wiley and Sons, New York, p. 1521-1554.

Savin S.M. and Lee M., 1988, Isotopic studies of phyllosilicates. In : Hydrous Phyllosilicates, Bailey S.W. ed., Mineralogical Society of America Reviews in Mineralogy v. 19, p. 189-224.

Seeman U., 1979, Diagenetically formed interstitial clay minerals as a factor in Rotliegend sandstone reservoir quality in the Dutch sector of the North Sea : Journal of Petroleum Geology v. 1, p. 55-62.

Schmidt V. and McDonald D.A., 1979 The role of secondary porosity in the course of sandstone diagenesis, In: Scholle, P.A. and Schluger, P.R. (eds) Aspects of diagenesis Soc Econ Palaeontol Mineral Spec Publ 26, Tulsa, Oklaholma, p. 175-208.

Shackleton N.J., 1967, Oxygen isotope analyses and Pleistocene temperatures reassessed : Nature v. 215, p. 15-17.

_____ and Kennett J.P.,1975, Palaeotemperature history of the Cenozoic and the initiation of Antarctic glaciation : oxygen and carbon isotope analyses in DSDP sites 277, 279 and 281. In Kennett J.P., Houtz R.E. et al., eds., " Initial Reports of the Deep Sea Drilling Project ", XXIX, Washington, p. 743-755 .

Shepherd T.J., 1981, Temperature programmable, heating-freezing stage for microthermometric analysis of fluid inclusions : Economic Geology v. 76, p. 1244-1247.

Sheppard S.M.F., 1986, Characterization and isotopic variations in natural waters. In : Stable isotopes in high temperature geological processes, Valley J.W., Taylor H.P. and O'Neil J.R. eds., Reviews in Mineralogy v. 16, Mineralogical Society of America, Washington D.C..

_____ and Charef A., 1986, Eau organique : caracterisation isotopique et evidence de son role dans le gisement Pb-Zn de Fedj-el-Adoum, Tunisie : C.R. Acad. Sci. Paris, t. 302, serie II, no. 19, p. 1189-1192

Shock E.L., 1988, Organic acid metastability in sedimentary basins : Geology v. 16, p. 886-890.

Smith A.G. and Briden J.C., 1977, Mesozoic and Cenozoic Palaeocontinental Maps, Cambridge University Press, 63pp..

Sweeney R.E. and Kaplan I.R., 1973, Diagenetic sulphate reduction in marine sediments : Marine Chemistry v. 9, p. 165-174.

Surdam R.C., Boese S.W. and Crossey L.J., 1984, The chemistry of secondary porosity. In McDonald D.A. and Surdam R.C. eds., Clastic diagenesis : American Association of Petroleum Geologists Memoir 37, p. 127-150.

Taylor H.P.Jr., and Forester R.W.,1971, Low $\delta^{18}O$ igneous rocks from the intrusive complexes of Skye, Mull and Ardnamurchan, Western Scotland : Journal of Petrology v.12, p. 465-497 .

_____ 1979, Oxygen and hydrogen isotope relationships in hydrothermal mineral deposits. In : Barnes H.L., ed., Geochemistry of hydrothermal ore deposits 2nd edition, John Wiley and Sons, New York, p. 236-277.

Thode H.G., Monster J. and Dunford H.B., 1961, Sulphur isotope geochemistry : Geochimica et Cosmochimica Acta v. 25, p. 150-174.

Trudinger P.A. and Chambers L.A., 1973, Reversibility of bacterial sulphate reduction and its relevance to isotopic fractionation : Geochimica et Cosmochimica Acta v. 37, p. 1775-1778.

Walderhaug O. , 1990, A fluid inclusion study of quartz cemented sandstones from offshore mid-Norway - possible evidence for continued quartz cementation during oil emplacement : Journal of Sedimentary Petrology v. 60 no. 2, p. 203-210.

Welton J.E., 1984, Chlorite, in SEM Petrology Atlas, Methods in Exploration Series, American Association of Petroleum Geologists, Tulsa, p. 46-47, pp237.

Whitney G. and Northrop H.R., 1987, Diagenesis and fluid flow in the San Juan Basin, New Mexico - regional zonation in the mineralogy and stable isotope composition of clay minerals in sandstone : American Journal of Science v. 287, p. 353-382.

Wilson M.D., 1982, Formation damage in sandstones : Course notes for Poroperm Laboratories.

Yeh H-W, 1980, D/H ratios and late stage dehydration of shales during burial : Geochimica et Cosmochimica Acta v. 44, p. 341-352.

Zinkernagel U., 1978, Cathodoluminescence of quartz and its application to sandstone petrology : Contributions to Sedimentology v. 8, p. 1-69.

4.14 TABLES

DEPTH (m)	Mqz	Pqz	K-flr	Plag	Mica	Sid	Ank	Kaol	Q o/g	Poro	Pyr	Det	Gnt
2938.3	48.1	2.2	15.2	3.8	1.8	0.1	0.1	4.8	5.0	14.8	1.4	2.6	0.2
2945.7	45.6	3.1	18.1	1.6	1.8	0.9	0.1	3.2	4.7	15.4	1.8	2.4	0.8
2954.5	46.7	1.9	19.2	3.4	1.6	0.6	0.0	2.4	3.4	17.3	0.6	2.2	0.8
2963.4	48.1	2.4	18.0	2.0	2.6	1.4	0.0	2.6	3.8	13.5	0.8	4.0	1.0
2971.4	46.2	2.6	17.5	1.2	1.0	0.4	0.0	3.0	7.6	18.3	0.4	1.4	0.4
2975.5	43.1	2.5	19.5	2.2	0.4	1.7	0.3	2.4	3.8	19.7	1.2	2.8	0.4
2978.6	44.7	3.0	18.6	1.6	0.8	0.9	2.1	4.4	3.6	15.8	0.4	4.0	0.2
2983.7	49.4	2.7	19.1	1.2	1.8	0.1	0.2	4.8	2.6	12.1	1.4	4.0	0.6

Table 1 : Point count results (500 counts per thin section) : 211/12-1. Mqz = monocrystalline quartz, Pqz = poycrystalline quartz, K-flr = K-feldspar, Plag = plagioclase, Sid =magnesian siderite, Ank = ankerite, Kaol = kaolinite, Q o/g = quartz overgrowths, Poro = porosity, Pyr = pyrite, Det = detrital clay, heavy and unidentified minerals, Gnt = garnet.

DEPTH (m)	Mqz	Pqz	K-flr	Plag	Mica	Sid	Ank	Kaol	Q o/g	Poro	Pyr	Det
2946.5	51.7	3.3	8.0	3.7	0.2	0.8	6.2	2.4	8.2	14.6	1.2	2.4
2962.1	48.3	2.9	11.2	3.2	1.2	0.8	7.2	3.2	3.6	13.8	1.2	3.6
2986.5	53.2	4.6	11.8	4.6	0.6	0.6	4.4	4.4	0.6	12.0	1.6	1.6
3006.3	56.1	4.3	13.4	4.2	0.8	2.4	2.0	3.0	1.0	9.8	1.6	1.4
3026.8	58.9	3.3	14.8	2.4	2.2	0.4	0.0	2.2	1.4	10.8	1.4	3.2
3040.4	54.6	3.6	12.8	1.8	1.2	1.6	0.0	3.4	4.2	11.6	1.8	3.4
3052.7	51.3	4.1	10.4	1.2	1.0	0.2	0.0	3.4	7.0	16.0	1.2	4.2
3073.9	51.6	4.4	8.6	1.0	0.6	1.7	3.9	5.0	7.4	7.8	2.6	5.4

Table 2 : Point count results (500 counts per thin section) : 211/12a-M1. Mqz = monocrystalline quartz, Pqz = poycrystalline quartz, K-flr = K-feldspar, Plag = plagioclase, Sid =magnesian siderite, Ank = ankerite, Kaol = kaolinite, Q o/g = quartz overgrowths, Poro = porosity, Pyr = pyrite, Det = detrital clay, heavy and unidentified minerals.

DEPTH (m)	Mqz	Pqz	K-flr	Plag	Mica	Sid	Ank	Kaol	Q o/g	Poro	Pyr	Det
3184.5	57.3	1.9	12.8	1.4	0.8	0.3	0.3	9.2	3.6	6.8	1.0	4.6
3194.1	46.6	2.2	16.0	2.0	2.6	0.5	1.7	5.0	4.2	7.4	1.0	10.8
3206.0	44.3	3.1	13.8	2.6	1.0	0.4	7.6	7.0	5.0	9.0	1.8	4.4
3229.5	46.9	4.5	15.2	1.4	0.6	1.2	0.0	7.8	5.0	11.0	1.4	5.0
3240.0	53.9	3.7	14.4	1.4	1.8	0.6	0.2	9.4	4.4	4.2	1.4	5.6
3248.0	47.3	4.1	13.8	2.6	1.2	0.0	21.8	4.6	3.2	0.0	0.8	0.6
3262.7	48.9	2.3	12.6	2.8	0.8	0.3	0.3	7.8	7.2	11.2	0.6	5.2
3280.0	54.7	2.5	11.6	2.0	1.4	4.8	0.0	4.6	2.8	10.2	0.4	5.0
3291.4	49.9	4.5	14.0	1.0	1.6	2.4	0.0	4.6	6.4	12.8	0.4	2.4
3308.7	48.6	2.0	9.2	1.0	2.0	1.6	0.0	12.4	7.0	7.0	1.6	7.4
3313.3	53.9	3.9	11.8	3.8	0.8	0.8	0.0	8.8	4.4	6.8	1.4	3.6
3338.5	54.8	4.8	12.6	2.2	0.8	2.8	0.0	5.0	4.4	4.6	2.2	5.8
3345.3	47.1	1.5	11.6	2.0	0.4	7.7	2.9	3.6	6.6	10.8	1.8	4.0
3355.3	54.6	1.8	10.6	1.0	0.2	3.0	9.2	4.0	1.2	8.8	1.2	4.4
3363.8	55.4	4.4	15.6	0.6	1.6	0.4	0.0	2.6	0.6	8.6	1.0	3.2
3374.8	55.5	3.9	14.2	1.2	0.4	0.4	0.0	3.8	4.0	14.0	0.4	2.2
3380.5	49.1	2.3	11.8	2.0	0.6	0.2	0.2	5.2	5.8	4.0	1.6	17.2

Table 3 : Point count results (500 counts per thin section) : 211/12a-9. Mqz = monocrystalline quartz, Pqz = poycrystalline quartz, K-flr = K-feldspar, Plag = plagioclase, Sid =magnesian siderite, Ank = ankerite, Kaol = kaolinite, Q o/g = quartz overgrowths, Poro = porosity, Pyr = pyrite, Det = detrital clay, heavy and unidentified minerals.

DEPTH (m)	%Feldspar Dissolution	Calc % Qtz o/g	P count % o/g	Calc % Kaolinite	P count% Kaolinite
2938.3	5.8	2.2	5.0	3.6	4.8
2945.7	9.1	3.6	4.7	5.5	3.2
2954.5	6.7	2.7	3.4	4.0	2.4
2963.4	8.4	3.4	3.8	5.0	2.6
2971.4	7.6	3.0	7.6	4.6	3.0
2975.5	8.2	3.3	3.8	4.9	2.4
2978.6	6.9	2.8	3.6	4.1	4.4
2983.7	6.4	2.6	2.6	3.8	4.8

Table 4 : Feldspar dissolution and comparison of calculated and point counted percentages of resultant quartz overgrowths and kaolinite : 211/12-1.

DEPTH (m)	%Feldspar Dissolution	Calc % Qtz o/g	P count % o/g	Calc % Kaolinite	P count% Kaolinite
2946.5	8.2	3.3	8.2	4.9	2.4
2962.1	7.6	3.0	3.6	4.6	3.2
2986.5	4.2	1.7	0.6	2.5	4.4
3006.3	4.4	1.8	1.0	2.6	3.0
3026.8	5.0	2.0	1.4	3.0	2.2
3040.4	6.7	2.7	4.2	4.0	3.4
3052.7	7.0	2.8	7.0	4.2	3.4
3073.9	7.7	3.1	7.4	4.6	5.0

Table 5 : Feldspar dissolution and comparison of calculated and point counted percentages of resultant quartz overgrowths and kaolinite : 211/12a-M1.

DEPTH (m)	%Feldspar Dissolution	Calc % Qtz o/g	P count % o/g	Calc % Kaolinite	P count% Kaolinite
3184.5	6.5	2.6	3.6	3.9	9.2
3194.1	4.9	2.0	4.2	2.9	5.0
3206.0	9.3	3.7	5.0	5.6	7.0
3229.5	3.0	1.2	5.0	1.8	7.8
3240.0	7.5	3.0	4.4	4.5	9.4
3248.0	3.3	1.3	3.2	2.0	4.6
3262.7	9.6	3.8	7.2	5.8	7.8
3280.0	3.0	1.2	2.8	1.8	4.6
3308.6	6.9	2.8	7.0	4.1	12.4
3313.3	5.6	2.2	4.4	3.4	8.8
3338.5	6.1	2.4	4.4	3.7	5.0
3355.3	8.3	3.3	1.2	5.0	4.0
3380.5	7.9	3.2	5.8	4.7	5.2

Table 6 : Feldspar dissolution and comparison of calculated and point counted percentages of resultant quartz overgrowths and kaolinite : 211/12a-9.

211/12-1

DEPTH (m)	%Overgrowth from SEM CL	Point count % Overgrowth	Point count % as %Total Quartz
2938.3	18.6	5.0	9.9
2963.4	18.3	3.8	7.5
2971.4	19.3	7.6	15.6
211/12a-9			
3291.4	19.1	6.4	11.8
3345.3	18.5	6.6	13.6
3361.5	17.5	8.6	11.0

Table 7 : SEM CL versus petrographic quartz overgrowth abundances.

WELL	DEPTH (m)	SIZE (μm)	AGE (myr)	REPEAT
211/12a-9	3184.5	<0.1	56.6 ±2.3	54.3 ±2.4
211/12a-9	3184.5	0.1-0.5	82.2 ±2.7	83.5 ±2.7
211/12a-9	3262.7	0.1-0.5	41.8 ±1.3	50.1 ±2.5

Table 8 : Illite K/Ar age dates.

DEPTH (m)	SIEVED SIZE FRACTION (μm)				
	20-53	53-85	85-106	106-160	160-250
3184.5		12.81	12.19	12.65	13.75
3206.0	13.12	12.93	12.58	12.80	14.17
3240.0		11.44	11.84	12.64	13.13
3262.7	11.01	12.14	12.34	12.08	13.67
3313.3		12.00	12.17	12.20	14.57
3355.3		12.35	12.59	13.39	13.72

Table 9 : Quartz overgrowth $\delta^{18}O$ results by the method of Lee and Savin (1985).

WELL	DEPTH (m)	$\delta^{18}O$ det +o/g	$\delta^{18}O$det core	%qtz o/g	$\delta^{18}O$qtz o/g
211/12-1	2938.3	12.5	11.9	18.6	23.9
211/12-1	2963.4	12.8	11.9	18.3	24.3
211/12-1	2971.4	12.3	11.4	19.3	25.9
211/12a-9	3291.4	14.4	12.0	19.1	28.6
211/12a-9	3345.3	15.2	11.5	18.5	30.1
211/12a-9	3361.5	15.1	11.4	17.5	28.2

Table 10 : Quartz oxygen isotopes: assume that the detrital core has a constant $\delta^{18}O = \delta c$ and overgrowths have a constant $\delta^{18}O = \delta o$. The measured $\delta^{18}O = \delta m = 1/100\{\%\delta o + (100-\%)\delta c\}$. det = detrital, o/g = overgrowth.

Garnet 211/12a-9 3355.3m $\delta^{18}O$ 12.7

WELL	DEPTH (m)	SIZE (μm)	δ^{18}Osmow	δD
211/12-1	2945.7	2-5	13.7	-91.6
211/12-1	2945.7	5-10	14.0	-61.1
211/12-1	2954.5	2-5	14.9	-90.7
211/12-1	2971.4	2-5	12.9	-81.6
211/12-1	2971.4	5-10	13.7	-85.1
211/12-1	2975.5	2-5	12.5	
211/12-1	2975.5	5-10	13.4	
211/12-1	2978.6	2-5	12.9	-101.4
211/12-1	2978.6	5-10	12.9	
211/12-1	2983.7	2-5	14.3	-80.8
211/12-1	2983.7	5-10	13.9	-94.1
211/12a-M1	2936.6	5-10	14.4	
211/12a-M1	2952.1	5-10	13.8	
211/12a-M1	2976.6	1-2	14.2	
211/12a-M1	2976.6	2-5	13.7	
211/12a-M1	2976.6	5-10	13.9	
211/12a-M1	2996.3	2-5	13.9	
211/12a-M1	2996.3	5-10	13.8	
211/12a-M1	3064.0	5-10	15.3	
211/12a-9	3184.5	2-5	16.7	-63.0
211/12a-9	3184.5	5-10	17.5	-68.7
211/12a-9	3206.0	5-10	15.5	-81.0
211/12a-9	3262.7	2-5	16.3	-60.2
211/12a-9	3313.3	2-5	15.9	
211/12a-9	3313.3	5-10	16.6	

Table 11 : Kaolinite oxygen and hydrogen isotope data (‰).

WELL	DEPTH (m)	$\delta^{34}S$	HOST
211/12a-M1	2912.8	-47.7	Cret. Lst.
211/12a-9	3184.5	+4.4	Sst.
211/12a-9	3206.0	-13.0	Sst.
211/12a-9	3240.0	+7.8	Sst.
211/12a-9	3248.0	+15.7	Thin sst. in mudstone.
211/12a-9	3262.7	-0.3	Sst.
211/12a-9	3313.3	-8.7	Sst.
211/12a-9	3355.3	-1.2	Sst.

Table 12 : Pyrite sulphur isotopes (‰).

WELL	DEPTH (m)	$\delta^{13}C$	$\delta^{18}Opdb$	$\delta^{18}Osmow$
211/12-1	2963.4	-9.2	-15.0	15.2
211/12-1	2975.4	-11.8	-13.8	16.4
211/12-1	2976.6	-10.2	-13.5	16.7
211/12-1	2978.6	-14.1	-16.6	13.6
211/12-1	2983.7	-8.0	-12.0	18.2
211/12a-M1	3030.2	-9.4	-12.0	18.3
211/12a-M1	3030.4	-9.0	-14.0	16.2
211/12a-M1	3042.8	-11.1	-12.8	17.4
211/12a-M1	3059.8	-9.7	-12.5	17.7
211/12a-M1	3064.0	-9.4	-11.8	18.4
211/12a-9	3184.5	-14.6	-16.0	14.1
211/12a-9	3240.0	-11.9	-11.6	18.6
211/12a-9	3262.7	-11.7	-13.5	16.7
211/12a-9	3313.3	-11.0	-12.5	17.7
211/12a-9	3355.3	-8.8	-12.8	17.4

Table 13 : Magnesian siderite carbon and oxygen isotopic data (‰).

WELL	DEPTH (m)	$\delta^{13}C$	$\delta^{18}Opdb$	$\delta^{18}Osmow$
211/12-1	2954.5	-10.6	-11.8	19.1
211/12-1	2971.4	-12.1	-13.5	17.1
211/12-1	2978.6	-13.6	-13.8	17.1
211/12a-M1	2936.6	-10.7	-11.2	19.4
211/12a-M1	2951.9	-12.8	-10.7	20.3
211/12a-M1	2952.1	-11.5	-9.7	20.4
211/12a-M1	2976.4	-10.4	-10.1	20.5
211/12a-M1	2976.6	-9.7	-10.3	20.3
211/12a-M1	2996.1	-10.8	-10.2	20.4
211/12a-M1	2996.2	-9.5	-10.2	20.5
211/12a-M1	3042.8	-9.3	-11.2	19.3
211/12a-M1	3064.0	-11.4	-11.3	19.2
211/12a-9	3206.0	-10.6	-9.0	21.3
211/12a-9	3248.0	-13.4	-8.7	21.6
211/12a-9	3249.2	-11.9	-8.9	21.4
211/12a-9	3355.3	-7.7	-9.3	20.9
211/12-3A	3069.9	-9.9	-7.6	23.1
211/12-3A	3074.6	-10.1	-7.8	22.8
211/12-6	3019.9	-6.7	-8.4	22.2
211/12-6	3081.1	-6.1	-8.2	22.4

Table 14 : Ankerite carbon and oxygen isotopic data (‰).

WELL	DEPTH (m)	SIZE (μm)	δ^{18}Osmow	δD
211/12-1	2938.3	<0.1	9.1	-103.8
211/12-1	2938.3	0.1-0.5	11.4	-100.5
211/12-1	2945.7	<0.1	12.8	
211/12-1	2945.7	0.1-0.5	12.7	-102.4
211/12-1	2954.5	0.1-0.5	12.2	
211/12-1	2963.4	<0.1	9.2	-101.3
211/12-1	2963.4	0.1-0.5	13.0	-76.4
211/12-1	2975.5	<0.1		-81.8
211/12-1	2975.5	0.1-0.5		-125.3
211/12a-M1	2936.6	<0.1	11.7	-89.7
211/12a-M1	2936.6	0.1-0.5	12.7	-90.9
211/12a-M1	2936.6	0.5-1.0	12.9	
211/12a-M1	2952.1	<0.1	11.3	
211/12a-M1	2952.1	0.1-0.5	11.0	
211/12a-M1	2952.1	0.5-1.0	10.1	
211/12a-M1	2976.6	0.5-1.0	12.8	
211/12a-M1	2993.3	<0.1	11.3	-89.8
211/12a-M1	2996.3	0.1-0.5	11.8	
211/12a-M1	2996.3	0.5-1.0	11.0	
211/12a-M1	3016.8	<0.5	11.4	
211/12a-M1	3030.4	<1.0	11.7	
211/12a-M1	3042.8	<0.1	9.8	
211/12a-M1	3042.8	0.1-0.5	12.2	
211/12a-M1	3042.8	0.5-1.0	11.6	
211/12a-M1	3064.0	<0.1	9.5	
211/12a-M1	3064.0	0.1-0.5	12.3	
211/12a-M1	3064.0	0.5-1.0	11.7	
211/12a-9	3184.5	<0.1	12.9	-64.5
211/12a-9	3184.5	0.1-0.5	15.5	-58.5
211/12a-9	3262.7	0.1-0.5	15.5	-75.3

Table 15 : Illite oxygen and hydrogen isotope data (‰).

4.14 FIGURE CAPTIONS

Figure 1 : Location of the Magnus oilfield.

Figure 2 : Magnus stratigraphic succession and reservoir reference section (after De'Ath and Schuyleman, 1981).

Figure 3 : The Magnus oilfield is defined to the east by the oil/water contact and to the west by subcrop of the Magnus Sandstone beneath Cretaceous marine sediments, and by depositional pinchout to the north and south.

Figure 4a : Cross-section through the Magnus oilfield showing the location of the three wells studied, and the Magnus Sandstone between the Upper and Lower Kimmeridge Clay Formations (UKCF, LKCF) below the mid-Cretaceous unconformity. Well -1 to well-9 is 3km.

Figure 4b : Burial history curve for the Magnus Sandstone. K/Ar dates constrain illite (the last diagenetic phase) formation to 55-42Ma.

Figure 5 : Generalised paragenetic sequence for the Magnus Sandstone.

Figure 6 : Early diagenetic illite (I) developed perpendicular to detrital grain surface, and overgrown by later quartz (Q). SEM image, 3291.4m, 211/12a-9.

Figure 7 : Pyrite framboids (P) composed of octahedral crystallites. SEM image3206.0m, 211/12a-9.

Figure 8 : Early fine-grained blocky kaolinite (K) enclosed by later quartz (Q). SEM image, 3313.3m, 211/12a-9.

Figure 9 : Small K-feldspar overgrowths (KO) developed on skeletal dissolved detrital K-feldspar grain. SEM image, 2954.4m, 211/12-1.

Figure 10 : Rare albite (AO) overgrowths form a grain-rimming cement around detrital plagioclase. Note also diagenetic fracture-filling K-feldspar (FF) and overgrowths (KO) on Detrital K-feldspar. Backscattered electron image (BSEM), 3345.3m, 211/12a-9.

Figure 11a : Dissolved detrital K-feldspar grain with diagenetic K-feldspar overgrowth (KO) developed on adjacent K-feldspar grain. SEM image, 3016.8m, 211/12a-M1.

Figure 11b : Garnet (G) dissolution by organic acids results in rhombic crystal faces. After dissolution, the pore was infilled by kaolinite 2 (K). Thin section photomicrograph, 3229.5m, 211/12a-9.

Figure 12a : Small inividual quartz overgrowth euhedra (Q). SEM image, 2954.5m, 211/12-1.

Figure 12b : Well developed prismatic quartz overgrowths (Q) predate pore-filling kaolinite (K). SEM image, 3291.4m, 211/12a-9.

Figure 13 : SEM cathodoluminescence (SEM CL) photomicrograph showing diagenetic quartz (Q) outgrowth. 2975.5m, 211/12-1.

Figure 14 : Thin section photomicrograph in crossed polars showing poor definition of detrital quartz (DQ)/overgrowth (Q) boundary.3248.0m, 211/12a-9. Note also that the sandstone is completely cemented by silica(Q) and later ankerite (A).

Figure 15 : Three stages of quartz overgrowth (Q) development are clearly defined in this SEM CL image. 2936.6m, 211/12a-M1.

Figure 16 : Precipitation of quartz (Q) forms stepped overgrowths, which encloses early kaolinite 1. SEM image, 2952.1m, 211/12a-9.

Figure 17 : Diagenetic quartz (Q) intergrown with the ends of illite (I) fibres. SEM image, 3042.8m, 211/12a-9.

Figure 18 : Vermiform morphology typical of crestal kaolinite 2 (K) - 2963.4m, 211/12-1. SEM image.

Figure 19 : Blocky morphology typical of deeper kaolinite (K) - 3290.5m, 211/12a-9. SEM image.

Figure 20 a, b and c : In all 3 wells more quartz cement exists than can be accounted for by feldspar dissolution alone. d, e and f : In crestal wells 211/12-1 and 211/12a-M1 less kaolinite was point counted than should be present if Al^{3+} released through feldspar dissolution was conserved. In deep well 211/12a-9 more Al^{3+} been conserved and more kaolinite precipitated after feldspar dissolution. This was probably the result of a higher concentration of Al^{3+} complexing organic acids in the porefluids of deeper, more shale-rich, well 211/12a-9. Calc % Qtz and Calc % Kaol = Theoretical percentages of diagenetic quartz and kaolinite that would be expected if the equation Feldspar -> 40%quartz + 60% kaolinite (by volume) were observed without loss. PC = point counted from thin sections, 500 counts per section. FELD DISS = Feldspar dissolution, as determined by 500-per-thin-section point counts. Stipple=mud, white=sand.

Figure 21 : Backscattered electron image showing intimate growth of magnesian siderite (S) through ion supply from detrital biotite (B) and mud clasts (MC). Bright specks are pyrite. 3262.7m, 211/12a-9

Figure 22 : Magnesian siderite (S) replacing pore-filling kaolinite (K) : thin section photomicrograph, 3240.0m, 211/12a-9.

Figure 23 : Magnesian siderite (S) developed inside the shell of a dissolved feldspar grain (F) : SEM photomicrograph, 2963.4m, 211/12-1.

Figure 24 : Backscattered electron image showing zoned magnesian siderite (S) enclosed and post-dated by ankerite (A), 3355.3m, 211/12a-9.

Figure 25 : Chlorite (C) showing rare "beehive" texture, and being enclosed by later quartz (Q). SEM image, 2976.6m, 211/12a-M1.

Figure 26 : Intergrowth of late diagenetic ankerite (A), illite (I) and quartz (Q). SEM photomicrograph, 3355.3m, 211/12a-9.

Figure 27 : Late diagenetic illitization of kaolinite. SEM photomicrograph, 3206.0m, 211/12a-9.

Figure 28 : Feldspar dissolution and diagenetic quartz and kaolinite distribution in 211/12-1 as determined by point counting.(500 counts per section). Stippled areas are thick mudrocks, single lines are thin mudrocks.

Figure 29 : Feldspar dissolution and diagenetic quartz and kaolinite distribution in 211/12a-M1 as determined by point counting.(500 counts per section). Stippled areas are thick mudrocks, single lines are thin mudrocks.

Figure 30 : Feldspar dissolution and diagenetic quartz and kaolinite distribution in 211/12a-9 as determined by point counting.(500 counts per section). Stippled areas are thick mudrocks, single lines are thin mudrocks.

Figure 31 : Magnesian siderite and ankerite distribution in 211/12-1 as determined by point counting (500 counts per section). Stippled areas are thick mudrocks, single lines are thin mudrocks.

Figure 32 : Magnesian siderite and ankerite distribution in 211/12a-9 as determined by point counting (500 counts per section). Stippled areas are thick mudrocks, single lines are thin mudrocks.

Figure 33 : Magnesian siderite and ankerite distribution in 211/12a-9 as determined by point counting.(500 counts per section). Stippled areas are thick mudrocks, single lines are thin mudrocks.

Figure 34 : Plot of the ranges of measured quartz overgrowth $\delta^{18}O$ (‰) against porewater $\delta^{18}O$ (‰) and temperature (°C) for crestal well 211/12-1 and deep well 211/12a-9.

Figure 35 : Plot of temperature against carboxylic acid concentration (after Surdam, 1984).

Figure 36 : Plot of the ranges of measured kaolinite 2 $\delta^{18}O$ (‰) against porewater $\delta^{18}O$ (‰) and temperature (°C) for crestal wells 211/12-1, 211/12a-M1 and deep well 211/12a-9.

Figure 37 : Plot of the ranges of measured magnesian siderite $\delta^{18}O$ (‰) against porewater $\delta^{18}O$ (‰) and temperature (°C) for crestal wells 211/12-1, 211/12a-M1 and deep well 211/12a-9.

Figure 38 : Plot of the ranges of measured ankerite $\delta^{18}O$ (‰) against porewater $\delta^{18}O$ (‰) and temperature (°C) for crestal wells 211/12-1, 211/12a-M1 and deep well 211/12a-9.

Figure 39 : Plot of the ranges of measured illite $\delta^{18}O$ (‰) against porewater $\delta^{18}O$ (‰) and temperature (°C) for crestal wells 211/12-1, 211/12a-M1 and deep well 211/12a-9.

Figure 40 : Constraints on the interpretaion of Magnus Sandstone isotopic data

Figure 41a : Model for the isotopic evolution of the porewater in the Magnus Sandstone in crestal well 211/12-1 during burial diagenesis. The model was constrained by the paragentic sequence, measured isotope values for the diagenetic minerals and the initial and final parameters shown in Figure 40.

Figure 41b : Model for the isotopic evolution of the porewater in the Magnus Sandstone in crestal well 211/12a-M1 during burial diagenesis. The model was constrained by the paragentic sequence, measured isotope values for the diagenetic minerals and the initial and final parameters shown in Figure 40.

Figure 41c : Model for the isotopic evolution of the porewater in the Magnus Sandstone in deep well 211/12a-9 during burial diagenesis. The model was constrained by the paragentic sequence, measured isotope values for the diagenetic minerals and the initial and final parameters shown in Figure 40.

Figure 42a : Plot of kaolinite and illite $\delta^{18}O$ (‰) vs. depth showing more negative values for shallower crestal samples from well 211/12-1.

Figure 42b : Plot of kaolinite and illite δD (‰) vs. depth showing more negative values for shallower crestal samples from well 211/12-1.

Figure 43 : Kaolinite and illite $\delta^{18}O$ and δD data. Crestal and downdip samples are ringed separately ; crestal samples have more negative values and grew in a porewater with a larger component of meteoric-derived water than the deeper samples.

Figure 44 : The diagenetic and isotopic evolution of the Magnus sandstones from deposition through burial to present day depth and temperature.

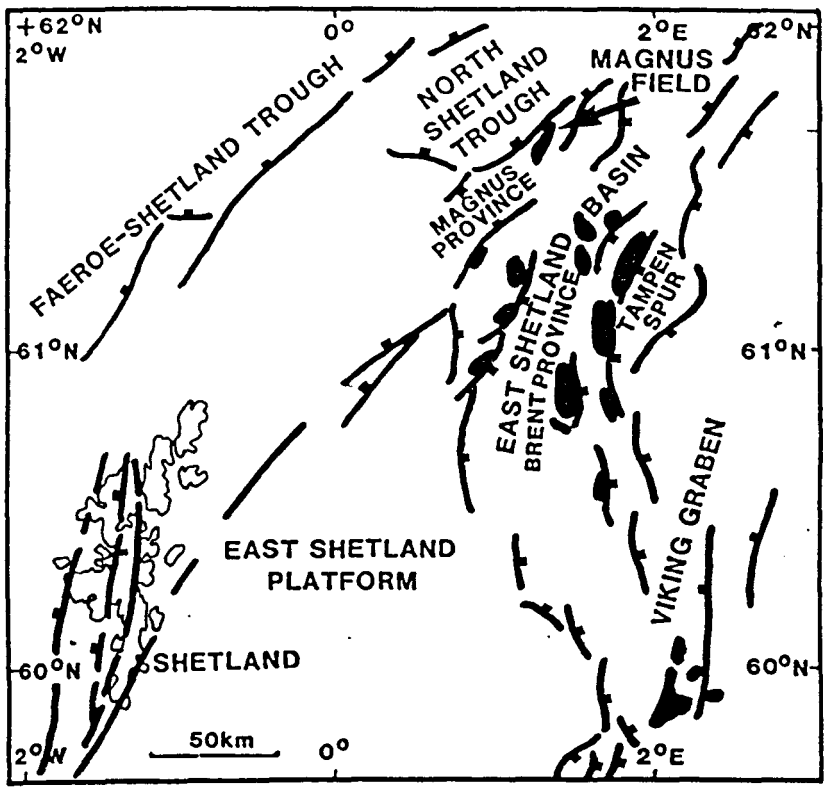
+62°N
2°W
0°
2°E
62°N
FAEROE-SHETLAND TROUGH
NORTH SHETLAND TROUGH
MAGNUS FIELD
MAGNUS PROVINCE
BASIN
EAST SHETLAND BRENT PROVINCE
TAMPEN SPUR
61°N
61°N
EAST SHETLAND PLATFORM
VIKING GRABEN
SHETLAND
60°N
60°N
50km
2°W
0°
2°E

Figure 1

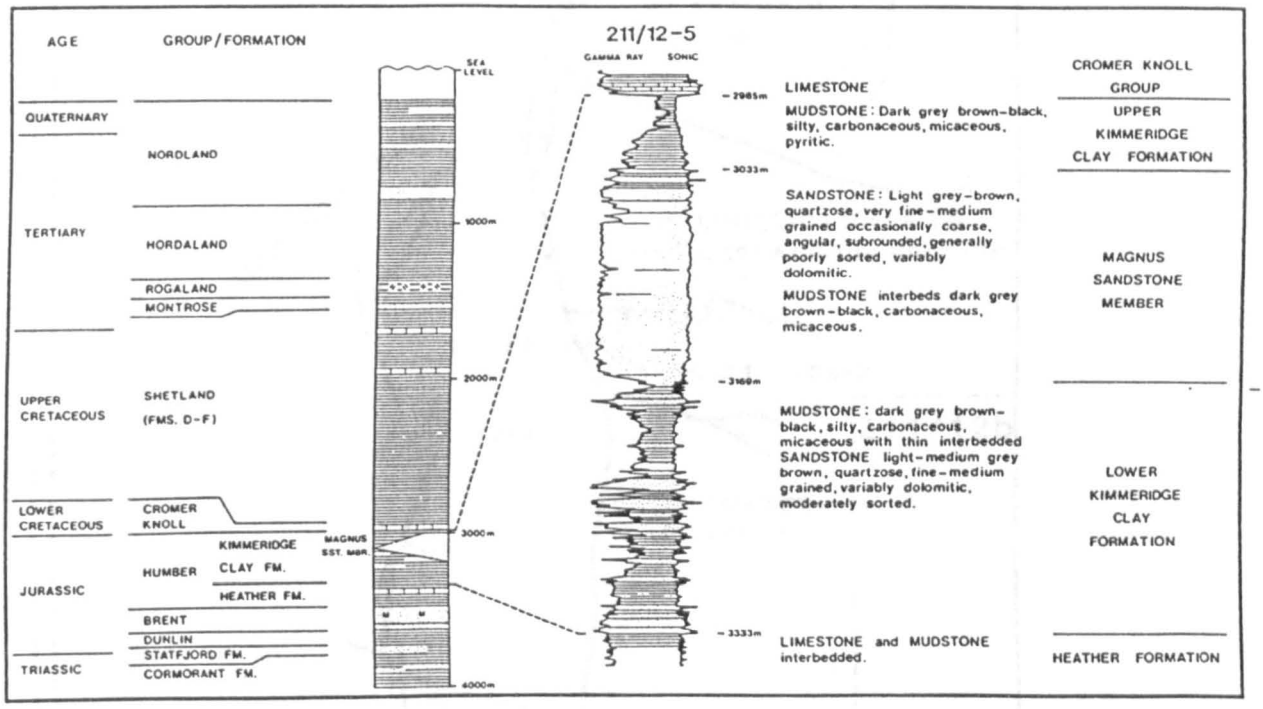
AGE
GROUP / FORMATION
211/12-5
GAMMA RAY
SONIC
SEA LEVEL
QUATERNARY
NORDLAND
TERTIARY
HORDALAND
ROGALAND
MONTROSE
UPPER CRETACEOUS
SHETLAND
(FMS. D-F)
LOWER CRETACEOUS
CROMER KNOLL
KIMMERIDGE CLAY FM.
HUMBER
HEATHER FM.
JURASSIC
BRENT
DUNLIN
STATFJORD FM.
TRIASSIC
CORMORANT FM.
MAGNUS SST. MBR.
1000m
2000m
3000m
4000m
-2985m
-3033m
-3169m
-3333m
LIMESTONE
MUDSTONE: Dark grey brown-black, silty, carbonaceous, micaceous, pyritic.
SANDSTONE: Light grey-brown, quartzose, very fine-medium grained occasionally coarse, angular, subrounded, generally poorly sorted, variably dolomitic.
MUDSTONE interbeds dark grey brown-black, carbonaceous, micaceous.
MUDSTONE: dark grey brown-black, silty, carbonaceous, micaceous with thin interbedded SANDSTONE light-medium grey brown, quartzose, fine-medium grained, variably dolomitic, moderately sorted.
LIMESTONE and MUDSTONE interbedded.
CROMER KNOLL GROUP
UPPER KIMMERIDGE CLAY FORMATION
MAGNUS SANDSTONE MEMBER
LOWER KIMMERIDGE CLAY FORMATION
HEATHER FORMATION

Figure 2

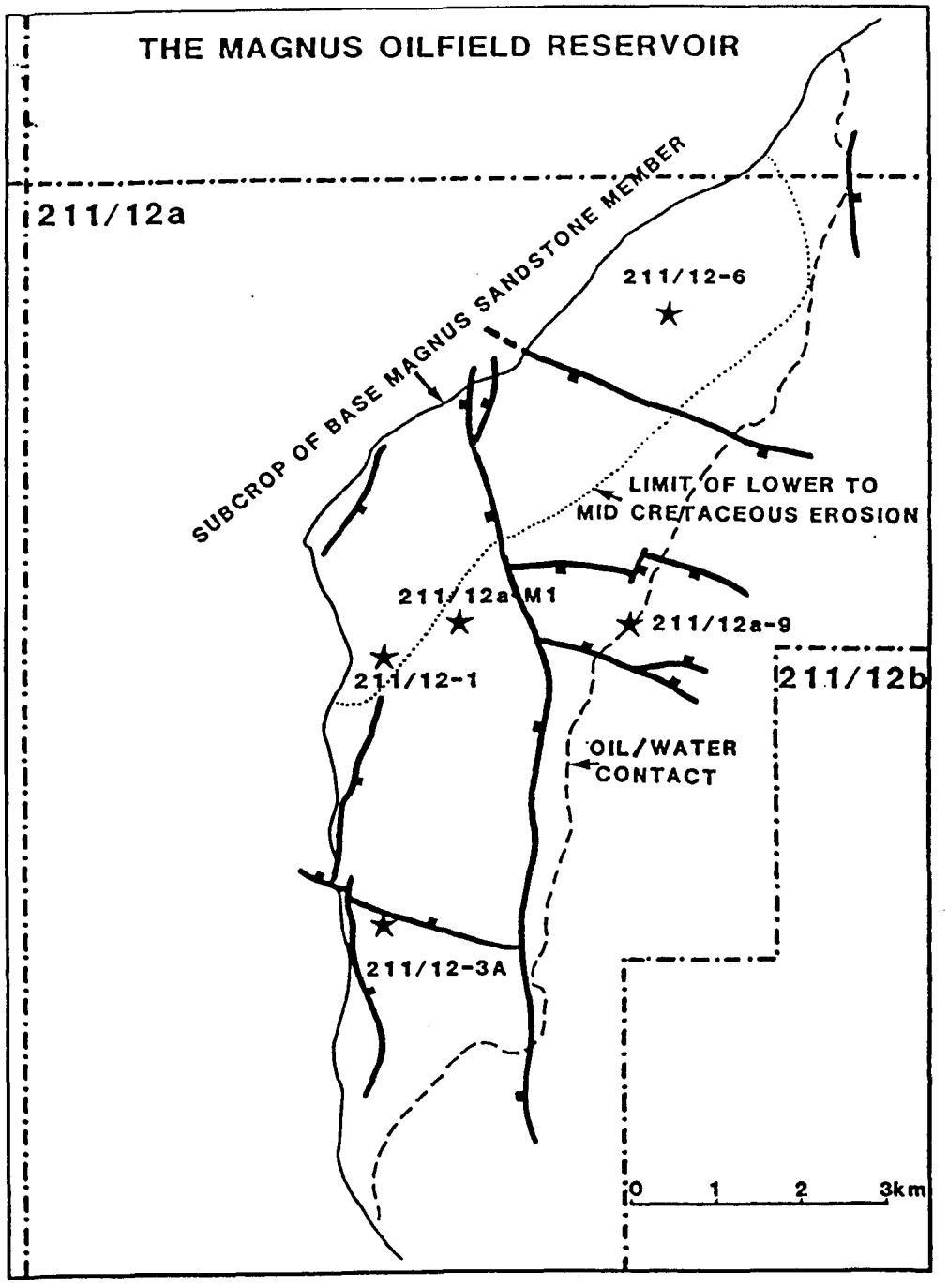
THE MAGNUS OILFIELD RESERVOIR
211/12a
SUBCROP OF BASE MAGNUS SANDSTONE MEMBER
211/12-6
LIMIT OF LOWER TO MID CRETACEOUS EROSION
211/12a-M1
211/12a-9
211/12-1
211/12b
OIL/WATER CONTACT
211/12-3A
0 1 2 3km

Figure 3

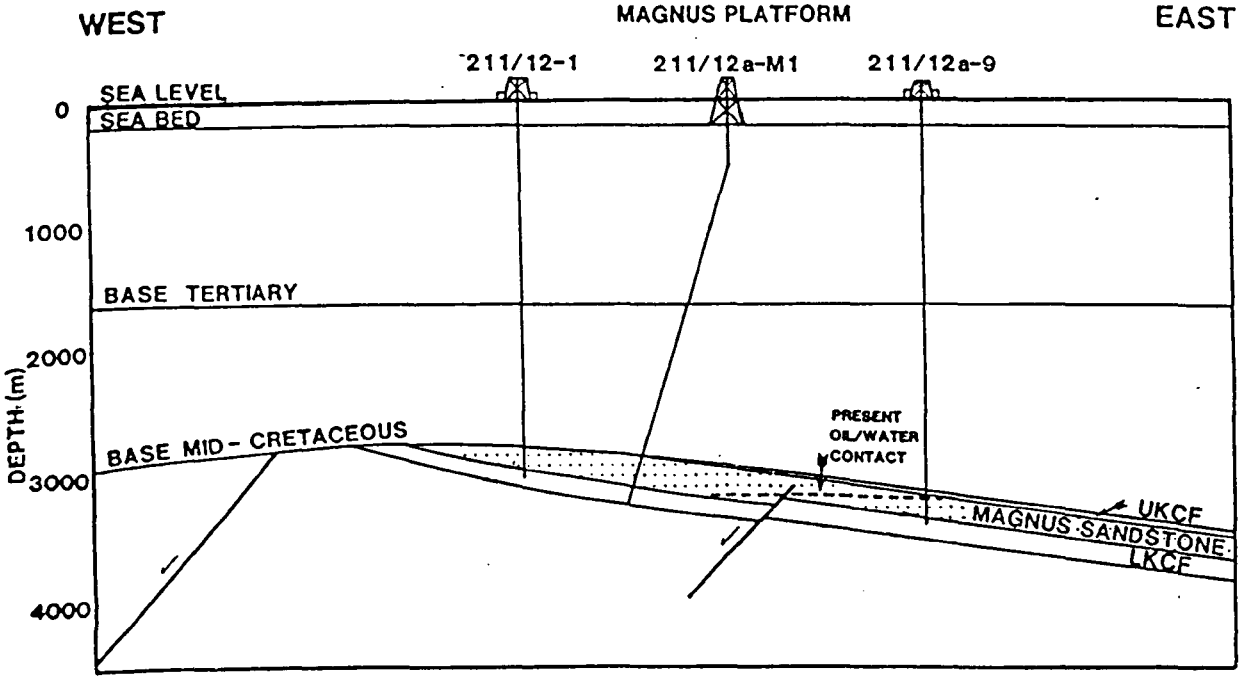
WEST
MAGNUS PLATFORM
EAST
211/12-1
211/12a-M1
211/12a-9
SEA LEVEL
SEA BED
0
1000
BASE TERTIARY
2000
DEPTH (m)
BASE MID-CRETACEOUS
3000
PRESENT
OIL/WATER
CONTACT
UKCF
MAGNUS SANDSTONE
LKCF
4000

Figure 4a

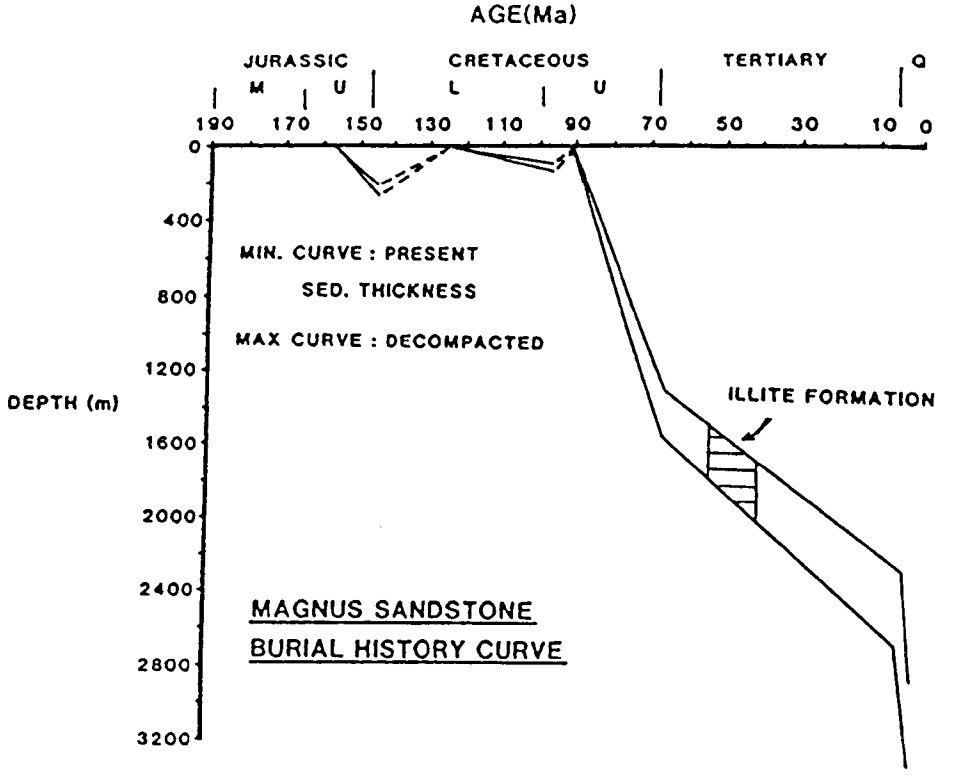
AGE(Ma)
JURASSIC
M
U
CRETACEOUS
L
U
TERTIARY
Q
190
170
150
130
110
90
70
50
30
10
0
0
400
800
1200
1600
2000
2400
2800
3200
DEPTH (m)
MIN. CURVE : PRESENT
SED. THICKNESS
MAX CURVE : DECOMPACTED
ILLITE FORMATION
MAGNUS SANDSTONE
BURIAL HISTORY CURVE

Figure 4b

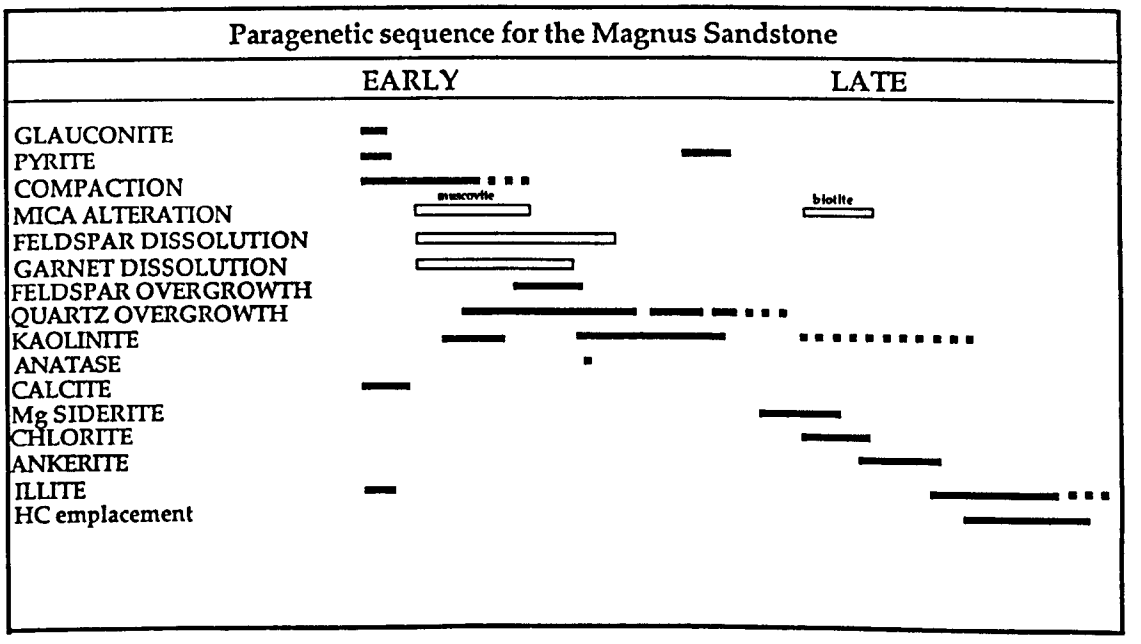
Paragenetic sequence for the Magnus Sandstone
EARLY
LATE
GLAUCONITE
PYRITE
COMPACTION
MICA ALTERATION
muscovite
biotite
FELDSPAR DISSOLUTION
GARNET DISSOLUTION
FELDSPAR OVERGROWTH
QUARTZ OVERGROWTH
KAOLINITE
ANATASE
CALCITE
Mg SIDERITE
CHLORITE
ANKERITE
ILLITE
HC emplacement

Figure 5

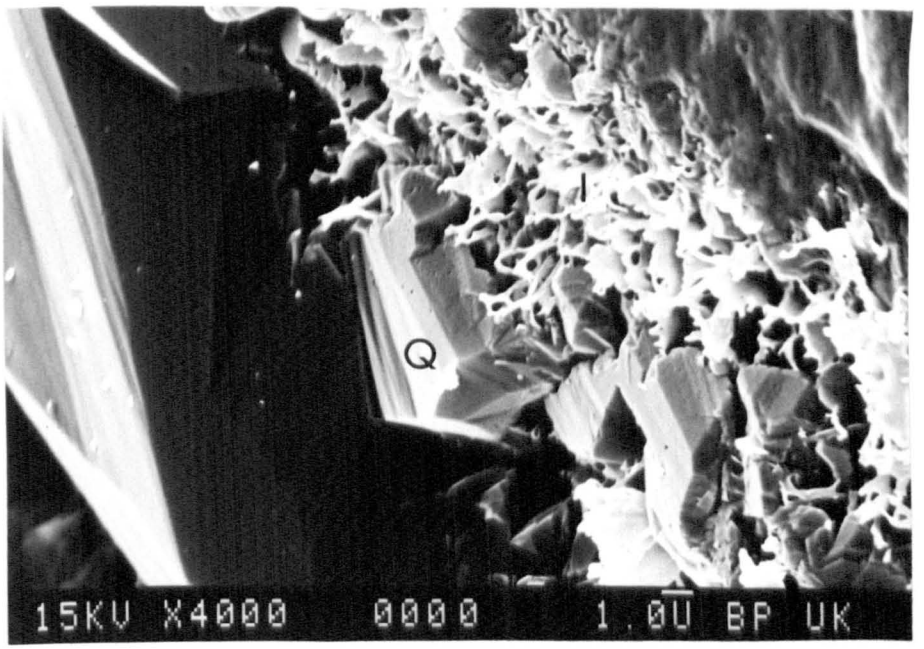

Figure 6

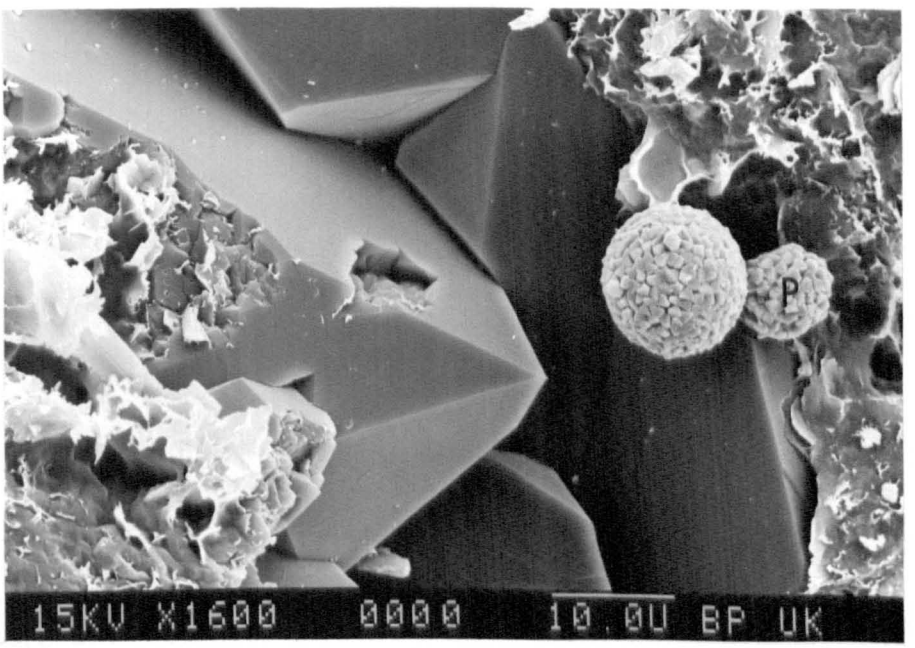

Figure 7

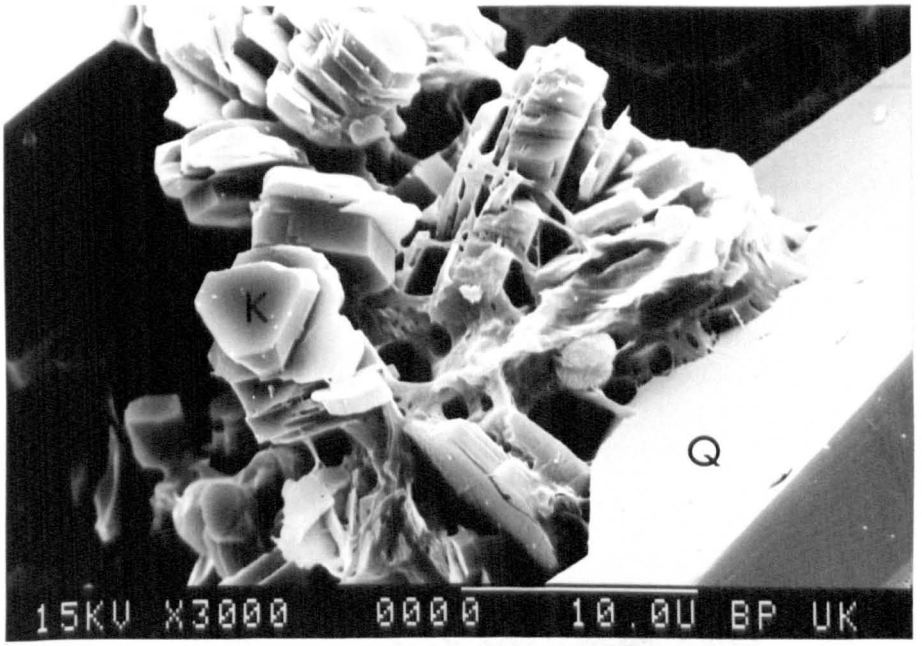

Figure 8

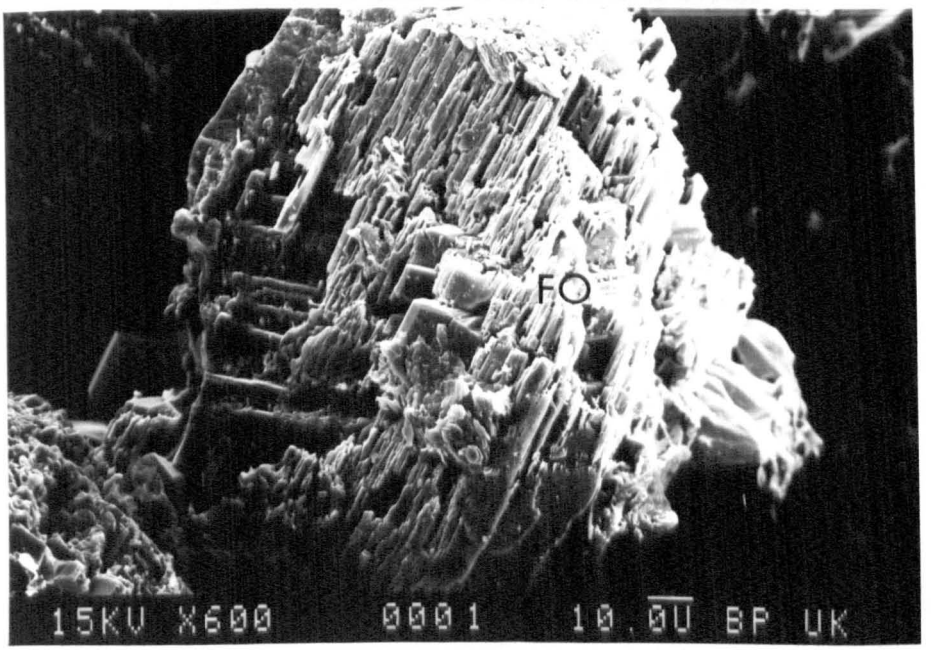

Figure 9

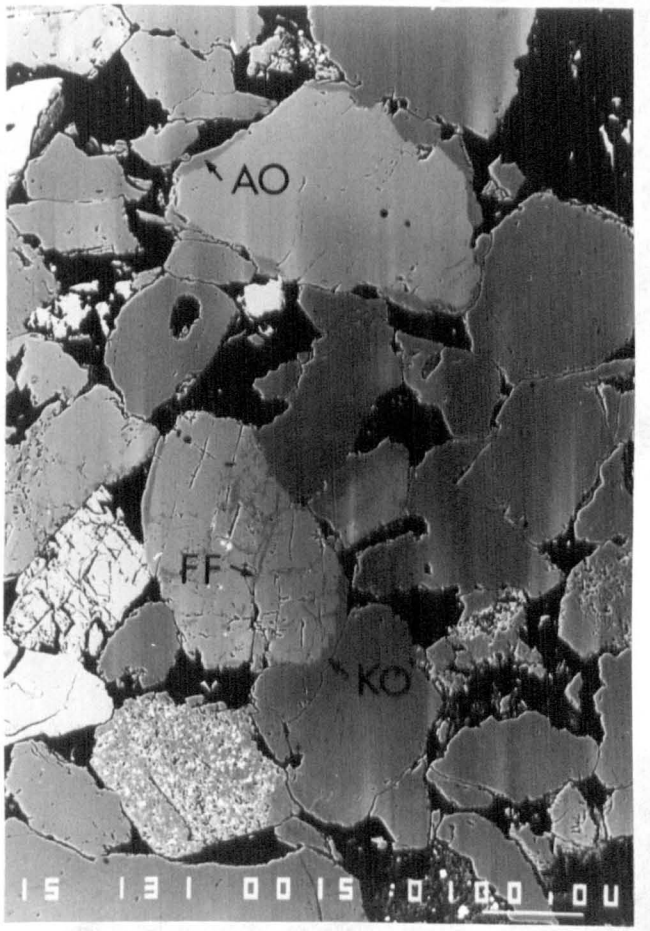

Figure 10

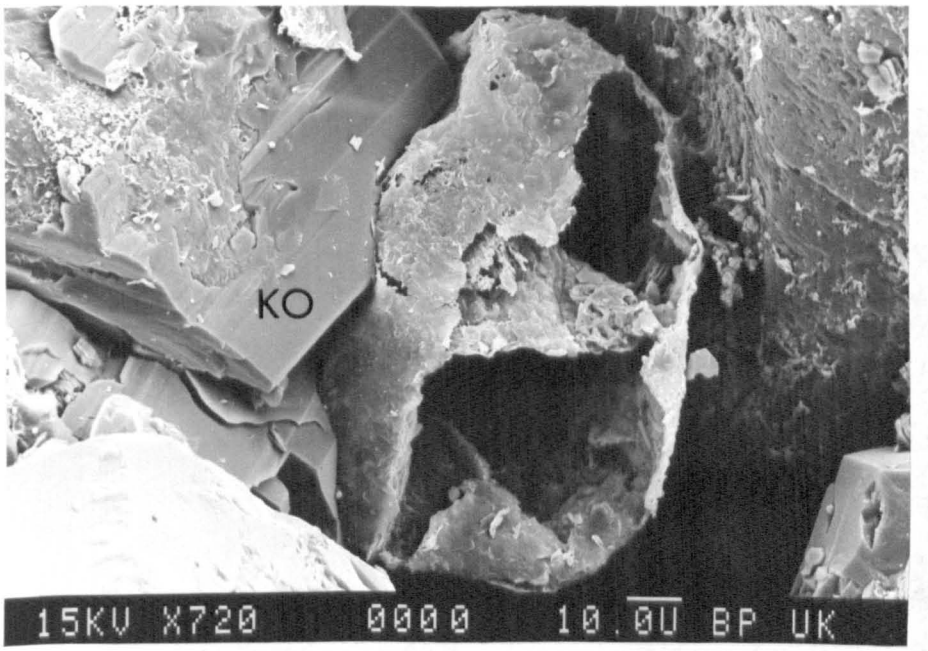

Figure 11a

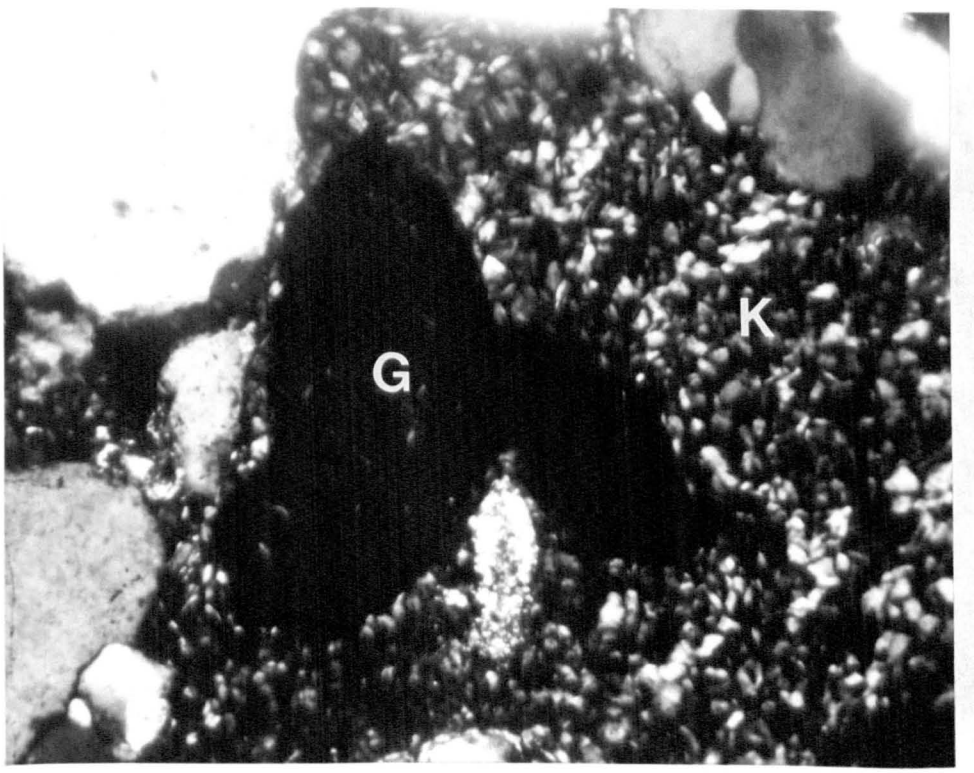

Figure 11b

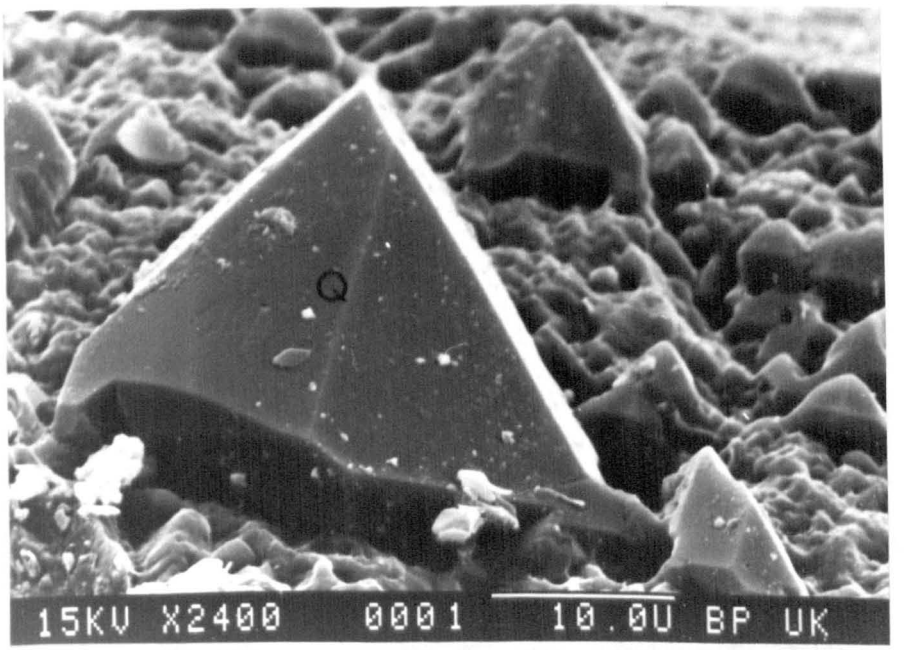

Figure 12a

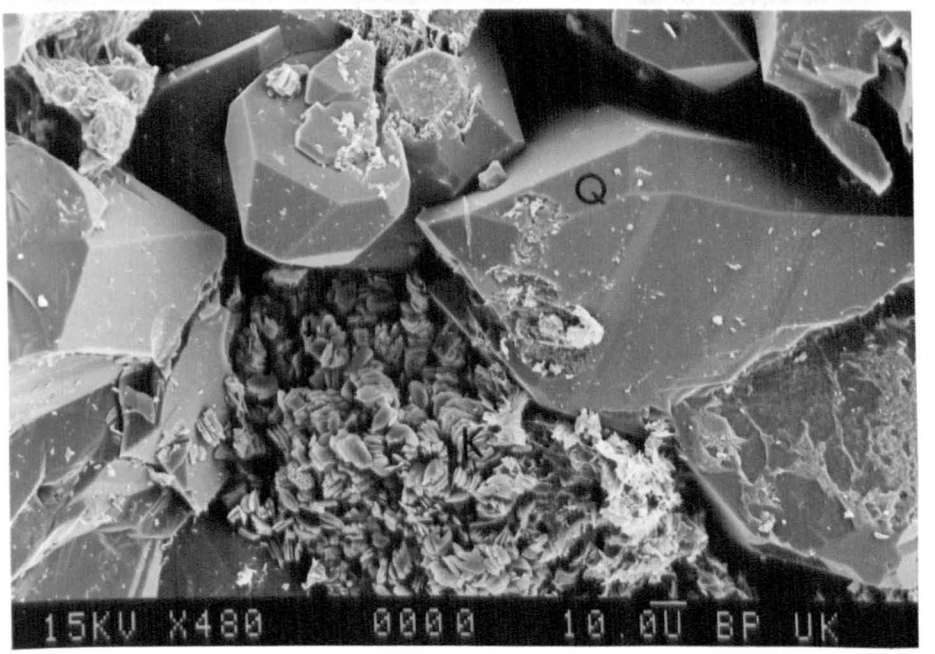

Figure 12b

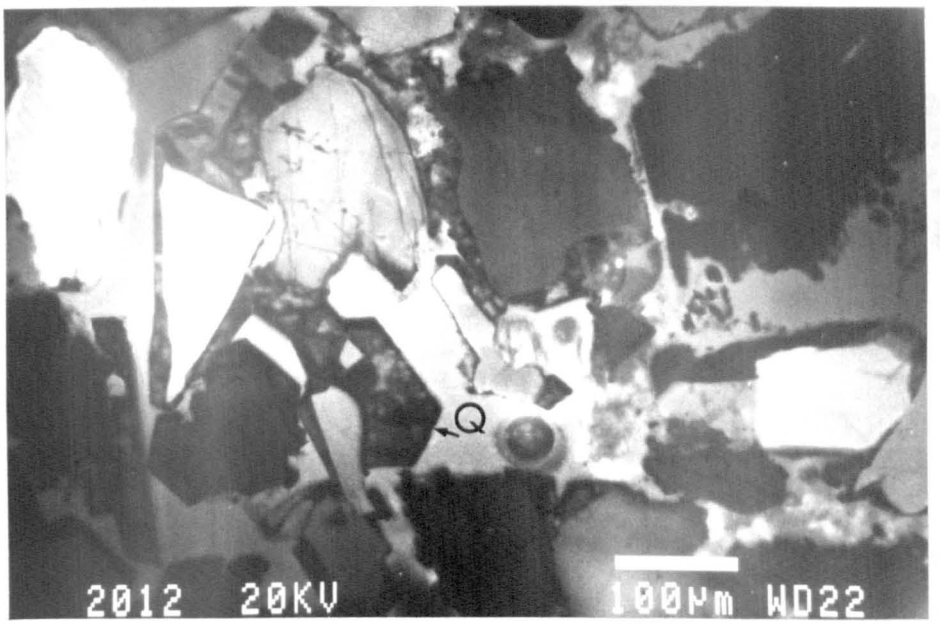

Figure 13

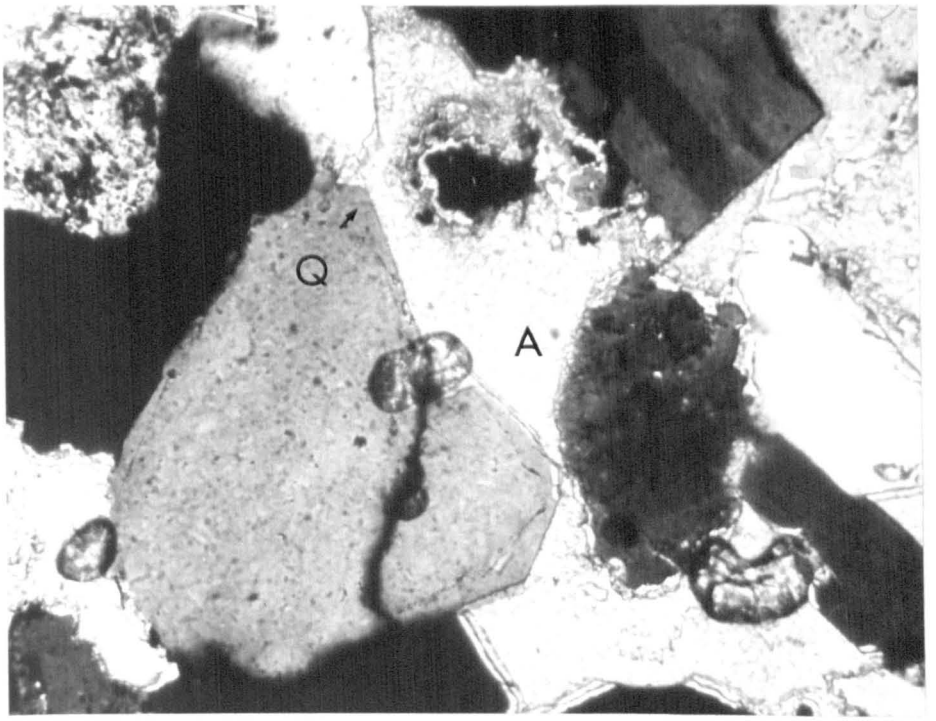

Figure 14

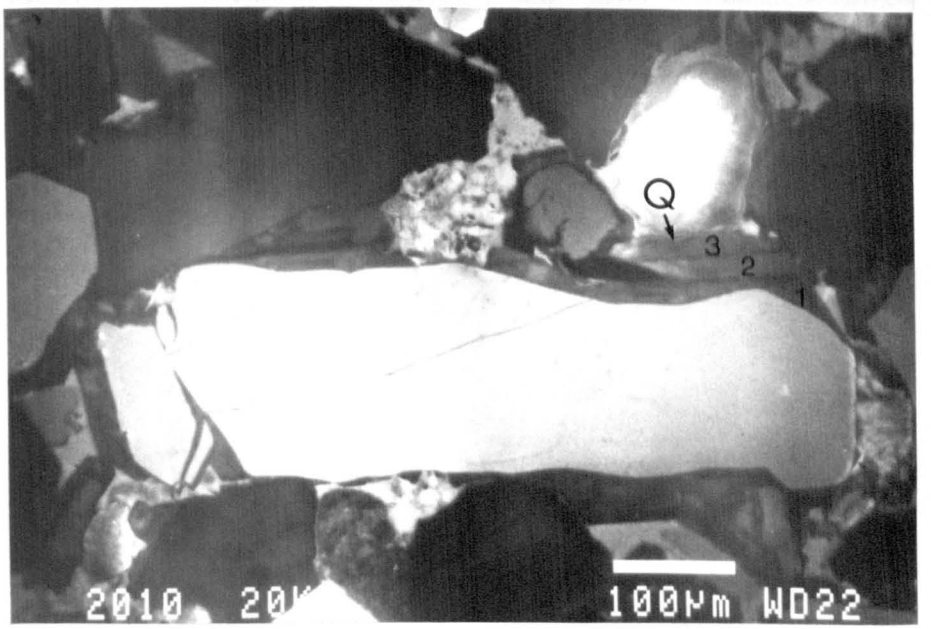

Figure 15

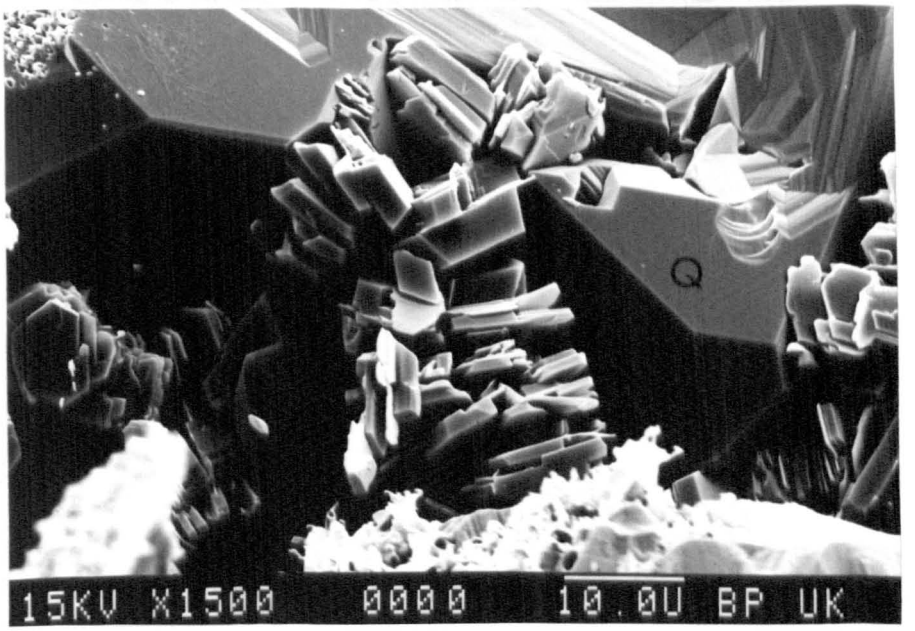

Figure 16

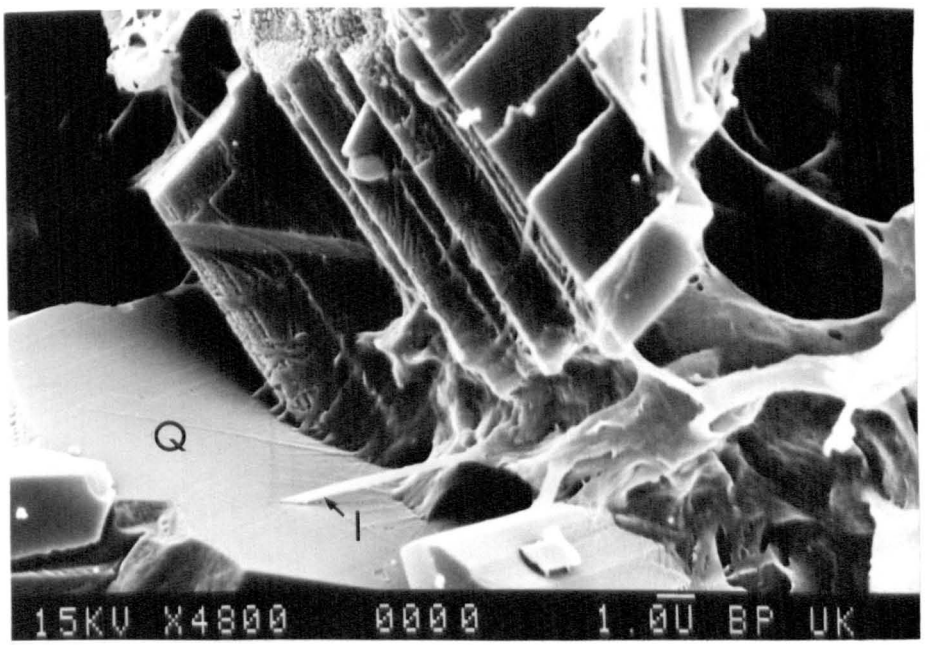

Figure 17

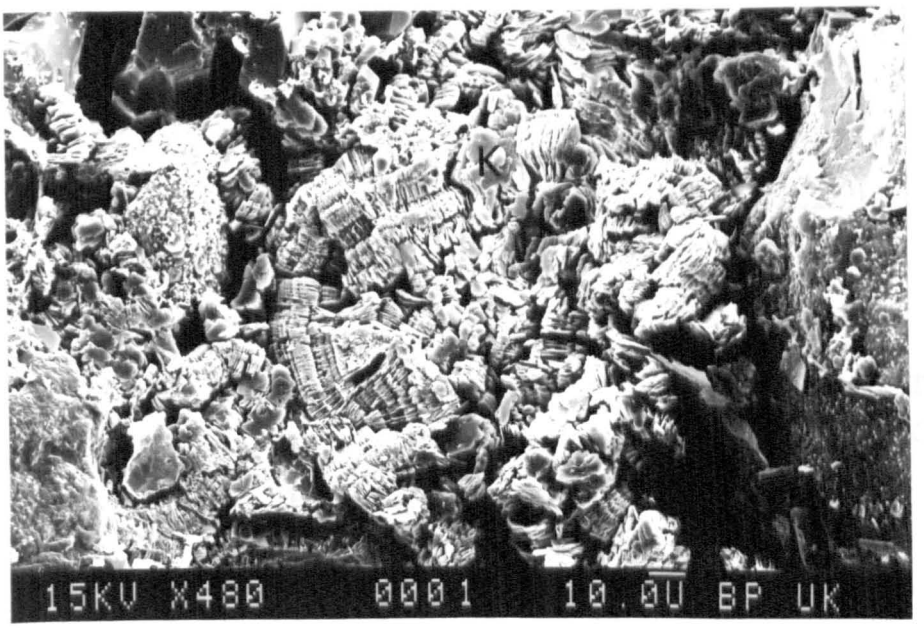

Figure 18

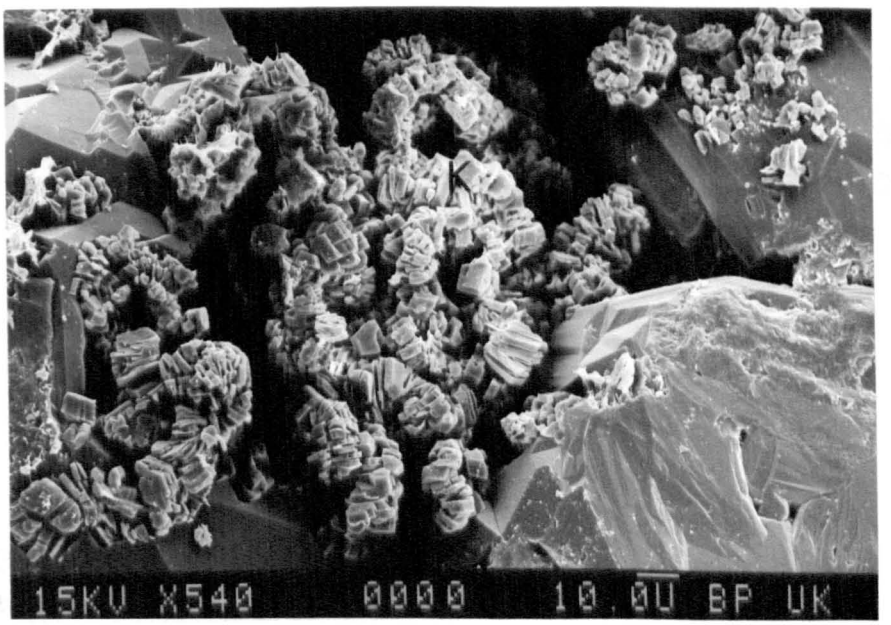

Figure 19

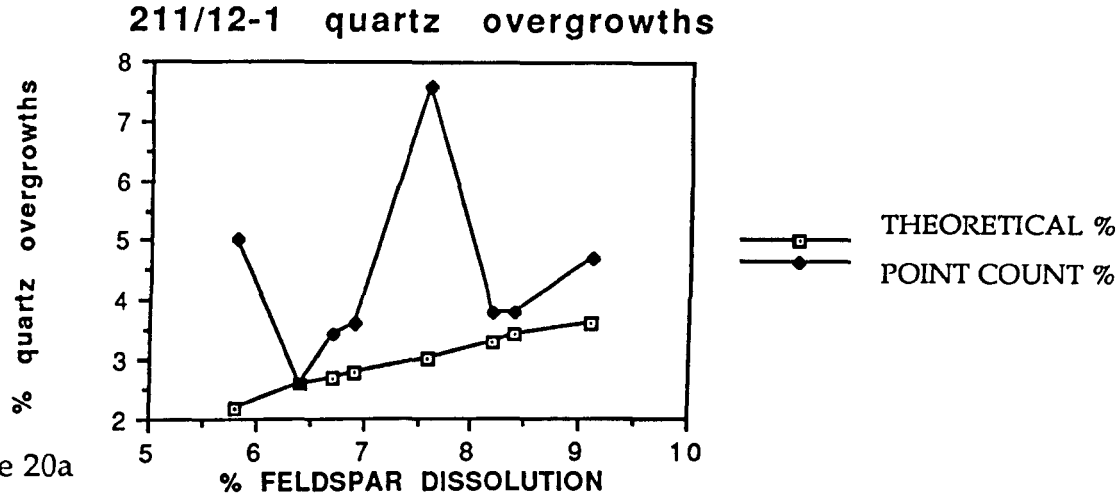

Figure 20a

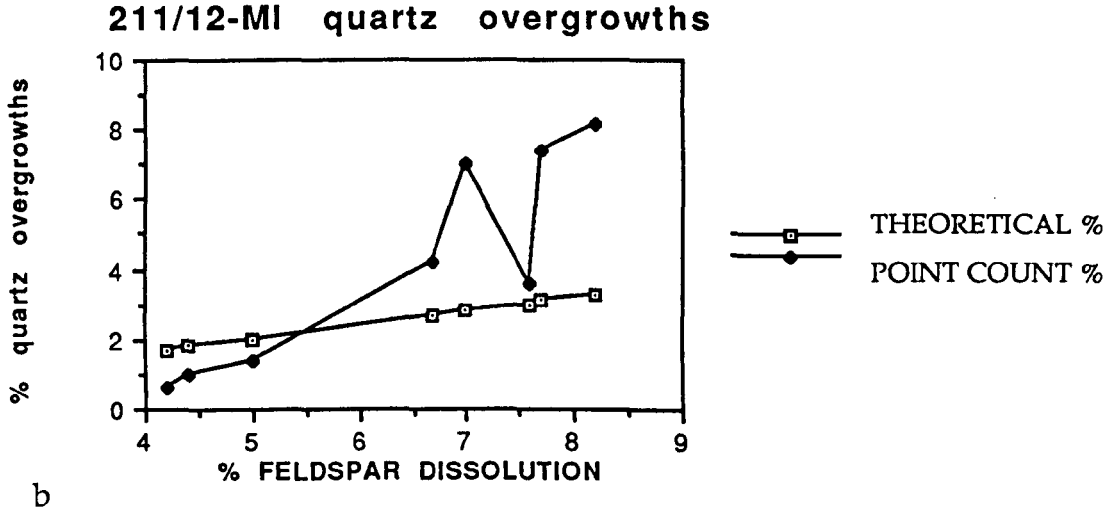

b

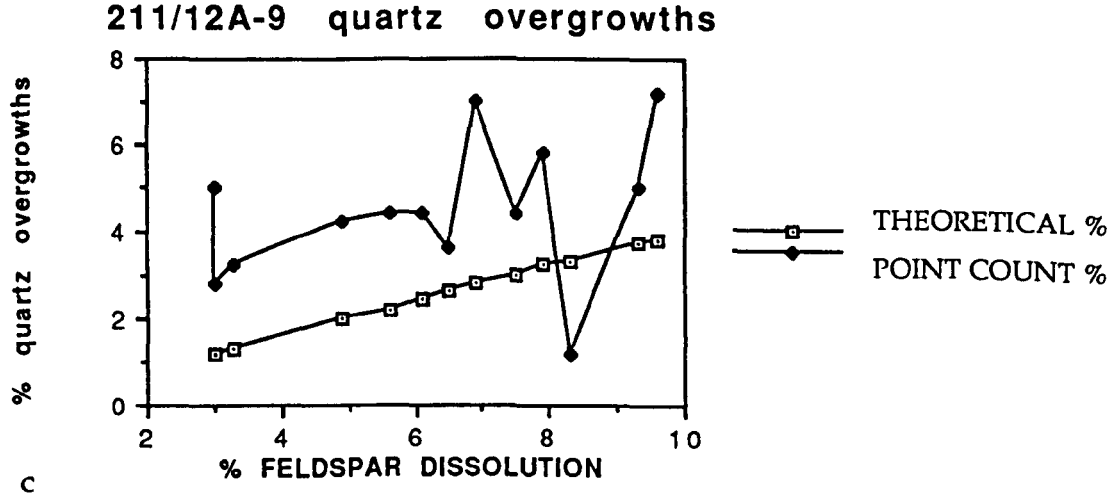

c

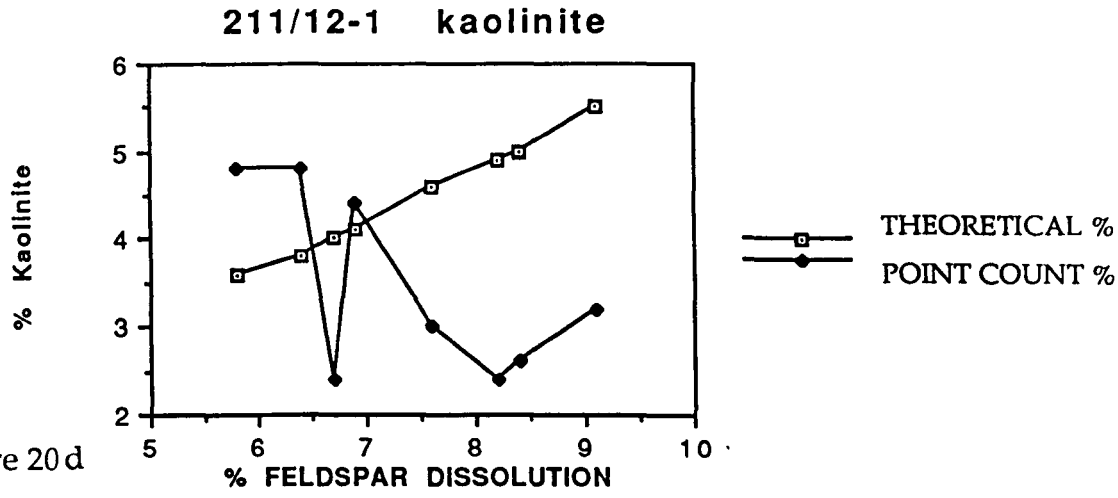

Figure 20 d

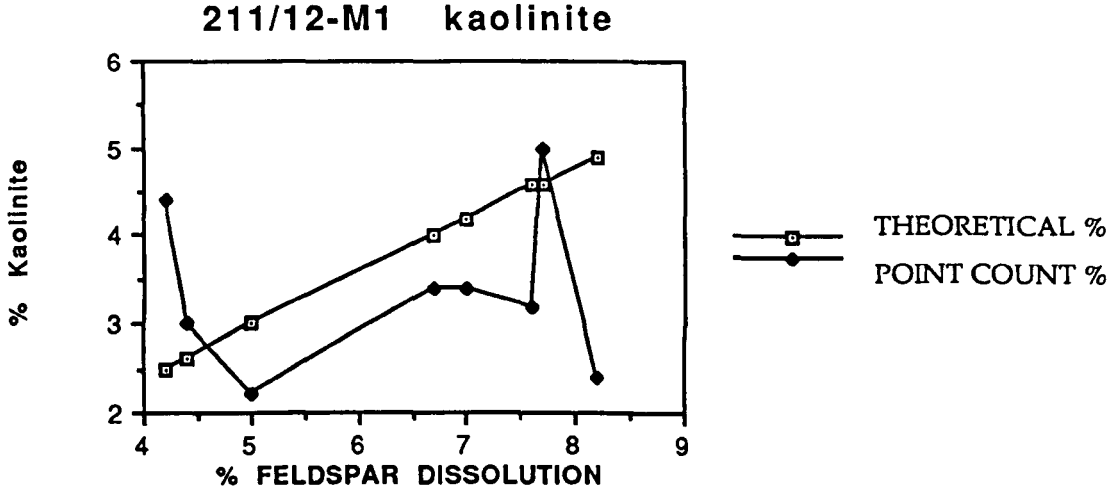

e

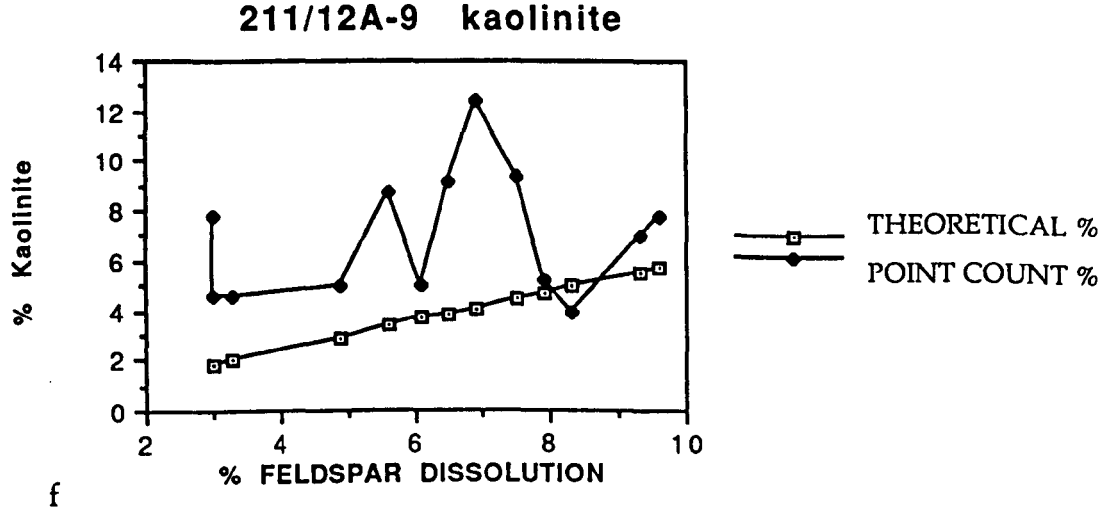

f

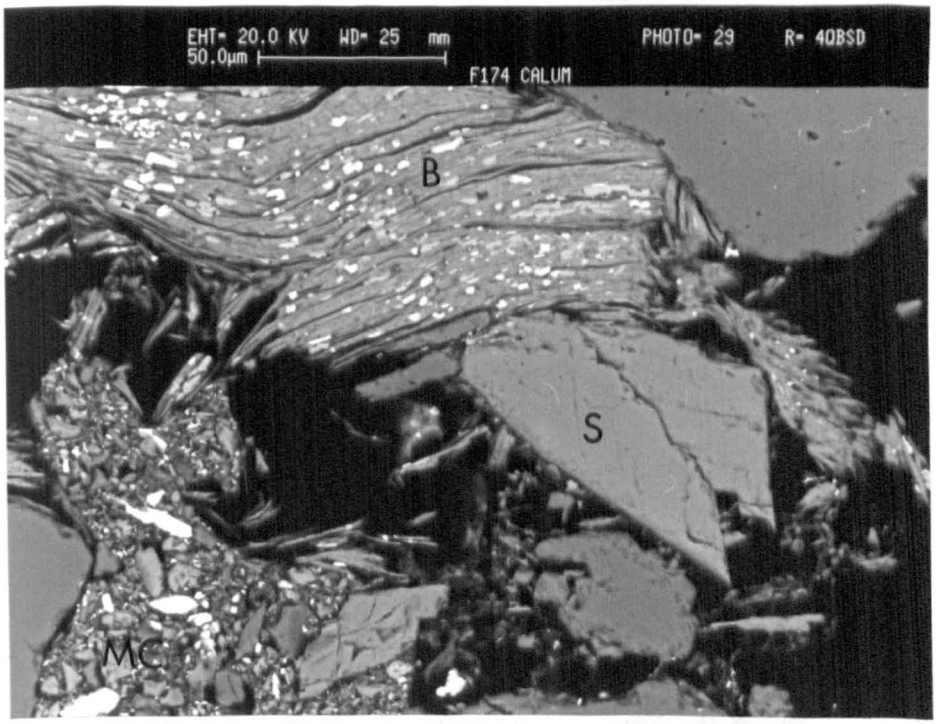

Figure 21

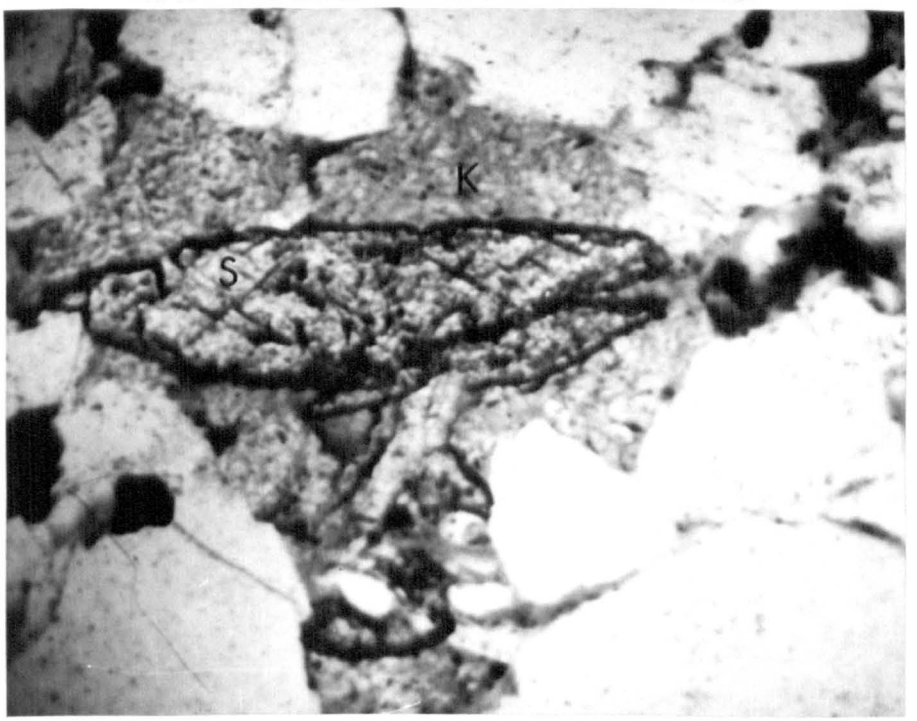

Figure 22

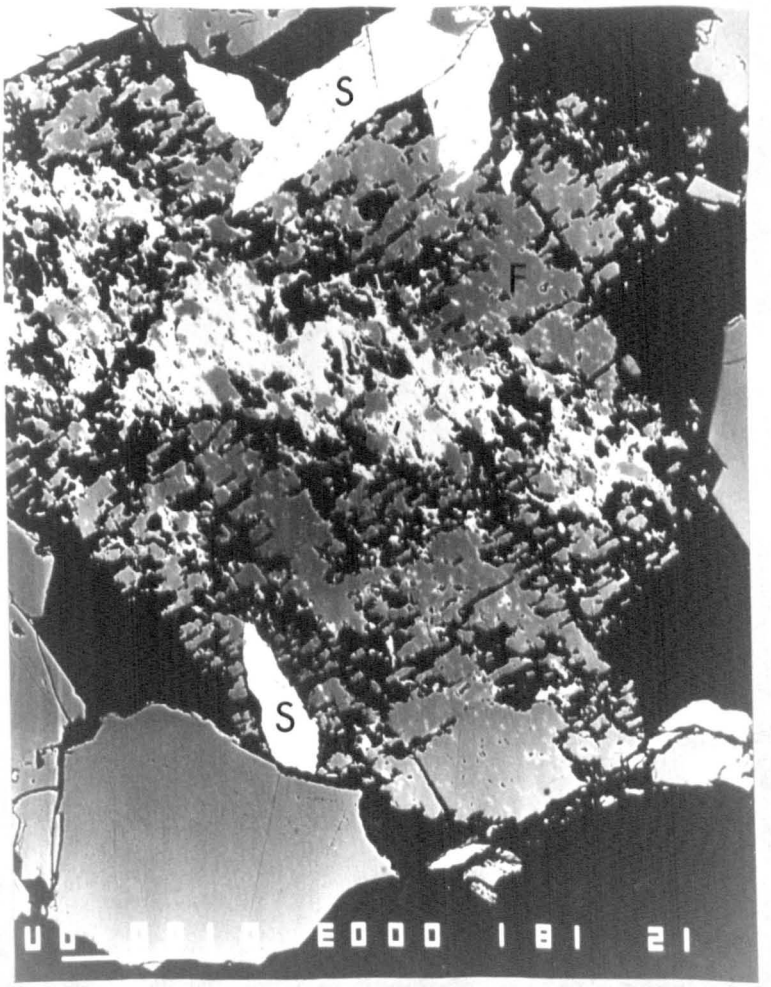

Figure 23

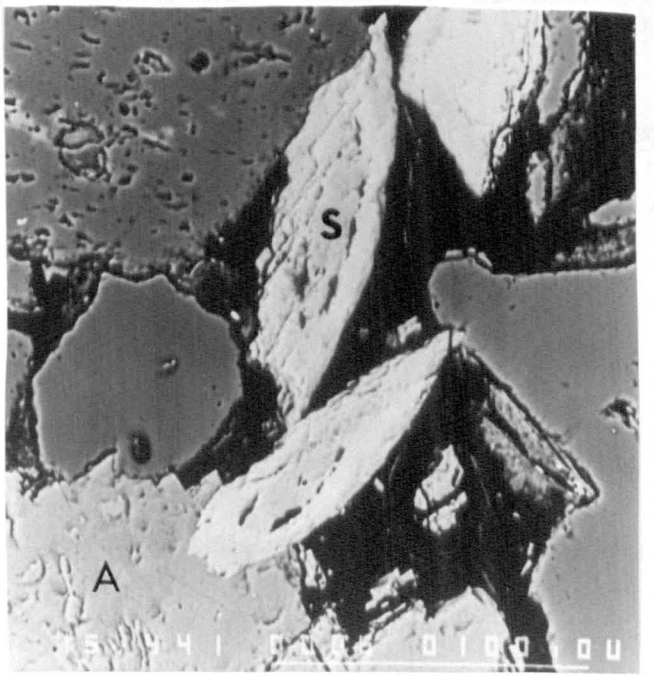

Figure 24

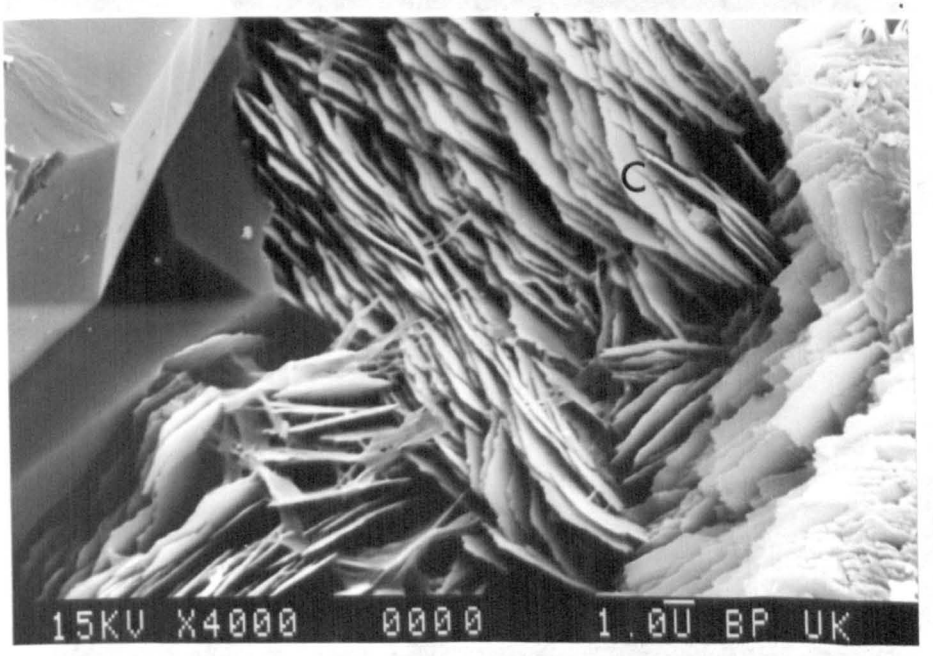

Figure 25

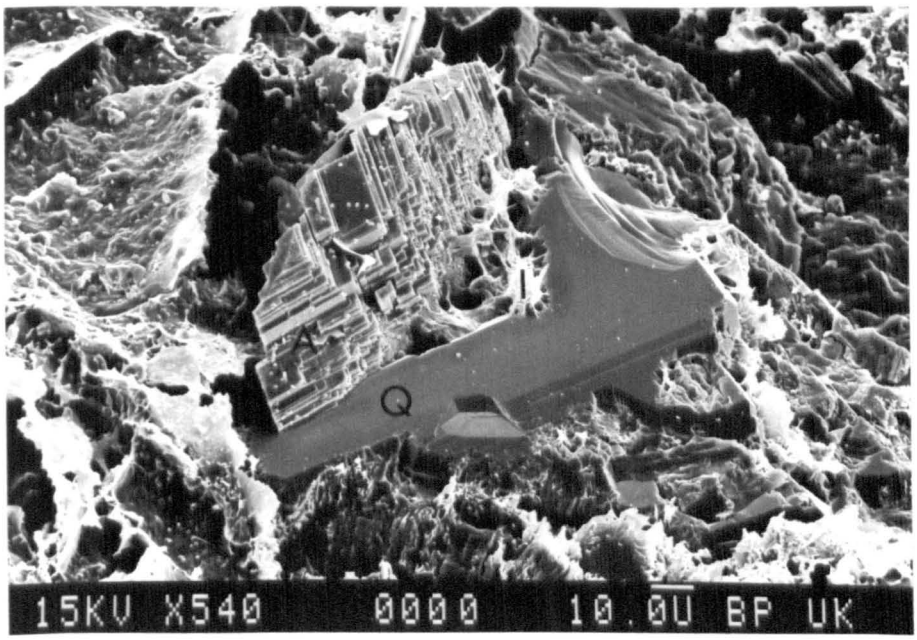

Figure 26

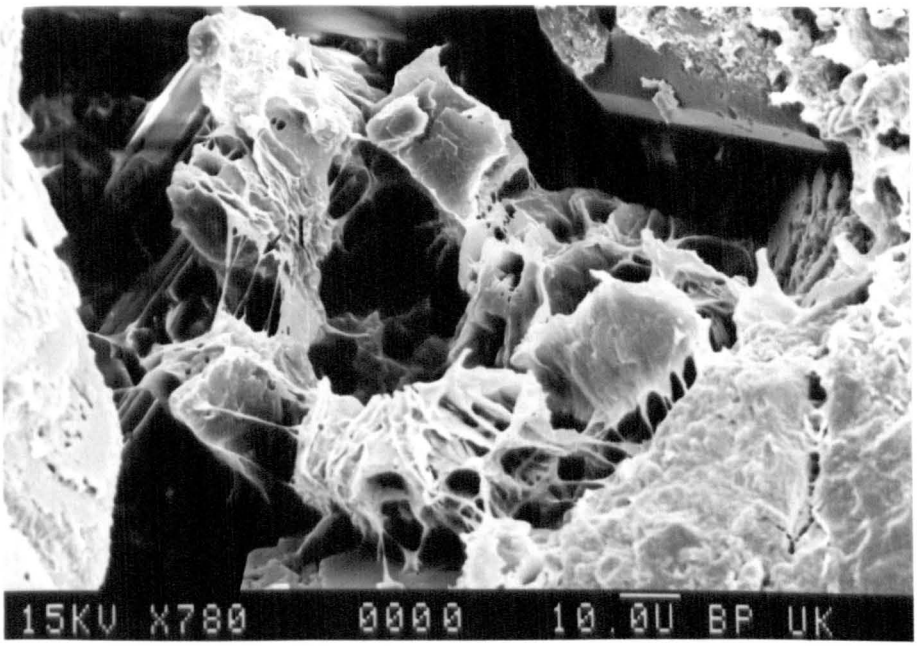

Figure 27

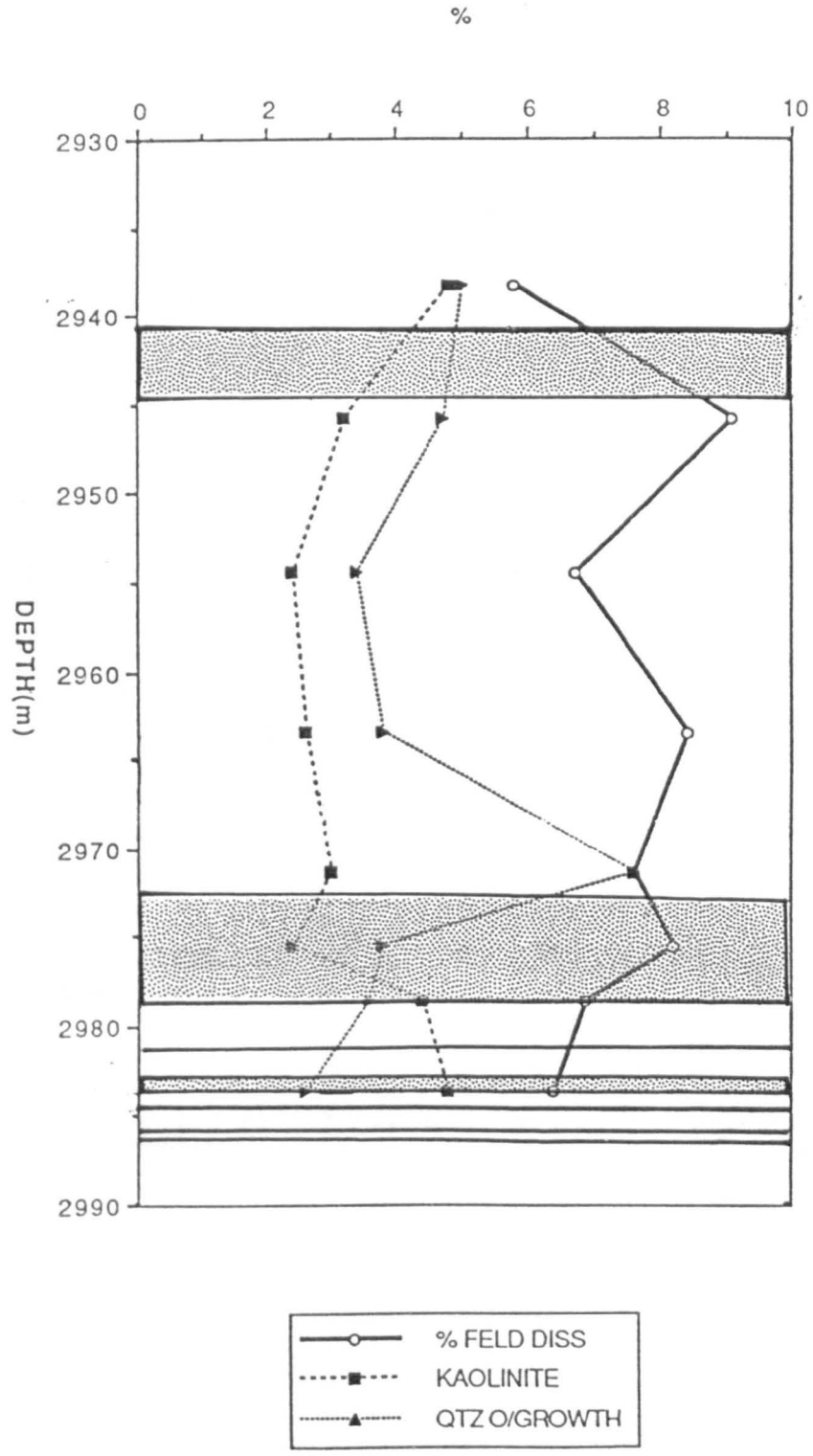
%
0
2
4
6
8
10
2930
2940
2950
2960
2970
2980
2990
DEPTH(m)
% FELD DISS
KAOLINITE
QTZ O/GROWTH

Figure 28

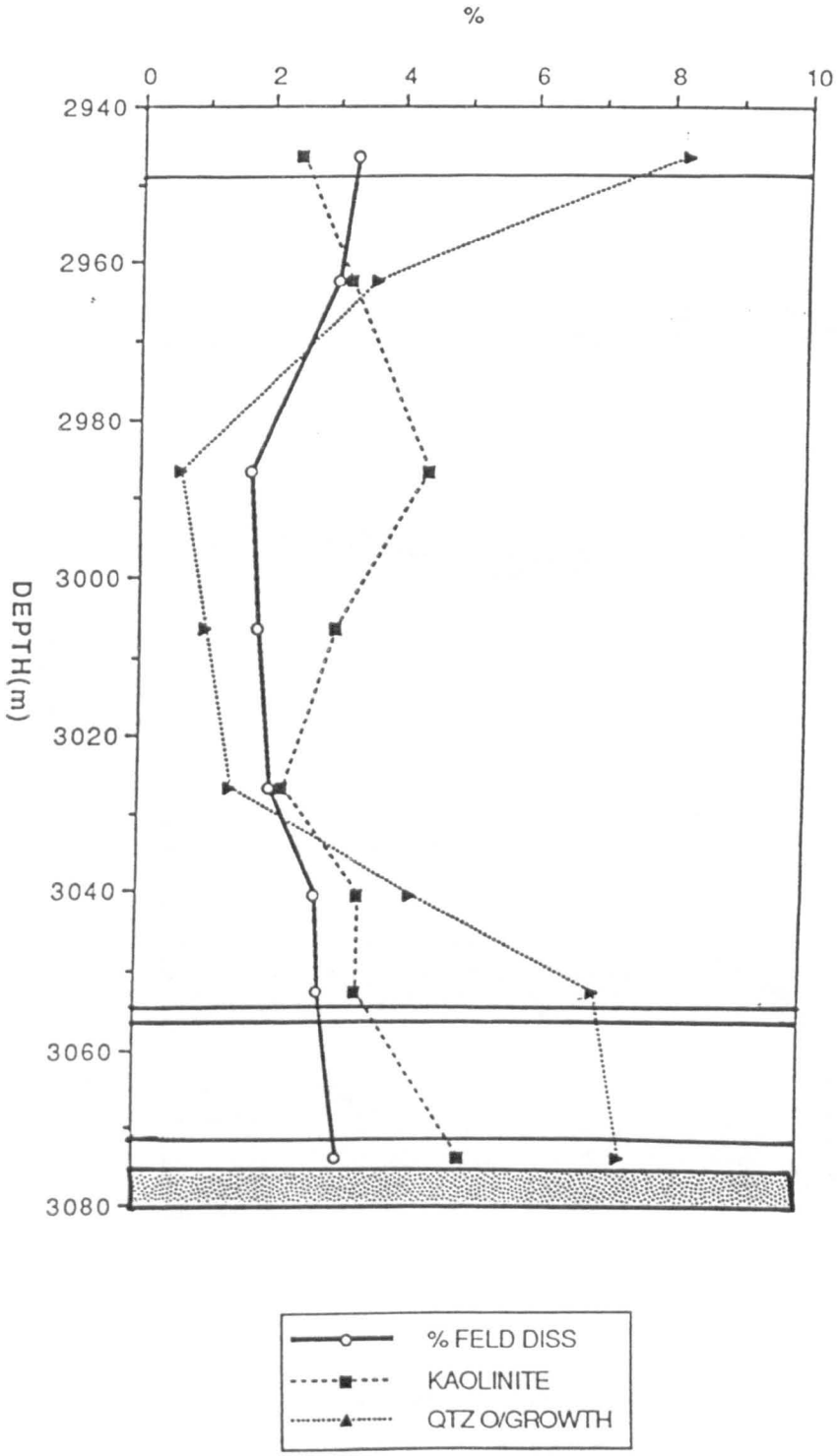
%
0
2
4
6
8
10
2940
2960
2980
3000
3020
3040
3060
3080
DEPTH(m)
% FELD DISS
KAOLINITE
QTZ O/GROWTH

Figure 29

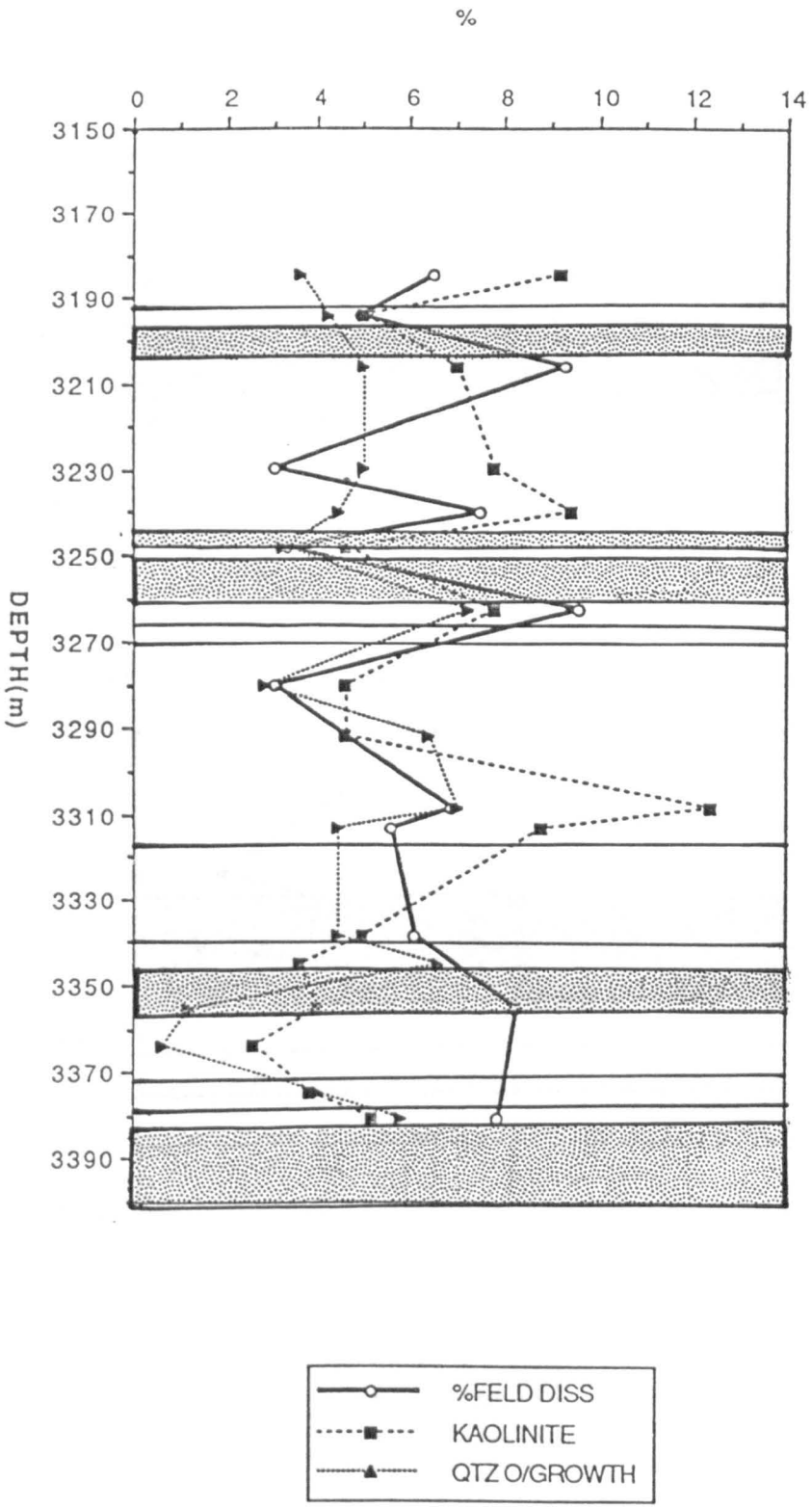
%
0
2
4
6
8
10
12
14
3150
3170
3190
3210
3230
3250
3270
3290
3310
3330
3350
3370
3390
DEPTH(m)
%FELD DISS
KAOLINITE
QTZ O/GROWTH

Figure 30

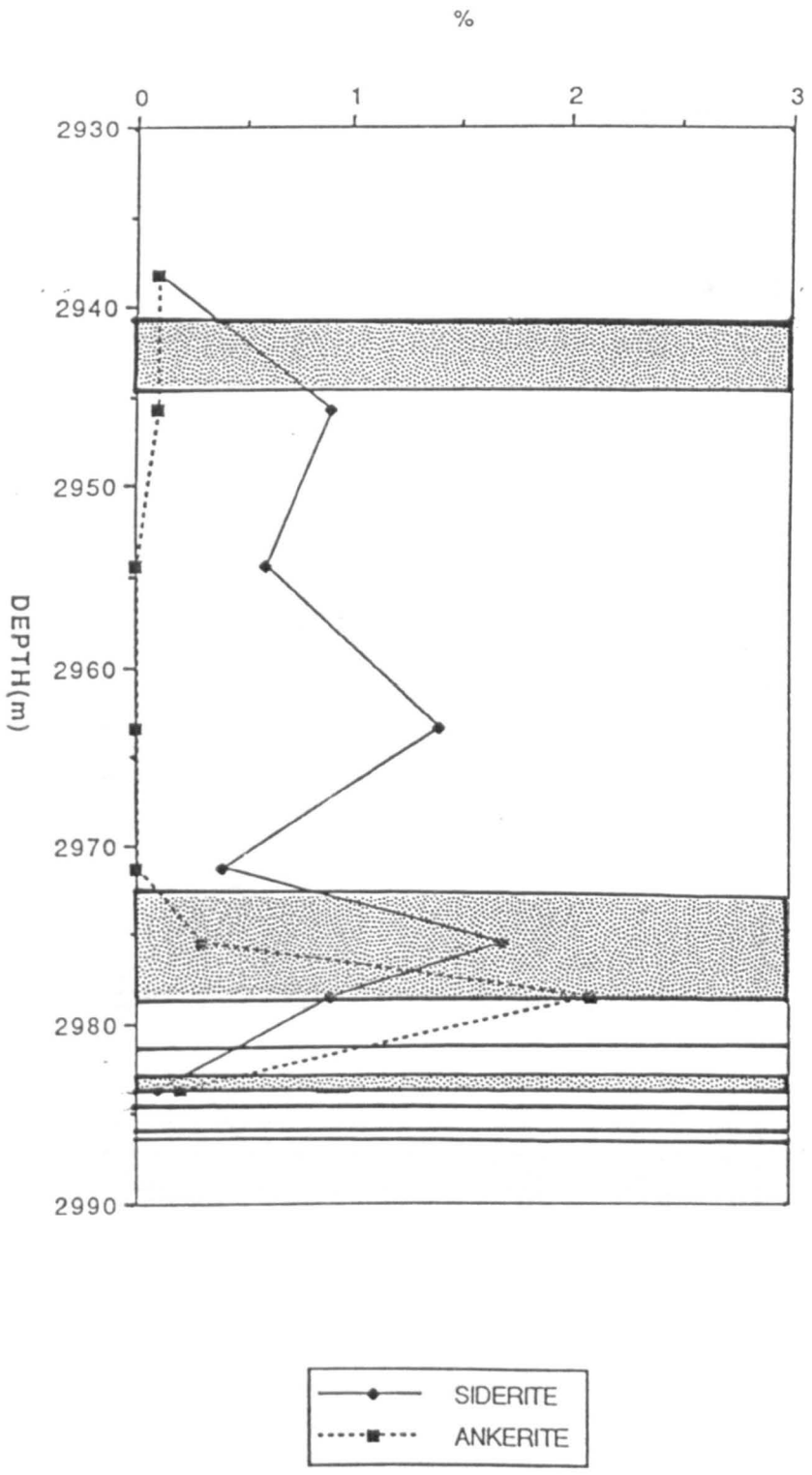
%
0
1
2
3
2930
2940
2950
2960
2970
2980
2990
DEPTH(m)
SIDERITE
ANKERITE

Figure 31

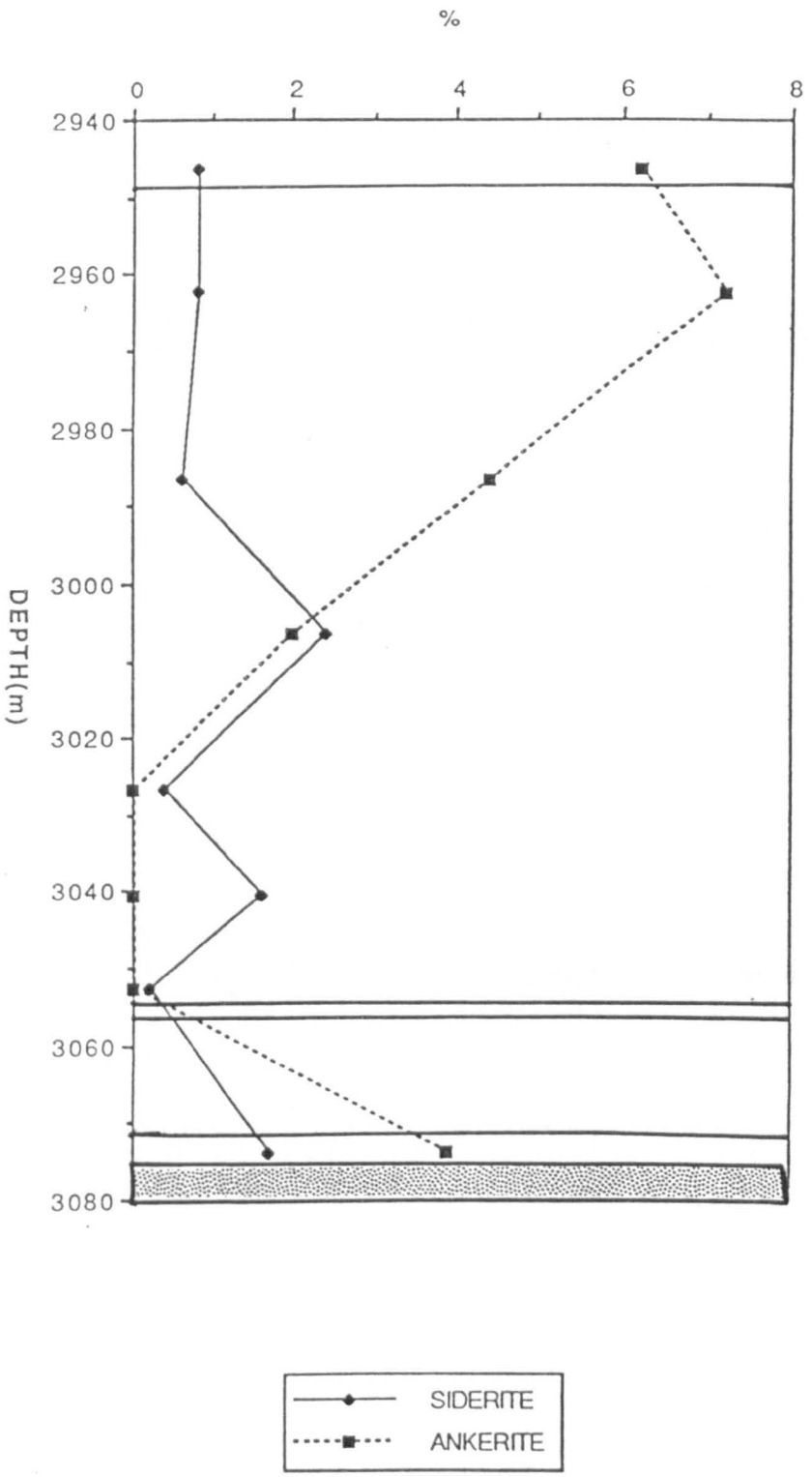
%
0
2
4
6
8
2940
2960
2980
3000
3020
3040
3060
3080
DEPTH(m)
SIDERITE
ANKERITE

Figure 32

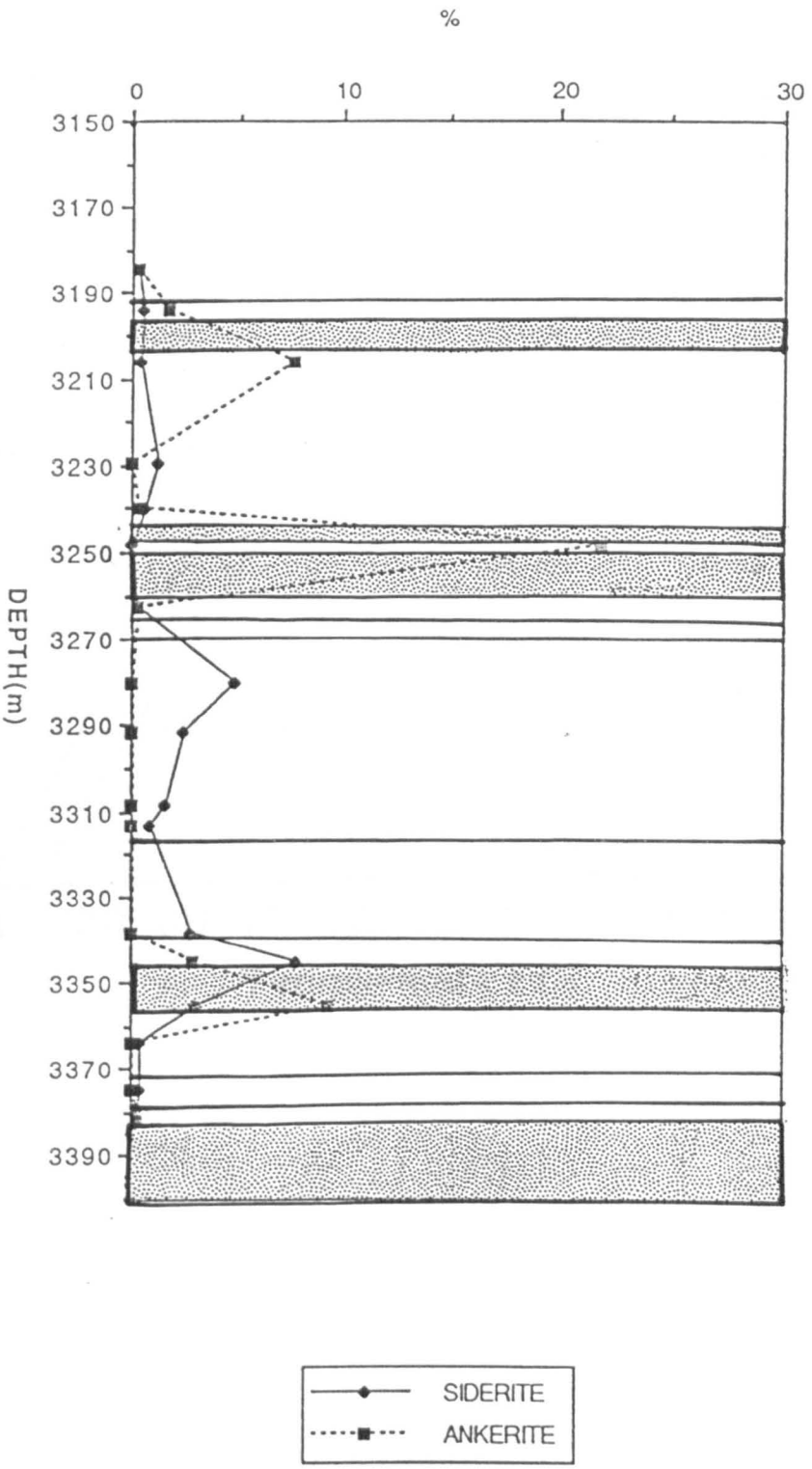
%
0
10
20
30
3150
3170
3190
3210
3230
3250
3270
3290
3310
3330
3350
3370
3390
DEPTH(m)
SIDERITE
ANKERITE

Figure 33

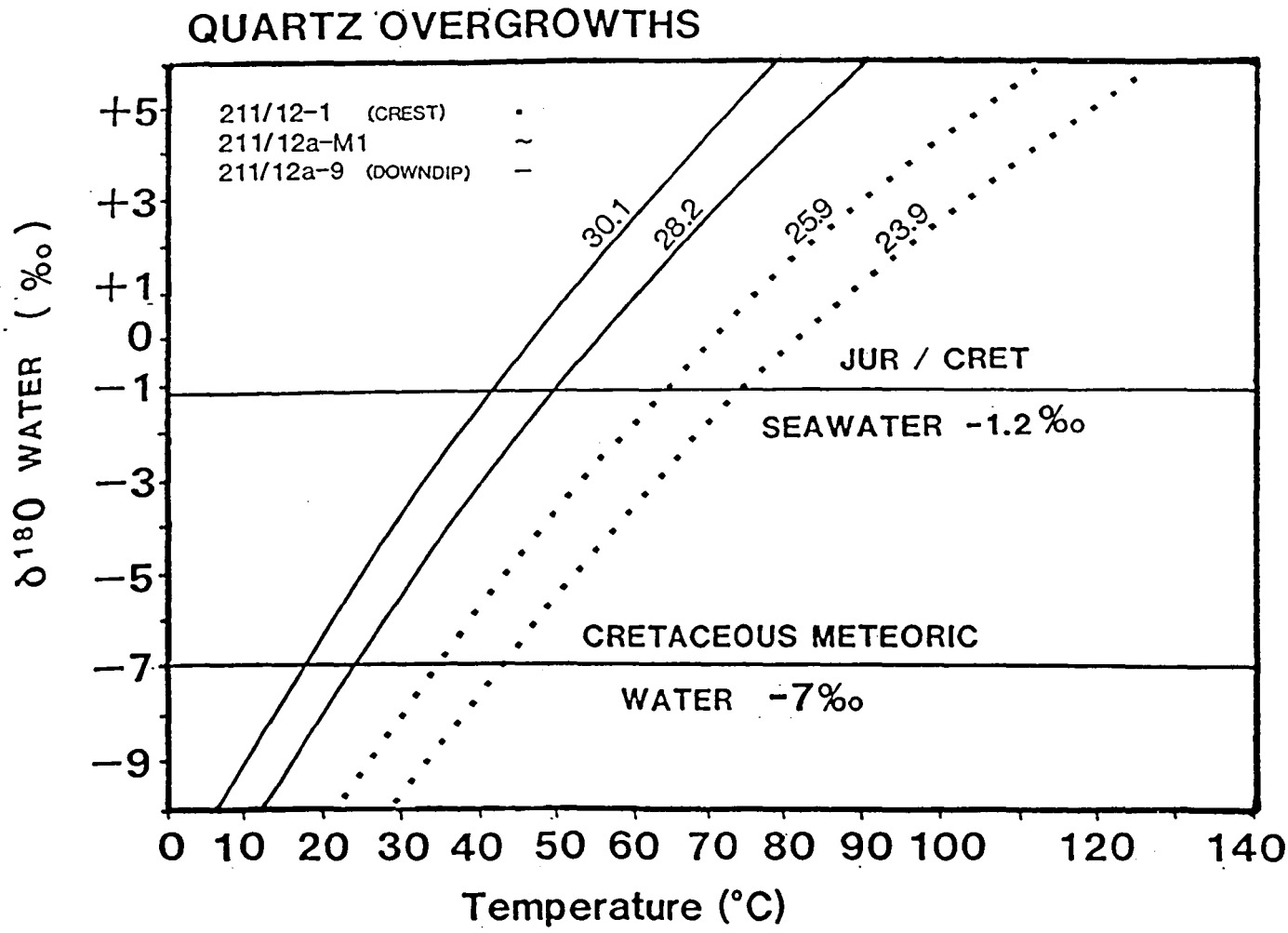
QUARTZ OVERGROWTHS
211/12-1 (CREST)
211/12a-M1
211/12a-9 (DOWNDIP)
30.1
28.2
25.9
23.9
JUR / CRET
SEAWATER -1.2‰
CRETACEOUS METEORIC
WATER -7‰
δ18O WATER (‰)
+5
+3
+1
0
−1
−3
−5
−7
−9
0 10 20 30 40 50 60 70 80 90 100 120 140
Temperature (°C)

Figure 34

Figure 35

Concentration of Carboxylic Acids (mg/l.)
10
100
1000
10,000
40
60
80
100
120
140
160
TEMPERATURE (°C)
Bacterial destruction of short-chained carboxylic acids
If $SO_4^{=}$ > 25 mg/l; $SO_4^{=} + CH_3COO^- \rightarrow 2HCO_3^- + HS^-$ $\delta^{13}C < 0$
If $SO_4^{=}$ < 25 mg/l; $CH_3COO^- + H_2O \rightarrow HCO_3^- + CH_4$ $\delta^{13}C > 0$
Elevated Pco_2 & buffered pH = carbonate cement
THERMAL DESTRUCTION OF BACTERIA
Short-chained carboxylic acid dominance
Thermocatalytic degradation of Kerogen → CH_3COO^-
Alkalinity controlled by short-chained carboxylic acids
Elevated concentrations of short-chained carboxylic acids = carbonate decementation
THERMAL DESTRUCTION OF SHORT-CHAINED CARBOXYLIC ACIDS
Thermal degradation of short-chained carboxylic acids
$CH_3COO^- + H_2O \rightarrow CH_4 + HCO_3^-$ $\delta^{13}C < 0$
Elevated Pco_2 & buffered pH = carbonate cement
POROSITY DESTRUCTION
POROSITY ENHANCEMENT
POROSITY DESTRUCTION

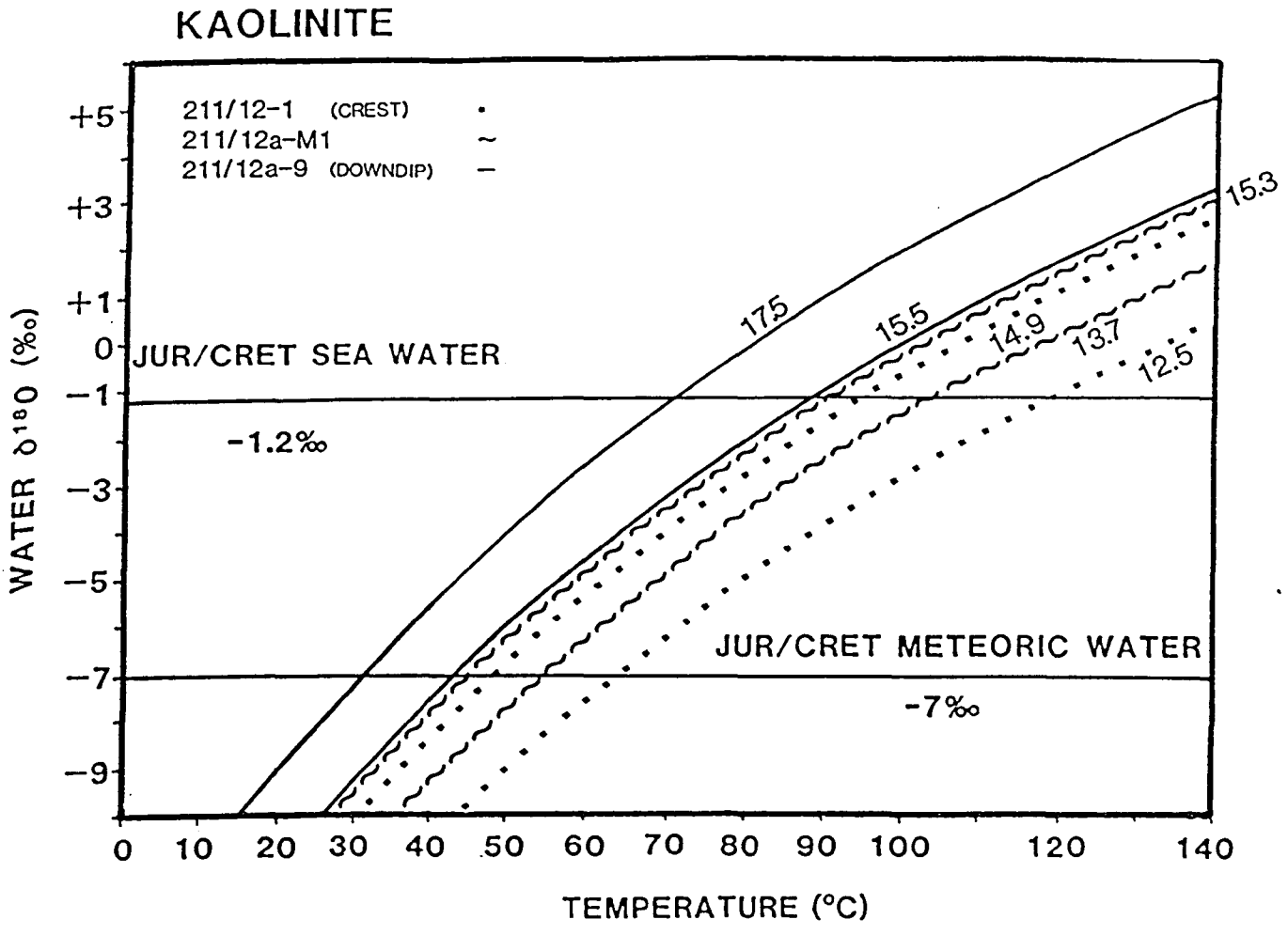
KAOLINITE
211/12-1 (CREST)
211/12a-M1
211/12a-9 (DOWNDIP)
+5
+3
+1
0
−1
−3
−5
−7
−9
WATER δ18O (‰)
JUR/CRET SEA WATER
-1.2‰
JUR/CRET METEORIC WATER
-7‰
17.5
15.5
14.9
13.7
12.5
15.3
0
10
20
30
40
50
60
70
80
90
100
120
140
TEMPERATURE (°C)

Figure 36

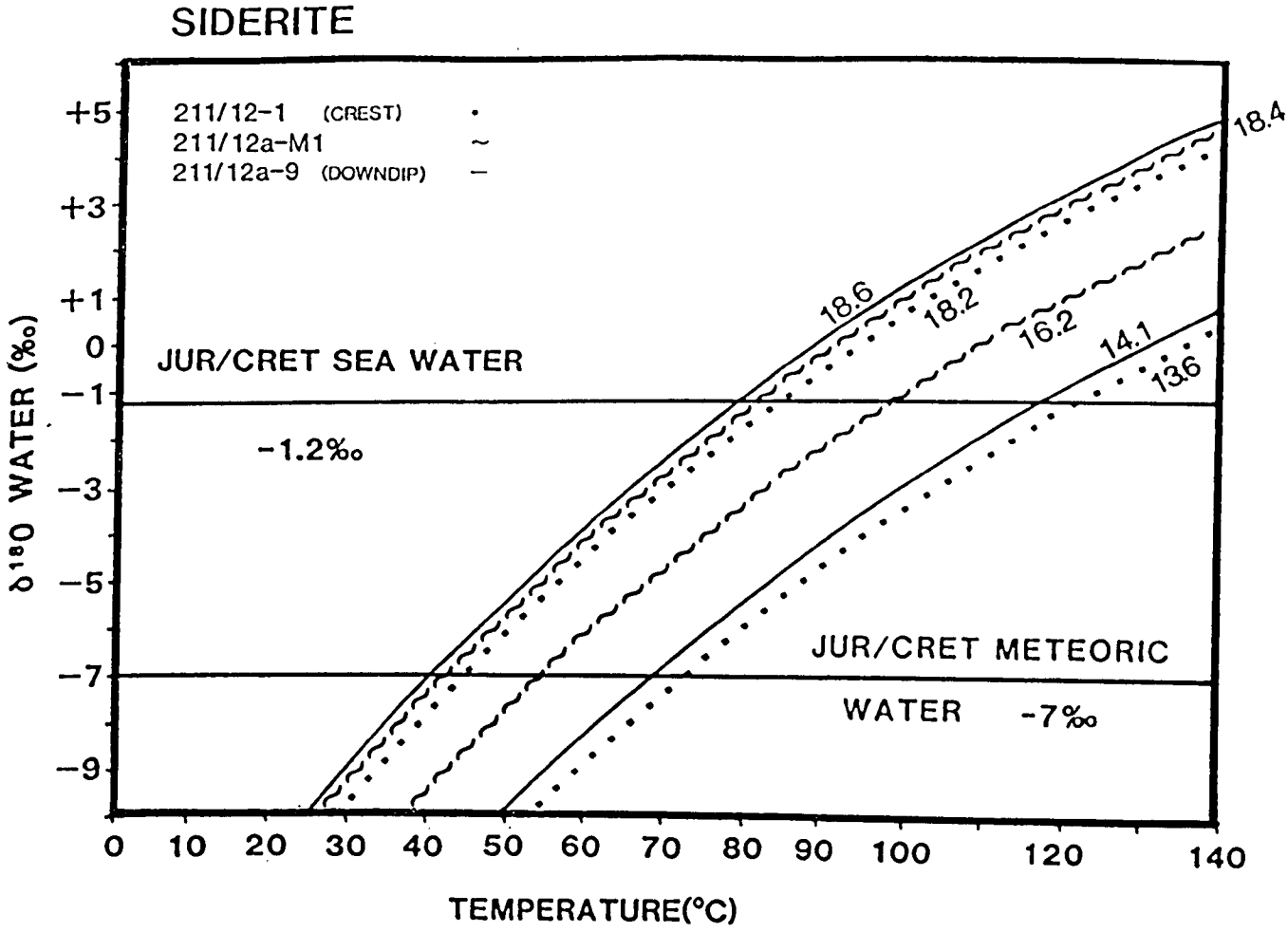
SIDERITE
211/12-1 (CREST)
211/12a-M1
211/12a-9 (DOWNDIP)
+5
+3
+1
0
−1
−3
−5
−7
−9
δ18O WATER (‰)
JUR/CRET SEA WATER
-1.2‰
JUR/CRET METEORIC
WATER -7‰
18.6
18.2
16.2
14.1
13.6
18.4
0 10 20 30 40 50 60 70 80 90 100 120 140
TEMPERATURE(°C)

Figure 37

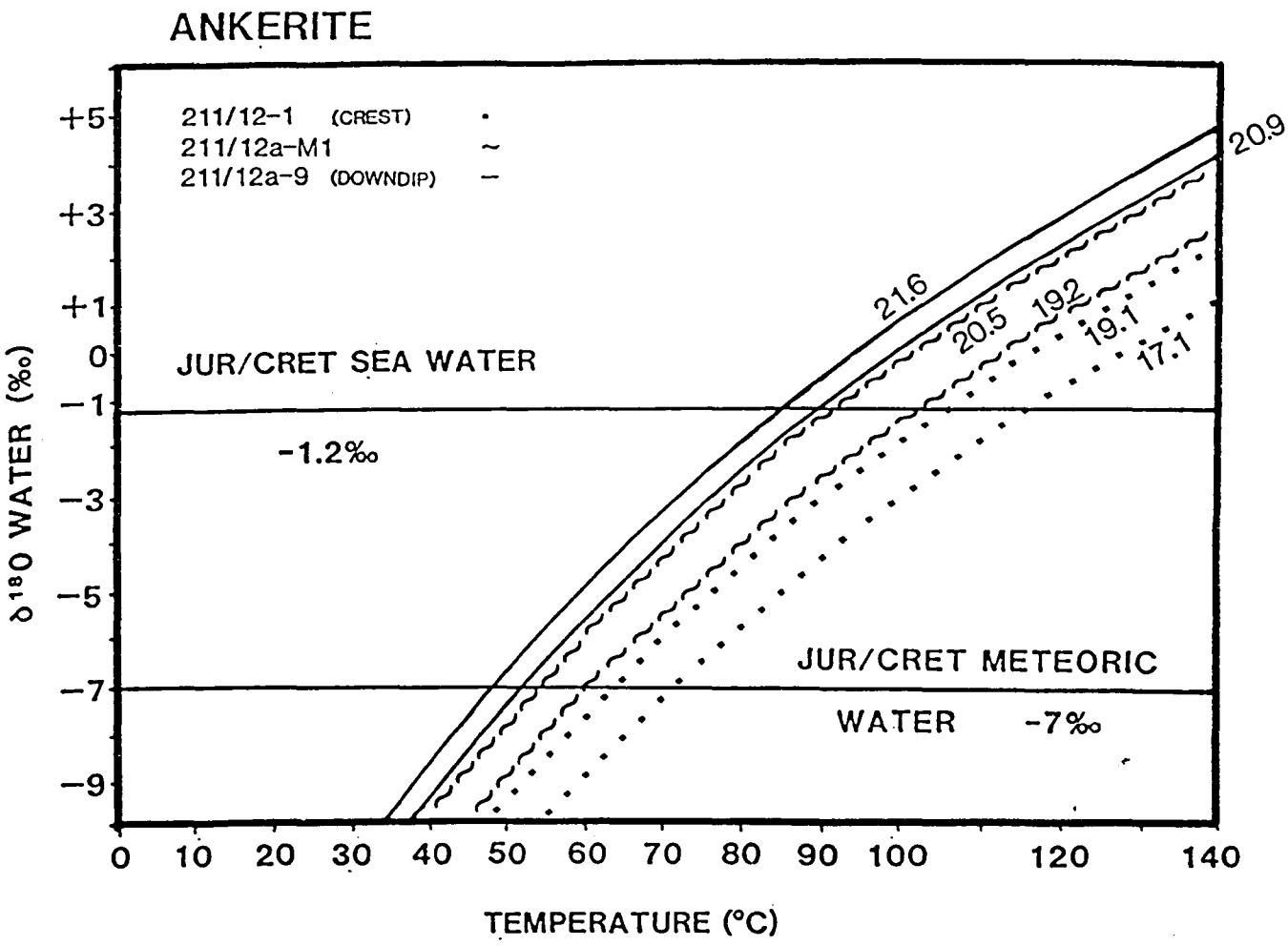
ANKERITE
211/12-1 (CREST)
211/12a-M1
211/12a-9 (DOWNDIP)
+5
+3
+1
0
−1
−3
−5
−7
−9
δ18O WATER (‰)
JUR/CRET SEA WATER
-1.2‰
JUR/CRET METEORIC
WATER -7‰
21.6
20.5
19.2
19.1
17.1
20.9
0 10 20 30 40 50 60 70 80 90 100 120 140
TEMPERATURE (°C)

Figure 38

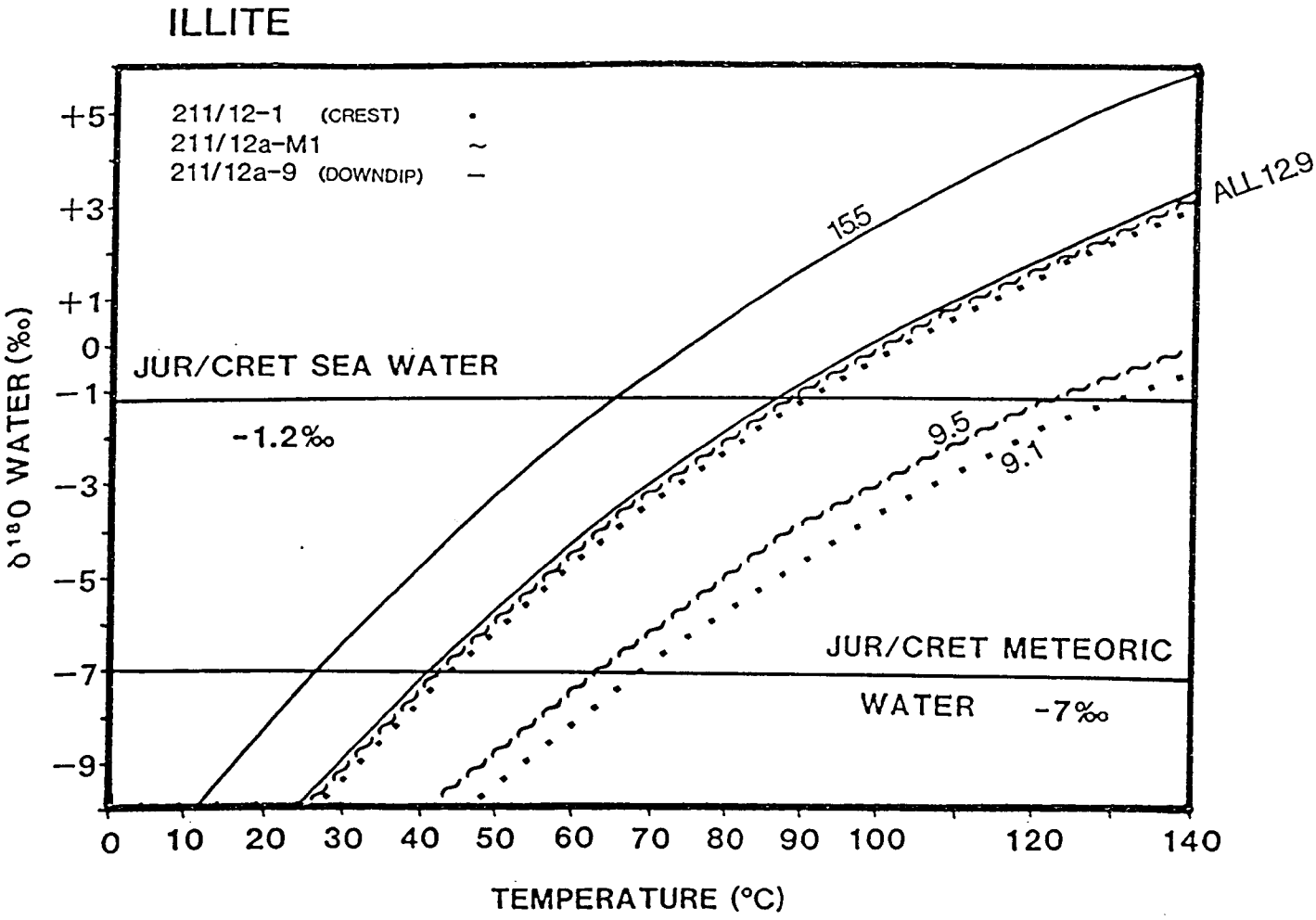
ILLITE
211/12-1 (CREST)
211/12a-M1
211/12a-9 (DOWNDIP)
+5
+3
+1
0
−1
−3
−5
−7
−9
δ18O WATER (‰)
JUR/CRET SEA WATER
-1.2‰
155
ALL 129
9.5
9.1
JUR/CRET METEORIC
WATER -7‰
0 10 20 30 40 50 60 70 80 90 100 120 140
TEMPERATURE (°C)

Figure 39

INITIAL PARAMETERS	INTERPRETATION	FINAL PARAMETERS
	---------->	
Cretaceous surface temperature 15°C	Diagenetic sequence	Present max reservoir temperature 120°C
Initial water isotopic composition : Meteoric $\delta^{18}O$ -7‰ , marine $\delta^{18}O$ -1.2‰	Diagenetic mineral $\delta^{18}O$, δD, $\delta^{13}C$,$\delta^{34}S$	Present formation water $\delta^{18}O$ +2‰, salinity half that of seawater
	System open/closed?	
	Isotopic evolution and exchange?	Illite K/Ar date 55Myr
	Redox conditios?	Illite growth at 100°C
	Mass transport?	Burial history
		Geothermal history

Figure 40

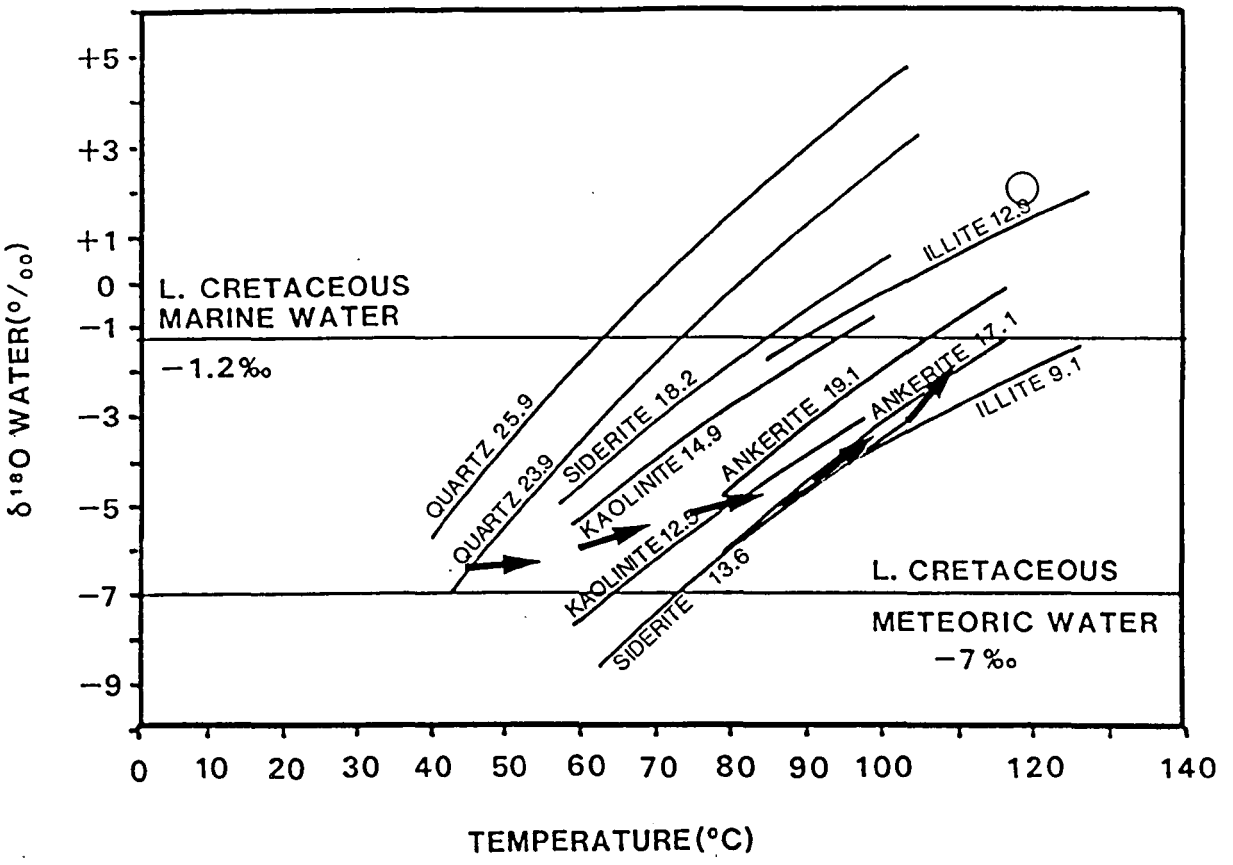

Figure 41a

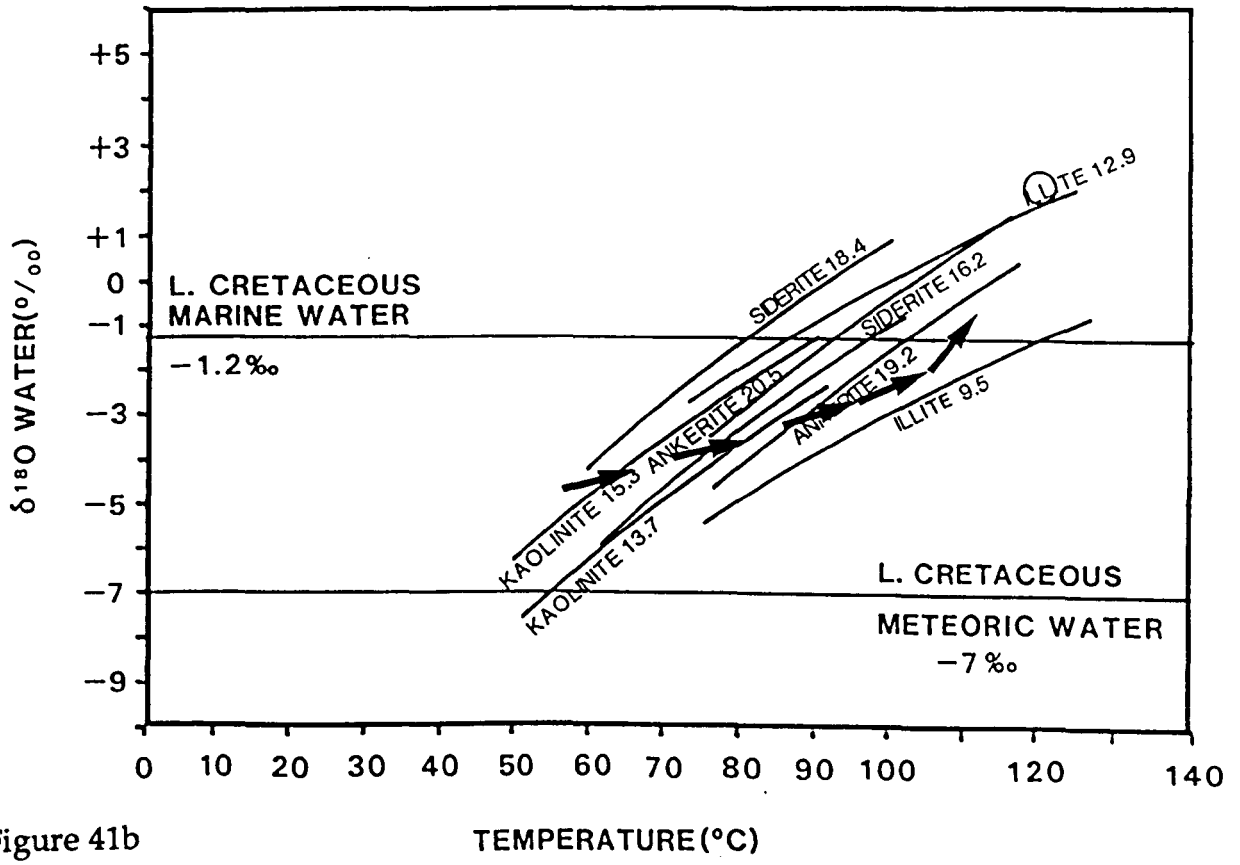

Figure 41b

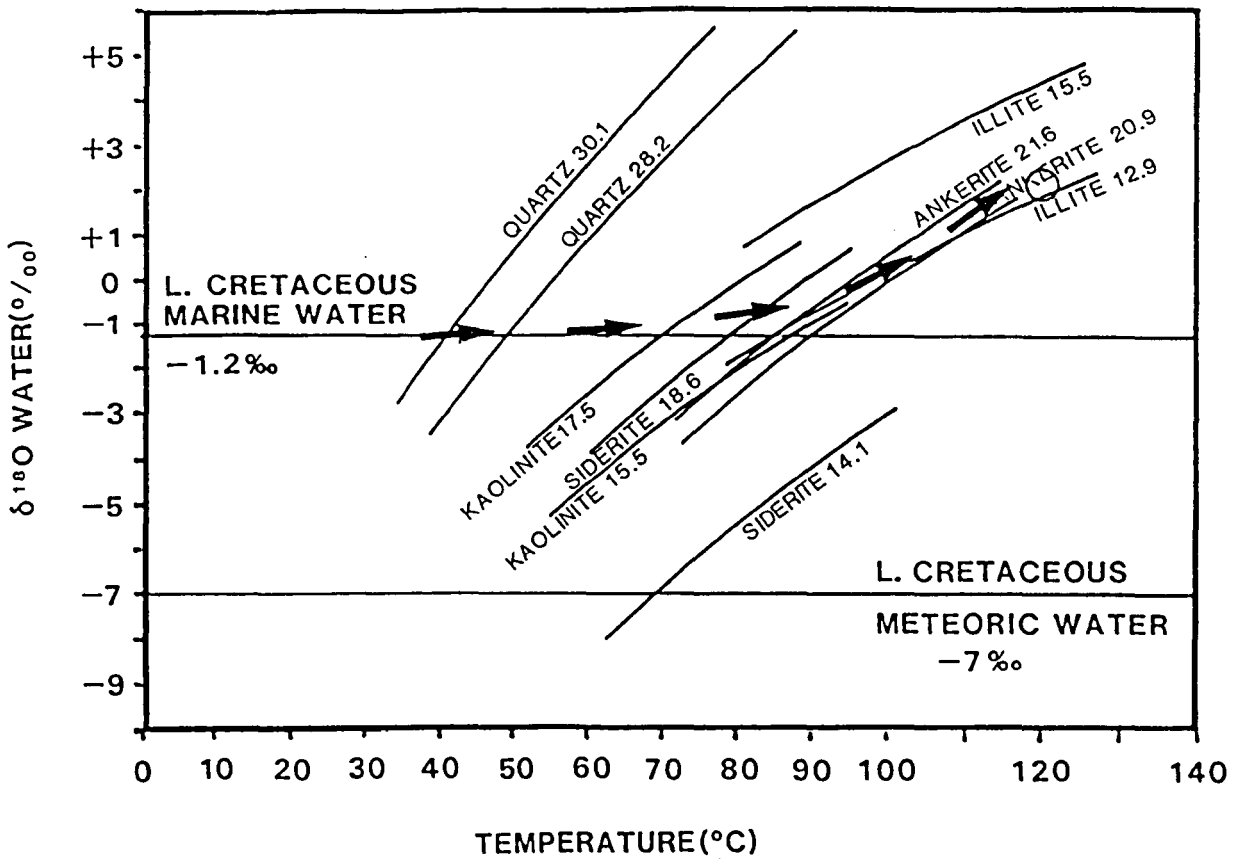
+5
+3
+1
0
−1
−3
−5
−7
−9
δ¹⁸O WATER(°/₀₀)
L. CRETACEOUS
MARINE WATER
−1.2‰
QUARTZ 30.1
QUARTZ 28.2
ILLITE 15.5
ANKERITE 21.6
ANKERITE 20.9
ILLITE 12.9
KAOLINITE17.5
SIDERITE 18.6
KAOLINITE 15.5
SIDERITE 14.1
L. CRETACEOUS
METEORIC WATER
−7‰
0
10
20
30
40
50
60
70
80
90
100
120
140
TEMPERATURE(°C)

Figure 41c

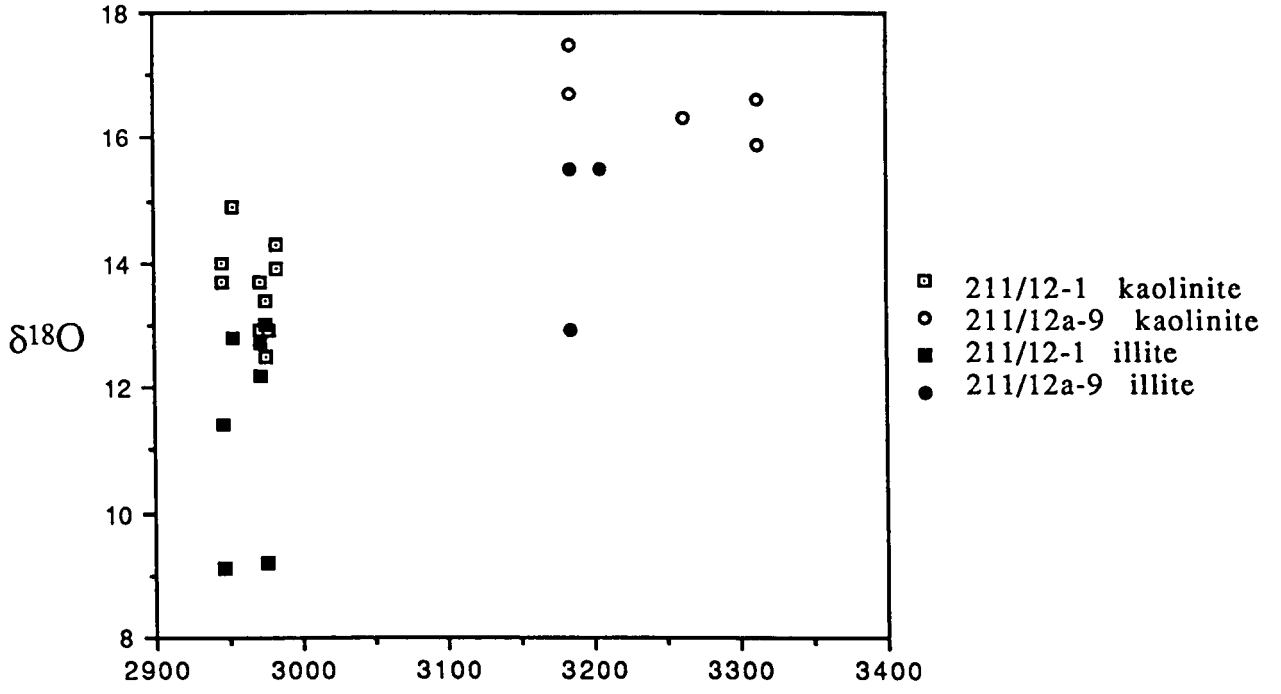

Figure 42a

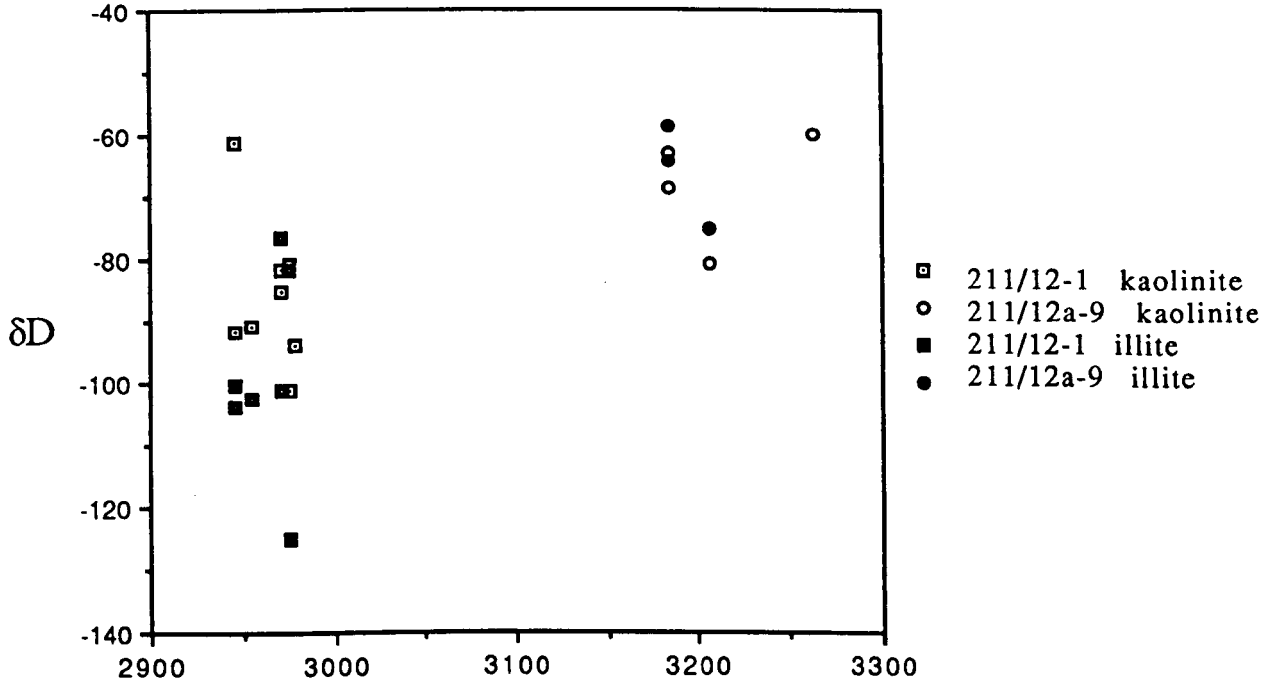

Figure 42b

Figure 43

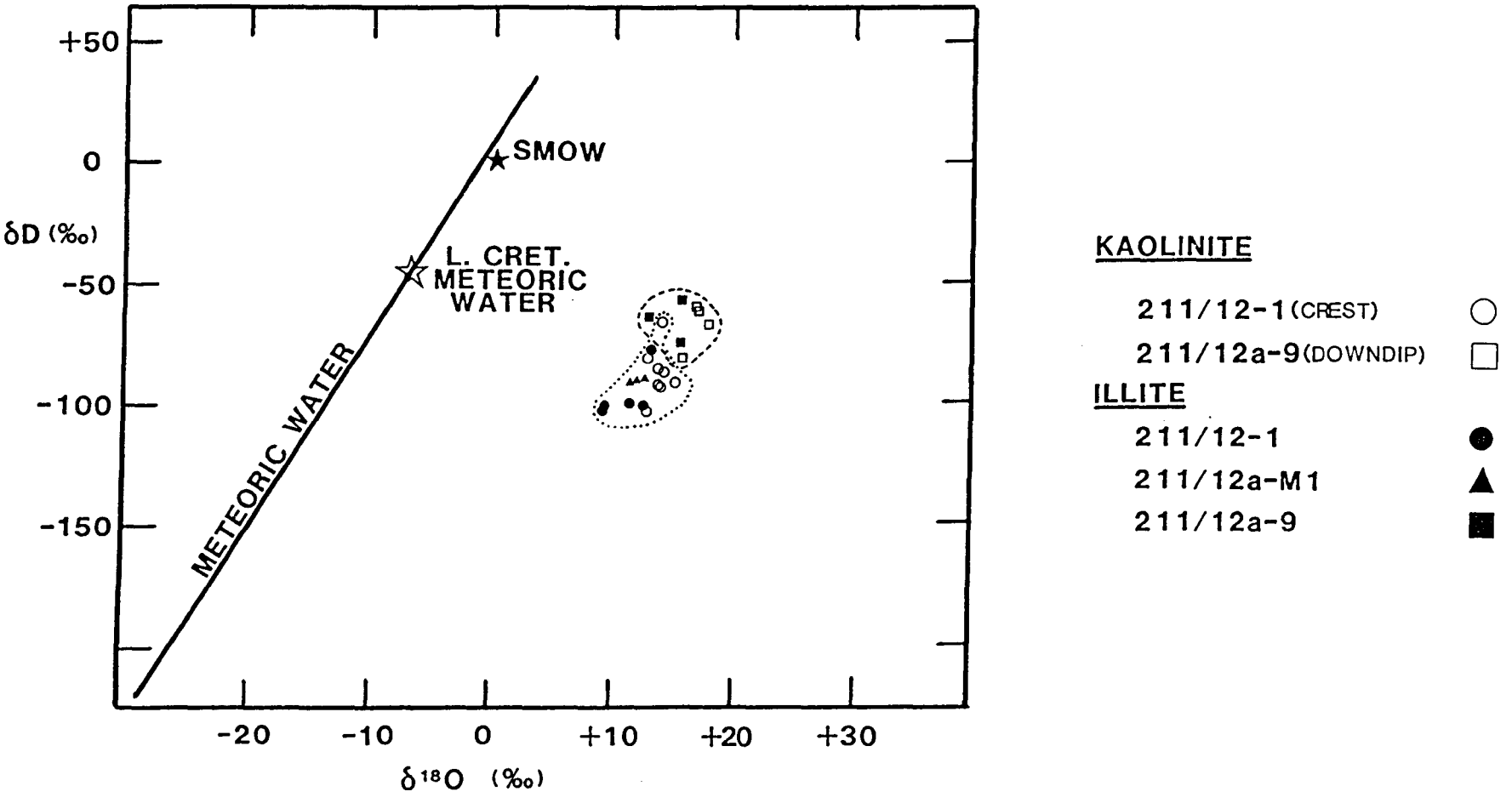
+50
0
-50
-100
-150
δD (‰)
SMOW
L. CRET.
METEORIC
WATER
METEORIC WATER
-20
-10
0
+10
+20
+30
δ18O (‰)
KAOLINITE
211/12-1 (CREST)
211/12a-9 (DOWNDIP)
ILLITE
211/12-1
211/12a-M1
211/12a-9

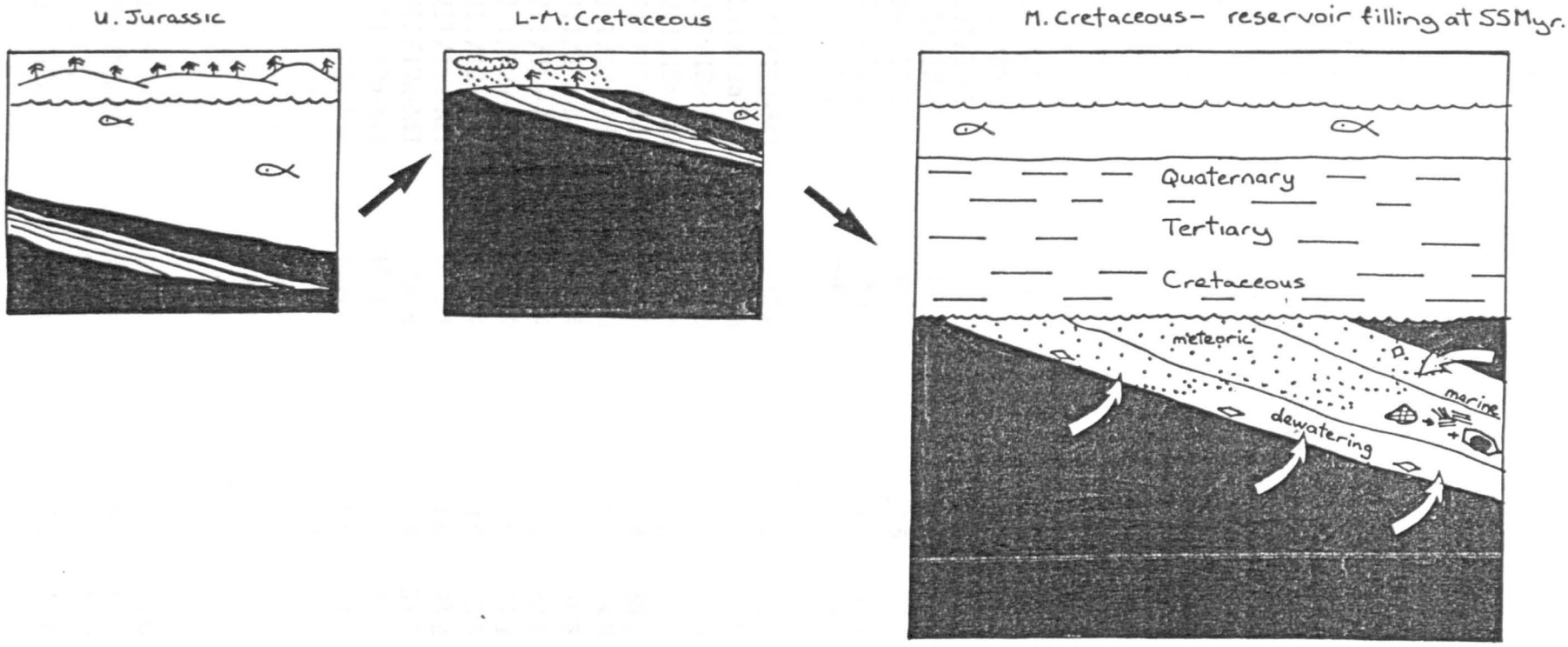
U. Jurassic
L-M. Cretaceous
M. Cretaceous- reservoir filling at 55Myr.
Quaternary
Tertiary
Cretaceous
meteoric
marine
dewatering

Figure 44

APPENDIX 1 - ELECTRON MICROPROBE ANALYSES
(mol%, normalised to 100)

Siderite

WELL	DEPTH (m)	Ca	Mg	Fe+Mn
211/12-1	2963.4	1.2	12.0	86.8
211/12-1	2963.4	4.0	12.4	83.6
211/12-1	2963.4	5.7	13.3	80.9
211/12-1	2963.4	6.4	15.5	78.1
211/12-1	2963.4	6.3	16.3	77.4
211/12-1	2963.4	6.4	13.3	80.3
211/12-1	2983.7	3.6	34.1	62.2
211/12-1	2983.7	4.0	30.9	64.9
211/12-1	2983.7	3.7	34.7	61.6
211/12-1	2983.7	4.1	34.5	61.4
211/12-1	2983.7	3.2	32.3	64.5
211/12-1	2983.7	2.6	30.2	67.2
211/12-1	2983.7	4.0	33.3	62.7
211/12-1	2983.7	2.6	32.5	64.9
211/12-1	2983.7	4.5	27.3	68.2
211/12-1	2983.7	3.5	33.0	63.5
211/12-1	2983.7	4.0	35.1	60.9
211/12-1	2983.7	1.7	28.1	69.5
211/12a-M1	2936.6	1.1	36.5	62.2
211/12a-M1	2936.6	1.1	38.5	60.4
211/12a-M1	2936.6	0.9	34.4	64.7
211/12a-M1	2936.6	0.5	33.5	66.0
211/12a-M1	2936.6	1.4	33.2	65.5
211/12a-M1	2936.6	1.4	34.3	66.5
211/12a-M1	3030.4	1.1	36.5	62.5
211/12a-M1	3030.4	1.1	38.5	60.4
211/12a-M1	3030.4	0.9	34.4	64.7
211/12a-M1	3030.4	0.5	33.5	65.6
211/12a-M1	3030.4	1.4	33.2	65.5
211/12a-M1	3030.4	1.4	33.5	65.1
211/12a-M1	3064.0	1.7	38.2	60.2
211/12a-M1	3064.0	1.5	38.9	58.2
211/12a-M1	3064.0	2.7	37.4	59.9
211/12a-M1	3064.0	2.9	40.2	56.9
211/12a-M1	3064.0	1.7	33.9	64.5
211/12a-M1	3064.0	1.5	32.4	66.1
211/12a-9	3206.0	2.4	44.6	53.0
211/12a-9	3206.0	6.6	40.3	57.3
211/12a-9	3206.0	7.5	31.7	60.1
211/12a-9	3206.0	3.2	37.6	47.1

211/12a-9	3206.0	3.2	43.1	53.7
211/12a-9	3206.0	2.7	41.7	55.6
211/12a-9	3206.0	4.1	38.2	57.7
211/12a-9	3206.0	3.3	41.7	55.0
211/12a-9	3206.0	1.7	46.2	53.1
211/12a-9	3206.0	6.6	40.6	52.8
211/12a-9	3355.3	7.9	35.1	57.0
211/12a-9	3355.3	3.3	44.3	51.2
211/12a-9	3355.3	3.5	44.2	52.3
211/12a-9	3355.3	8.6	42.4	49.0
211/12a-9	3355.3	1.8	43.0	55.2
211/12a-9	3355.3	7.3	36.3	56.4
211/12a-9	3355.3	5.0	42.1	52.9
211/12a-9	3355.3	3.5	41.7	54.8
211/12a-9	3355.3	6.9	37.9	49.4

Ankerite

WELL	DEPTH (m)	Ca	Mg	Fe+Mn
211/12-1	2963.4	66.2	22.7	11.1
211/12-1	2963.4	65.5	21.7	12.8
211/12-1	2963.4	57.5	18.4	24.1
211/12-1	2963.4	58.1	17.9	24.0
211/12-1	2978.6	59.0	26.4	14.5
211/12-1	2978.6	58.6	23.3	18.1
211/12-1	2978.6	58.6	25.3	16.1
211/12-1	2978.6	58.3	24.4	17.2
211/12-1	2978.6	58.6	25.8	15.6
211/12-1	2978.6	59.0	25.7	15.3
211/12-1	2978.6	58.7	23.3	18.0
211/12-1	2978.6	58.4	25.9	15.6
211/12-1	2978.6	58.8	26.4	14.8
211/12a-M1	2936.6	63.0	25.8	11.2
211/12a-M1	2936.6	62.7	24.2	13.1
211/12a-M1	2936.6	66.5	28.4	5.1
211/12a-M1	2936.6	65.8	30.6	3.6
211/12a-M1	2936.6	62.2	25.8	12.0
211/12a-M1	3030.4	47.8	35.7	16.5
211/12a-M1	3030.4	48.2	39.1	12.7
211/12a-9	3206.0	52.6	45.2	2.2
211/12a-9	3206.0	48.9	46.3	4.8
211/12a-9	3206.0	54.1	38.4	7.5
211/12a-9	3206.0	50.5	36.6	12.9
211/12a-9	3206.0	48.9	37.6	13.5
211/12a-9	3206.0	52.2	39.9	7.9

211/12a-9	3206.0	51.5	45.1	3.4
211/12a-9	3206.0	53.9	38.2	7.9
211/12a-9	3206.0	49.7	40.3	10.0
211/12a-9	3206.0	50.1	45.1	4.8
211/12a-9	3355.3	49.9	38.2	11.9
211/12a-9	3355.3	53.8	39.3	6.9
211/12a-9	3355.3	52.0	44.2	3.8
211/12a-9	3355.3	52.3	42.4	5.3

Appendix 2

Fluid inclusion data from the Magnus field, analysed and provided by BP. None of the wells from which fluid inclusion data have been measured are the same as those studied in this paper. Well 211/7A-3 is 2.5km northeast of 211/12-6 (Figure 3), 211/12A-M12 is 2km northwest of 211/12a-M1 and 211/12A-11 is 2km east of 211/12-3A. Statistical student's t-tests on the quartz-hosted fluid inclusion data reveal no significant differences in the temperature populations between wells.